

https://dspace.org/

A comparison of estimation methods for evaluating iron ore bodies

Machaka, Elelwani

2015-05-04
http://hdl.handle.net/10539/17604

Downloaded from a DSpace repository. https://dspace.org/

A COMPARISON OF ESTIMATION METHODS FOR EVALUATING IRON ORE BODIES

Elelwani Machaka



A research report submitted to the Faculty of Engineering and the Built Environment, University of the Witwatersrand, Johannesburg, in partial fulfilment of the requirements for the degree of Master of Science in Engineering.

Johannesburg, 2014

DECLARATION

I, Elelwani Machaka student number **385412** hereby declares this research report to be my own unaided work. It is being submitted in partial fulfilment for the degree of Master of Science in Engineering at the University of the Witwatersrand. It has not been submitted before for any degree or examination in any other University.

_____

Signature of Candidate

On this _____ day of_____ (year)_____

ABSTRACT

The estimation of iron (Fe) ore deposits presents a challenge in the mining industry, given the inter-relationship that may exist between the different variables and to preserve the relationship thereof.

Samples are collected at many locations and for each of them analyses for several chemical components are made. For multivariate data it is observed that apart from the spatial correlations(namely using variograms and cross-variograms) amongst the variables, there is also a more or less strong relationship that may exist between the variables(statistical relationships that are expressed as scatterplots and correlations). Any estimation method utilised must be able to preserve the relationship that might exist between variables. The aim of this research was to compare two different estimation methods that could be used in iron ore deposits, with both primary and secondary variables sampled at the same locations. To compare the different estimation methods, a block model was created and four grade variables (%Fe, %SiO_2, %Al_2O_3 and RD) were kriged into each block model, using two different estimation methods namely:

- *Ordinary Kriging(OK),*
- *Ordinary Co-Kriging(OCK).*

The dataset used in this project comprises 21 drillholes which in turn have a total of 292 samples from block 9 of Kapstevel North, found at Kolomela Mine in the Northern Cape. This dataset is isotopic, given that 98% of the variables of interest, %Fe, %SiO_2, %Al_2O_3 and RD, are present in all locations for most of the samples, if not all.

Point Simulation at a very fine mesh was run and re-blocked to *Block Simulation. Point Simulation* was compared to the raw data to check for representativity and to satisfy the *Conditional Simulation* properties. *Conditional Simulation* properties are as follows:

- Simulated grades must honour the raw data
- Simulated grades must honour the histogram of the raw data

- Simulated grades must honour the variograms of the raw data

Point Simulation was re-blocked to *Block Simulation* for comparison with the blocked kriged estimates. *Twenty Conditional Simulations* were run in order to formulate ground truth to compare the kriged estimates with, but only five which adequately represented the input dataset was used in the study.

The results thereof were compared and summarised thus looking at Pearson correlation coefficient between the kriged estimates and the ground truth, kriging variance, slope of regression for all two estimation methods.

Results from the study have shown that OK and OCK perform equally when the primary and secondary variables are sampled at the same locations(isotopic) and have strong correlation; however the study has demonstrated the benefit of using Ordinary Co-kriging when dataset is partially heterotopic(opposite of isotopic).

ACKNOWLEDGEMENTS

The author would like to thank the following people:

- Mr Fanie Nel for his encouragement and permission to utilise the applicable dataset;
- Dr Michael Harley at Anglo American, for his mentoring and advice;
- Dr Alastair Cornah at Anglo American, for the advice and information.

GLOSSARY

The definitions listed below apply to this document.

Acronym	Definition
Al_2O_3	Alumina
BEF	Block Estimation File
BIF	Banded Iron Formation
CaO	Calcium Oxide
CDF	Cumulative Distribution Function
CGT	Conglomeratic Ore
CoV	Coefficient of Variation
EDA	Exploratory Data Analysis
FE	Iron (elemental)
HEM	Hematite
KIO	Kumba Iron Ore
KV	Kriging Variance
OK	Ordinary Kriging
OCK	Ordinary Cokriging
QKNA	Quantitative Kriging Neighbourhood Analysis
RC	Reverse Circulation
RD	Relative Density
SCR	Screed
SIO_2	Silica
SH	Shale
SK	Simple Kriging
SCK	Simple Cokriging
SR	Slope of Regression

TABLE OF CONTENTS

DECLARATION ii

ABSTRACT iii

ACKNOWLEDGEMENTS v

GLOSSARY vi

Table of Contents vii

LIST OF FIGURES ix

List of tables xii

1 INTRODUCTION 14

2 RESEARCH GOAL 16

2.1 RESEARCH WORKFLOW 17

3 GENERAL INFORMATION OF THE PROJECT AREA 18

3.1 PROJECT AREA AND DESCRIPTION 18

3.2 ORE TYPES AND DISTRIBUTION 19

3.3 BRECCIATED ORE 19

3.4 CONGLOMERITIC ORE 19

3.5 LAMINATED AND MASSIVE IRON ORE 20

3.6 ORE GENESIS 20

4 DATA ANALYSIS 22

4.1 DATA ACQUISITION 22

4.2 DATA VALIDATION 24

4.3 EXPLORATORY DATA ANALYSIS 25

4.3.1 DRILLHOLE COUNT 25

4.3.2 DRILL-HOLE VARIABILITY 29

4.3.3 DATA COMPOSITING 30

4.3.4 PERCUSSION vs. DIAMOND DRILLED SAMPLES 31

4.3.5 CLASSICAL STATISTICS 35

4.3.6 %Fe HISTOGRAM OF 1M COMPOSITES 36

4.3.7 % SiO_2 HISTOGRAM OF 1M COMPOSITES 37

4.3.8 %Al_2O_3 HISTOGRAM OF 1M COMPOSITES 38

4.3.9 RD HISTOGRAM OF 1M COMPOSITES 39

4.3.10 CONCLUSION 40

4.4 VARIABLES SCATTER PLOTS 41

4.4.1 %Fe vs. %SiO_2 41

4.4.2 %Fe vs. %Al_2O_3 42

4.4.3 %Fe vs. RD 43

4.4.4 Multivariate Analysis 45

5 METHODOLOGY 48

5.1 VARIOGRAPHY 49

5.2 EXPERIMENTAL VARIOGRAM MODEL 50

5.3 QUANTITATIVE KRIGING NEIGHBOURHOOD ANALYSIS 53

5.4 ESTIMATION - KRIGING 59

5.4.1 ORDINARY KRIGING 59
5.4.2 APPLICATION OF ORDINARY KRIGING IN THE RESEARCH 62
5.5 ESTIMATION - COKRIGING 63
5.5.1 CROSS VARIOGRAMS 63
5.5.2 ORDINARY COKRIGING 67
5.5.3 APPLICATION OF ORDINARY COKRIGING IN THE RESEARCH 70
6 INVESTIGATIONAL RESULTS 70
6.1 CONDITIONAL SIMULATION 71
6.2 COMPARISONS OF STATISTICS 80
7 DISCUSSION 95
8 CONCLUSION 98
9 REFERENCES 100

LIST OF FIGURES

FIGURE 1: RESEARCH PROJECT LOCALITY AND SIMPLIFIED GEOLOGY OF THE SISHEN-POSTMANSBURGSUBREGION (CAIRNCROSS AND DIXON, 1995) 18
FIGURE 2: LOCATION OF BLOCK 9(HIGHLIGHTED IN BLUE) WITH FAULTING HIGHLIGHTED IN RED. 23
FIGURE 3: LOCATION OF BLOCK 9 BOREHOLE DATA. 24
FIGURE 4: VARIABILITY - DRILL TYPE 26
FIGURE 5: ISOTOPIC AND PARTIAL HETEROTOPIC DATA 28
FIGURE 6: FULLY HETEROTOPIC DATA, AL_2O_3 PRIMARY VARIABLE; FE,SIO_2 AND RD SECONDARY VARIABLES. 28
FIGURE 7: BOX AND WHISKER PLOT SHOWING VARIABILITY - LITHOLOGY 29
FIGURE 8: DISTRIBUTION OF SAMPLE LENGTH. 30
FIGURE 9: PERCUSSION DRILL-HOLE SAMPLE DISTRIBUTION 31
FIGURE 10: DIAMOND DRILL-HOLE SAMPLE DISTRIBUTION 31
FIGURE 11: CDF PLOT DIAMOND VS PERCUSSION DRILLING 32
FIGURE 12: X Y PLOT PERCUSSION VS. DIAMOND DRILLING LOCATION 32
FIGURE 13: Y Z PLOT PERCUSSION VS. DIAMOND DRILLING LOCATION 33
FIGURE 14: DISTRIBUTION OF THREE RANDOMLY SELECTED DIAMOND HOLES AND DISTRIBUTION OF THE TOTAL DIAMOND DRILLED HOLES. 34
FIGURE 15: DISTRIBUTION OF SELECTED DIAMOND HOLES CLOSEST TO PERCUSSION HOLES AND DISTRIBUTION OF THE TOTAL DIAMOND DRILLED HOLES. 35
FIGURE 16: %FE DISTRIBUTION AND CDF PLOT 37
FIGURE 17: %SIO_2 DISTRIBUTION AND CDF PLOT 38
FIGURE 18: %AL_2O_3 DISTRIBUTION AND CDF PLOT 39
FIGURE 19: RD DISTRIBUTION AND CDF PLOT 40
FIGURE 20: SCATTER PLOT %FE VS %SIO_2 42
FIGURE 21: SCATTER PLOT FE VS AL_2O_3 43
FIGURE 22: SCATTER PLOT FE VS RD 44
FIGURE 23: BIVARIATE FIT OF RD AGAINST %FE 45
FIGURE 24: SCATTER PLOT MATRIX ORE TYPE 230 46
FIGURE 25: SEMIVARIOGRAM IN ALONG STRIKE DIRECTION AND DOWN-HOLE DIRECTION 51
FIGURE 26: CONCEPT OF ZONAL ANISOTROPY AND ZONE OF INFLUENCE (WELMER, 1998). 52
FIGURE 27: ELLIPSE ALONG STRIKE DIRECTION 53
FIGURE 28: BLOCKS FOR QKNA STUDY 55
FIGURE 29: BLOCK SIZE - WELL INFORMED AREA 56
FIGURE 30: MAXIMUM NO. OF SAMPLES - WELL INFORMED AREA 57
FIGURE 31: MINIMUM NO. OF SAMPLES - WELL INFORMED AREA 57
FIGURE 32: DISCRETISATION INTERVAL - WELL INFORMED AREA 58
FIGURE 33: SEARCH RADIUS - WELL INFORMED AREA 59

FIGURE 34: SCHEMATIC DIAGRAM OF SAMPLE DISTRIBUTION WITH BLOCK OF INTEREST 60
FIGURE 35: CROSS VARIOGRAM: %FE, %SIO_2, %AL_2O_3 AND RD; DIRECTION 1 N0 (RED LINE) AND DIRECTION 2 D-90(PURPLE LINE). 65
FIGURE 36: %FE TRANSFORMED THROUGH GAUSSIAN ANAMORPHOSIS. 73
FIGURE 37: %FE TRANSFORMATION GAUSSIAN MODEL. 74
FIGURE 38: %FE RAW DATA HISTOGRAM DISPLAYED IN RED LINES, WITH SIMULATED %FE_SIM1 HISTOGRAM OF ALL FIVE SIMULATIONS RAN. 75
FIGURE 39: EXPERIMENTAL VARIOGRAMS RAW DATA FE_NS AND SIMULATED GRADES FE_SIM11 (00005). 76
FIGURE 40: REBLOCKING OF %FE (POINT SIMULATION INTO %FE_SIM1_MEAN BLOCK SIMULATION. 80
FIGURE 41: %FE_KRIGED HISTOGRAM OF OK KRIGED ESTIMATE DISPLAYED IN RED LINE AND %FE_SIM1_MEAN HISTOGRAM OF SIMULATED DATA. 83
FIGURE 42: OK KRIGEDESTIMATES (FE_KRIGED_OK) VS GROUND TRUTH (FE_SIM1_MEAN) SCATTER PLOT; KRIGING VARIANCE VS SLOPE OF REGRESSION SCATTER PLOT. 84
FIGURE 43: SCATTER PLOT OF SLOPE OF REGRESSION (SOR_FE) AGAINST DISTANCE OF SAMPLES (OK) (DISTANCE_FE). 85
FIGURE 44: HISTOGRAMS FE OCK KRIGED AND FE MEAN (SIMULATED DATA) 88
FIGURE 45: CORRELATION COEFFICIENT BETWEEN OCK KRIGED (FE_KRIGED_CK) AND GROUND TRUTH (FE_SIM11(005)), SLOPE OF REGRESSION (SOR_FE_CK) AGAINST KRIGING VARIANCE (KRIGVAR_FE_CK). 88
FIGURE 46: MEAN DISTANCE (MEAN_DISTANCE_FE_COK) OF SAMPLES FROM BLOCKS AGAINST SLOPE OF REGRESSION (OCK) (SOR_FE_COK). 89
FIGURE 47: HISTOGRAM FOR OK AND FOR OCK FOR 19% THRESHOLD 91
FIGURE 48: CORRELATION COEFFICIENT BETWEEN OK AND GROUND TRUTH; THAT OF OCK AND GROUND TRUTH AT 19% THRESHOLD. 91
FIGURE 49: HISTOGRAM FOR OK AND OCK FOR 22% THRESHOLD. 92
FIGURE 50: CORRELATION COEFFICIENT BETWEEN OK AND GROUND TRUTH; THAT OF OCK AND GROUND TRUTH AT 22% THRESHOLD. 92
FIGURE 51: HISTOGRAM FOR OK AND FOR OCK FOR 44% THRESHOLD 93
FIGURE 52: CORRELATION COEFFICIENT BETWEEN OK AND GROUND TRUTH; THAT OF OCK AND GROUND TRUTH AT 44% THRESHOLD. 93
FIGURE 53: HISTOGRAM FOR OK AND FOR OCK FOR 66% THRESHOLD 94
FIGURE 54: CORRELATION COEFFICIENT BETWEEN OK AND GROUND TRUTH; THAT OF OCK AND GROUND TRUTH AT 66% THRESHOLD. 94
FIGURE 55: CORRELATION COEFFICIENT FOR %FE AGAINST GROUND TRUTH. 95

FIGURE 56: CORRELATION COEFFICIENT FOR %AL_2O_3 ATDIFFERENT PERCENTAGE OF SAMPLES MISSING AGAINST GROUND TRUTH. 97
FIGURE 57: %FE GRADE VARIATION IN DIFFERENT ROCK TYPES 102
FIGURE 58: %SIO_2 VARIATION IN DIFFERENT ROCK TYPES 102
FIGURE 59: %AL_2O_3 VARIABILITY IN DIFFERENT ROCK TYPES 103
FIGURE 60: RD VARIATION IN DIFFERENT ROCK TYPES 103
FIGURE 61: SCATTERPLOT OF %FE VS %SIO_2 104
FIGURE 62: SCATTERPLOT %FE VS %AL_2O_3 104
FIGURE 63: SCATTERPLOT %FE VS RD 105
FIGURE 64: EXPERIMENTAL VARIOGRAM %SIO_2VARIOGRAM 106
FIGURE 65: EXPERIMENTAL VARIOGRAM %AL_2O_3 VARIOGRAM 107
FIGURE 66: EXPERIMENTAL VARIOGRAM RD VARIOGRAM 108
FIGURE 67: %SIO_2 GAUSSIAN ANARMORPHOSIS TRANSFORMATION 109
FIGURE 68: %SIO_2 GAUSSIAN ANARMORPHOSIS TRANSFORMATION MODEL. 109
FIGURE 69: %AL_2O_3 GAUSSIAN ANARMORPHOSIS TRANSFORMATION 110
FIGURE 70: %AL_2O_3 GAUSSIAN ANARMORPHOSIS TRANSFORMATION MODEL 110
FIGURE 71: RD GAUSSIAN ANARMORPHOSIS TRANSFORMATION 111
FIGURE 72: RD GAUSSIAN ANARMORPHOSIS TRANSFORMATION MODEL. 111
FIGURE 73: %SIO_2 CONDITIONAL PROPERTIES 115
FIGURE 74: %AL_2O_3 CONDITIONAL PROPERTIES 119
FIGURE 75: RD CONDITIONAL PROPERTIES 123
FIGURE 76: SIO_2 RESULTS 126
FIGURE 77: AL_2O_3 RESULTS 129
FIGURE 78: RD RESULTS 132
FIGURE 79: SIO_2 RESULTS 136
FIGURE 80: AL_2O_3 RESULTS 139
FIGURE 81: RD RESULTS 143

LIST OF TABLES

TABLE 1: **SAMPLES COUNT PER DRILL TYPE.** 26
TABLE 2: **DRILLHOLE COUNT PER VARIABLE** 27
TABLE 3: **CLASSICAL STATISTICS OF COMPOSITED DATA INCLUSIVE OF BOTH PERCUSSION AND DIAMOND.** 36
TABLE 4: **CORRELATIONS BETWEEN ALL THE VARIABLES** 47
TABLE 5: **VARIOGRAM MODEL PARAMETERS** 51
TABLE 6: **SUMMARY OUTLINING THE COREGIONALISATION MATRICES FOR VARIABLES %FE, %, SIO_2, %AL_2O_3 AND RD.** 64
TABLE 7: **SUMMARY OF EXPERIMENTAL CROSS VARIOGRAMS FOR VARIABLES %FE, %, SIO_2, %AL_2O_3 AND RD** 66
TABLE 8: **CO-REGIONALISATION MATRICES FOR THE 10 CROSS VARIOGRAMS OF VARIABLES %FE, %, SIO_2, %AL_2O_3 AND RD.** ... 66
TABLE 9: **CORRELATION BETWEEN %FE, %, SIO_2, %AL_2O_3 AND RD SIMULATED VARIABLES** 77
TABLE 10: **SUMMARY OF THE RESULTS OF THE TWO ESTIMATION METHODS** 99

APPENDICES

APPENDIX: 1 STATISTICS 102

APPENDIX: 2 VARIOGRAM BOREHOLE DATA WITH BOTH DIAMOND DRILLED AND PERCUSSION SAMPLES 106

APPENDIX: 3 GAUSSIAN ANARMORPHOSIS TRANSFORMATION 109

APPENDIX: 4 CONDITIONAL SIMULATION PROPERTIES 112

APPENDIX: 5 ORDINARY KRIGING 124

APPENDIX: 6 ORDINARY COKRIGING 133

APPENDIX: 7 CORRELATION COEFFICIENT FOR % SiO_2, Al_2O_3 and RD AGAINST GROUND TRUTH 144

APPENDIX: 8 QUANTITATIVE NEIGHBOURHOOD ANALYSIS 145

1 INTRODUCTION

An aim for performing resource estimate is to develop the *best estimate* describing the quantity of material and the qualities of that material inherent in any ore body so that high levels of confidence in the results are produced. This, therefore, requires that all available and valid information are being utilised to the fullest extent.

A resource estimate is based on interpolation of the physical characteristics of a mineral deposit through:

* The collection of data (i.e. sampling; logging rock type, texture, colour etc.)
* Analysis of the data (i.e. chemical analysis, grade distribution etc.), and
* Modelling the geometry of the ore and waste components, size, shape and grade of the deposit (i.e. data interpretation, geological domaining, grade estimation into different domains etc.).

Important physical characteristics of the ore body that must be determined include:

(i) The size, shape, and continuity of ore zones,

(ii) The frequency distribution of the mineral grade, and

(iii) The spatial variability of the mineral grade.

These characteristics of the mineral deposit are never completely known but are estimated from sample data.

The estimation of laminated iron (Fe) ore is the focal point of this research. The main constraint in dealing with Fe ore bodies is to preserve the stratigraphy and spatial continuity of grades during estimation. It must be noted that there are

several estimation methods that are being utilised in the industry and the application of each method may depend on the *complexity of the ore body* as well as *the availability of data*.

There are several geostatistical techniques utilised in estimation processes, however, the following estimation methods will be investigated for the iron (Fe) study:

- *Ordinary Kriging and Ordinary Co-kriging.*

The dataset is from Block 9 of Kapstevel North at Kolomela Mine, which is the area of interest for this research focusing on *ore-type 230* which is laminated ore. The dataset comprises 21 drill-holes which in turn have 292 samples.

The data is isotopic in that for each sample location, all the four variables, %Fe, $\%SiO_2$, $\%Al_2O_3$ and RD, are present, thus primary and secondary variables are sampled at the same locations.

2 RESEARCH GOAL

The purpose of this research is to compare two estimation methods that can be utilised optimally to estimate Fe ore bodies; with isotopic dataset. The following were investigated in the research:

- *Ordinary Kriging (OK)*
- *Ordinary Co-kriging (OCK).*

The dataset used in the research is isotopic[1] with respect to the four variables of interest (%Fe, $\%SiO_2$, $\%Al_2O_3$ and RD) to test which of the two estimation methods OK and OCK will be a preferred method under such condition.

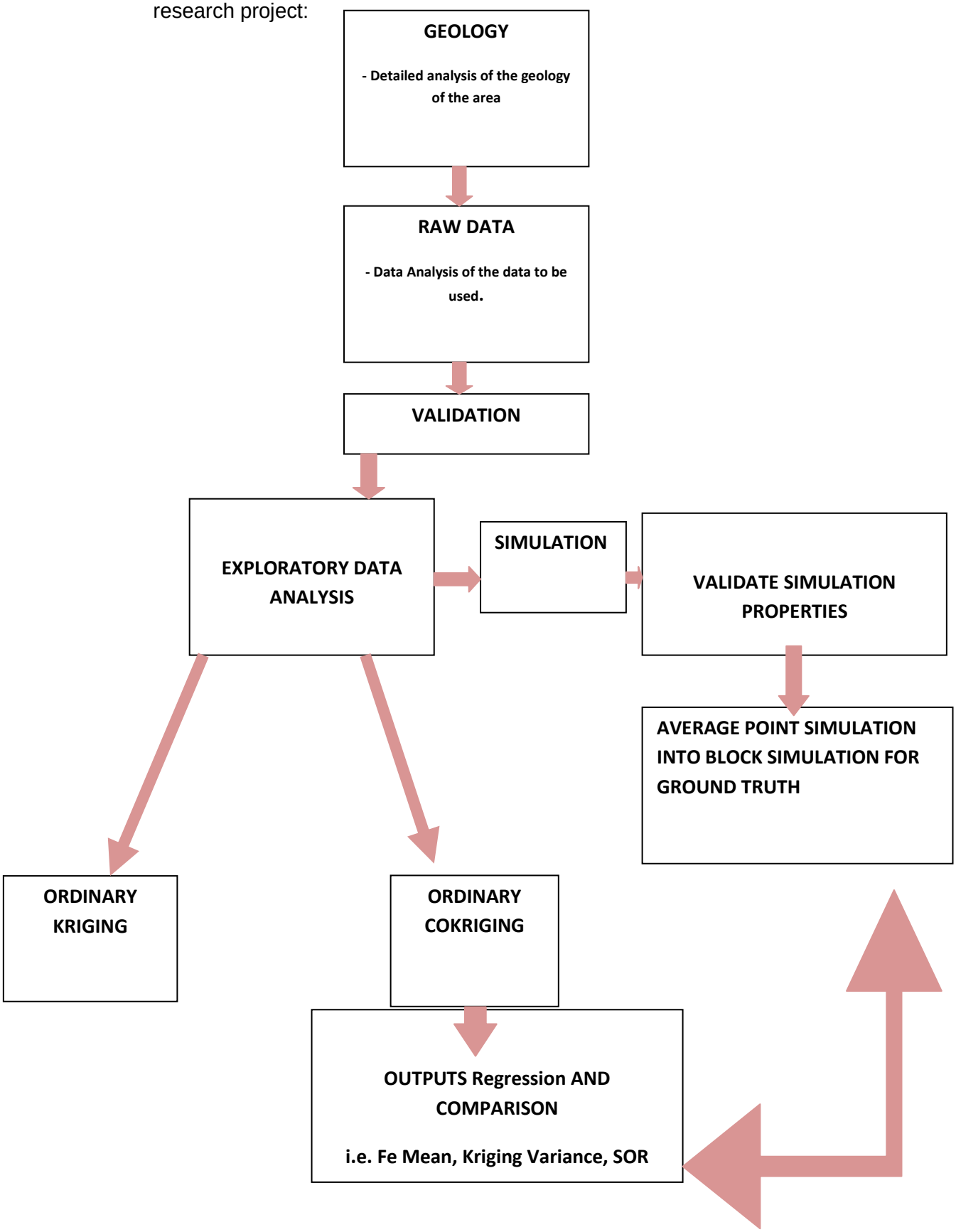
A block model was created and four variables were estimated into the block model using each of the two estimation methods. The results of each estimation method were compared by detailed investigation of grade continuity, kriging variances, correlation coefficient and slope of regression (SOR), etc.

A very fine mesh simulation was generated and re-blocked to the same block size to that of the kriged estimates blocks which were then compared with. For the purpose of this research estimates were performed in *Isatis* software.

[1] Isotopic all the variables of interest in all the locations, Heterotopic not all the variables occur at the same position

2.1 RESEARCH WORKFLOW

The following is a schematic description of the workflow applied during this research project:



3 GENERAL INFORMATION OF THE PROJECT AREA

3.1 PROJECT AREA AND DESCRIPTION

The Kapstevel North project area is located within Kumba Iron Ore's Kolomela Mine licence area, near the town of Postmansburg, in the Northern Cape Province of South Africa (see **Figure 1**). This region is known for the occurrence of high-grade iron ore and manganese deposits. The mining area is located about 10km from Postmansburg town.

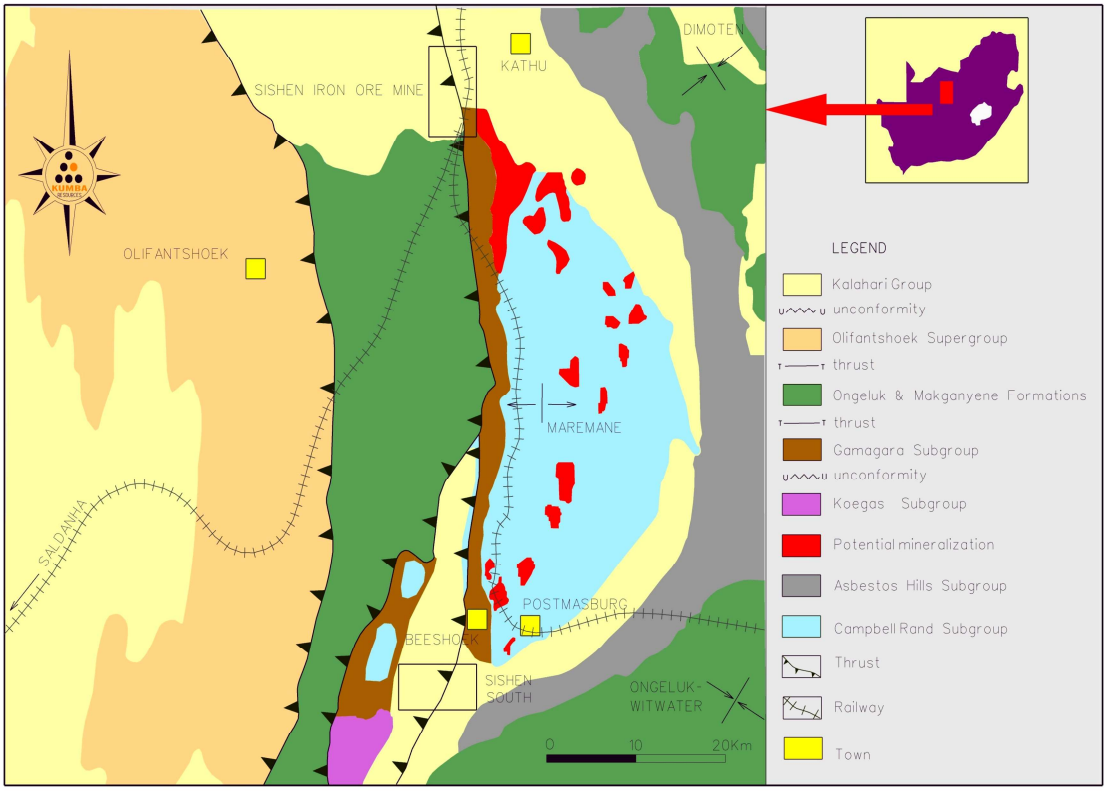


Figure 1: Research Project locality and simplified Geology of the Sishen-Postmansburg Subregion (Cairncross and Dixon, 1995).

3.2 ORE TYPES AND DISTRIBUTION

The ores at Sishen and Kolomela are very similar. They are composed of hematite and specular hematite, with minor to trace amounts of limonite. Four distinct ore types can be classified as *brecciated*, *conglomeratic, laminated* and *massive*, ores. The ores have been developed in specific depositional environments hence each has a unique chemical, physical and metallurgical properties; and the range of chemical and physical properties are specific to each ore type. The genesis of each ore-type has been influenced by regional tectonics and the preservation of each ore type is primarily determined by local geological structures. The laminated and massive ores are best developed in basinal and pseudo-graben structures. Brecciated ores are preserved within deep palaeosinkholes that have developed within the dolomites. The conglomeratic ores are found in the overlying clastic succession of conglomerates, shales and quartzites.

3.3 BRECCIATED ORE

Brecciated ores consist of a chaotic arrangement of very angular and poorly sorted fragments of laminated and massive ore types. The breccias fill palaeosinkholes developed in the carbonates. Angular fragments of BIF and some argillitic material are also found in the collapse breccia. Specularite is very common in the porous breccia matrix.

3.4 CONGLOMERITIC ORE

The conglomeratic ores are invariably situated adjacent to, or are in close proximity to, laminated and massive ore bodies. The lower ore conglomerates are usually poorly-sorted and clast-supported. Clasts tend to be angular fragments of laminated and massive ore in a groundmass of finer, detrital hematite grains and crystalline specularite. This ore unit is thought to represent

ferruginised Gamagara Formation conglomerates, which unconformably overly the laminated and massive ores. Ore conglomerates often lie on, or are found very close to the Gamagara unconformity.

3.5 LAMINATED AND MASSIVE IRON ORE

Two ore types namely *laminated* and *massive* ore have been identified as the most important resource of high-grade, lump ore in the region, with hematite ore which grades upwards into thickly-bedded, contorted and even massive ores.

The laminated and massive ores are best preserved in basinal and pseudo-graben type structures. The textures displayed by the thickly-bedded and massive ores suggest elements of clastic input were present during deposition (van Schalkwyk and Beukes, 1986).

3.6 ORE GENESIS

Two models give reference to the origin of high grade hematite deposits in banded iron formation; supergene related origin and hydrothermal related origin. The distinct difference between the two deposits (supergene and hydrothermal) is likely linked to the different processes and temperature of ore formation. Sishen deposit is believed to be of supergene origin formed as results of the influence of meteoric at low temperature (van Schalkwyk and Beukes 1986). In contrast, the Thabazimbi deposit appears to be hydrothermal in origin with sparitic calcite and dolomite forming cogenetically with the ore-forming micro-platy hematite (Netshiozwi, 2002). The author concurs with the opinion of many researchers including van Schalkwyk and Beukes (1986) and Moore et al (2001) that the laminated and massive ores at Sishen are a product of supergene enrichment of primary BIF, which has a similar genetic model to that of Kolomela.

This mineralisation process at Kolomela is deduced from the following field, pit and drill core relationships:

- hematite mineralisation crosscuts primary sedimentary bedding (van Schalkwyk and Beukes, 1986),
- the contact between the host BIF and overlying laminated ore is always gradational,
- remnant lenses of BIF occur within the ore bodies,
- the ore and the original BIF have identical textures such as laminae, slump folds and diagenetic cracks,
- brecciated iron-formation is often partially or completely ferruginised
- van Schalkwyk and Beukes (1986) also explain the porosity of the alternating hematite laminae as evidence of leaching of primary silica by alkaline fluids which points to ferric hydroxide as a precursor to goethite and eventually hematite.

The above mentioned observations indicate that the primary BIF's were leached of silicates, chert and carbonates; and enriched by hydrated iron oxides, whilst in a brittle and lithified state resulting in additional Fe. This was followed by the growth of hematite plates and goethite from the hydrated iron oxides, a process that stopped before all the iron oxides had been altered. Finally, solution of the remaining goethite led to high grade hematite ores (Morris et al, 1980). The process preserved original textures and diagenetic features. The energy source, mechanism and events required to enrich the ore in this manner, are, however, less clear.

However for supergene processes to take place, there must have been some mobility of fluids. The groundwater responsible for the solution of the dolomites would have been acidic. These waters could also leach iron bearing minerals from the lower portion of the overlying BIF. Over time, voids would develop and the groundwater would become increasingly alkaline (van Schalkwyk and Beukes, 1986). Collapse of overlying strata into the voids could explain the origin

of brecciated, supergene enriched ore, preserved in deep sinkhole structures. Although the fluids would be forced upward, into the overlying strata, the theory does not satisfactorily explain why the main ore bodies would develop just beneath the pre-Gamagara erosion surface. Nel (pers comm.) has speculated that basinal dewatering could have played a major role in the supergene enrichment process. It is possible that fluctuating groundwater and basinal dewatering continued during and after the deposition of the Gamagara Subgroup. Migratory fluids hematized conglomerates and adjacent shales at specific stratigraphic horizons. The conglomerates probably offered an ideal plumbing system for the fluids to move through.

The complexity of the iron ore bodies is clearly outlined from the sections above; mineralisation, local geology and ore genesis. Any estimation method considered must take cognisance of the complexities of the genesis of ore bodies. This will have to ensure optimal estimates are obtained which are accurate reflections of the geology.

4 DATA ANALYSIS

4.1 DATA ACQUISITION

The dataset for the project was drawn from the holes that were drilled by the following methods:

- percussion
- reverse circulation
- diamond drilling

The Kapstevel area is *divided* into different blocks due to the high density of faulting present in the area as shown in **Figure 2**. The area below filled with boreholes was the area of interest for this project.

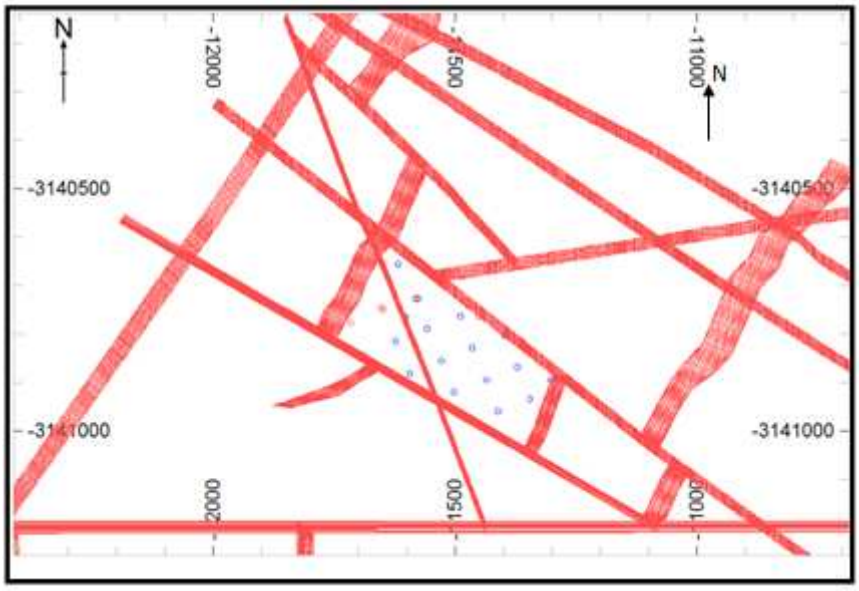


Figure 2: Location of Block 9(Highlighted in Blue) with faulting highlighted in red.

For the purpose of this study, only Block 9 drill-hole data (**Figure 2**) was used as displayed in **Figure 3**.

Figure 3 depicts the relative locations of the drill-holes used in the study; red being the diamond drilled samples, blue percussion drilled samples, yellow piloting samples and cyan RC drilled samples. A total of 27 boreholes were initially available, but only 24 holes were available for use in the research (three holes were missing coordinates). However further three holes were taken off the database, due to data interrogation analysis illustrated in **Section 4.2** and a total of 21 holes was then available for use in the study.

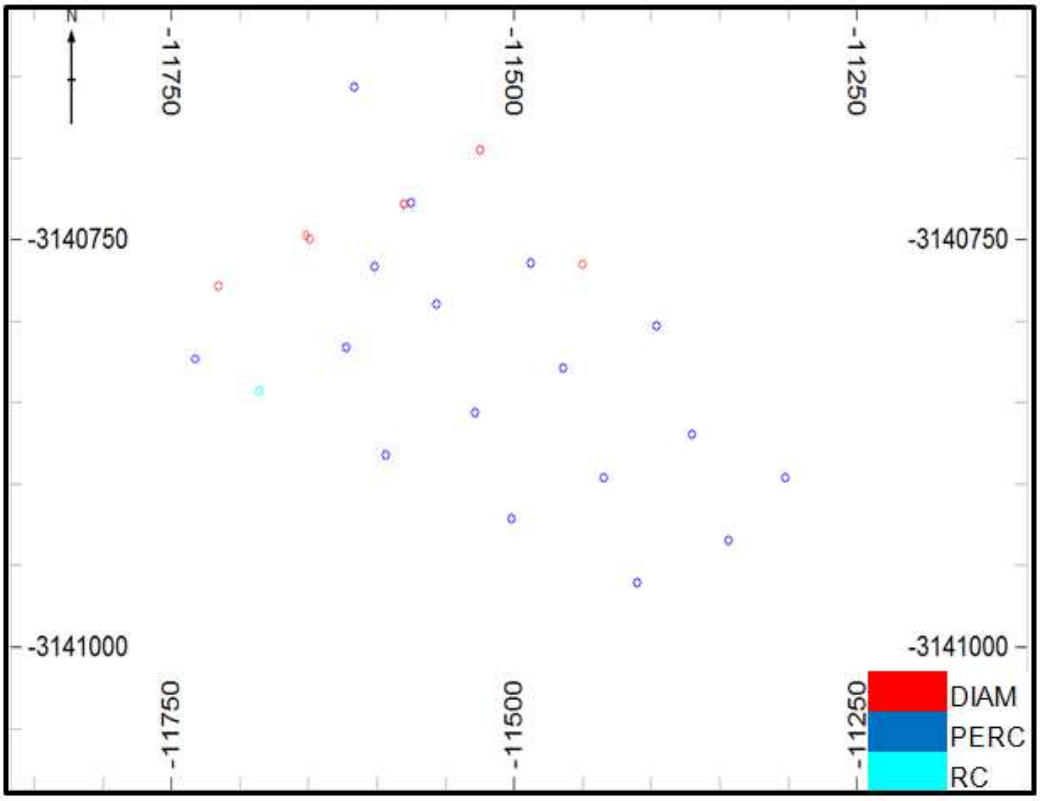


Figure 3: Location of Block 9 Borehole Data.

4.2 DATA VALIDATION

It is important to ensure that the quality of data and information being used is thoroughly checked. The quality of the decisions made in the mining industry rests most significantly on the quality (accuracy and reproducibility) of the data, hence the need for proper validation of the data prior to being used. The database used for the study was subjected to rigorous validation protocols which looked at:

- Overlaps in both the geology and assays
- Drill-holes with no assay data
- Geological logging not available up to the end of the hole
- Non – unique collar co-ordinates
- Drill-holes plotting outside of the interpretation area

- Incorrect down hole survey data
- Very large deviations in down hole survey and dips
- No solid wireframing to support drill-holes
- Gaps in assays
- Zero values in the database (true value or not?)
- Extreme assay values
- Sample length exceeding maximum allowed value
- Extreme total oxide values

The dataset available for the study was fairly clean with an exception of three holes that had spurious collars or downhole survey (one hole collar was significantly above topography); two holes protrude significantly above topography.

The problematic samples were highlighted and investigated; those with significant problems did not form part of the final data set used in the research, which resulted in three boreholes out of 24 being deemed not suitable for use in the study.

4.3 EXPLORATORY DATA ANALYSIS

4.3.1 DRILLHOLE COUNT

The dataset comprises 24 boreholes in total. The dataset displayed in **Table 1** comprises percussion, reverse circulation and diamond drill-holes; with a significant amount of data from diamond drilling. **Table 1** outlines a total of 340 samples collected from each drilling type, with 107 samples sampled between 0.5 and 1m sampling length; 54 samples sampled at 1m sampling length and 179 samples between 1 and 1.5m sampling length.

Table 1: Samples Count per Drill Type.

DRILL TYPE	N(Samples)
UNDEFINED	7
DIAM	306
PERC	24
PILO	2
RC	1

The sample population is mostly made up of diamond drill core followed by chips from percussion drilling as illustrated by **Figure 4**, given the length drilled through ore by different drilling types.

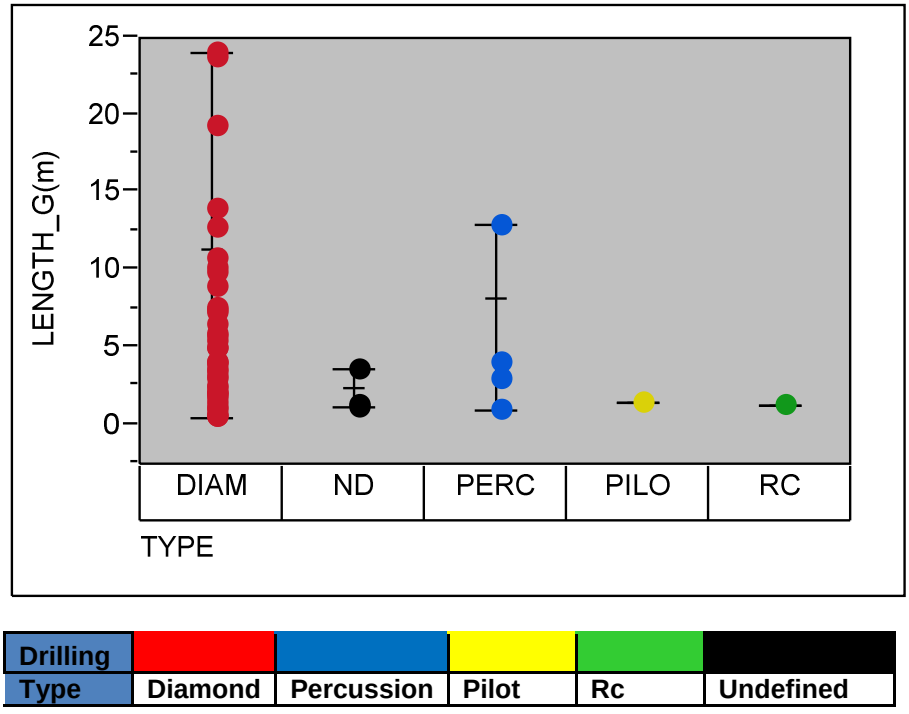


Figure 4: Variability - Drill type

It is also important to account the total number of assays for each variable of interest per sample in all drill-holes; as this signifies whether the dataset is heterotopic or isotopic. The relationship between %Fe, %SiO_2, %Al_2O_3 and RD which are the variables of interest in the study is of importance, hence the need to establish if all variables are present for each sample at every location. **Table 2** outlines the number of assays for each variable per drill-hole sample which is

important mainly for Co-kriging. N (Rows) in **Table 2** below defines the total number of samples collected in each borehole.

Table 2: Drillhole Count per Variable

BHID	COUNT	N(Rows)	N(Fe)	N(SiO_2)	N(Al_2O_3)	N(K_2O)	N(P)	N(RD)
WV011_O	1	4	0	0	0	0	0	0
WV047_O	2	20	20	20	20	20	20	20
WV048_O	3	10	10	10	10	10	10	10
WV072_O	4	28	27	27	27	27	27	27
WV073_O	5	8	8	8	8	8	8	8
WV074_O	6	8	8	8	8	8	8	8
WV115_A	7	24	24	24	24	24	24	24
WV115_O	8	24	24	24	24	24	24	24
WV145_O	9	2	2	2	2	2	2	2
WV152_O	10	26	26	26	26	26	26	26
WV154_O	11	10	10	10	10	10	10	10
WV155_O	12	6	6	6	6	6	6	6
WV156_O	13	14	14	14	14	14	14	14
WV157_O	14	5	5	5	5	5	5	5
WV158_O	15	2	2	2	2	2	2	2
WV182_O	16	9	8	8	8	8	8	8
WV184_O	17	25	25	25	25	25	25	25
WV185_O	18	13	13	13	13	13	13	13
WV187_O	19	8	8	8	8	8	8	8
WV191_O	20	1	1	1	1	1	1	1
WV193_O	21	30	30	30	30	30	30	30
WV196_O	22	32	32	32	32	32	32	32
WV197_O	23	11	11	11	11	11	11	11
WV209_O	24	20	19	19	19	19	19	0

The conclusion drawn from **Table 2** is that the sampling of the 24 boreholes is practically isotopic (the complement of heterotopic); meaning that most if not all of the variables are fully sampled at every sample location as clearly shown in **Table 2** by the number of variables sampled in each borehole with WV011_O having no results at all and WV209_O not having RD results (**Table 2**). This is important in that most if not all of the four variables will be estimated in the first search volume passed for the individual blocks.

An isotopic dataset (see **Figure 5**) has both the primary and secondary data that have the sample sites shared or at the same location, and the dataset used in the

study is isotopic, given that 98% of the samples have all four variables at the same location. A heterotopic dataset has primary and secondary datasets at different locations or sampling points or may partially share some locations (**Figure 5** and **Figure 6**).

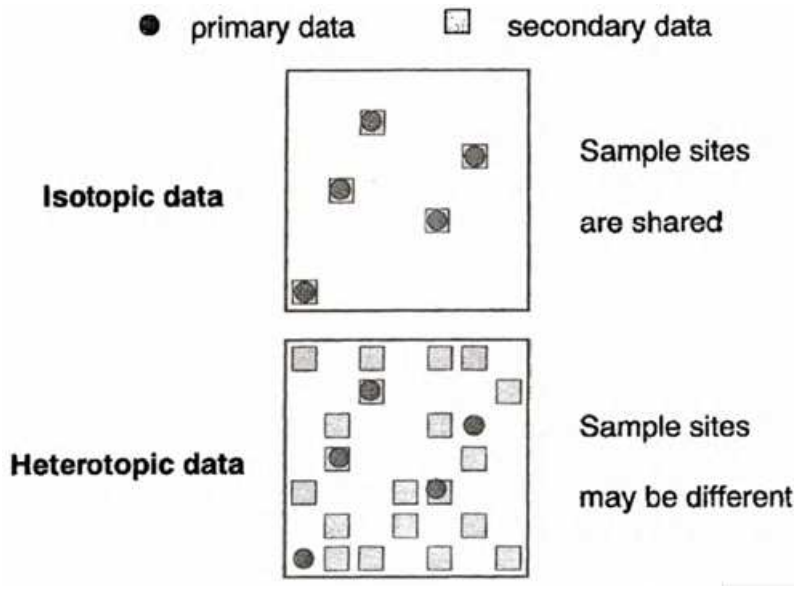


Figure 5: **Isotopic and partial heterotopic data**

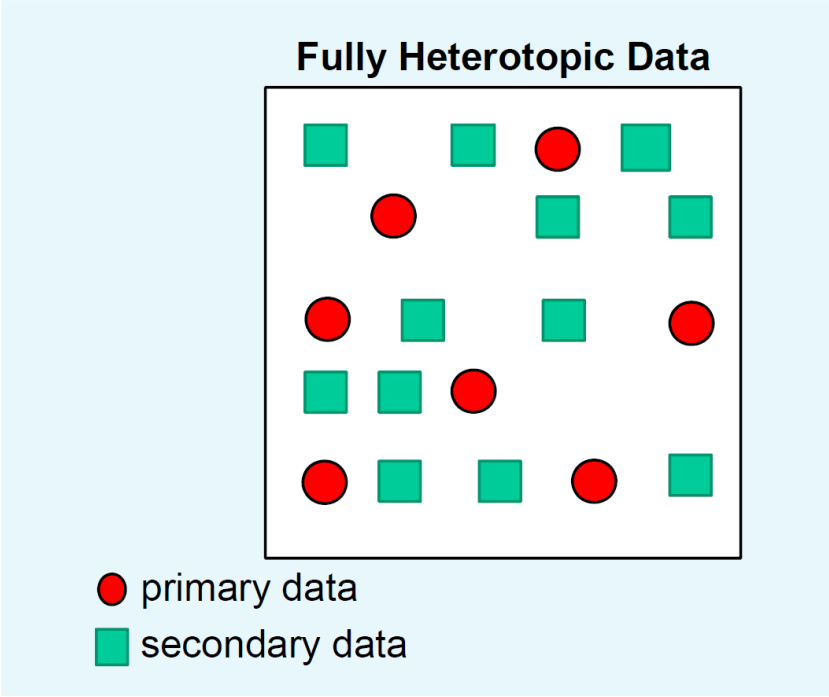


Figure 6: **Fully Heterotopic data, Al_2O_3 primary variable; Fe, SiO_2 and RD secondary variables.**

This research will also create a partial heterotopic dataset, with Al_2O_3 as a primary variable undersampled in relation to Fe, SiO_2 and Rd to test at what threshold of missing data of Al_2O_3 will OK or OCK estimation method is a preferred estimation method over the other (**Figure 5**).

4.3.2 DRILL-HOLE VARIABILITY

Lots of samples in the dataset used for this research were collected from diamond drilling as shown in **Figure 4**. It is a norm in this area that some holes will be percussion drilled to a certain depth and then diamond drilled down to completion or fully drilled either percussion or diamond drilled. Furthermore it is clearly depicted in **Figure 7** that the majority of samples were logged as hematite which is the main carrier of ore in the *ore-type230*. The presence of banded iron formation (BIF), conglomeratic ore (CGT), Scree (SCR) and shale (SH) as shown in **Figure 7** could be attributed to the genesis of this ore type (see **Section 3.6**). According to the wire-framing (3D delineation of geological interpretation) and according to Kumba Iron Ore's protocol, any waste material less than 3m cannot be modelled separately, therefore the presence of this waste material intercalated within ore. This has then resulted in the inclusion of the said waste material in the ore estimate.

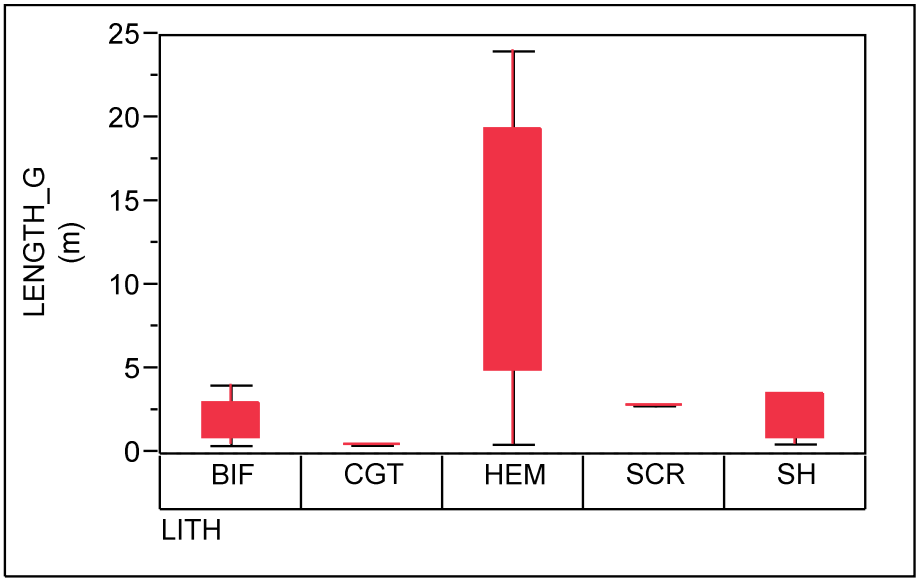


Figure 7: Box and Whisker Plot showing Variability - Lithology

As expected, the focus is within the ore zone as most of the samples were collected from the main ore-type, hematite, as show in **Figure 7**.

4.3.3 DATA COMPOSITING

An array of different compositing methods exists in the various Resource estimation software packages; however no technique exists which is capable of providing composites of exactly equal volumetric support whilst at the same time honouring geological contacts and preserving the metal content of the sample dataset. This is because distances between the geological boundaries that are encountered in drillholes and the various thicknesses in the dataset are highly unlikely to all be exactly divisible by a single length.

Run length compositing was carried out to the dominant sample length of 1m, which is the dominant sampling length as shown in **Figure 8**. Samples were composited by lithology to 1m lengths. Some restrictions were applied for example, if a sample was longer than 1m it was subdivided into two or more samples, each 1m long. Samples less than 1m in length were composited with full length samples (from the same lithology) with the provision that no sample was shorter than 0.50m or longer than 1.5m. If, at the end of a hole, a short sample could not be combined with another sample, it was retained as it is. **Figure 8** highlights distribution of the sampling length of composited data, with a minimum of 0.5 and maximum of 1.43 as required.

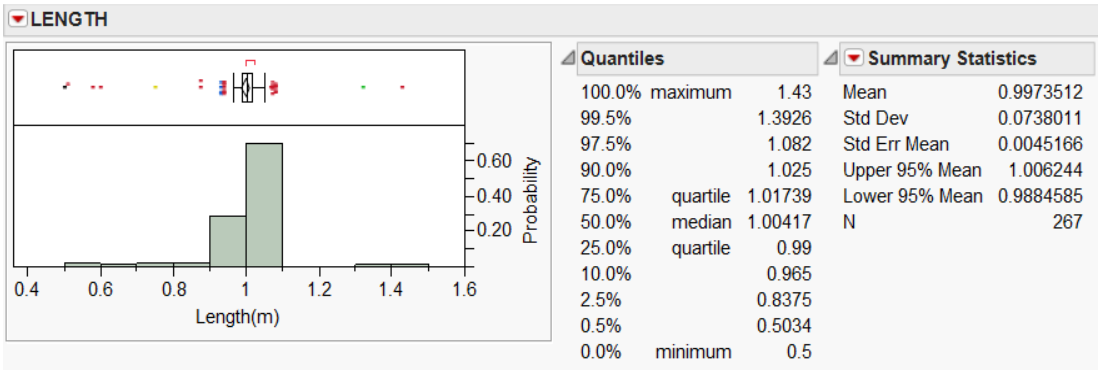
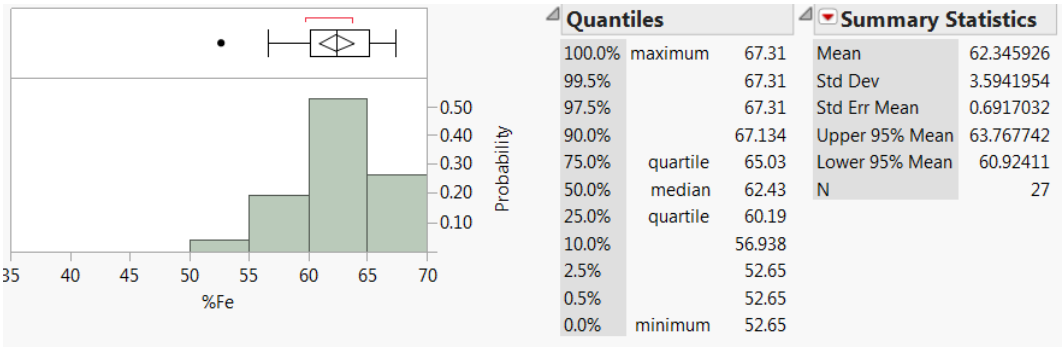


Figure 8: Distribution of sample length.

4.3.4 PERCUSSION vs. DIAMOND DRILLED SAMPLES

Evidence of differences between diamond and percussion data is evident on overall at Kolomela; however given that the study is only focussed on one ore type with limited number of samples, diamond and percussion samples have separate distributions as displayed by %Fe in the figures below. As such, this raises the question whether or not to combine the two dataset for variography and estimation.

The distinction between the two populations is illustrated in **Figure 9**, **Figure 10** and **Figure 11**. The cumulative distribution function(CDF) plots of the two drilling types display similar trends, with diamond drilling data displaying a smoother trend because of more sample data support.



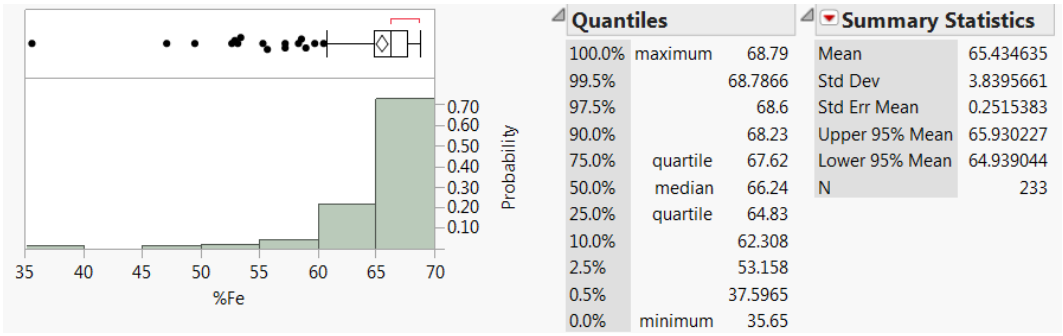
Quantiles

100.0%	maximum	67.31
99.5%		67.31
97.5%		67.31
90.0%		67.134
75.0%	quartile	65.03
50.0%	median	62.43
25.0%	quartile	60.19
10.0%		56.938
2.5%		52.65
0.5%		52.65
0.0%	minimum	52.65

Summary Statistics

Mean	62.345926
Std Dev	3.5941954
Std Err Mean	0.6917032
Upper 95% Mean	63.767742
Lower 95% Mean	60.92411
N	27

Figure 9: Percussion drill-hole sample distribution



Quantiles

100.0%	maximum	68.79
99.5%		68.7866
97.5%		68.6
90.0%		68.23
75.0%	quartile	67.62
50.0%	median	66.24
25.0%	quartile	64.83
10.0%		62.308
2.5%		53.158
0.5%		37.5965
0.0%	minimum	35.65

Summary Statistics

Mean	65.434635
Std Dev	3.8395661
Std Err Mean	0.2515383
Upper 95% Mean	65.930227
Lower 95% Mean	64.939044
N	233

Figure 10: Diamond drill-hole sample distribution

Figure 11 is a display of **Figure 9**(percussion drill-hole sample distribution) overlain on top of **Figure 10**(diamond drill-hole sample distribution), and there is some differences on the two dataset as already elaborated above, however the impact of data support(27 percussion samples and 233 diamond samples) of the two could justify the differences.

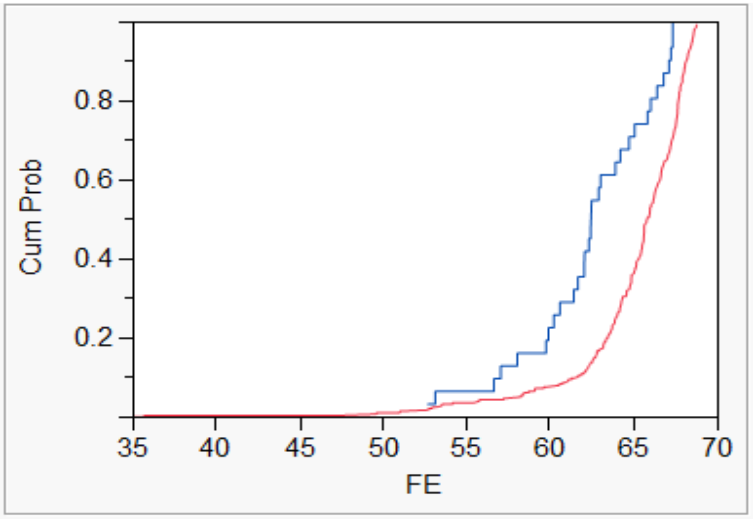


Figure 11: CDF Plot Diamond vs Percussion Drilling

Percussion Drilling Diamond Drilling

Figure 12 shows the location of the two populations on the XY plane. Subsequently, **Figure 13** shows the location of the two populations on the YZ plane.

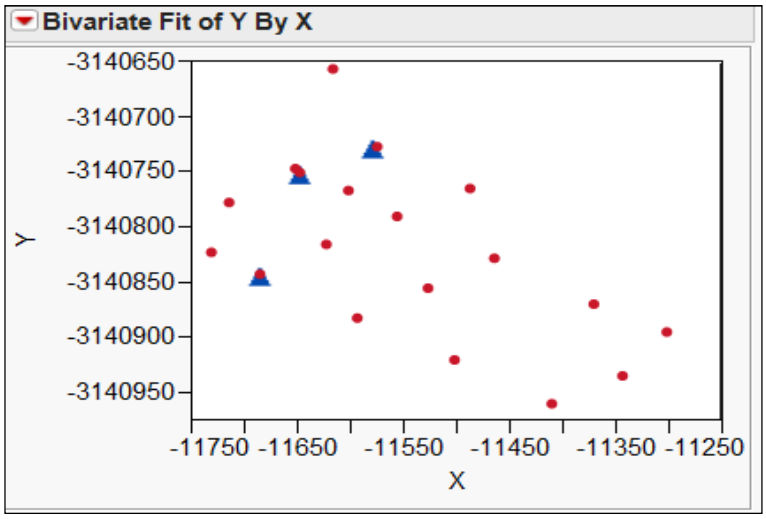


Figure 12: X Y Plot Percussion vs. Diamond Drilling location

Diamond Drilled Percussion Drilled

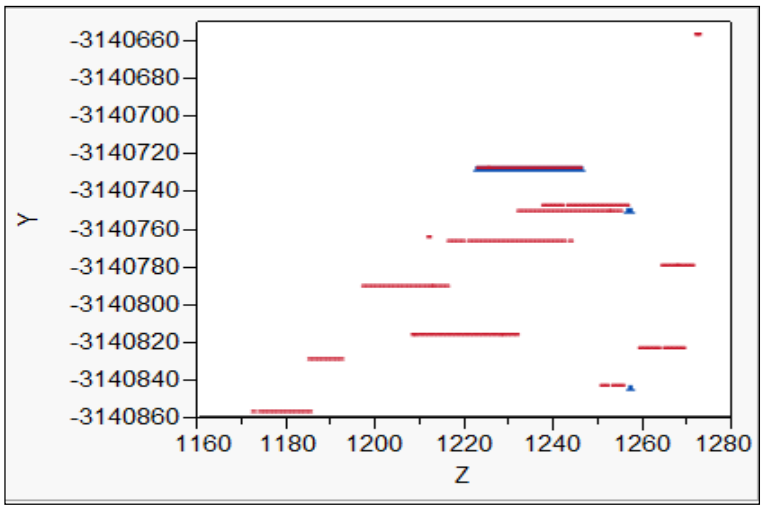
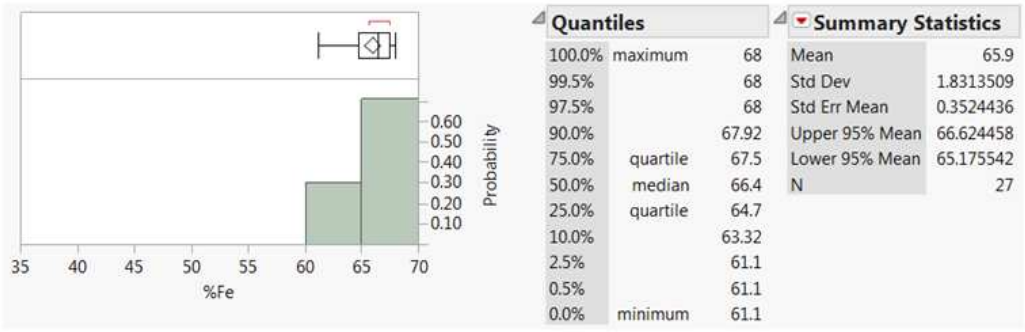


Figure 13: Y Z Plot Percussion vs. Diamond drilling location

Ideally the two populations must be separated out, however the number of percussion samples contributes very little to the total dataset, and the impact of its usage would not be that significant. This has been confirmed also by variograms generated with and without percussion samples and no change was observed as there is not much percussion samples data.

Further testwork was carried out to see if significant differences are eminent between percussion and diamond samples. Three random diamond drilled holes were selected and compared to the total diamond drillholes (**Figure 14**).

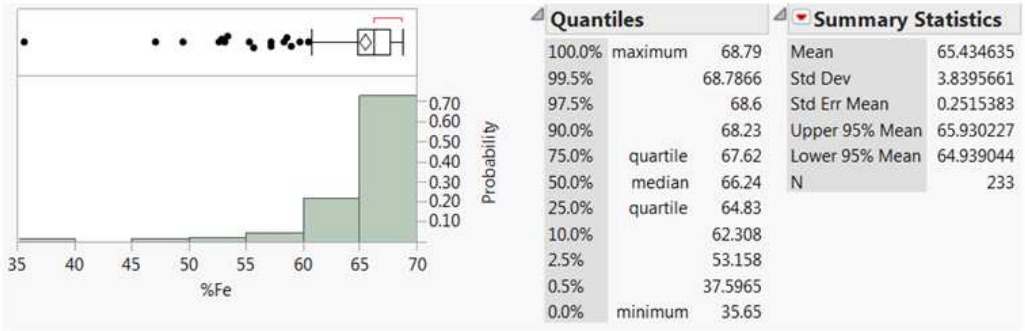
3 – DD



Quantiles		
100.0%	maximum	68
99.5%		68
97.5%		68
90.0%		67.92
75.0%	quartile	67.5
50.0%	median	66.4
25.0%	quartile	64.7
10.0%		63.32
2.5%		61.1
0.5%		61.1
0.0%	minimum	61.1

Summary Statistics	
Mean	65.9
Std Dev	1.8313509
Std Err Mean	0.3524436
Upper 95% Mean	66.624458
Lower 95% Mean	65.175542
N	27

All_Diamond



Quantiles		
100.0%	maximum	68.79
99.5%		68.7866
97.5%		68.6
90.0%		68.23
75.0%	quartile	67.62
50.0%	median	66.24
25.0%	quartile	64.83
10.0%		62.308
2.5%		53.158
0.5%		37.5965
0.0%	minimum	35.65

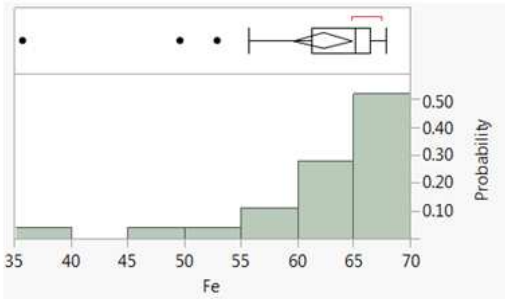
Summary Statistics	
Mean	65.434635
Std Dev	3.8395661
Std Err Mean	0.2515383
Upper 95% Mean	65.930227
Lower 95% Mean	64.939044
N	233

Figure 14: Distribution of three randomly selected diamond holes and distribution of the total diamond drilled holes.

Distributions of the two dataset (**Figure 14**) do appear different due to the number of holes and samples of the two (27 samples for the three selected holes and 233 samples for the total diamond holes). However the mean remain fairly the same between the two dataset.

Furthermore diamond holes closest to the percussion holes were selected and compared to that of percussion drilled holes (**Figure 15**).

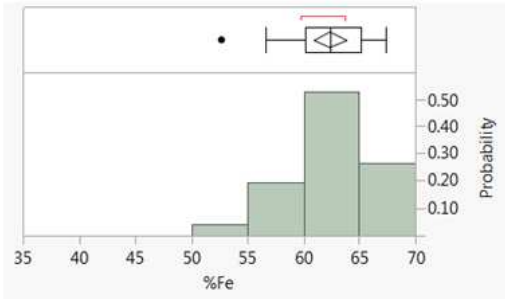
DD-PERC



Quantiles		
100.0%	maximum	67.8
99.5%		67.8
97.5%		67.8
90.0%		67.2
75.0%	quartile	66.4
50.0%	median	65.1
25.0%	quartile	61.3
10.0%		52.9
2.5%		35.7
0.5%		35.7
0.0%	minimum	35.7

Summary Statistics	
Mean	62.234483
Std Dev	6.8148617
Std Err Mean	1.265488
Upper 95% Mean	64.826718
Lower 95% Mean	59.642248
N	29

PERCUSSION



Quantiles		
100.0%	maximum	67.31
99.5%		67.31
97.5%		67.31
90.0%		67.134
75.0%	quartile	65.03
50.0%	median	62.43
25.0%	quartile	60.19
10.0%		56.938
2.5%		52.65
0.5%		52.65
0.0%	minimum	52.65

Summary Statistics	
Mean	62.345926
Std Dev	3.5941954
Std Err Mean	0.6917032
Upper 95% Mean	63.767742
Lower 95% Mean	60.92411
N	27

Figure 15: Distribution of selected diamond holes closest to percussion holes and distribution of the total diamond drilled holes.

Distributions of the two dataset (**Figure 15**) do appear different but not much change on the mean of the two dataset.

The testwork carried above further affirms the usage of the two dataset together for both variography and estimation; and the amount of dataset available is not enough to advocate separation of the two dataset diamond and percussion.

4.3.5 CLASSICAL STATISTICS

The statistical analysis listed in **Table 3** is derived from the composited data within the mineralised zone of *ore-type 230*. The table represents the actual composited data as it is with no cutting/capping being applied.

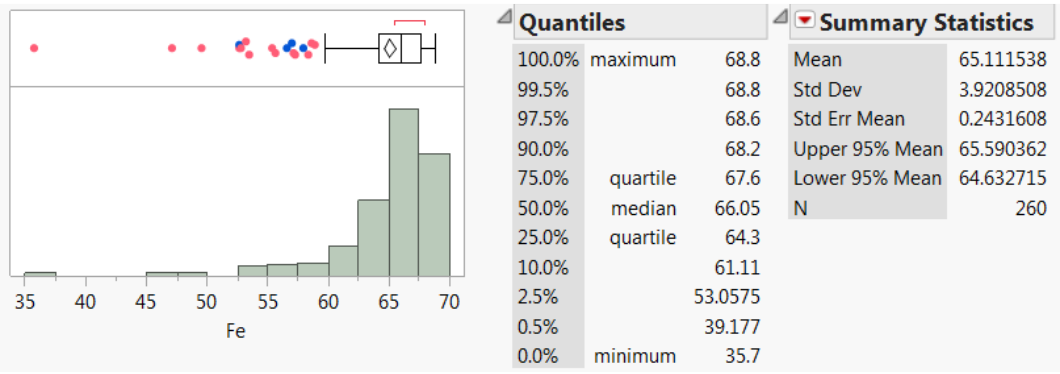
The statistical analysis is listed for %Fe, %SiO_2, %Al_2O_3 and RD. The mean values for %Fe, %SiO_2 and %Al_2O_3 are 65.11, is 3.97 and 1.15 respectively. The mean RD is 4.78.

Table 3: Classical Statistics of Composited Data inclusive of both Percussion and Diamond.

FIELD	RECORDS	MINIMUM	MAXIMUM	MEAN	STANDDEV	VARIANCE
%FE	267	35.70	68.79	65.11	3.92	15.37
%SIO_2	267	0.45	47.35	3.97	4.65	21.62
%Al_2O_3	267	0.16	9.37	1.15	1.08	1.17
RD	267	3.40	5.22	4.78	0.26	0.0067

4.3.6 %Fe HISTOGRAM OF 1M COMPOSITES

The %Fe distribution shows that the data is negatively skewed with a minimum value of 35.65% and a maximum of 68.78% with a mean of 65.11% as shown in **Figure 16**. This observation is in line with what one expects from a high-grade bulk commodity like iron ore. The standard deviation is 3.92 with 2.5% of the data below 53% Fe which can be attributed to the less than 3m of waste material intercalated within the ore (see **Figure 7**). Cumulative distribution function (CDF) displays a low probability of low values less than 60% Fe and high probability of high grade values greater than 60% Fe.



Quantiles		
100.0%	maximum	68.8
99.5%		68.8
97.5%		68.6
90.0%		68.2
75.0%	quartile	67.6
50.0%	median	66.05
25.0%	quartile	64.3
10.0%		61.11
2.5%		53.0575
0.5%		39.177
0.0%	minimum	35.7

Summary Statistics	
Mean	65.111538
Std Dev	3.9208508
Std Err Mean	0.2431608
Upper 95% Mean	65.590362
Lower 95% Mean	64.632715
N	260

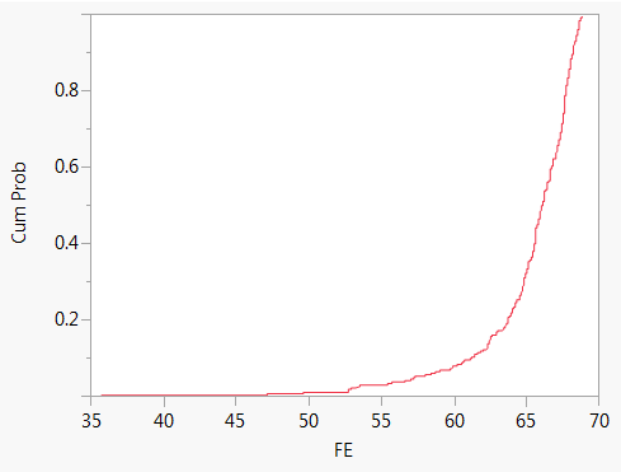


Figure 16: %Fe Distribution and CDF Plot

4.3.7 % SiO_2 HISTOGRAM OF 1M COMPOSITES

The % SiO_2 is positively skewed with a minimum value of 0.45% and a maximum value of 47.34% with a mean of 3.92% as shown in **Figure 17**. The standard deviation is 4.65 with 10% of the data above 8% SiO_2, which also can be attributed to the less than 3m of waste material intercalated within the ore as this cannot be modelled out separately. CDF displays low probability of high values greater than 10% SiO_2 and high probability of low grade values less than 10% SiO_2.

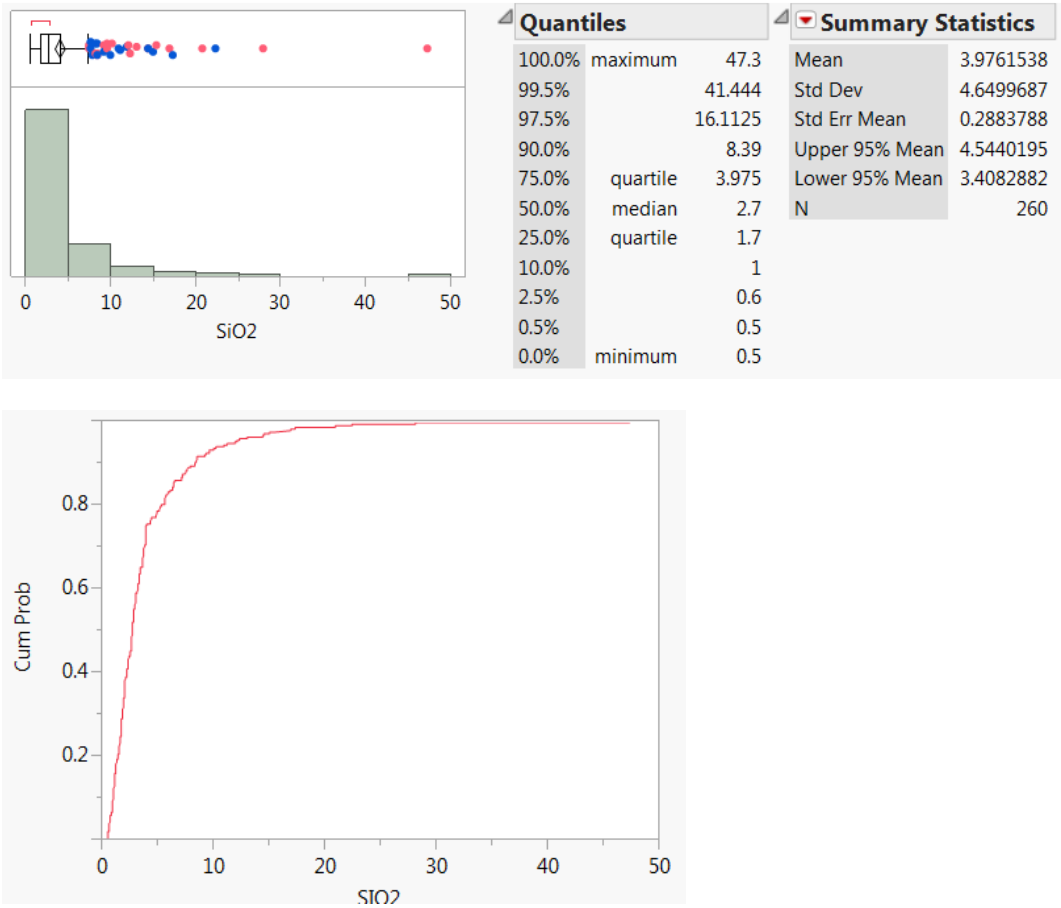


Figure 17: %SiO_2 Distribution and CDF Plot

4.3.8 %Al_2O_3 HISTOGRAM OF 1M COMPOSITES

The %Al_2O_3 is positively skewed with a minimum value of 0.16% and maximum value of 9.37% with a mean of 1.15% as shown in **Figure 18**. The Standard deviation is 1.09 with 10% of the data above 8% Al_2O_3 and as with %Fe and %SiO_2 distributions, this can also be attributed to the less than 3m of waste material intercalated within the ore as this cannot be modelled out separately. Waste material is from the shale's and conglomeratic ore present within the laminated ore. CDF displays low probability of high values greater than 2% Al_2O_3 and high probability of low grade values less than 2% Al_2O_3.

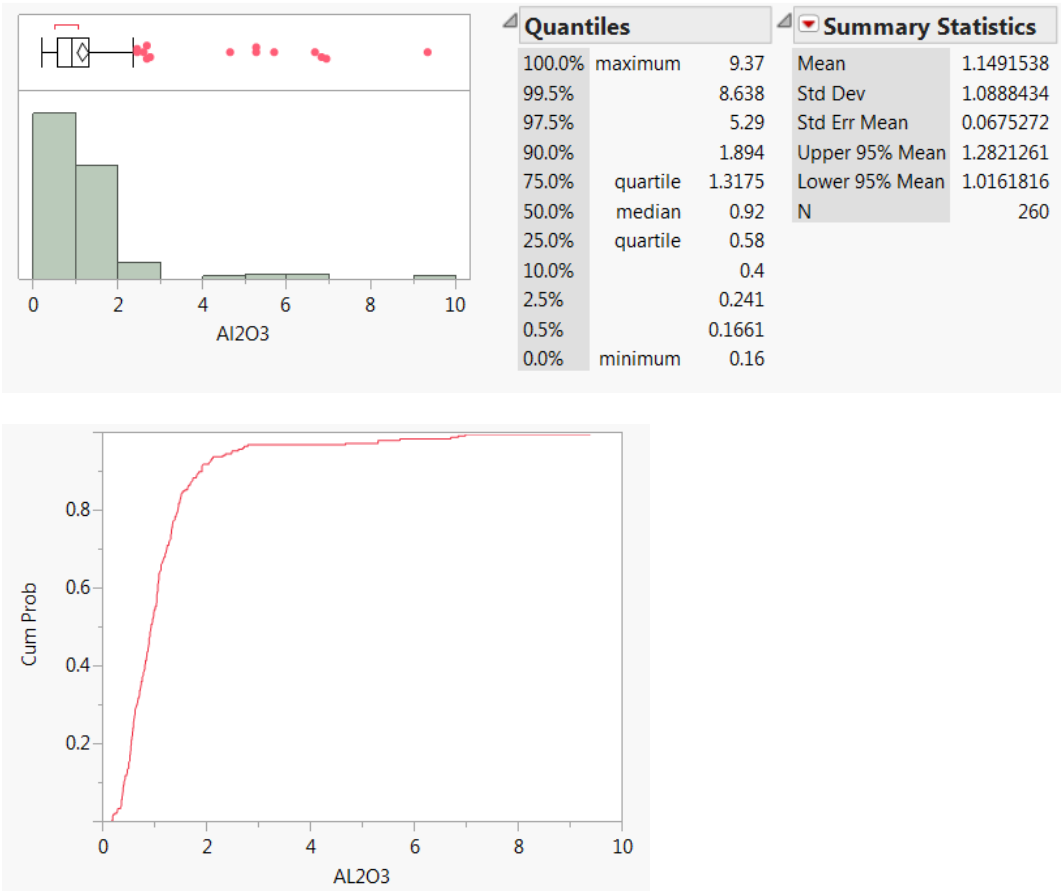


Figure 18: %Al_2O_3 Distribution and CDF Plot

4.3.9 RD HISTOGRAM OF 1M COMPOSITES

The RD is negatively skewed with a minimum value of 3.40 and maximum of 5.22 with a mean of 4.78. Standard deviation is 0.26 and as with the other variables the 2.5% of data has a density less than 4.1 which again relates to the waste material present within the ore (see **Figure 19**). CDF displays low probability of low RD values <4 and high probability of high RD values of greater than 4.

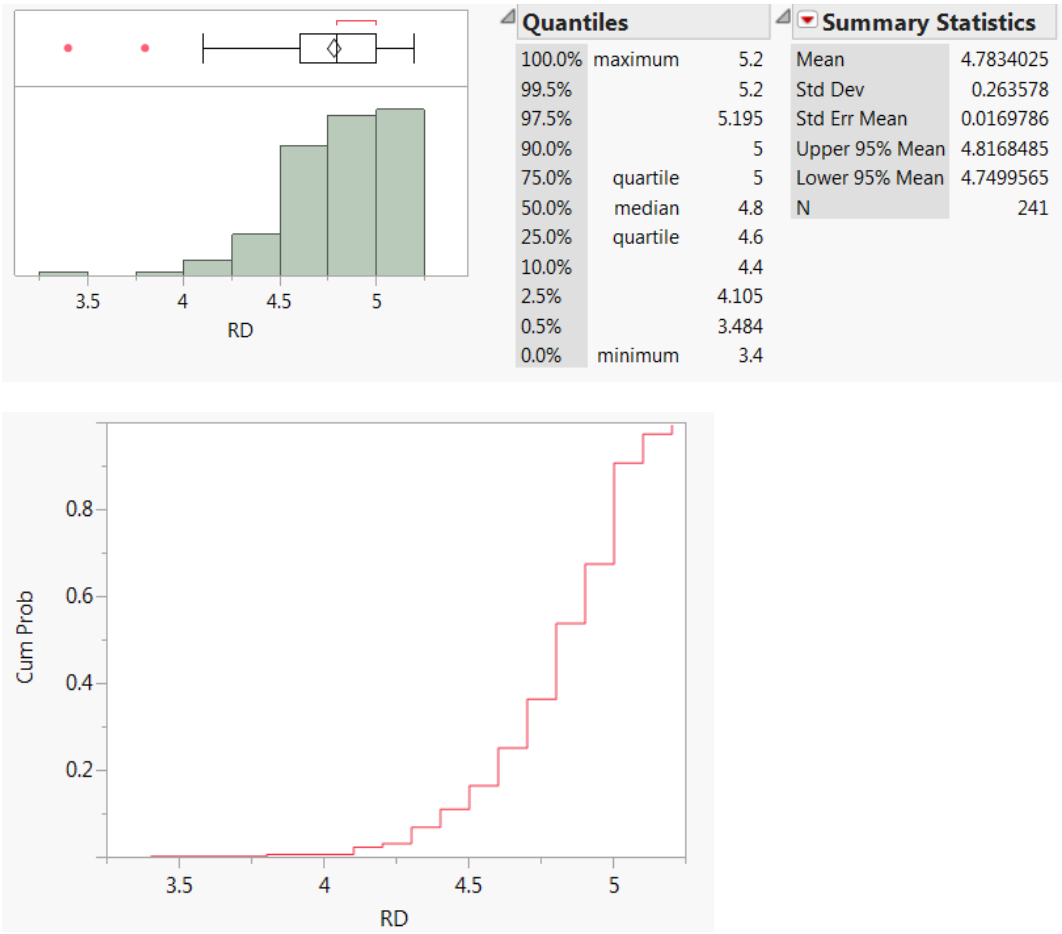


Figure 19: RD Distribution and CDF Plot

4.3.10 CONCLUSION

The histograms are strongly negatively skewed for %Fe and RD but strongly positively skewed for %SiO_2 and %Al_2O_3. Extreme outliers can bias the estimates towards the extreme value, especially when there are only a few samples available. Welmer (1998) defines the use of Coefficient of Variation (CoV) to understand the degree of skew-ness and the need to apply a top cut in the effect when the distribution is positively skewed. To top cut a data means to re-set any composites grades that are higher than the top cut value to the top cut value. This ensures the high grades are still included in subsequent analyses, but the extremity of their grades does not overly influence on the statistics.

CoV is calculated as follows:

CoV = Standard Deviation/Mean

%Al_2O_3 CoV = 1.14/1.16 = 0.98

RD CoV = 0.24/4.82 = 0.49

According to Welmer (1998);

- Datasets with CoV greater than 1.2 generally need to be top cut
- Datasets with CoV less than 1.0 generally do not need to be top cut
- High CoV greater than 3 is indicative of mixed distributions and more domains may be necessary.

The conclusion drawn from the CoV values of the variables %Al_2O_3 and RD is that top-cutting of extreme values is not necessary in this case as the calculated CoV is close to 1.2. However bottom cutting of the low grade values was considered for %Fe to 40% and to 4 for RD given the outliers present for the two variables.

4.4 VARIABLES SCATTER PLOTS

4.4.1 %Fe vs. %SiO_2

Figure 20 clearly shows a strong inverse relationship between %Fe and %SiO_2. However, from the Fe vs SiO_2 scatter plot there is an indication of two populations in the data set. This observation is not defined in the histograms, hence the absence of a bimodal distribution. A possible explanation to this could be attributed to the two drilling methods in the dataset diamond drilling and percussion drilling as displayed in **Figure 20**. Another possible explanation could be attributed to the waste material intercalated within the ore, thus a makeup of two different populations each with its own %Fe, %SiO_2, %Al_2O_3 and RD.

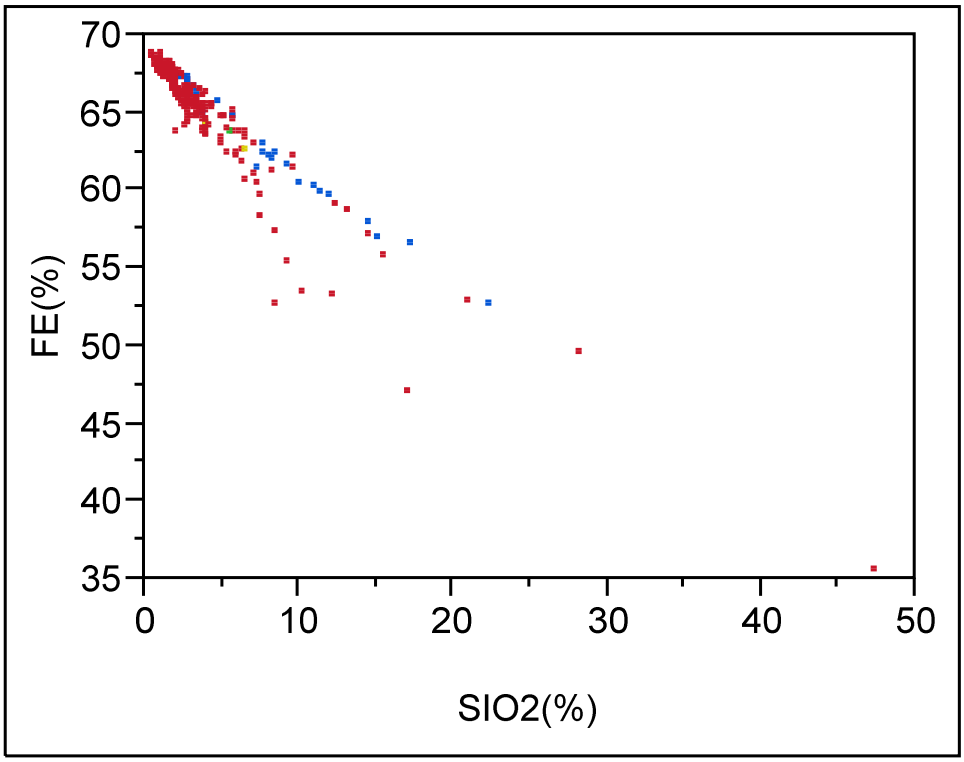


Figure 20: Scatter plot %Fe vs %SiO_2

Diamond Drilled Percussion Drilled Pilot Drilled RC Drilled

4.4.2 %Fe vs. %Al_2O_3

There is an inverse relationship between %Fe and %Al_2O_3 (see **Figure 21**) similar to that of %Fe vs. %SiO_2. However, as in the case of %Fe vs. %SiO_2, two populations are observed which could also be attributed to the drilling type, given that percussion samples are chips which could be contaminated with some of the material above and below the ore type of interest. However a zone defined above 5% Al_2O_3 in **Figure 21** could be indicative of ferruginised shale remnants present in the ore type of interest and presence of cherty BIF.

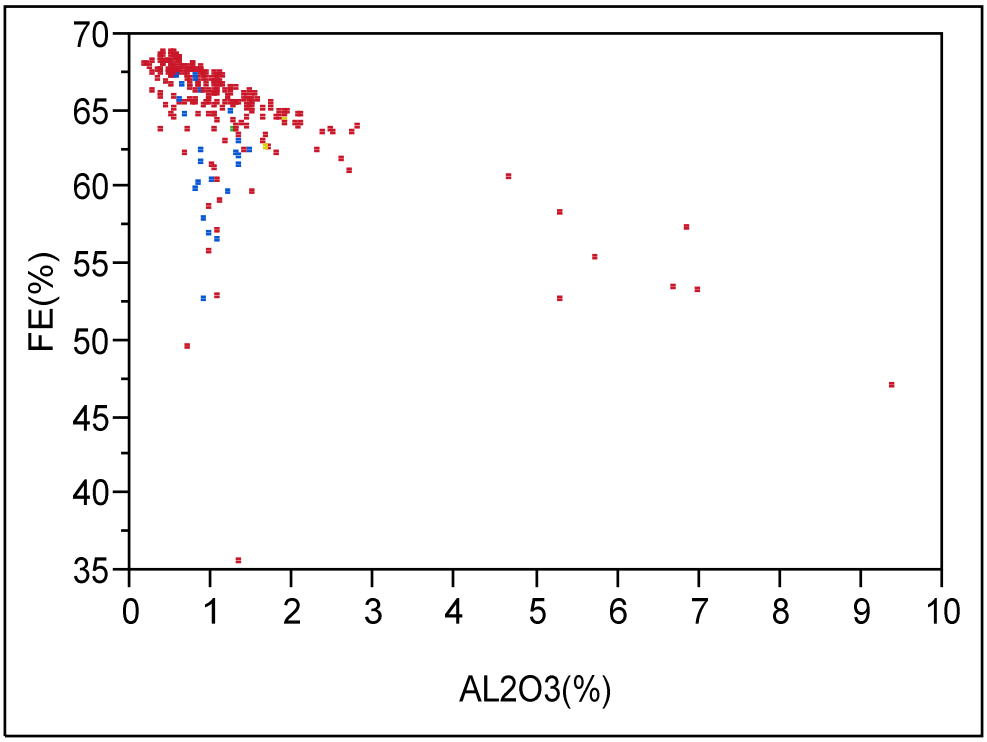


Figure 21: Scatter plot Fe vs Al_2O_3

Diamond Drilled Percussion Drilled Pilot Drilled RC Drilled

4.4.3 %Fe vs. RD

A strong positive relationship between %Fe and RD is defined in **Figure 22**. However, as observed in the scatter plots for the other variables, two populations are observed as well with %Fe vs. RD.

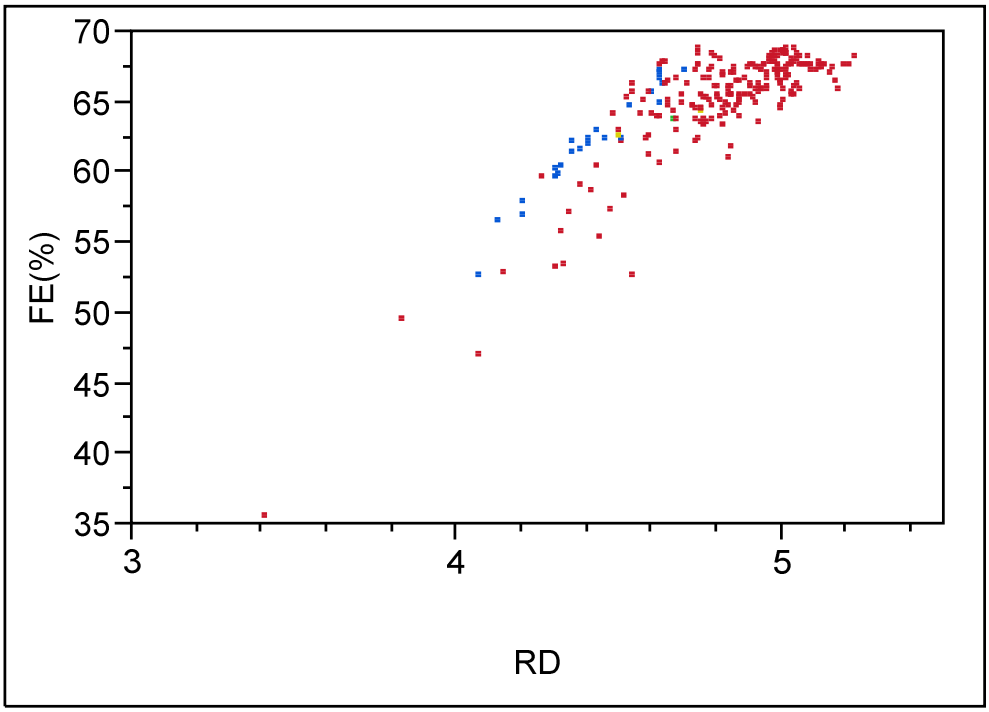


Figure 22: Scatter plot Fe vs RD

Diamond Drilled Percussion Drilled Pilot Drilled RC Drilled

The two populations are defined by the circles; red indicating diamond drilled samples and blue circles indicating percussion drilled samples. Given the methodology used for analysis (pycnometer), the fact that DD give a higher density than RC indicates that there is porosity preserved in the RC cuttings than that, which has been destroyed by pulping the DD cores.

The %Fe increases as the sample RD increases and as expected, %Fe and RD are positively correlated. This is further depicted in **Figure 23** displayed by quantile density contours highlighting areas where the plotted points are concentrated. About 90% of the data points are enclosed within the red contours and this is expected given that the research is only focusing on the high-grade *ore-type 230,* which is laminated hematite. It is important to note that within the red contours, %Fe grades range between 66% and 68%, similarly, the RD also ranges between 4.5 and 5. However, as already indicated in **Section 4.3.2** that there are other waste materials intercalated within this zone and this can also be observed within the blue and purple contours which make up about 10% of the data points with RD values ranging between 3.6 and 4.5 with %Fe of between 40% and 59%.

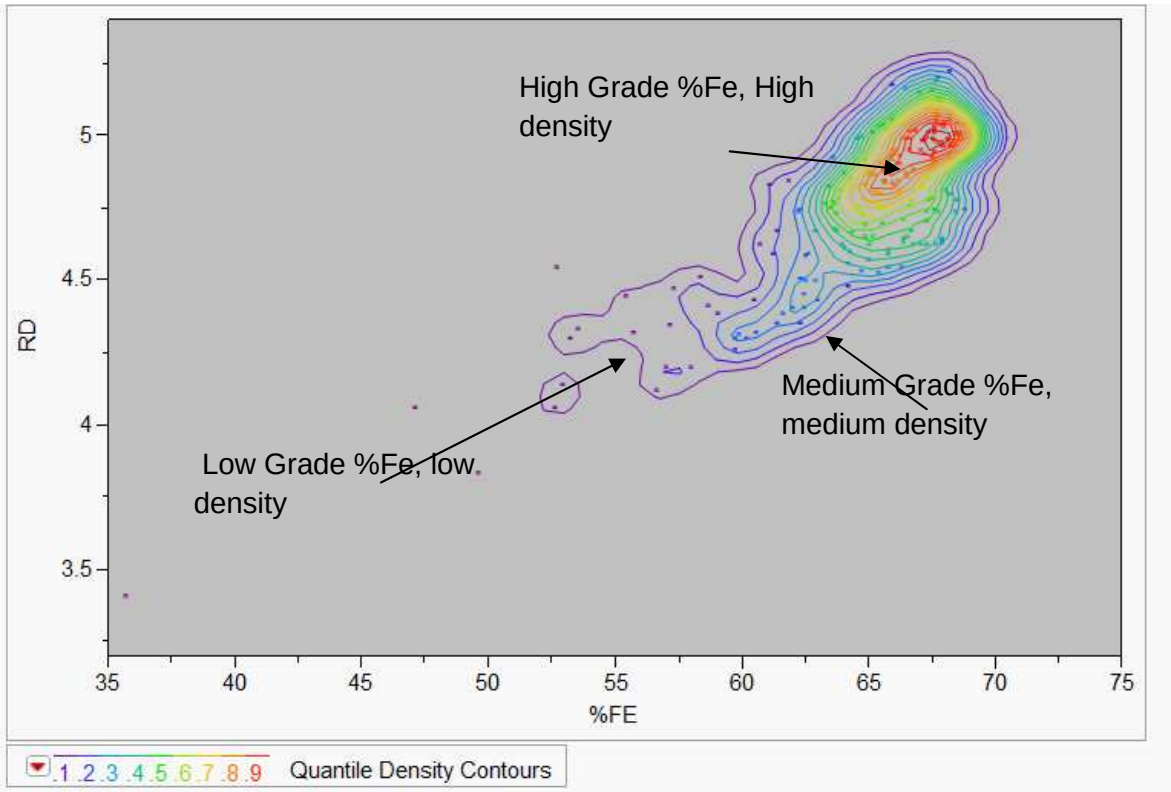


Figure 23: Bivariate Fit of RD against %Fe

4.4.4 Multivariate Analysis

Multivariate statistical analysis is the simultaneous analysis of more than one statistical variable. As with any spatial analysis, data is divided into similar homogenous units, which can be attributed to the geological continuity or similar grade distribution, etc. The drilling-type colour coding used in all scatter plots in **Figure 4** was preserved to distinguish the two populations as shown in **Figure 24**; red being the diamond-drilled samples and blue being the percussion- drilled samples. Multivariate analysis was carried out to get the correlation coefficient between the variables, which was important in this study given that co-kriging is the estimation method looked at.

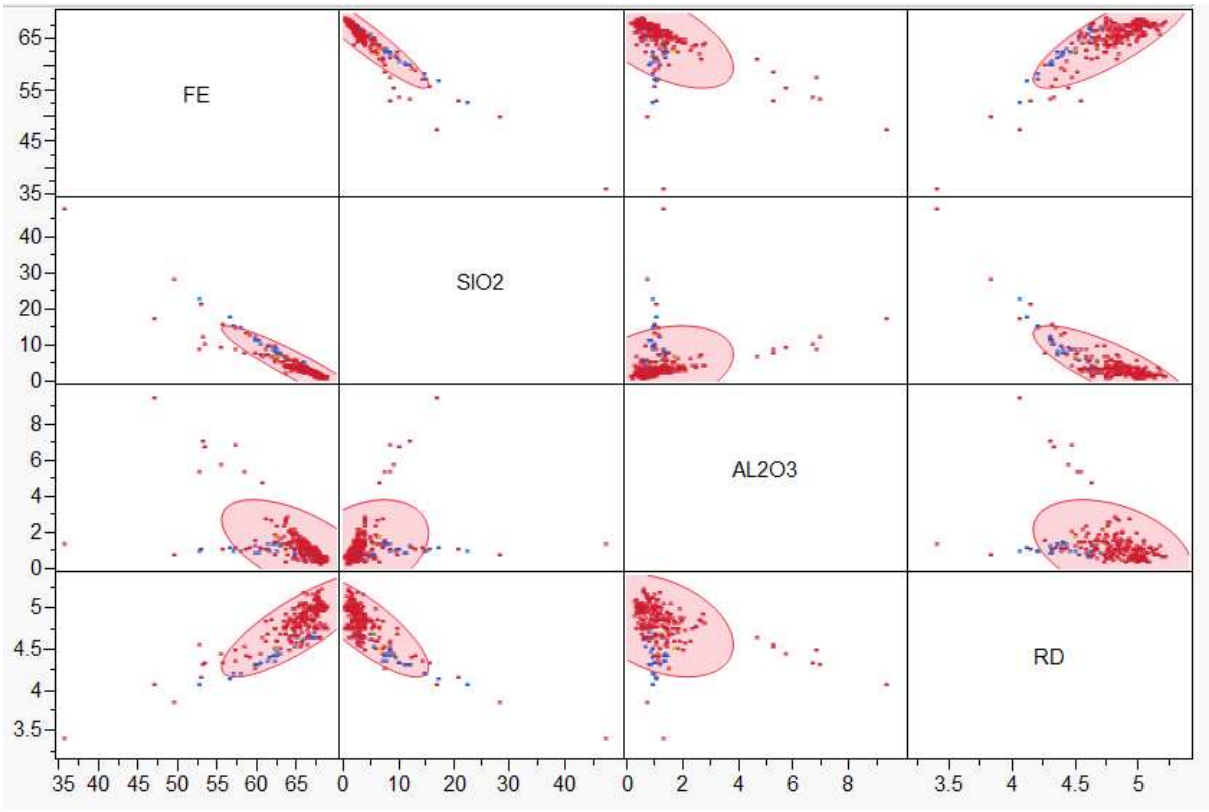


Figure 24: Scatter plot Matrix Ore Type 230

If two variables are highly correlated, the ellipse enclosing the data will be very long and narrow as this is evident with the pink ellipse defining the relationship between %Fe and % SiO_2. In contrast, if the two variables are not correlated, the ellipse will be more circular in that the major and minor axes of the ellipse surrounding the data points are both similar in length.

The Pearson's correlation coefficient was used to measure the linear relationship between all four variables as shown in **Figure 24** and **Table 4**. In the case, the correlation coefficient is a number between -1 and 1; where negative 1 implies a perfect negative correlation and positive 1 implies a perfect positive correlation and 0 implies no correlation.

The Formula for the Pearson's correlation coefficient is as follows:

$$r_{xy} = \frac{\sum xy - \frac{\left(\sum x\right)\left(\sum y\right)}{n}}{\sqrt{\left[\left(\sum x^2 - \frac{\left(\sum x\right)^2}{n_x}\right)\left(\sum y^2 - \frac{\left(\sum y\right)^2}{n_y}\right)\right]}}$$

- ΣX: This simply tells one to add up all the *x* scores
- ΣY :This tells one to add up all the y scores
- ΣX2: This tells one to square each *x* score and then add them up
- ΣX2 :This tells one to square each *y* score and then add them up
- ΣXY: This tells one to multiply each *x* score by its associated Y score and then add the resulting products together (this is called a “cross-products”)
- n: This refers to the number of “pairs” of data one has.[7]

The following relationships are evident as displayed in **Figure 24** and **Table 4** %Fe is strongly negatively correlated with $\%SiO_2$ and slightly negatively correlated with $\%Al_2O_3$. The correlation between %Fe and $\%\ SiO_2$ is the strongest with r=-0.9 %Fe is positively correlated to RD with r=0.8.

- The correlation between $\%SiO_2$ and $\%Al_2O_3$ is weak with r=0.3, but the strongest with RD r=-0.8.
- The correlation between RD and Al_2O_3 is also weak with r=-0.4.

Table 4: Correlations between all the variables

	Raw Data			
	Fe	**SiO_2**	**Al_2O_3**	**RD**
Fe	1	-0.929	-0.638	0.824
SiO_2	-0.929	1	0.353	-0.788
Al_2O_3	-0.638	0.353	1	-0.463
RD	0.824	-0.788	-0.463	1

5 METHODOLOGY

Snowden (1996) describes the process of estimating mineral resources as a process that can only take place after the estimator is convinced of the soundness of the fundamentals underlying the estimation process. When deciding on the estimation method it is ideal as the base to have a good understanding of the genesis of the ore body, have a sampling database that must have integrity and the results thereof yielded must reflect the internal consistency of the geology and mineralization of the ore body. There are a variety of estimation methods with a common objective of estimating a distribution of grades into either a point or block.

Kriging which is one of the most widely used linear estimation methods and it is of interest in this study, hence the comparison between *Ordinary Kriging and Ordinary Co-Kriging* as stated later in this report.

Kriging is named after Dr. D.G Krige, a South African mining engineer, who first developed a moving average technique for estimating gold grades to remove the regression effect. This method was later on improved by Prof G. Matheron and he coined the idea and name of *Kriging* (Bohling, 2005).

Kriging is well-known to provide the '*best linear unbiased estimate'* of local block grades and is unique in the sense that the weights are estimated so that the estimation variance is minimised for whatever search neighbourhood is selected. The kriged block model's global and local grade distribution(Global distribution could be a deposit or large zone and local distribution could be a regionalised variable over a limited domain, its dimension being smaller to that of the deposit) within each estimation domain are determined by a combination of the sample data values, their geometric organisation, their spatial continuity (as defined by the variogram model) and the parameters which are associated with the

estimation neighbourhood. At the time of estimation, *domaining* decisions can be made, the data values and their geometrical organisation are pre-defined and the spatial continuity model is designed to best fit the data. Neighbourhood parameters therefore present the only remaining tool to control the estimated grade distribution within each *domain*. Decisions on their settings can materially impact the model's suitability for use in each of the various mine planning horizons (which may range from global strategic planning through to medium or short term scheduling). The chosen estimation parameters, therefore, should be tailored to align with the intended use of the model (Vann et al., 2003).

5.1 VARIOGRAPHY

Experimental variograms were generated for all four variables within the area of interest. They were no significant differences in the variograms generated using and not using the two datasets as the percussion dataset is very minimal; and variograms for the study were generated using combined diamond and percussion drilled data and for further processes in the project namely the estimation process.

The function for the variogram (*h*) is defined as (Isaaks and Srivastava, 1989):

$$\gamma(h) = \frac{1}{2N(h)} \sum_{(i,j)|hij=h} \left(v_i - v_j\right)^2$$

Where: *N* is the number of sample pairs separated by a distance of *h; V_i sample 1,* V_j *sample 2.*

All variograms were generated using *Isatis Software*. The nugget effect was modelled from the down-hole variogram.

5.2 EXPERIMENTAL VARIOGRAM MODEL

It is common practice in the industry to model variograms for the major constituents with the same ranges and with the same or similar relative contributions for each of the variogram structures(with total sill being rescaled for each variable) when variograms of variables show huge differences in structures. However this principle could probably apply to the variables that are strongly correlated, and not to the variables with less correlation. The same or at least similar neighbourhood parameters are then used for the major constituents; the intended purpose of this approach is to ensure that similar Kriging weights are applied to the major constituents of each composite.

Variograms were modelled with untransformed data and bottom cutting of the low grade values was considered for %Fe to 40% and to 4 for RD. The software allows the lag distance to be dynamically varied, so the determination of the nugget effect and spatial variance for the different structures was performed at appropriate lags. The down-hole variogram was used to determine the value for the nugget.

Continuity analysis was done in the omni directional direction and down-hole to determine the nugget effect along which the variograms were to be modelled.

All experimental variograms were modelled with a consistent number of structures, nugget effect plus two spherical structures for Fe, SiO_2, Al_2O_3 and RD to allow building of models that represent intrinsic correlation and thus avoid inconsistencies in resulting estimates. The Variogram model parameters are contained in **Table 5**; each experimental variogram and its fitted model for other variables are shown in **Appendix 3**. An example of experimental variogram and its fitted model is shown in **Figure 25**. This is Fe variable; nugget effect accounts for approximately 20% of sill, the first spherical structure range is 5 to 10m, the second structure is 10 to 100 for %Fe, %SiO_2 and %Al_2O_3 first range is 10 to 15 and second structure is 15 to 50; for RD first spherical structure range is 3 to 7m and the second structure range is 7 to 45m. Zonal anisotropy is evident with

more variation in the vertical direction due to the laminated nature of the ore type. The variogram is split into isotropic component and one in the vertical direction.

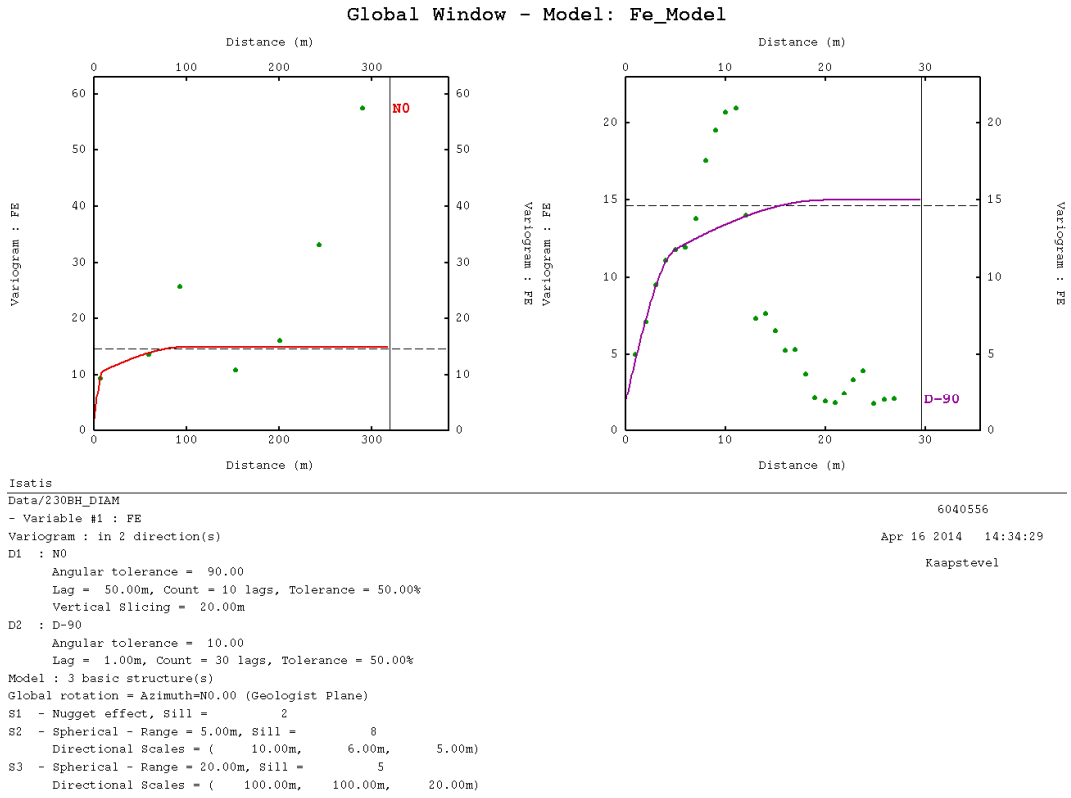


Figure 25: Semivariogram; Isotropic component and Vertical direction

Table 5: Variogram Model Parameters

		Structure 1					Structure 2				
	NUGGET	**Type**	**Sill**	**Range**	**Range**	**Range**	**Type**	**Sill**	**Range**	**Range**	**Range**
FE	2.00	Spherical	8.00	10	6	5	Spherical	5.00	100.00	100.00	20.00
SiO_2	3.00	Spherical	12.00	10.00	5.00	5.00	Spherical	7.00	100.00	100.00	11.00
Al_2O_3	0.039	Spherical	0.300	10.00	20.00	15.00	Spherical	0.300	50.00	60.00	100.00
RD	0.02	Spherical	0.01	3.60	3.60	7.00	Spherical	0.03	45.00	45.00	30.00

The concept of zonal anisotropy is illustrated in **Figure 26**.

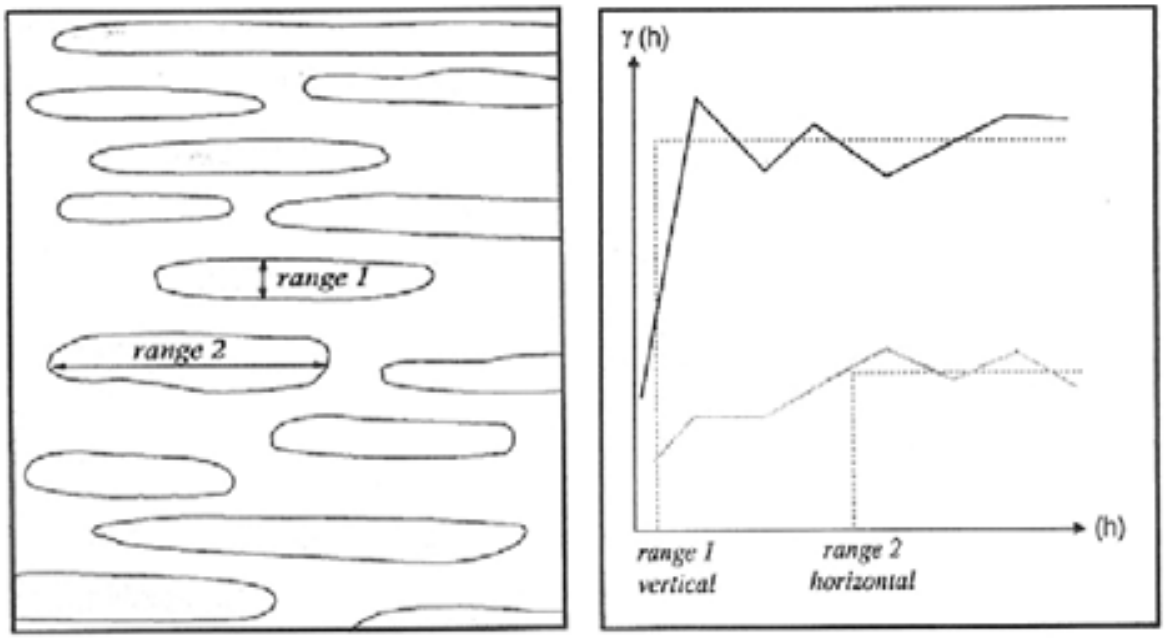


Figure 26: Concept of zonal anisotropy and zone of influence (Welmer, 1998).

The ellipse illustrated below represents the continuity of samples in the dataset being used in this research (laminated ore type), hence the shape of the ellipse as displayed in **Figure 27**, rapid change on vertical direction due to laminated nature of the ore type. The downhole variogram starts with minimum variance, which increases to a maximum and then drops to a minimum, suggesting that we may be traversing a single zone of ore and re-entering waste at the deepest parts of the drillholes.

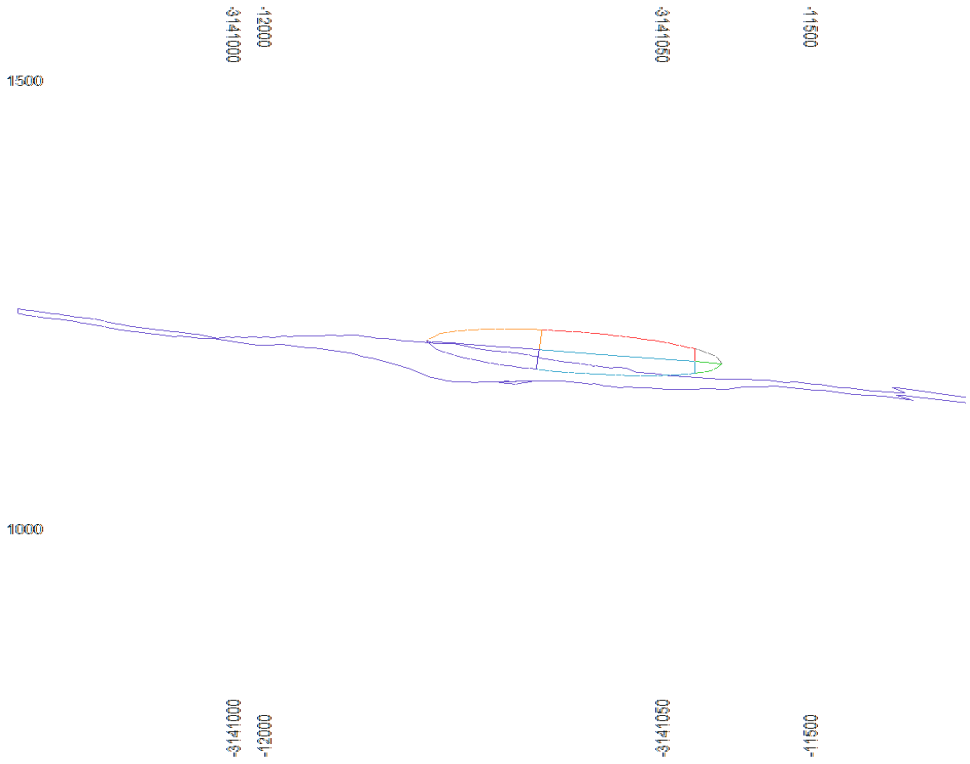


Figure 27: Ellipse along strike

5.3 QUANTITATIVE KRIGING NEIGHBOURHOOD ANALYSIS

Quantitative Kriging Neighbourhood Analysis (*QKNA*) was carried out on the data to determine the appropriate parameters to be used in both *Ordinary* and *Ordinary Cokriging*. This is very important in order to ensure that ideal parameters are used in the estimation process. *QKNA* study was done in *Datamine* software and the results were interpreted in *Excel* (*Microsoft*).

Three blocks were selected for *QKNA* as outlined in **Figure 28** in a "well-informed" area 7.1, in "moderately-informed" area 7.2 and in "poorly-informed" area 7.3. "Informed" areas are defined from well to poor based on the number of drill-holes surrounding block of interest.

The process works by defining a node(x,y) position in the model defined by 7.1, 7.2 and 7.3, varying different parameters and graphing the resultant grades, point variance, kriging variance, kriging efficiency and slope of regression to determine

optimal kriging parameters. Block 7.1 is analysed in **Figure 29** to **Figure 33**, block 7.2 and 7.3 analyses are listed in **Appendix 8**.

The *slope of regression* (*REG-SLOPE*) is a theoretical calculation that represents a calculated relationship between the estimated and the (unknown) true grades and should be as close as possible to 1 to ensure that the conditional unbiasedness property of kriging is realised. A rewriting of the expression for the slope of regression (*a*) in terms of correlation coefficient is possible:

$$a = \rho \frac{\sigma_{Z_v}}{\sigma_{Z_v^*}}$$

a is the slope of the linear regression

ρ is the linear(Pearson) correlation coefficient

σ_{Z_v} is the standard deviation of true block grades

$\sigma_{Z_v^*}$ is the standard deviation of estimated block grades(Vann et al., 2003).

From the above expression we can see that even for slope equalling one, the correlation may be less than one(because the smoothing effect of kriging necessitates that the variability of estimates is lower than that of true blocks.

The *kriging variance* (*KVAR*) provides an indication of relative estimation quality mainly in terms of data density and geometry and so is the *kriging efficiency* (*KE*) (Vann et al., 2003). (*FSTATS*) is the *Point variance*.

Kriging Variance is calculated by the following formula:

If '*V*' is the target block to be estimated, the variance of the error

$$Z_V^* - Z_V$$

can be expressed in terms of variogram as

$$\sigma^2 = 2\sum \lambda_i \bar{\gamma}(x_i, V) - \sum\sum \lambda_i \lambda_j \gamma(x_i, x_j) - \bar{\gamma}(V, V)$$

where

$\bar{\gamma}(x_i, V)$

is the average of the variogram between

x_i and the volume *V*.

$\bar{\gamma}(V, V)$ is the average of the variogram between any two points sweeping independently throughout the volume *V* (Armstrong (1998).

Kriging efficiency is calculated by the following formula:

KE = (BV - KV)/BV

BV = (1-FSTATS), using a standardised variogram(sill=1.00)

where, *Point variance* (*FSTATS*) is the error distribution between points within a block. BV is block variance = Point variance - Average Point variance

The parameters defined for estimation have significant influence on the kriging process and these parameters include model cell-dimensions, search radii, minimum/maximum number of sample and discretisation interval.

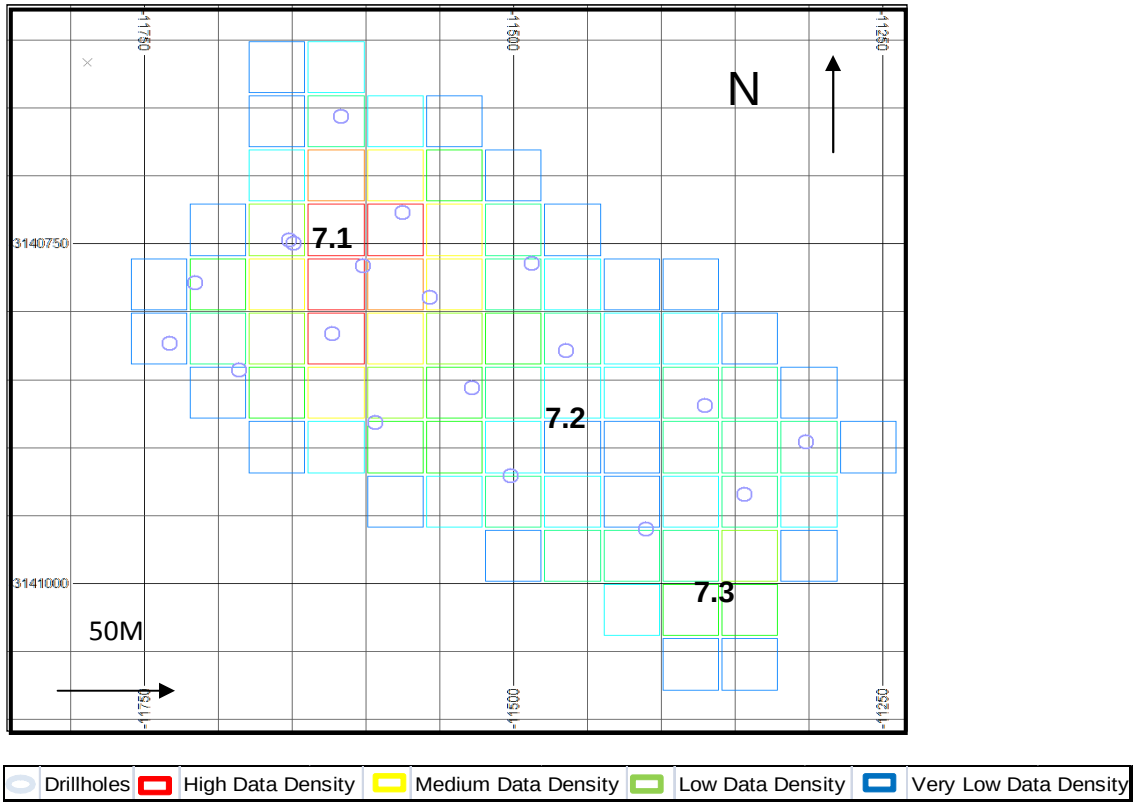


Figure 28: Blocks for QKNA study

As expected the Slope of Regression and Kriging Efficiency increase with increasing number of block sizes; and the Kriging Variance decreases with increasing number of block sizes. The Point Variance increases as the block becomes bigger. The optimal block size is 40 as observed from the graph (see **Figure 29**) as it is at this point moving forward that the Slope of Regression is constant at above 0.64.

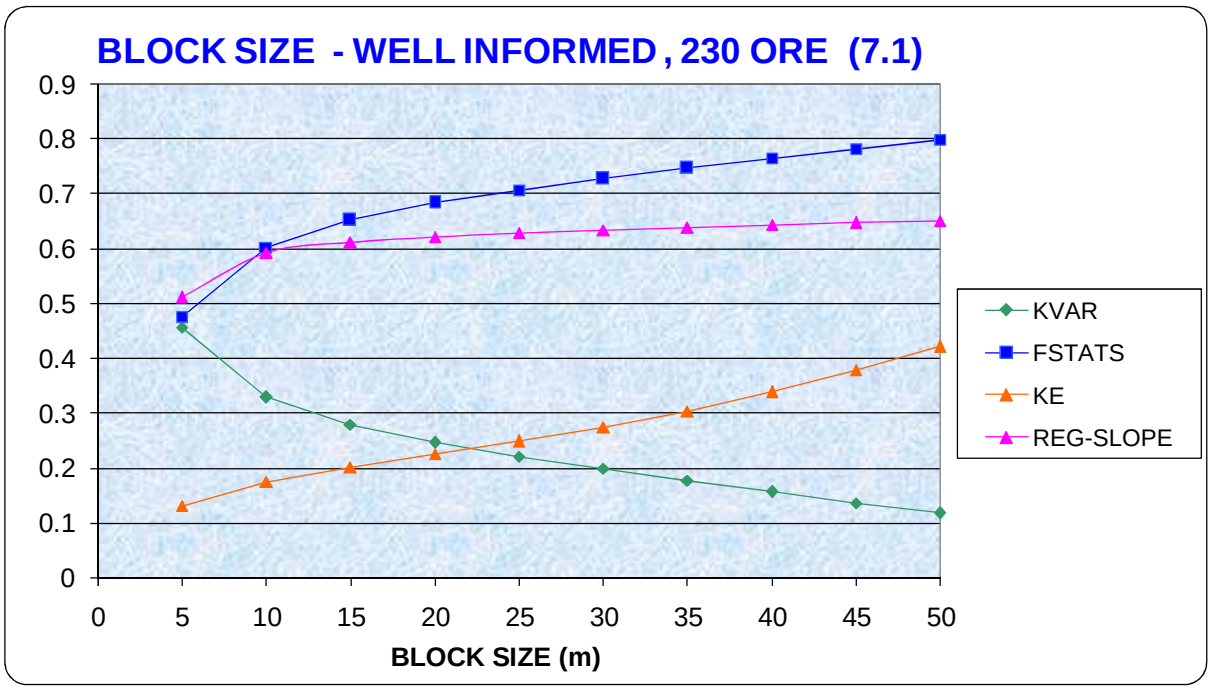


Figure 29: Block size - Well informed Area

Figure 30 confirms the expectation that as the number of samples included within the search neighbourhood incrementally increases, the Kriging Variance continues to incrementally decrease and the slope of regression remains fairly constant.

In fact this behavior will continue with increasing number of data values incorporated into the estimation neighbourhood until every sample available in the estimation domain is incorporated into the neighbourhood. However observation in **Figure 30** clearly displays 40 to be the optimal maximum number of samples with Kriging Variance being stable (0.15) and kriging efficiency becoming stable (0.32) from 40 maximum number of samples onwards.

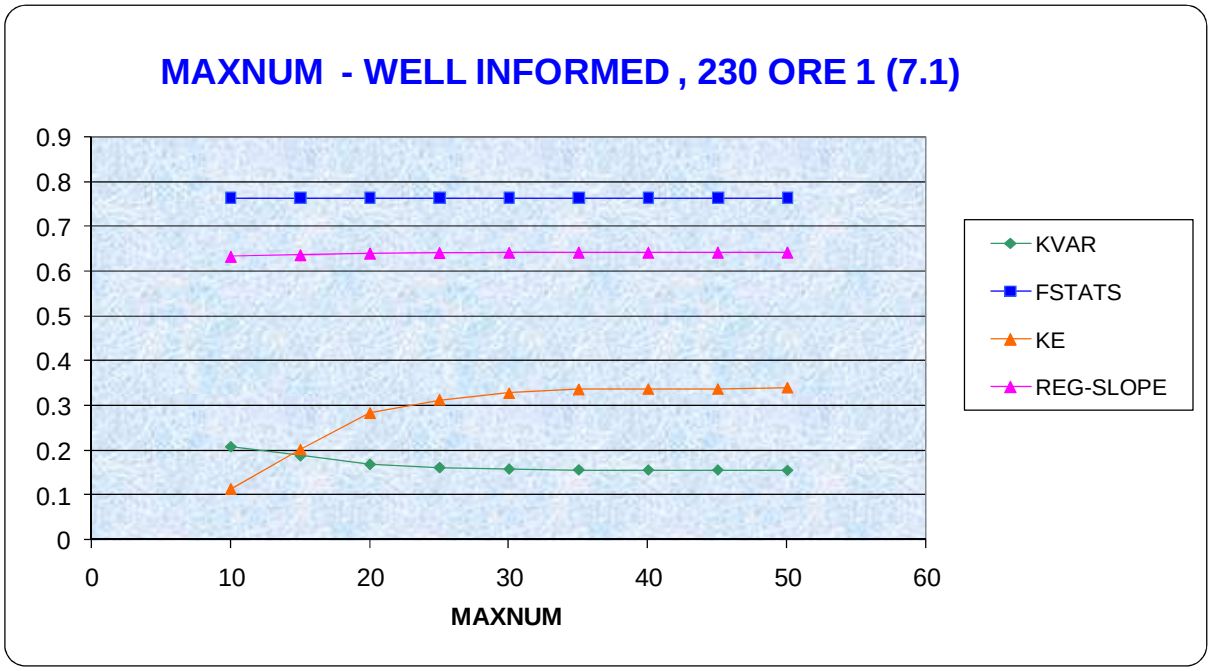


Figure 30: Maximum No. of Samples - Well informed Area

The Slope of Regression, Point Variance, Kriging Variance and Kriging Efficiency are stable (see **Figure 31**), throughout different number of minimum samples tested. For this project minimum of 8 samples were used given that the dataset is sparse.

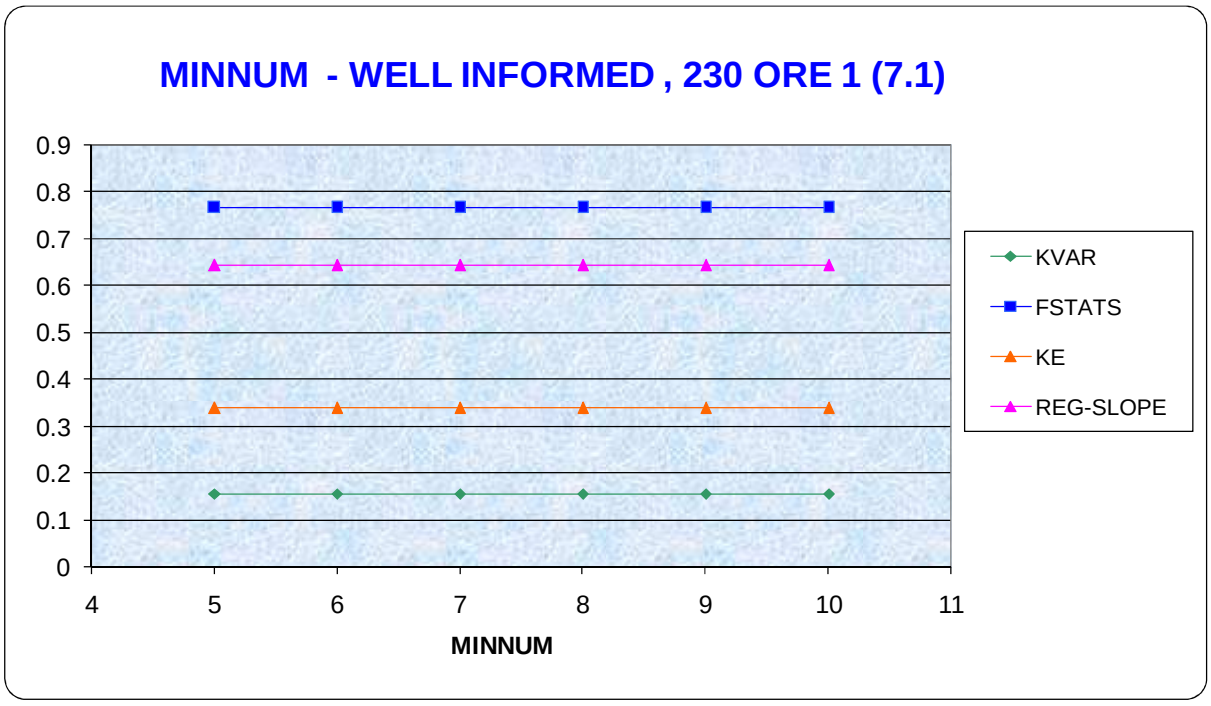


Figure 31: Minimum No. of Samples - Well informed Area

The Slope of Regression, Point Variance and Kriging Efficiency increases with increasing discretisation interval as Kriging Variance decreases resulting in 5 x 5 x 5 discretisation as the optimal number (see **Figure 32**). At 5 discretisation slope of regression is stable at 0.8 from that point onwards, with decreasing Kriging Variance at 0.15.

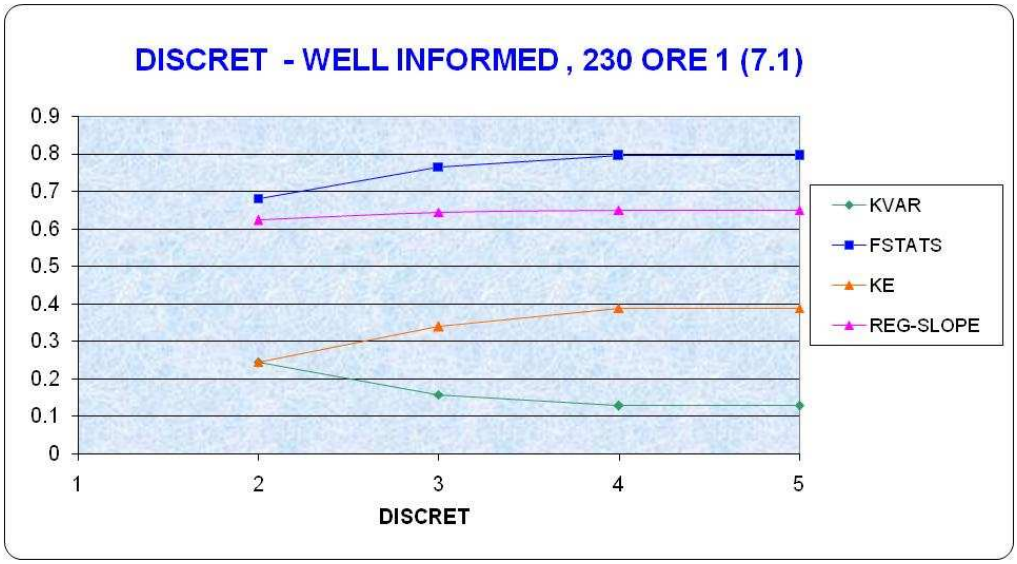


Figure 32: Discretisation interval - Well informed Area

The Slope of Regression, Point Variance, Kriging Variance and Kriging Efficiency are stable throughout different search radius(see **Figure 33**) tested for spatial relationship of samples. A 250m search radius was chosen given the amount samples available.

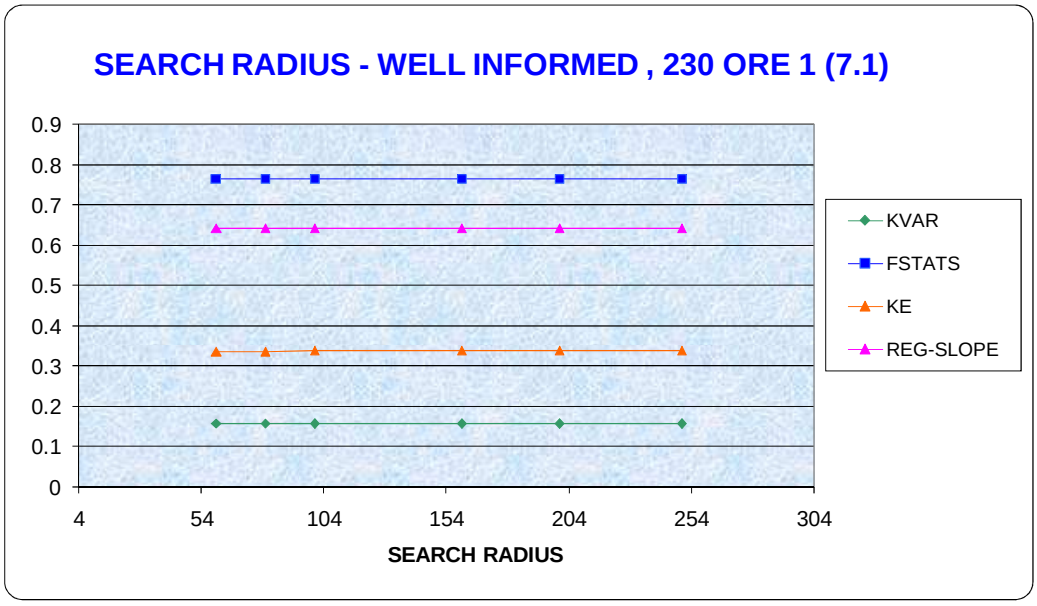


Figure 33: Search Radius - Well informed Area

5.4 ESTIMATION - KRIGING

Kriging, which is of interest in this project, can be synonymously referred to spatial interpolation; the reason being that it is an interpolation method that predicts unknown values from values at any given location taking into account weights associated with the samples used in the interpolation. This method utilises variograms to express the spatial variation that exists between values or data points and it minimises the error of the predicted values which are estimated by spatial distribution of the predicted values.

5.4.1 ORDINARY KRIGING

Ordinary Kriging (OK) is one of the estimation methods of interest in this research. According to Armstrong (1998), Ordinary Kriging is an estimation method that gives the best unbiased linear estimates of point values or of block averages.

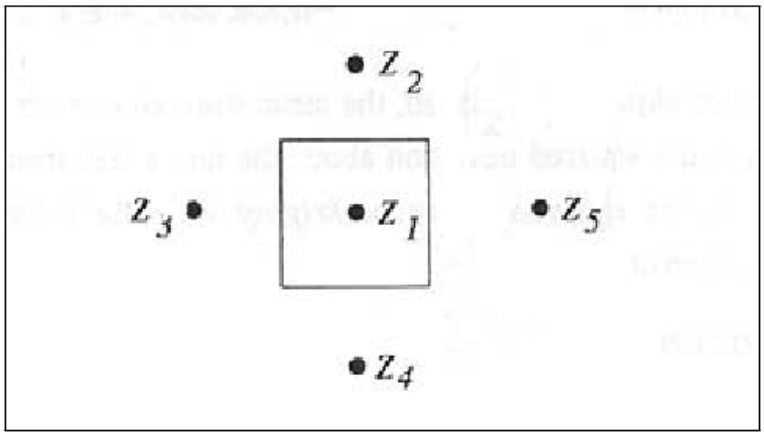


Figure 34: Schematic diagram of Sample distribution with block of interest

Consider an unsampled location *u* and *n* nearby sampled data locations u_α, *α=1,...n,*

This weighted linear estimate at the unsampled location is written as::

$$Z^{OK}(u) = \sum_{\alpha=1}^{n} \lambda_\alpha Z(u_\alpha)$$

where λ_α, α=1,…,*n* are the weights assigned to the n data.

Weights assigned to samples should be such that Z_u^{OK} is :

1. Unbiased: E[$Z_u^{OK} - Z_u$] = 0 and $\lambda_{\alpha=1}$

2. Minimum variance: Var [$Z_u^{OK} - Z_u$] is a minimum.

The target to be estimated can be a point or as large as the whole deposit "*V*".

Minimum variance, being the variance of the error [$Z_u^{OK} - Z_u$] can be expressed in terms of either the covariance or the variogram.

$$\sigma^2 = \sum \sum \lambda_i \lambda_j C(u_i, u_j) + \overline{C}(V, V) - 2\sum \lambda_i \overline{C}(u_i, V)$$
$$= 2\sum \lambda_i \overline{\gamma}(u_i, V) - \sum \sum \lambda_i \lambda_j \gamma(u_i, u_j) - \overline{\gamma}(V, V)$$

where,

$\overline{\gamma}(u_i, V)$ is the average of the variogram between (u_i) and the volume V .

The unbiased condition should further be satisfied, if it is ensured that the sum of weights is equal to 1, which is the main constraint when dealing with Ordinary Kriging. However, due to the constraint that sum of weights must be one the variance of the estimation error must be minimised hence the use of Lagrange multiplier(μ) (Armstrong,1998). Since the sum of the weights must be 1.0, adding the term in μ does not change the value of the expression.

$$\sum_{j=1}^{n} \lambda_j \gamma(u_i, u_j) + \mu = \overline{\gamma}(u_i, V) \qquad i=1,2,...n$$
$$\sum_{i}^{n} \lambda_i = 1$$

The minimum of the variance which is called the kriging variance, is given by:

$$\sigma_k^2 = \sum \lambda_i \overline{\gamma}(u_i, V) - \overline{\gamma}(V, V) + \mu$$

The equation could also have been obtained in terms of the covariance as:

$$\sigma_k^2 = \sum_{j=1} \lambda_j C(u_i, u_j) + \mu' = \overline{C}(u_i, V) \qquad i=1,2,...n$$
$$\sum_{i} \lambda_i = 1$$

Armstrong (1998).

The quality of this estimation method will however depend on the amount of data available and the quality of the variogram model coupled with the search parameters, hence it is imperative that quantitative kriging neighbourhood study is done so that optimal and quality estimates can be produced.

5.4.2 APPLICATION OF ORDINARY KRIGING IN THE RESEARCH

A polygon defining the project area of Block 9 was used to selectively cut the portion of the research. For estimation, *DATAMINE* cell dimensions of 40m*40m*10m were used in Northing, Easting and the elevation respectively. Cell discretisation of 5*5*5 in the X, Y and Z directions for all the 4 variables was used. Search volumes relates to the modelled ranges of the relevant variograms. The Ordinary Kriging process in this modelling required a minimum of 8 and a maximum of 40 samples to be located for a search volume 1 or 2 estimate to be performed. Where this was not achieved, then 40 samples were also required for a search volume 3 estimates. This phenomenon was apparent given the presence of the nested structure composed of short range of ~5m and long range of ~100m. The presence of nested structure is due to the physical make up of the ore type of interest which is laminated.

Confirmation of the above stated parameters was summarised in the kriging neighbourhood study tests completed for Fe variable as listed in **Section 5.3**. Nodes for this study were chosen from a relatively well-informed area to poorly-informed area as shown in **Figure 28**. The tests were carried out for block size, discretisation, search radius and maximum number of samples using KE, KVAR, FSTATS and REG-SLOPE.

The results of the kriging neighbourhood study on this project resulted in the decision to use the following parameters in its grade estimation using Ordinary Kriging:

- Block Size - 40m by 40m by 10m
- Discretisation level - 5 by 5 by 5
- Minimum no. of samples - 8
- Maximum no. of samples - 40

5.5 ESTIMATION - COKRIGING

Cokriging (CK) estimate is a linear combination of neighbouring primary and secondary data through cokriging system. Cokriging approach based on cross-variograms and a linear model of co-regionalisation will be discussed.

5.5.1 CROSS VARIOGRAMS

The concept of variogram, defined for the regionalisation of one variable, can be generalised to spatial coregionalisation of several variables (Journel and Huijbregts, 1978). In Iron Ore deposit, for example, the regionalisation of the Fe grade, $Z_1(u)$ and in SiO_2, $Z_2(u)$ grade are characterised by their respective variograms $2\gamma_1(h)$ and $2\gamma_2(h)$. However since the two variables are dependant of each other, a cross variogram for Fe and SiO_2 can be defined as:

$$2\gamma_{12}(h) = E\{[Z_1(x) - Z_1(x+h)][Z_2(x) - Z_2(x+h)]\}$$

Once the cross-variogram is calculated, a matrix will be formed as illustrated in **Table 6**.

Table 6: Summary outlining the coregionalisation matrices for variables %Fe, %, SiO_2, %Al_2O_3 and RD.

Variables	Variable Identifier
Fe	**1**
SiO_2	**2**
Al_2O_3	**3**
RD	**4**

	1	**2**	**3**	**4**
1	**11**	**12**	**13**	**14**
2	**21**	**22**	**23**	**24**
3	**31**	**32**	**33**	**34**
4	**41**	**42**	**43**	**44**

Cross Variograms were generated in order to run Cokriging in *Isatis* software. Isatis uses an algorithm similar to the Goulard and Voltz algorithm to generate coregionalisation matrices whilst maximising the quality of fit between the experimental variograms and the models.

Cross Variograms of four variables in the study were modelled %Fe, %SiO_2, %Al_2O_3 and RD resulting in 10 cross variograms as shown in **Figure 35** and summary of the cross variograms is outlined **Table 7**.

Fe is the primary variable while SiO_2, Al_2O_3, RD are secondary variables; and all samples are collocated to each other as shown in **Table 2.**

All experimental cross variograms were modelled with a consistent number of structure, nugget plus two exponential structures for Fe, SiO_2, Al_2O_3 and RD thus having one model fitting all ten crossvariograms. However, the data is so sparse and this results in short range and not so good variograms and cross variograms.

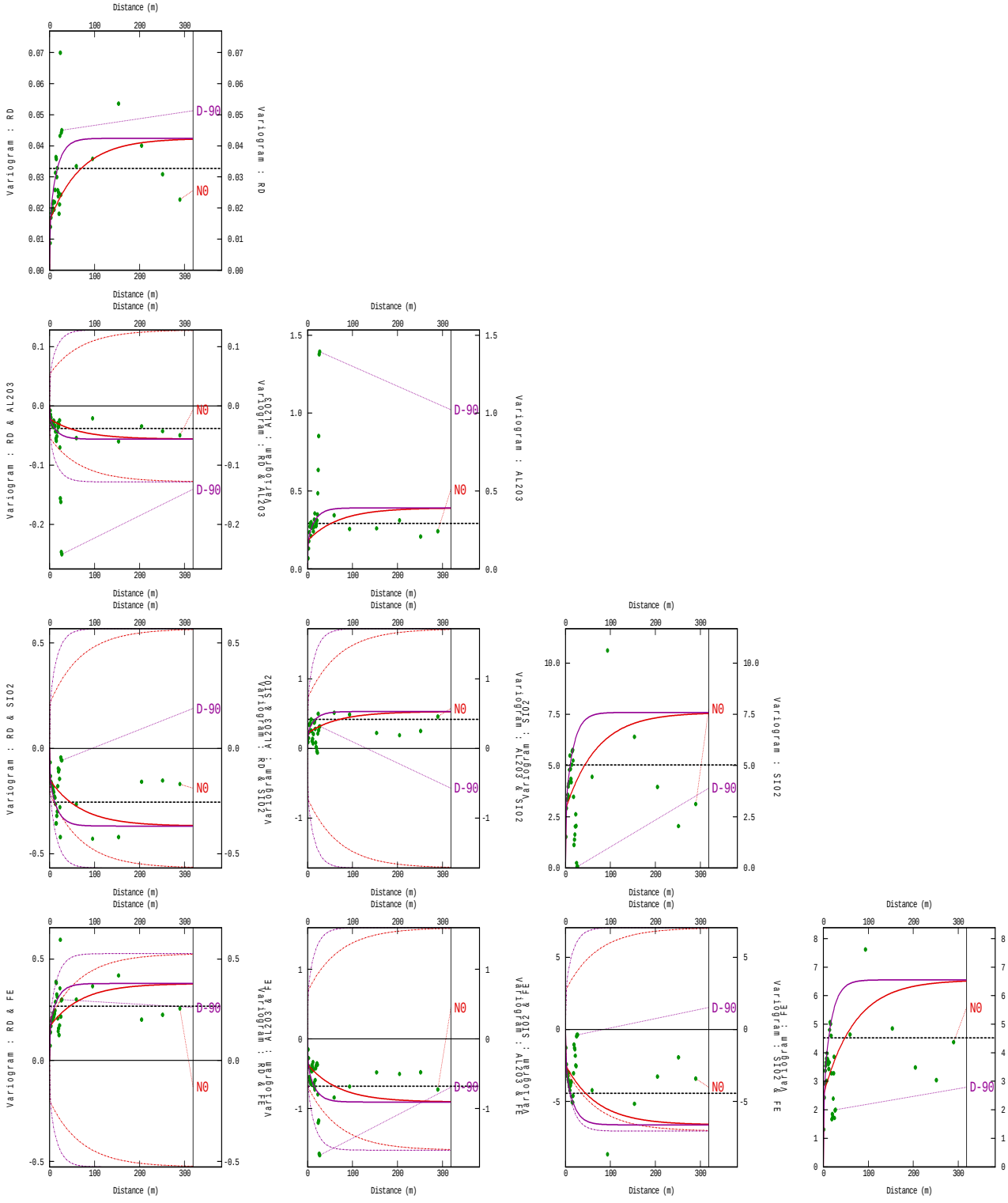


Figure 35: Cross Variogram: %Fe, %SiO_2, %Al_2O_3 and RD; Direction 1 N0 (Red line) and Direction 2 D-90(Purple line).

All ten cross variograms were modelled with the same exponential model hence the same structures and same ranges as outlined in **Table 7**.

Table 7: Summary of experimental cross variograms for variables %Fe, %, SiO_2, %Al_2O_3 and RD

Variables	Structure 1					Structure 2			
	Type	Range	Range	Range		Type	Range	Range	Range
Fe	Exponential	**0.5**	**0.5**	**3.62**		Exponential	229.53	229.53	102.84
SIO_2	Exponential	**0.5**	**0.5**	**3.62**		Exponential	229.53	229.53	102.84
Al_2O_3	Exponential	**0.5**	**0.5**	**3.62**		Spherical	229.53	229.53	102.84
RD	Exponential	**0.5**	**0.5**	**3.62**		Exponential	229.53	229.53	102.84

Detail summary of co-regionalisation matrix is outlined in **Table 8.** The modelling of co-regionalisation is essential in multivariate geo-statistics in that it highlights structural relations between variables; and it can improve the estimation of one variable using the other variable.

Table 8: Co-regionalisation matrices for the 10 cross variograms of variables %Fe, %, SiO_2, %Al_2O_3 and RD.

Structure 1

2.587	-2.553	-0.3934	0.1753
-2.553	2.911	0.2238	-0.1646
-0.3934	0.2238	0.193	-0.02777
0.1753	-0.1646	-0.02777	0.01712

Structure 2

4.656	-4.735	-0.5547	0.2319
-4.735	5.59	0.3969	-0.2305
0.5547	0.3969	0.2265	-0.02746
0.2319	-0.2305	-0.02746	0.02945

5.5.2 ORDINARY COKRIGING

The unbiased-ness condition of ordinary cokriging (OCK) is enforced by making the sum of weights of the primary variable to be 1, whereas the sum of weights of the secondary variable should be 0. This constraint does, however in some cases, cause problems in that most of the secondary variable weights tend to be small which might necessarily be negative and this might result in negative estimates.

Goovaerts (1998) denotes the formula of OCK estimator of Z_1 at u as:

Let

$$\{z_1(u_{\alpha 1}), \alpha_1 = 1,..., n_1\}$$

be the values of the primary attribute z_1 *at* n_1 locations $u_{\alpha 1}$. To alleviate notation consider the situation where there is only one secondary attribute z_2 measured at, possibly different, locations u_2,

$$\{z_2(u_{\alpha 2}), \alpha_2 = 1,..., n_2\}$$

$$Z^{(1)}_{OCK^{(u)}} = \sum_{\alpha 1=1}^{n1(u)} \lambda^{OCK}_{\alpha 1}(u) Z_1(u_{\alpha 1}) + \sum_{\alpha 2=1}^{n2(u)} \lambda^{OCK}_{\alpha 2}(u) Z_2(u_{\alpha 2})$$

That estimator is unbiased under the following constraints on the cokriging weights:

$$\sum_{\alpha 1=1}^{n1(u)} \lambda^{OCK}_{\alpha 1}(u) = 1, \sum_{\alpha 2=1}^{n1(u)} \lambda^{OCK}_{\alpha 2}(u) = 0$$

Minimisation of the error variance $\sigma^2_E(u)$ under the two constraints above yields the following system of (n_1 *(u)* + n_2 *(u)* + *2)* linear equations (Goovaerts, 1998):

$$\left\{ \sum_{\beta_1=1}^{n_1(u)} \lambda_{\beta_1}^{OCK}(u) C_{11}\left(u_{\alpha 1} - u_{\beta 1}\right) + \sum_{\beta 2=1}^{n_2(u)} \lambda_{\beta 2}^{OCK}(u) C_{12}\left(u_{\alpha 1} - u_{\beta 2}\right) + \mu_1^{OCK}(u) = C_{11}\left(u_{\alpha 1} - u\right), \alpha_1 = 1,..., n_1(u) \right\}$$

$$\left\{ \sum_{\beta_1=1}^{n_1(u)} \lambda_{\beta_1}^{OCK}(u) C_{21}\left(u_{\alpha 2} - u_{\beta 1}\right) + \sum_{\beta 2=1}^{n_2(u)} \lambda_{\beta 2}^{OCK}(u) C_{22}\left(u_{\alpha 2} - u_{\beta 2}\right) + \mu_2^{OCK}(u) = C_{21}\left(u_{\alpha 2} - u\right), \alpha_2 = 1,..., n_2(u) \right\}$$

$$\left\{ \sum_{\beta_1=1}^{n_2(u)} \lambda_{\beta_1}^{OCK}(u) = 1 \right\}$$

$$\left\{ \sum_{\beta 2=1}^{n_2(u)} \lambda_{\beta 2}^{OCK}(u) = 0 \right\}$$

where the two Lagrange parameters $\mu_1^{OCK}(\boldsymbol{u})$ and μ_2^{OCk} ($\boldsymbol{u}$) account for the two unbiased-ness constraints.

For this research with one primary variable (Fe) and three secondary variables(SiO_2, Al_2O_3 and RD) OCK denotes as follows as per matrices illustrated in **Table 6**;

$$\left\{\sum_{\beta_1=1}^{n_1(u)}\lambda_{\beta_1}^{OCK}(u)C_{11}(u_{\alpha 1}-u_{\beta 1})+\sum_{\beta 2=1}^{n_2(u)}\lambda_{\beta 2}^{OCK}(u)C_{12}(u_{\alpha 1}-u_{\beta 2})+\sum_{\beta 3=1}^{n_3(u)}\lambda_{\beta 3}^{OCK}(u)C_{13}(u_{\alpha 1}-u_{\beta 3})+\sum_{\beta 4=1}^{n_4(u)}\lambda_{\beta 4}^{OCK}(u)C_{14}(u_{\alpha 1}-u_{\beta 4})\right\}$$

$$+\mu_1^{OCK}(u)=C_{11}(u_{\alpha 1}-u),\alpha_1=1,...,n_1(u)$$

$$\left\{\sum_{\beta_1=1}^{n_1(u)}\lambda_{\beta_1}^{OCK}(u)C_{21}(u_{\alpha 2}-u_{\beta 1})+\sum_{\beta 2=1}^{n_2(u)}\lambda_{\beta 2}^{OCK}(u)C_{22}(u_{\alpha 2}-u_{\beta 2})+\sum_{\beta 3=1}^{n_3(u)}\lambda_{\beta 3}^{OCK}(u)C_{23}(u_{\alpha 2}-u_{\beta 3})+\sum_{\beta 4=1}^{n_4(u)}\lambda_{\beta 4}^{OCK}(u)C_{24}(u_{\alpha 2}-u_{\beta 4})\right\}$$

$$+\mu_2^{OCK}(u)=C_{21}(u_{\alpha 2}-u),\alpha_2=1,...,n_2(u)$$

$$\left\{\sum_{\beta_1=1}^{n_1(u)}\lambda_{\beta_1}^{OCK}(u)C_{31}(u_{\alpha 3}-u_{\beta 1})+\sum_{\beta 2=1}^{n_2(u)}\lambda_{\beta 2}^{OCK}(u)C_{32}(u_{\alpha 3}-u_{\beta 2})+\sum_{\beta 3=1}^{n_3(u)}\lambda_{\beta 3}^{OCK}(u)C_{33}(u_{\alpha 3}-u_{\beta 3})+\sum_{\beta 4=1}^{n_4(u)}\lambda_{\beta 4}^{OCK}(u)C_{34}(u_{\alpha 3}-u_{\beta 4})\right\}$$

$$+\mu_3^{OCK}(u)=C_{31}(u_{\alpha 3}-u),\alpha_3=1,...,n_3(u)$$

$$\left\{\sum_{\beta_1=1}^{n_1(u)}\lambda_{\beta_1}^{OCK}(u)C_{41}(u_{\alpha 4}-u_{\beta 1})+\sum_{\beta 2=1}^{n_2(u)}\lambda_{\beta 2}^{OCK}(u)C_{42}(u_{\alpha 4}-u_{\beta 2})+\sum_{\beta 3=1}^{n_3(u)}\lambda_{\beta 3}^{OCK}(u)C_{43}(u_{\alpha 4}-u_{\beta 3})+\sum_{\beta 4=1}^{n_4(u)}\lambda_{\beta 4}^{OCK}(u)C_{44}(u_{\alpha 4}-u_{\beta 4})\right\}$$

$$+\mu_4^{OCK}(u)=C_{41}(u_{\alpha 4}-u),\alpha_4=1,...,n_4(u)$$

$$\left\{\sum_{\beta_1=1}^{n_1(u)}\lambda_{\beta_1}^{OCK}(u)=1\right\}$$

$$\left\{\sum_{\beta 2=1}^{n_2(u)}\lambda_{\beta 2}^{OCK}(u)=0\right\}$$

$$\left\{\sum_{\beta 3=1}^{n_3(u)}\lambda_{\beta 3}^{OCK}(u)=0\right\}$$

$$\left\{\sum_{\beta 4=1}^{n_4(u)}\lambda_{\beta 4}^{OCK}(u)=0\right\}$$

5.5.3 APPLICATION OF ORDINARY COKRIGING IN THE RESEARCH

Cokriging was run in *Isatis* software with the same estimation parameters used in OK ;

- Block Size - 40m by 40m by 10m
- Discretisation level - 5 by 5 by 5
- Minimum no. of samples - 8
- Maximum no. of samples - 40

6 INVESTIGATIONAL RESULTS

According to Coombes (2008), one can follow certain matrices to assess the validity and efficiency of estimation. The results from the estimation for each of the four estimation methods of interest in this research will be assessed in the following manner:

- Statistics for each methodology will be scrutinised between block estimates and the original drill hole values to explore the differences,
- Conditional simulation properties will be assessed,
- Scatter plots between the ground truth and the estimates will be compared in order to calculate the correlation coefficient between the two.

Kriging variance is also a useful tool in determining the quality of the estimation as is Slope of regression. The kriging variance represents the minimum estimation variance and will give an idea of the quality of the estimation (Vann *et al,* 2003). The kriging variance generally depends on the distances between the samples. Similarly, the slope of regression often is another geostatistical tool that can be used to determine the quality of the estimate produced. All the

validation tools mentioned above will be used jointly in order to assess the quality of estimation for each of the options.

6.1 CONDITIONAL SIMULATION

Simulation can be defined in simpler terms as an attempt for sampling the unknown using constraints, e.g. statistical moments imposed by the data. If the simulations honour the data themselves by reproducing the data histogram and honouring the spatial variability of data, they are said to be "conditional simulations". Geostatistical simulation is much more computationally demanding than geostatistical estimation. However given the latest technology in computer processing and data storage significant number of simulations can be generated. The question still remains: 'how many simulated images are required to properly characterise a given domain'. To answer this, simulations must be tested to ensure they reasonably reproduce the input statistics.

The main differences between the geostatistical simulation models and geostatistical estimation or kriging models is that with simulation a series of realisations are generated and were as with kriging models there is only one best estimator.

In the study a Gaussian based method of TurningBands (TB) simulation was used. A Gaussian based method relies on raw data being transformed to have a Gaussian distribution. A Gaussian transform is a simple technique whereby a raw data population is transformed to have a normal distribution with zero mean and unit variance. For each raw data value a Gaussian equivalent is generated via the cumulative histograms for both the raw and Gaussian distributions. Gaussian distributions can then be transformed back to raw space.

Turning Bands was the first large-scale 3D Gaussian simulation algorithm to be implemented. The method works by simulating one-dimensional process on lines regularly spaced 3D. The one-dimensional simulations are then projected onto the spatial coordinates and averaged to give the required 3D simulated value. The method is very efficient for generating non-conditional simulations and

particularly good at replicating the variogram. Conditioning is obtained through a separate kriging step:

- Non-conditional simulations at all target points and all sample points $Z_s(u)$
- Krige values to all sample points using real data $Z_k(u)$
- Combine using $Z_{cs}(u) = Z_k(u) + [Z_s(u) - Z_{ks}(u)]$

The main advantage of TB is that it reproduces the variogram better than other methods more so for small simulated field (Journel and Huijbregts, 1978).

However for this study multivariate (co-simulation) was run. Conditional simulation (CS) as illustrated above deals with one variable. Conditional co-simulation (CCS) is conditional simulation of more than one variable. If an independent simulation of a multivariate set is performed, the results will not reproduce the correlation between these variables (Vann et al, 2002).

In order to provide a 'ground truth' against which to compare the estimates generated using each of the methods, twenty realisations of conditional co-simulation of % Fe, %SiO_2, % Al_2O_3 and RD grade were generated on a fine mesh of (5m x 5m x 1m) using the Turning Bands algorithm but only five simulations which adequately represented the statistical moments of the input data were used in the study. CS allows multiple images of the deposit to be generated which are realistically variable but are 'conditional' in the sense that they honour the known but limited drillhole sampling data from the deposit. The raw dataset was first de-clustered through cumulative kriging weights and transformed through Gaussian anamorphosis modelling (see **Figure 36** and **Figure 37**) for conditional simulation. Only transformations of %Fe is displayed below, the rest of the variables are displayed in **Appendix 3**.

5m x 5m x 1m point co-simulation was then re-blocked to 40m x 40m x 10m block co-simulation to get the average %Fe, %SiO_2, %Al_2O_3 and RD which will be the mean grade 'ground truth' to compare the kriged estimates with from the Ordinary and Ordinary Cokriging estimation methods tested in this project.

The mean grade from both the point and block simulation was checked for representativity of key statistics against the input data (raw data) more so to satisfy the three properties of conditional simulation listed below:

- Simulated grades must honour the raw data
- Simulated grade must honour the histogram of the raw data
- Simulated grades must honour the variograms of the raw data

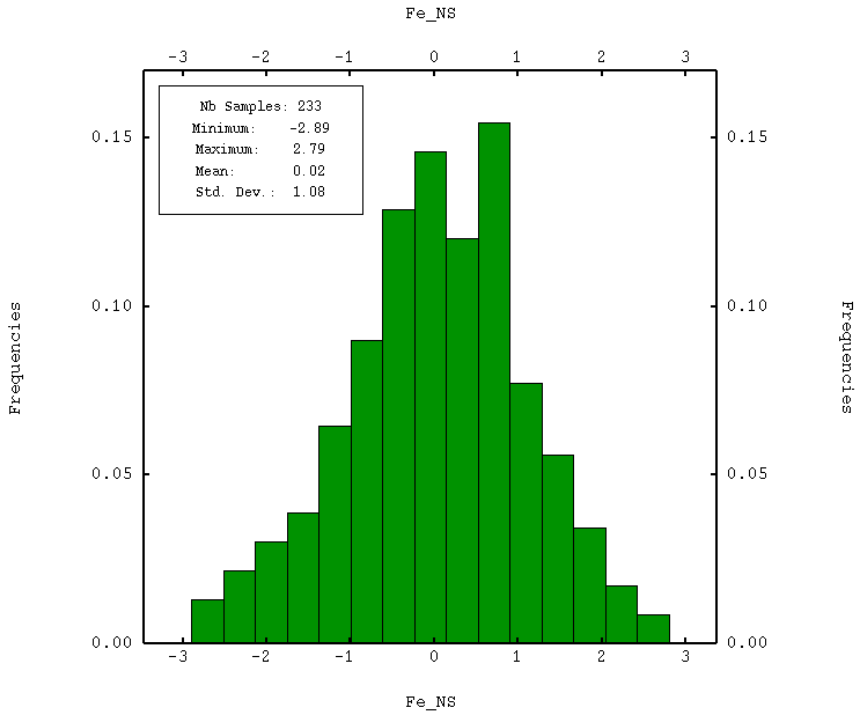


Figure 36: %Fe transformed through GAUSSIAN Anamorphosis.

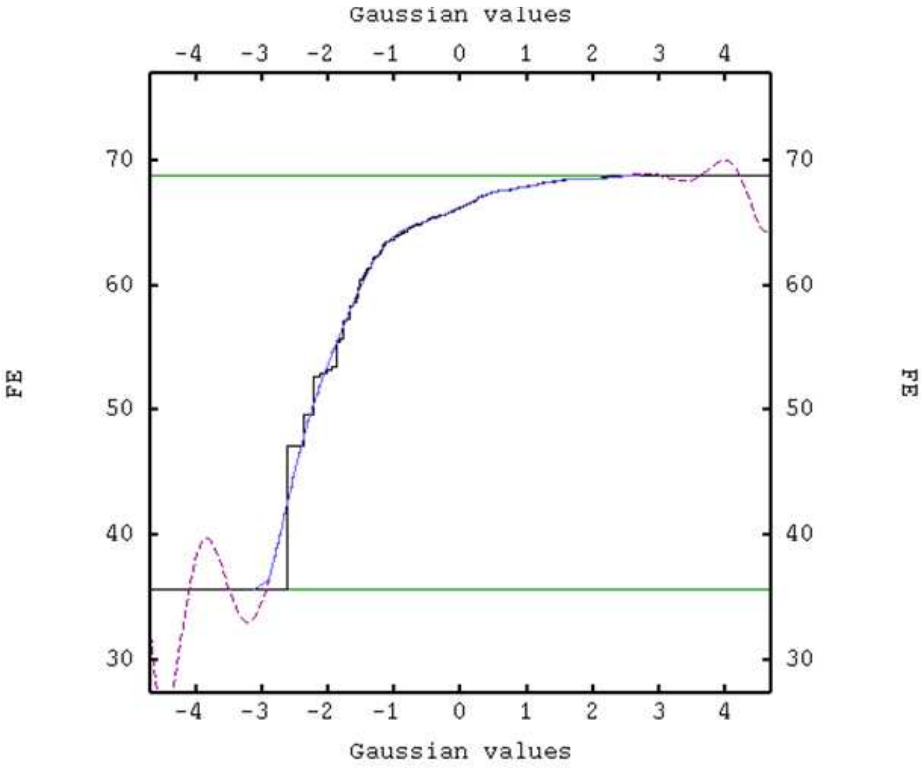


Figure 37: %Fe transformation GAUSSIAN model.

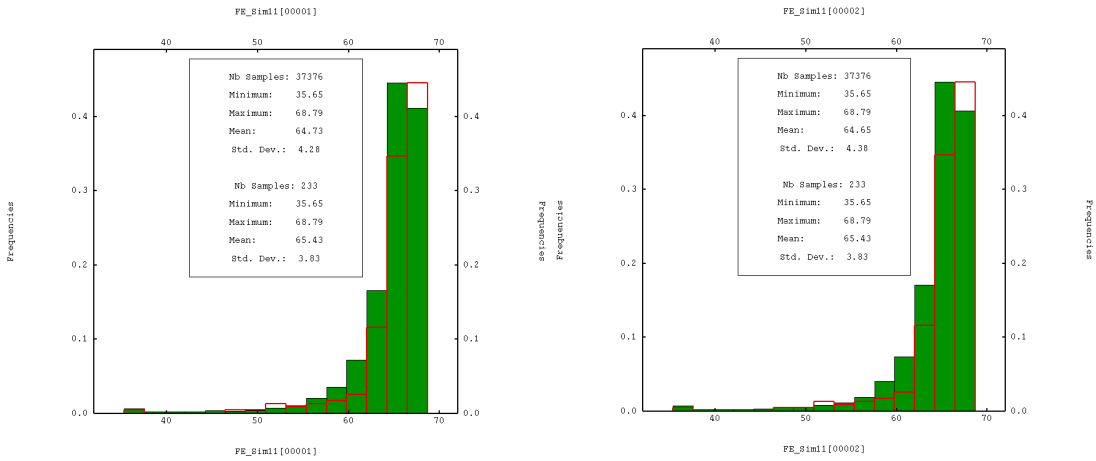


Figure 38: %Fe raw data histogram displayed in red lines superimposed over simulated %Fe_Sim1 histogram of five simulations.

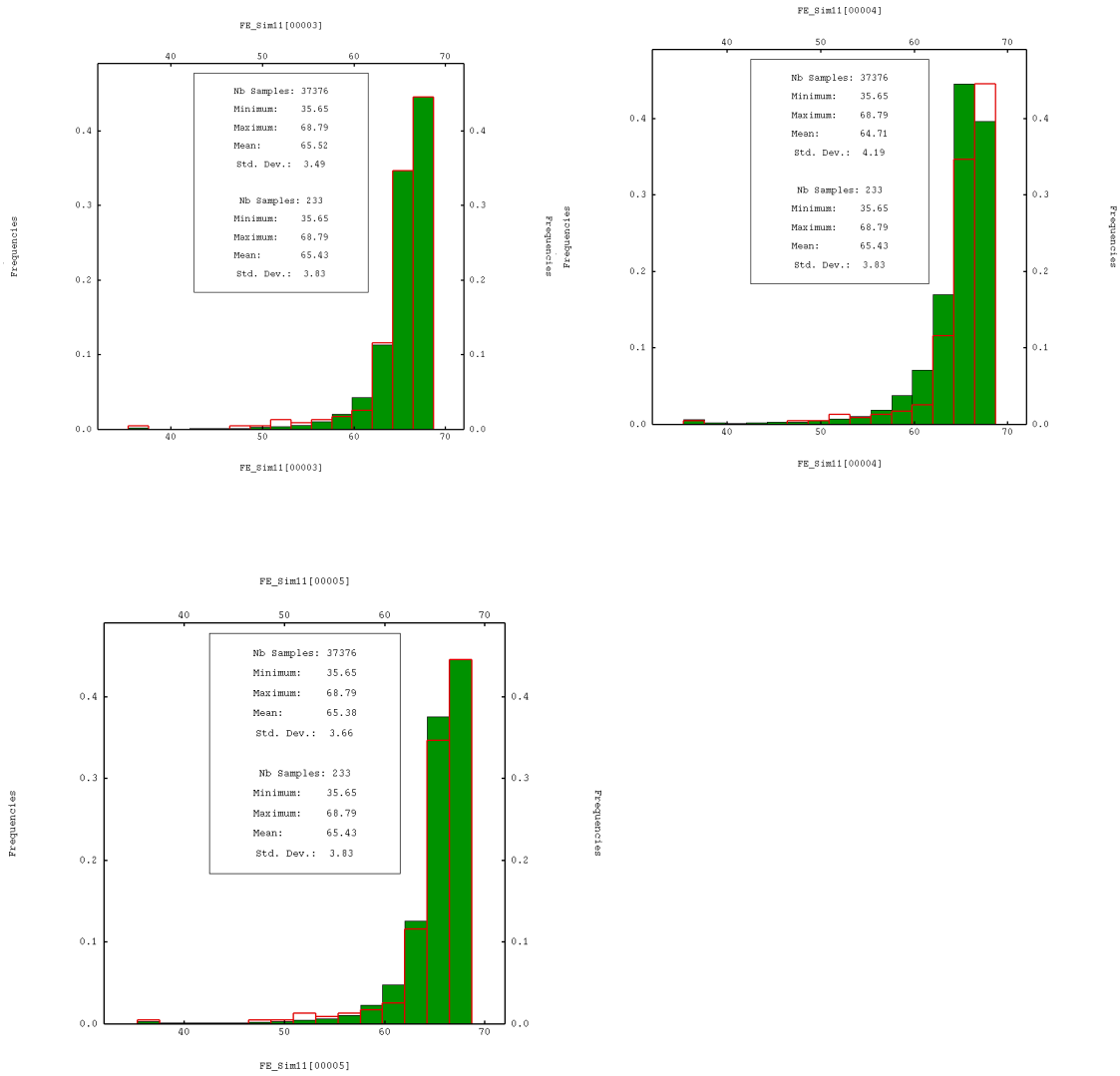


Figure 38(continued): %Fe raw data histogram displayed in red lines superimposed over simulated %Fe_Sim1 histogram of five simulations.

The mean of Fe for the raw data is 65.43 % and for simulated Fe_Sim1 (0005, which is the fifth realisation) grade is 65.38%. The third and fifth realisations have mean of 65.52% and 65.38%, which are the once close to the mean of the raw data of 65.43%. The standard deviation between the raw data and the simulated data is 3.83 for the raw data, 3.49 and 3.66 for third and fifth realisation. The shapes of the histograms of the third and fifth realisations look more or less the same to that of the raw data (**Figure 38**) and so is that of the

variograms of the two as displayed in **Figure 39**. This is a clear indication that the simulated data is a true reflection of the raw data.

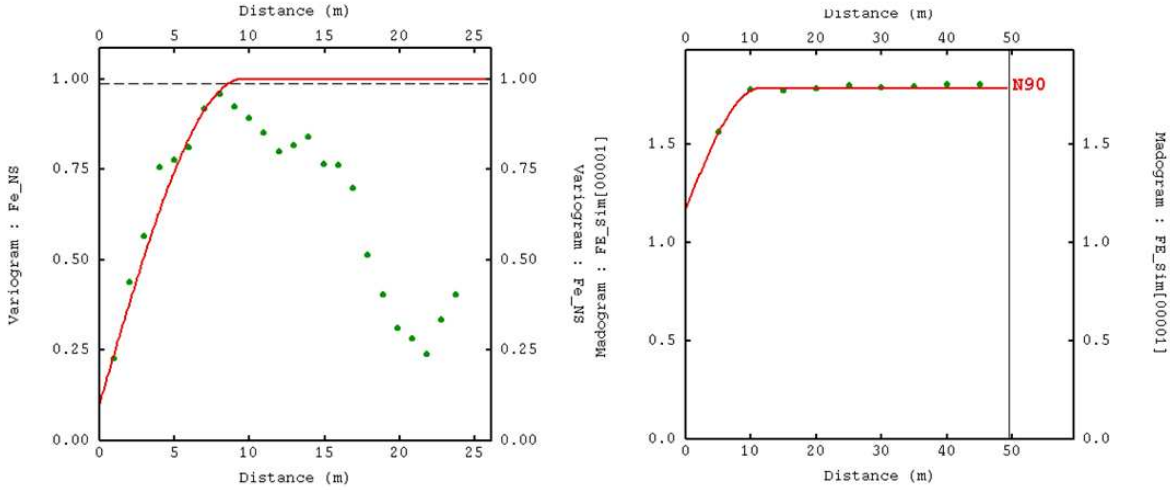


Figure 39: Experimental variograms raw data Fe_NS and simulated grades FE_Sim11 (00005).

If an independent simulation of a multivariate set is performed, the results will not reproduce the correlation between these variables (Vann et al, 2002).

Co-simulation was ran in the study and given the correlation between the four variables Fe, SiO_2 Al_2O_3, and RD outlined in **Section 4.4.4** on the raw data, the same correlation was verified in the five simulations, given that the simulated data should be a close reflection of the raw data. Realisation 3 and 5 displays close correlation to that of the raw data (**Table 9**), and this can also be seen in the histograms outlined in **Figure 38.**

Table 9: Correlation between %Fe, %, SiO_2, %Al_2O_3 and RD simulated variables

	Raw Data			
	Fe	**SiO_2**	**Al_2O_3**	**RD**
Fe	1	-0.929	-0.638	0.824
SiO_2	-0.929	1	0.353	-0.788
Al_2O_3	-0.638	0.353	1	-0.463
RD	0.824	-0.788	-0.463	1

	Point Simulation(0001)			
	Fe	**SiO_2**	**Al_2O_3**	**RD**
Fe	1	-0.821	-0.519	0.796
SiO_2	-0.821	1	0.304	-0.704
Al_2O_3	-0.519	0.304	1	-0.419
RD	0.796	-0.704	-0.419	1

	Point Simulation(0002)			
	Fe	**SiO_2**	**Al_2O_3**	**RD**
Fe	1	-0.862	-0.505	0.766
SiO_2	-0.862	1	0.331	-0.717
Al_2O_3	-0.505	0.331	1	-0.354
RD	0.766	-0.717	-0.354	1

	Point Simulation(0003)			
	Fe	**SiO_2**	**Al_2O_3**	**RD**
Fe	1	-0.832	-0.506	0.812
SiO_2	-0.832	1	0.311	-0.797
Al_2O_3	-0.506	0.311	1	-0.423
RD	0.812	-0.797	-0.423	1

Table 9(continued): Correlation between %Fe, %, SiO_2, %Al_2O_3 and RD simulated variables

	Point Simulation(0004)			
	Fe	**SiO_2**	**Al_2O_3**	**RD**
Fe	1	-0.85	-0.525	0.78
SiO_2	-0.85	1	0.344	-0.714
Al_2O_3	-0.525	0.344	1	-0.378
RD	0.78	-0.714	-0.378	1

	Point Simulation(0005)			
	Fe	**SiO_2**	**Al_2O_3**	**RD**
Fe	1	-0.856	-0.61	0.813
SiO_2	-0.856	1	0.324	-0.767
Al_2O_3	-0.61	0.324	1	-0.323
RD	0.833	-0.767	-0.323	1

5m x 5m x1m point co-simulation was run on the whole set of variables as they are collocated and have a spatial relationship; and then re-blocked to 40m x 40m x 10m block co-simulation to get the average Fe, SiO_2, Al_2O_3, and RD which will be the mean grade 'ground truth' to compare with for all five realisations (see **Figure 40**). The point simulation and the re-blocked simulation have the same mean of 65.38%; with a standard deviation of point simulation of 3.66 and for the re-blocked simulation is 1.11(%Fe_Sim1100005) as displayed in **Figure 40**, and is less due to change of support from points to blocks. This clearly demonstrates the key features of up-scaling from punctual to block support, the range and skewness of the distribution is reduced, but the mean is preserved.

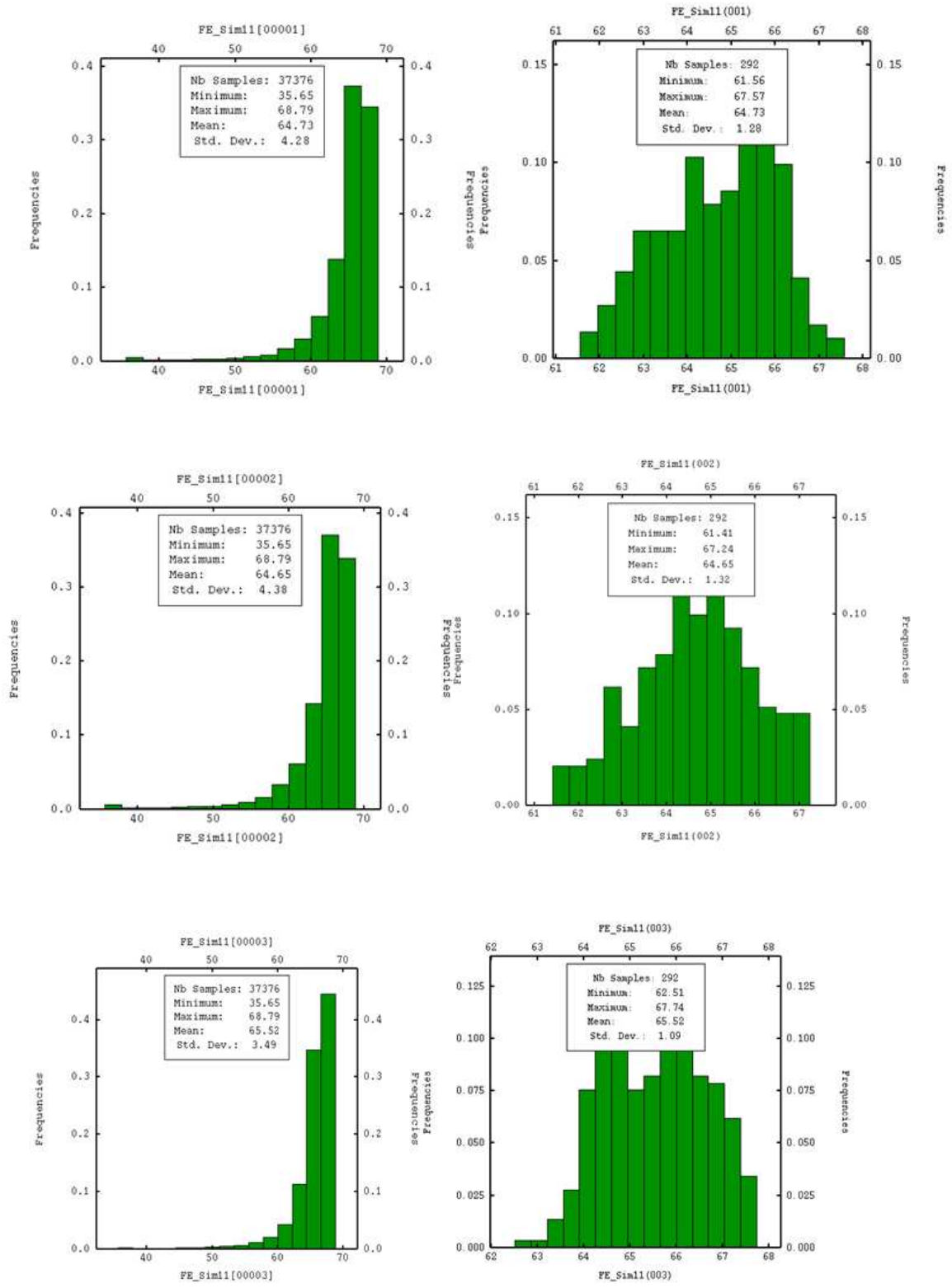


Figure 40: Reblocking of %Fe (point simulation into %Fe_Sim1_Mean block simulation.

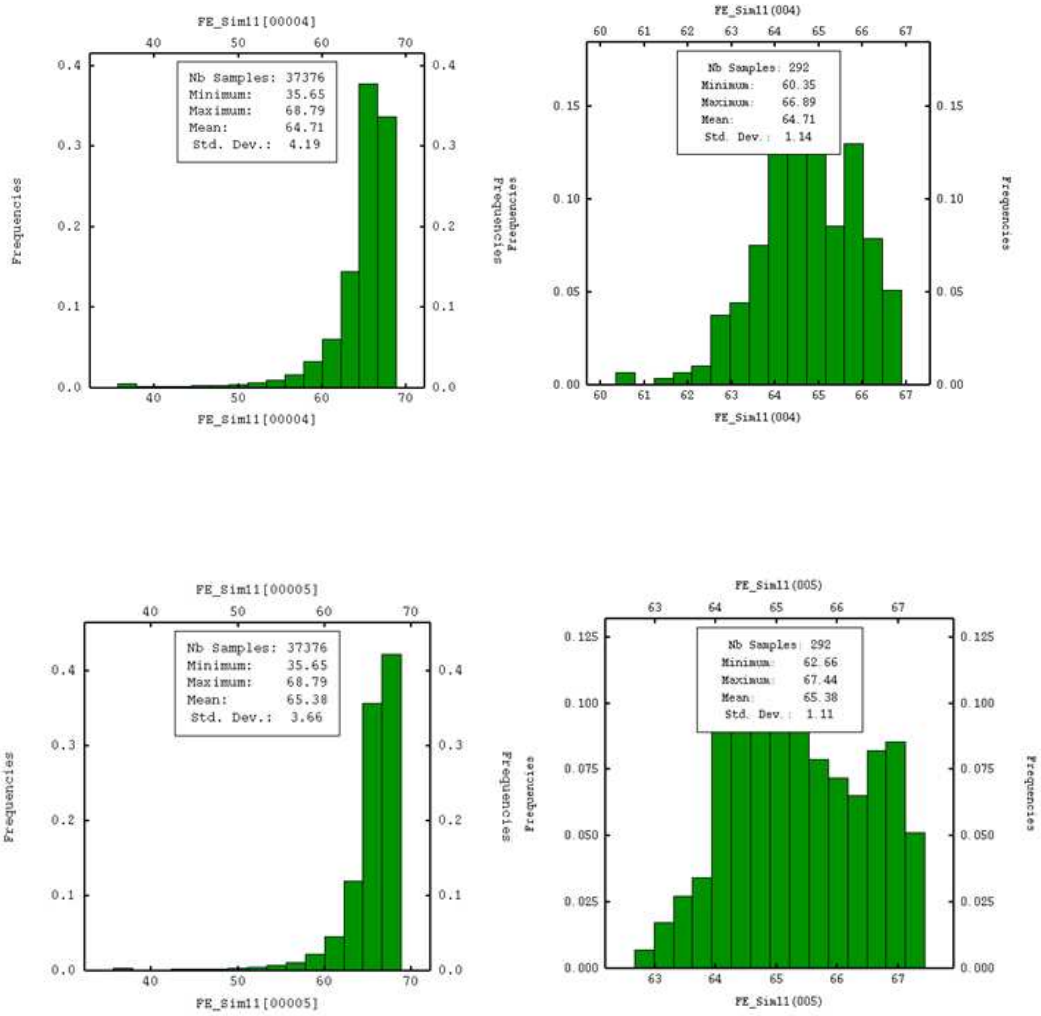


Figure 40(continued): Reblocking of %Fe (point simulation into %Fe_Sim1_Mean block simulation.

6.2 COMPARISONS OF STATISTICS

Each block estimate of %Fe, $\%SiO_2$, $\%Al_2O_3$ and RD were compared to the five ground truth simulations in order to get the correlation coefficient between simulated grades and estimates from OK and OCK estimation method. The Pearson correlation coefficient measures the linear dependency between Z and Z^{OK}, subsequently between Z and Z^{OCK}. Goovaerts (1998) have used similar methodology as the basis for comparison.

6.2.1 ORDINARY KRIGING

Variography for all four variables of interest were generated and OK was run. The results for each variable kriged %Fe, %SiO_2, %Al_2O_3 and RD were compared to the simulated grades (ground truth) for each variable (**Appendix 5**). Displayed below in **Figure** are histograms of %Fe kriged (outlined in red lines) against the %Fe ground truth from the simulation of the five realisations.

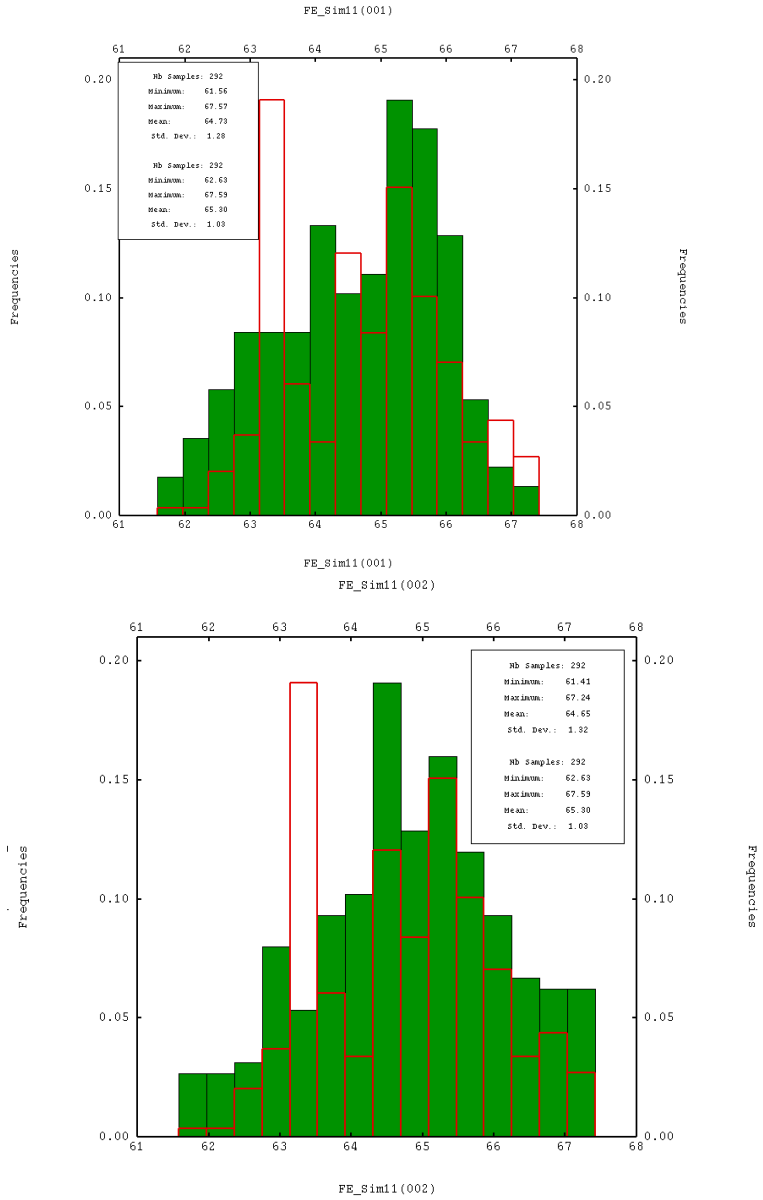


Figure 41: %Fe_Kriged histogram of OK kriged estimate displayed in red line superimposed over %Fe_Sim1_Mean histogram of simulated data

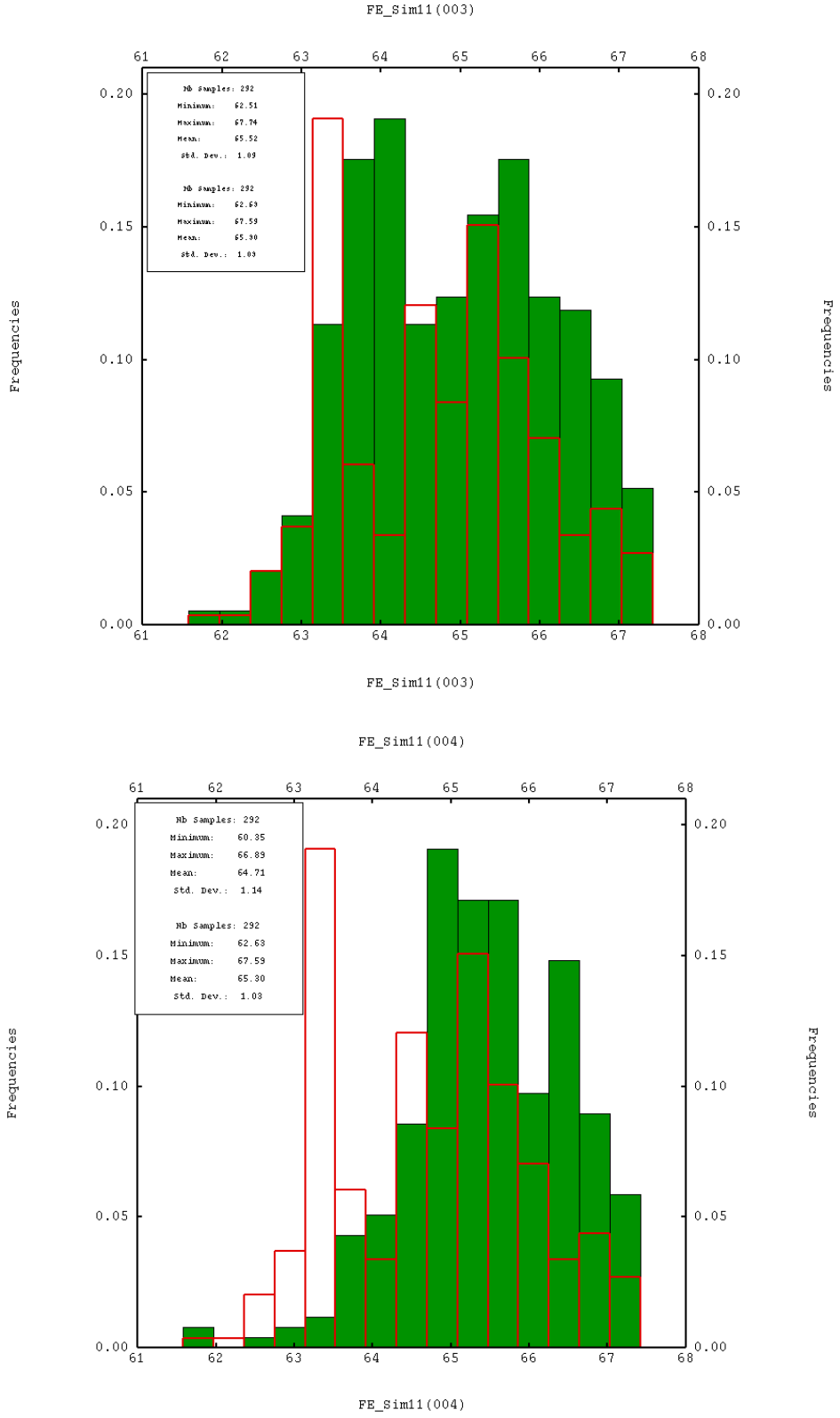


Figure 41(continued): %Fe_Kriged histogram of OK kriged estimate displayed in red line superimposed over %Fe_Sim1_Mean histogram of simulated data.

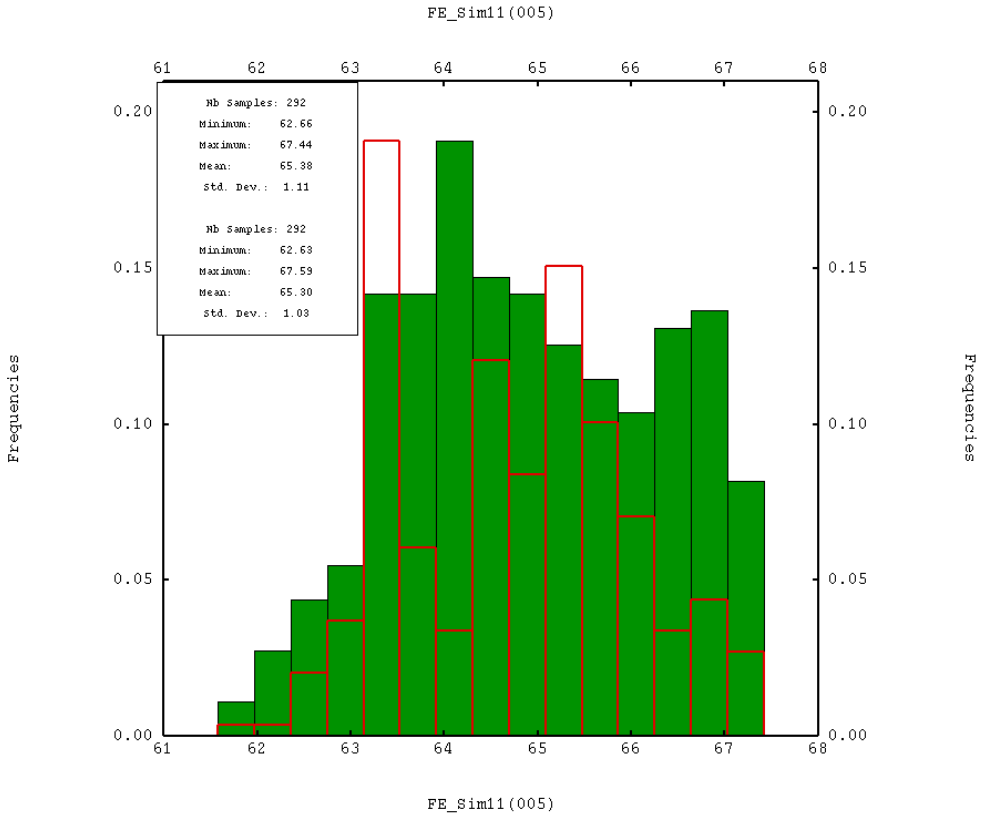


Figure 41(continued): %Fe_Kriged histogram of OK kriged estimate displayed in red line superimposed over %Fe_Sim1_Mean histogram of simulated data.

Kriged estimates have a bimodal distribution and the simulated grades have a bimodal distribution (for all five simulations) as well as displayed in **Figure 41** with kriged estimates mean of 65.30% and simulated grades with 65.38% mean (5^{th}realisation). The minimum of kriged estimates is 62.63% and the maximum is 67.59% while the simulated grade's minimum is 62.66% and the maximum is 67.44 %(5^{th}realisation).

However if the mean grades of the 20 simulations are collected and analysed;

- it is observed that the variance of this distribution (1.63) is much higher than that of the kriged estimates 1.23 for OK and 1.06 for OCK.
- the semivariogram of kriged estimates has a much smaller relative nugget than the semivariogram model of the simulated data, which

reflects the underestimation of the short range variability of Fe values(as displayed in **Figure 39**).

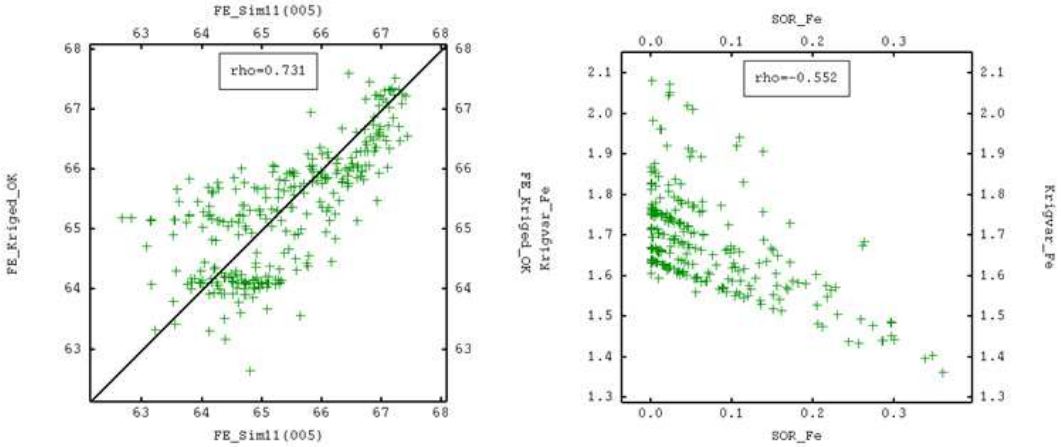


Figure 42: OK kriged Estimates (FE_Kriged_OK) vs Ground Truth (FE_Sim1_Mean) Scatter plot; Kriging Variance vs Slope of Regression Scatter plot.

The scatter plot on the left-hand side in **Figure 42** demonstrates that the correlation between Fe Kriged and Fe simulated is lower at the lower Fe grades. Correlation between kriged estimates and ground truth is at 0.731 correlation coefficient of the kriged estimate to that of the fifth simulation. Correlation between kriged estimates and the other simulations are illustrated in **Appendix 5**. Strong observation of proportional effect is noted from **Figure 42**, thus variance of estimation error is dependent on the mean grade as displayed on the left hand side scatterplot of kriged estimate against fifth simulation; with local variability and estimation error greatest between 63 and 65% Fe and least in high grades. The Slope of Regression and kriging variance are slightly correlated as this can be used to measure how good the estimate is. The Kriging variance is high and slope of regression is low. The Slope of regression and kriging variance are more driven by data density, and the results are as expected in that the data has sparse geometry; high kriging variance with less slope of regression. Results for other variables are indicated in **Appendix 5**.

The Slope of Regression as displayed in **Figure 43** increases with decreasing distance of samples from the block of interest, and it's more likely that better

estimates will be with blocks that have samples within 50m. For blocks that have samples further than 50m are more likely to have low values of slope of regression and relatively high kriging variance values.

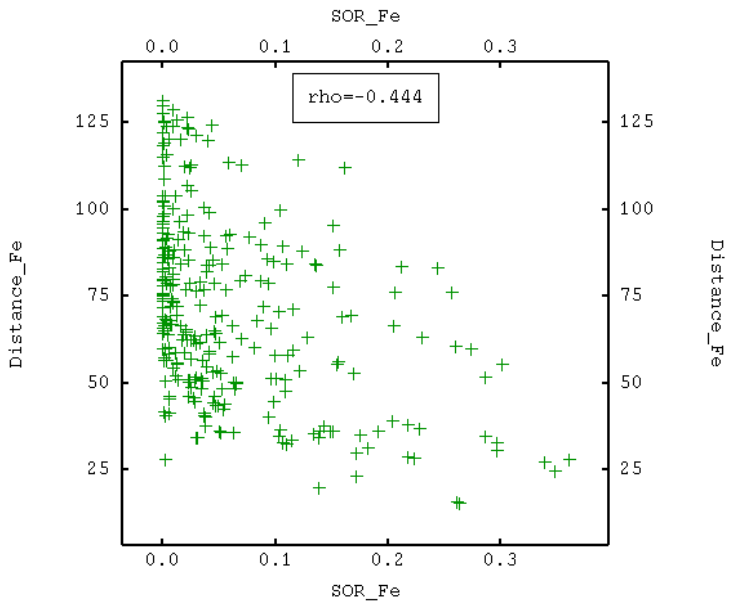


Figure 43: Scatter plot of slope of regression (SOR_Fe) against Distance of samples (OK) (Distance_Fe).

6.2.2 ORDINARY COKRIGING

Cross-variography for all four variables of interest were generated and OCK was ran; results for each variable kriged were compared to the simulated grades (ground truth) for each variable (**Appendix 6**). Analysis displayed in **Figure 44** is of %Fe.

Kriged estimate (FE_Kriged_CK) has a bimodal distribution, and the simulated grades also have a bimodal distribution for all five simulations. The mean of the two distributions (Co-kriged estimate and fifth simulation) is very close to each other thus 65.30% for cokriged estimates and 65.38% for co-simulated data, so is the standard deviation which is 1.04 and subsequently 1.11(5^{th} realisation).

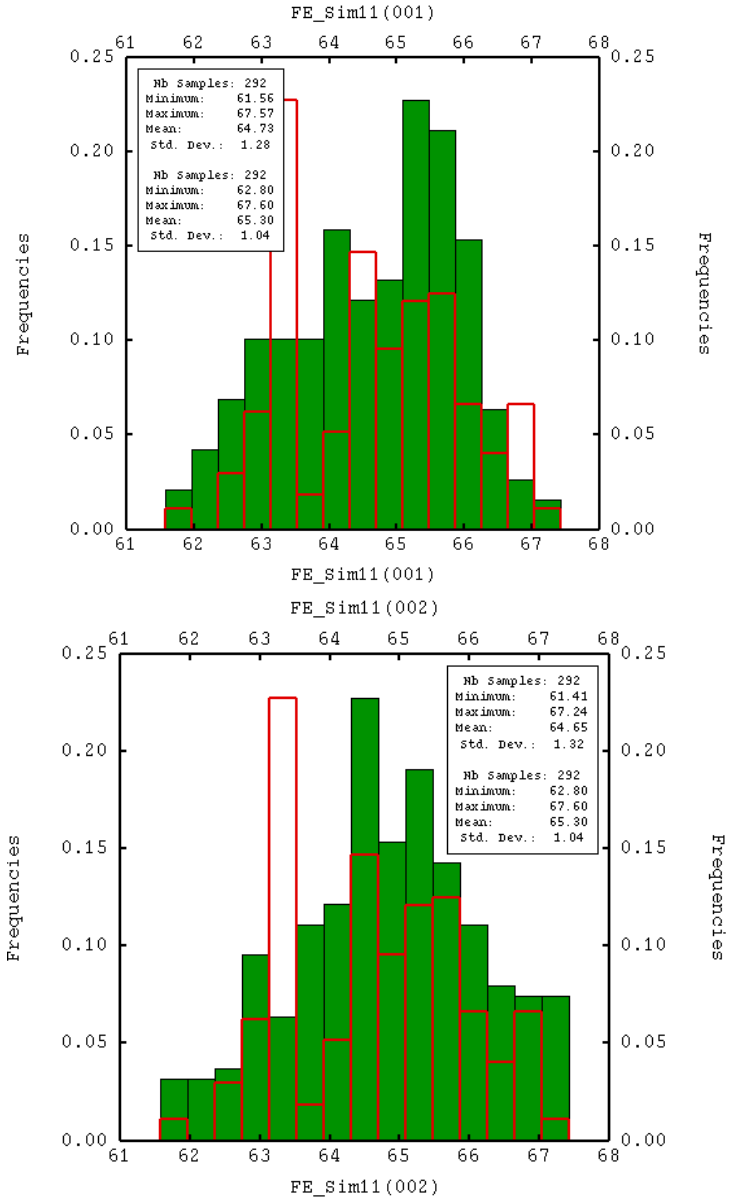


Figure 44: Histograms Fe OCK kriged displayed in red lines superimposed over Fe mean (simulated data).

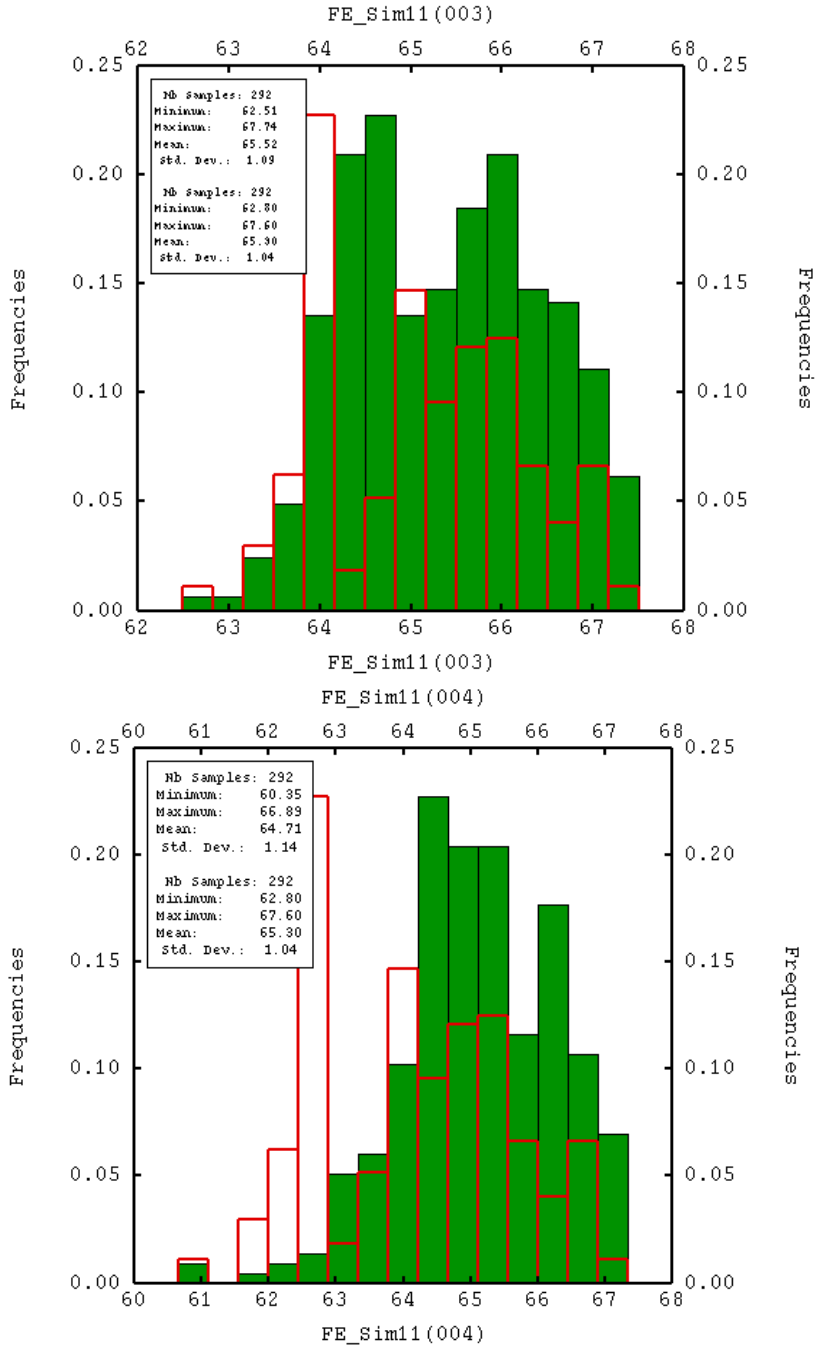


Figure 44(continued): **Histograms Fe OCK kriged displayed in red lines superimposed over Fe mean (simulated data).**

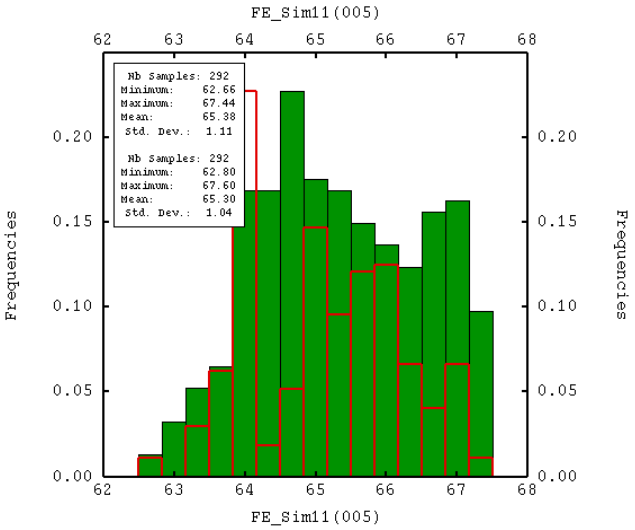


Figure 44(continued): Histograms Fe OCK kriged displayed in red lines superimposed over Fe mean (simulated data).

Correlation coefficient between the cokriged estimate and the ground truth is 0.730 with an error distribution between the two being slightly high around grades less than 65%Fe (Fe cokriged and fifth realisation). Another strong observation of proportional effect is noted from **Figure 45**, thus variance of estimation error is dependent on the mean grade. The kriging variance increases with decreasing slope of regression as shown in **Figure 45**. Kriging variance in general is slightly less than that of OK.

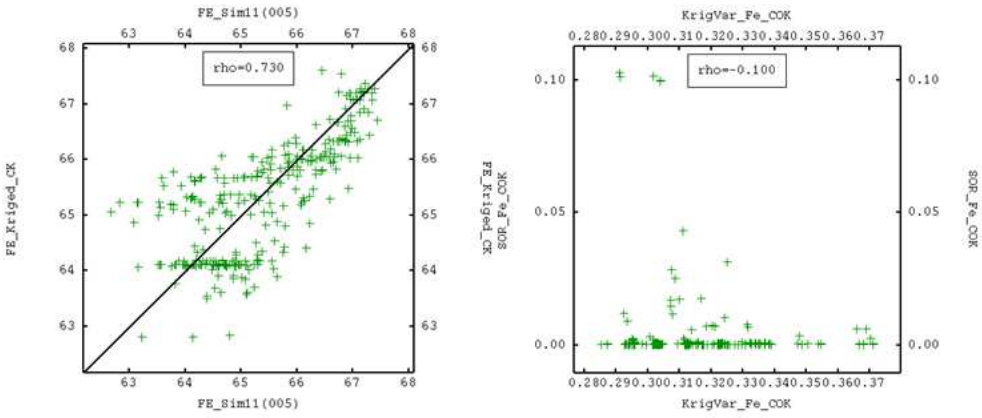


Figure 45: Correlation coefficient between OCK kriged (Fe_Kriged_CK) and ground truth (Fe_Sim11 (005)), slope of regression (SOR_Fe_CK) against kriging variance (KrigVar_Fe_CK).

Slope of Regression slightly high within blocks that have samples within 25m, not as high as in OK. The rest of the variables results are displayed in **Appendix 6**. Slope of regression is very low and this is a reflection of not so good quality on the estimates given that the data is sparse.

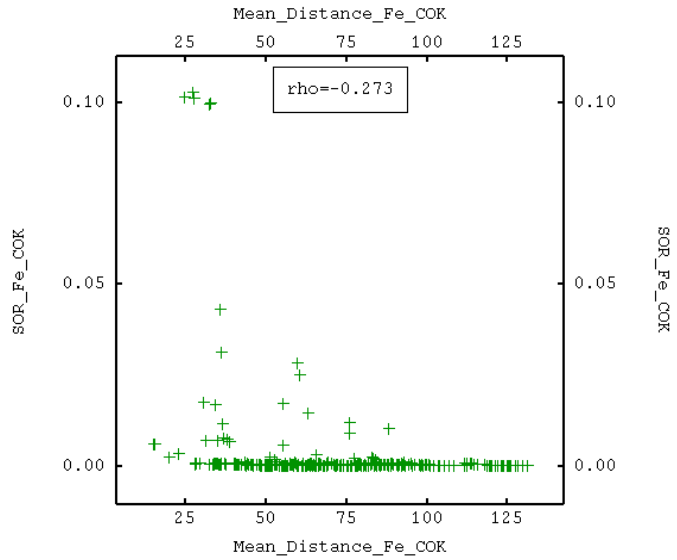


Figure 46: Mean distance (Mean_Distance_Fe_COK) of samples from blocks against slope of regression (OCK) (SOR_Fe_COK).

6.2.3 ORDINARY COKRIGING WITH DIFFERENT PERCENTAGE OF RD MISSING

Co-kriging allows samples of the secondary variable besides the primary variable to be used when predicting the target value in the un-sampled location. The secondary variable may be measured at the same points as the primary variable (thus collocated samples), or at other points, or both.

The most common application of cokriging is when the secondary variable has been more densely sampled, than the primary variable. The dataset in this research for both primary and secondary variables is densely sampled in that both primary and secondary samples are found at the same points or location. This section will outline a typical situation in a case were primary variable is under-sampled compared to the secondary variable. A case will be investigated to determine at what threshold is cokriging beneficial to use compared to OK when having heterotopic dataset. Correlation coefficient between the estimates

from both OK and OCK will be calculated against the simulated grade mean (ground truth).

OK and OCK were run for the following thresholds;

- OCK/OK with 22% of Al_2O_3 missing
- OCK/OK with 44% of Al_2O_3 missing
- OCK/OK with 66% of Al_2O_3 missing

Al_2O_3as a primary variable was under-sampled at different missing thresholds. This section is to investigate at what percentage of the missing variable OCK will improve the estimates compared to OK.

Cokriging requires that both the primary and secondary variables have a spatial structure that can be modelled, so the same cross-variogram used in OCK and subsequently variograms generated for OK can be used. A comparison between OCK and OK was done for different percentage of % Al_2O_3 missing with both OCK and OK estimates run for different thresholds and compared with the ground truth.

6.2.4 ORDINARY COKRIGING WITH 19% OF Al_2O_3 MISSING

The mean of the two distributions; OK with a mean of 1.22% and OCK mean of 1.25% as displayed in **Figure 47**. OCK displays more of what is expected of the Al_2O_3 distribution which is positively skewed. Correlation coefficient of OK, OCK against the ground truth, shows that with 19% of Alumina missing from the dataset OK displays better correlation than OCK thus 0.243 for OK and 0.231 for OCK (**Figure 48**).

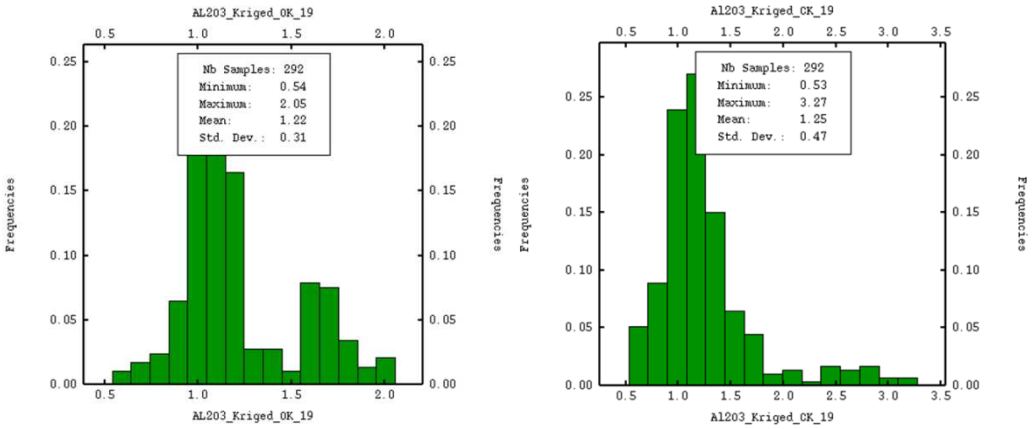


Figure 47: Histogram for OK and for OCK for 19% threshold

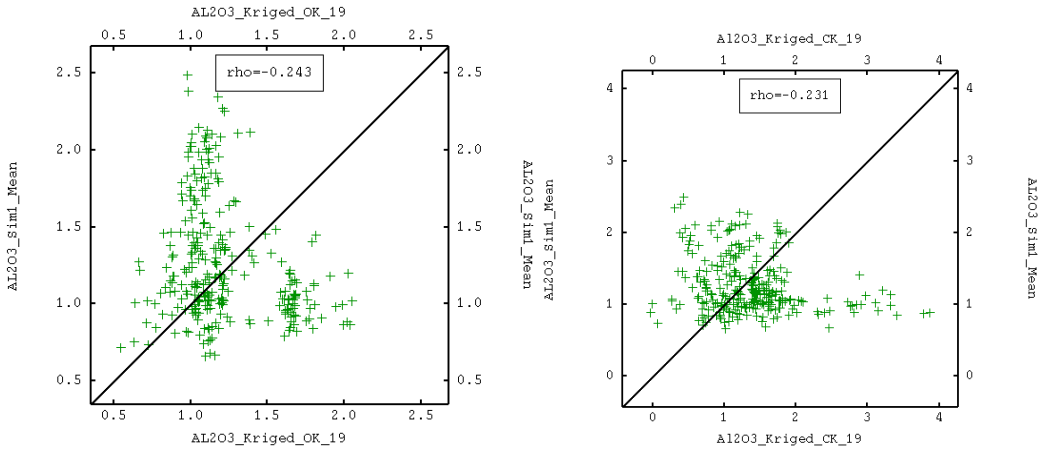


Figure 48: Correlation coefficient between OK and Ground truth; that of OCK and ground truth at 19% threshold.

6.2.5 ORDINARY COKRIGING WITH 22% OF Al_2O_3 MISSING

The mean of the two distributions differ slightly; OK with a mean of 1.21% and OCK mean of 1.26% as displayed in **Figure 49**. OCK displays a strongly positively skewed distribution. Correlation coefficient of OK, OCK against the ground truth, shows that with 22% of Alumina missing from the dataset OK displays better correlation with 0.240 than 0.027 of OCK (**Figure 50**).

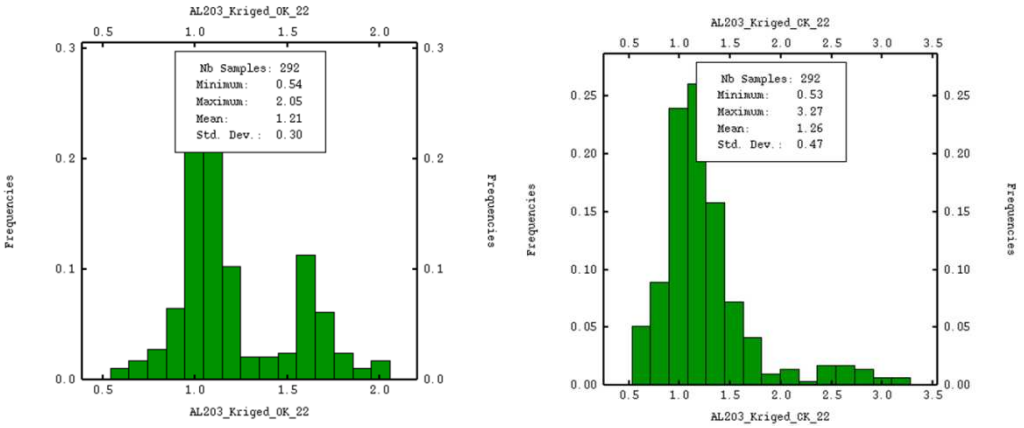


Figure 49: Histogram for OK and OCK for 22% threshold.

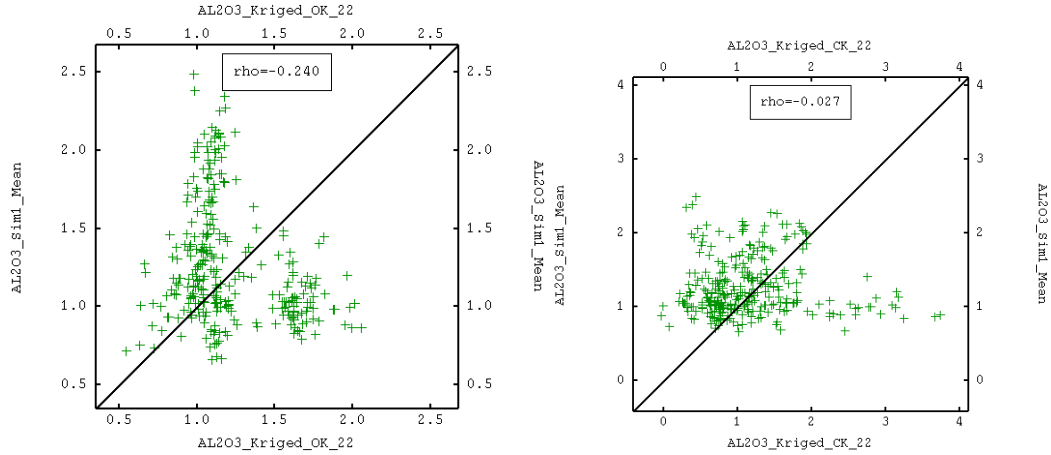


Figure 50: Correlation coefficient between OK and Ground truth; that of OCK and ground truth at 22% threshold.

6.2.6 ORDINARY COKRIGING WITH 44% OF Al_2O_3 MISSING

The two distributions have the same mean of 1.10% as displayed in **Figure 51**. OCK displays more of what is expected of the Al_2O_3 distribution which is positively skewed. A 44% threshold of alumina missing in the dataset seems to serve an advantage to OCK, in that the correlation coefficient between the estimates and the ground truth is high in OCK thus 0.402 than 0.081 in OK (**Figure 52**).

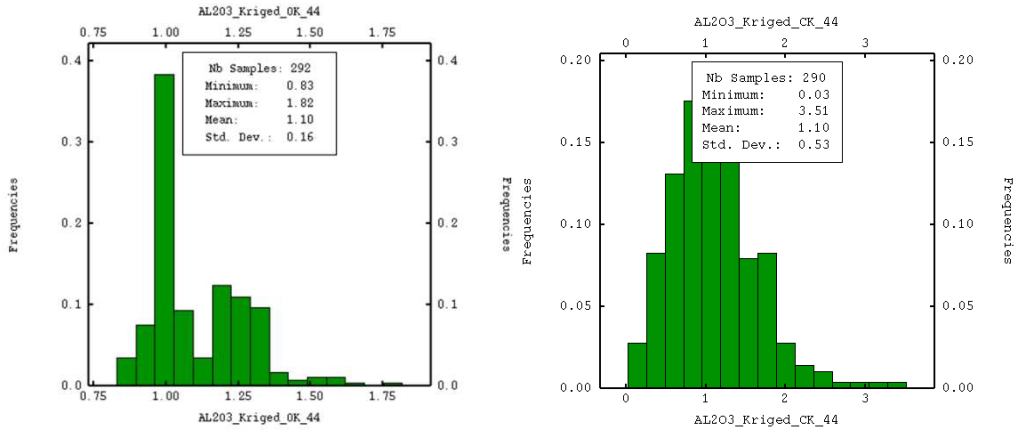


Figure 51: Histogram for OK and for OCK for 44% threshold

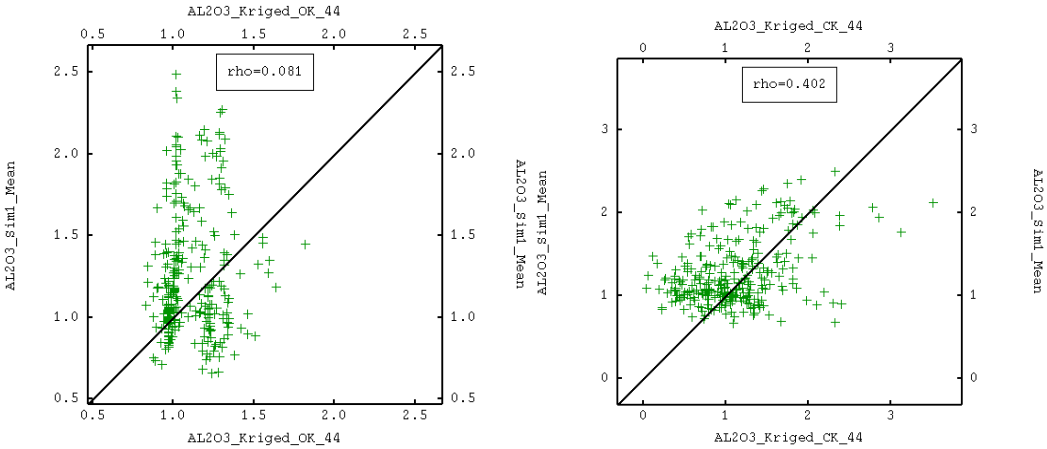


Figure 52: Correlation coefficient between OK and Ground truth; that of OCK and ground truth at 44% threshold.

6.2.7 ORDINARY COKRIGING WITH 66% OF Al_2O_3 MISSING

The mean of the two distributions is different; OK with a mean of 1.08% and OCK mean of 1.26% as displayed in **Figure 53**. OCK displays more of a positively skewed distribution. The correlation coefficient of OK, OCK against the ground truth, shows that with 66% of Alumina missing from the dataset OCK displays higher correlation of 0.507 than 0.245 of OK (**Figure 54**).

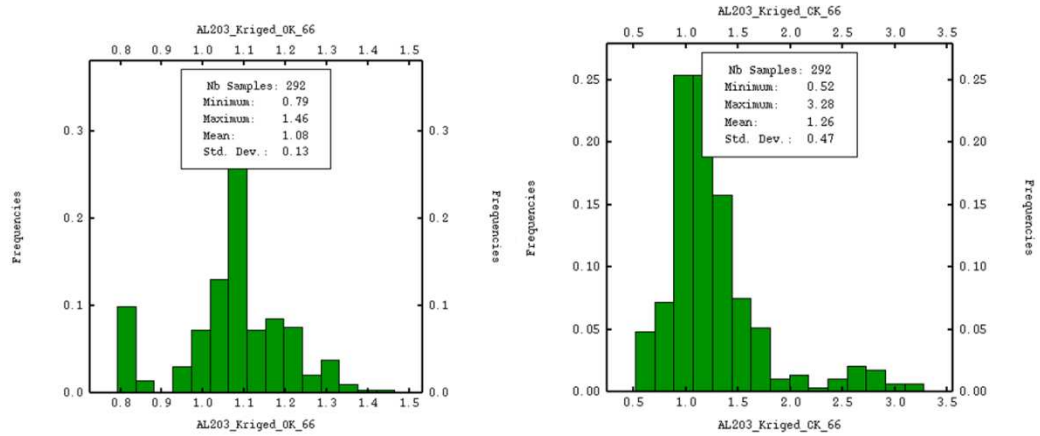


Figure 53: Histogram for OK and for OCK for 66% threshold

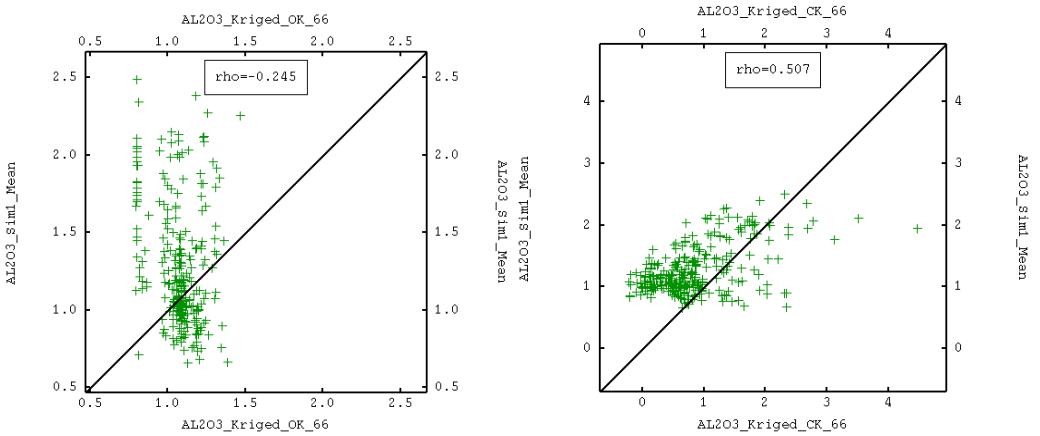
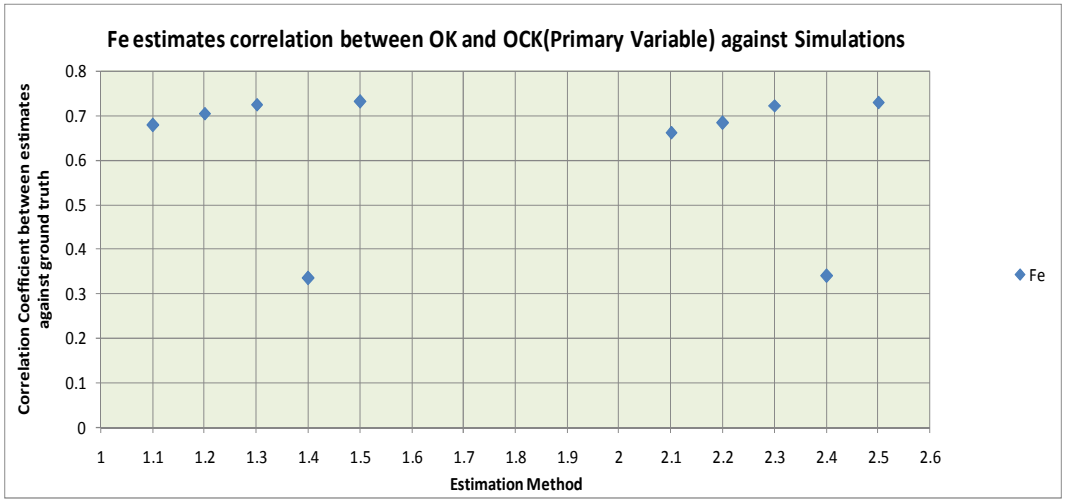


Figure 54: Correlation coefficient between OK and Ground truth; that of OCK and ground truth at 66% threshold.

7 DISCUSSION

In order to assess the relative benefit of the alternative estimation approaches, it is necessary to have a benchmark against which each can be compared. Averaging the underlying conditional simulated values (at 5m x 5m x 1m) into the blocks on which estimates are made gives the 'true' grade of the block. The true grade of each block of the five realisations were compared to the grade estimates made using the alternative estimation approaches discussed in **Section 6** above. Paired data was either plotted on scatter plot for visualisation, or the relationship between the two populations summarised using the correlation (Pearson) coefficient.

Two estimation methods were ran OK and OCK; the comparison against the ground truth is shown in **Figure 55**.



1- OK **2 - OCK**

Simulation vs Estimation Method	1st vs OK	2nd vs OK	3rd vs OK	4th vs OK	5th vs OK	1st vs OCK	2nd vs OCK	3rd vs OCK	4th vs OCK	5th vs OCK
	1.1	1.2	1.3	1.4	1.5	2.1	2.2	2.3	2.4	2.5

Figure 55: Correlation coefficient for %Fe against ground truth.

The framework adopted for this study then, compares the results derived from each of the estimation methods for the four variables %Fe, %SiO_2, %Al_2O_3 and

RD against the ground truth. Correlation coefficients for all four variables are displayed in **Appendix 7.**

In **Figure 55** OK and OCK displays more or less similar correlation coefficient for all 5 realisations tested for Fe estimated as a primary variable.

Third realisation displays weaker correlation coefficient compared to estimates for both OK and OCK; however similar trend is displayed in both cases.

Based on **Figure 55** analysis at all test locations shows that OK and OCK perform equally when the primary and secondary variables are sampled at the same locations. When the secondary information is available at the estimated location, one gains little by retaining other distant secondary data in the estimation (Goovaerts, 1998). The results of the research are as expected given that the dataset is isotopic and the variables of interest are also intrinsically correlated. Various authors including Journel and Huijbregts (1978) and Goovaerts (1998) suggest that Co-kriging is only worthwhile where correlations between variables are strong and the variable of interest is under-sampled with respect to secondary variable.

The various kriging and cokriging estimation methods differ in the way the trend component of the dataset is modelled. OK and OCK re-estimate the means within each search neighbourhood through the incorporation of one or several unbiased-ness constraints in the kriging and cokriging system.

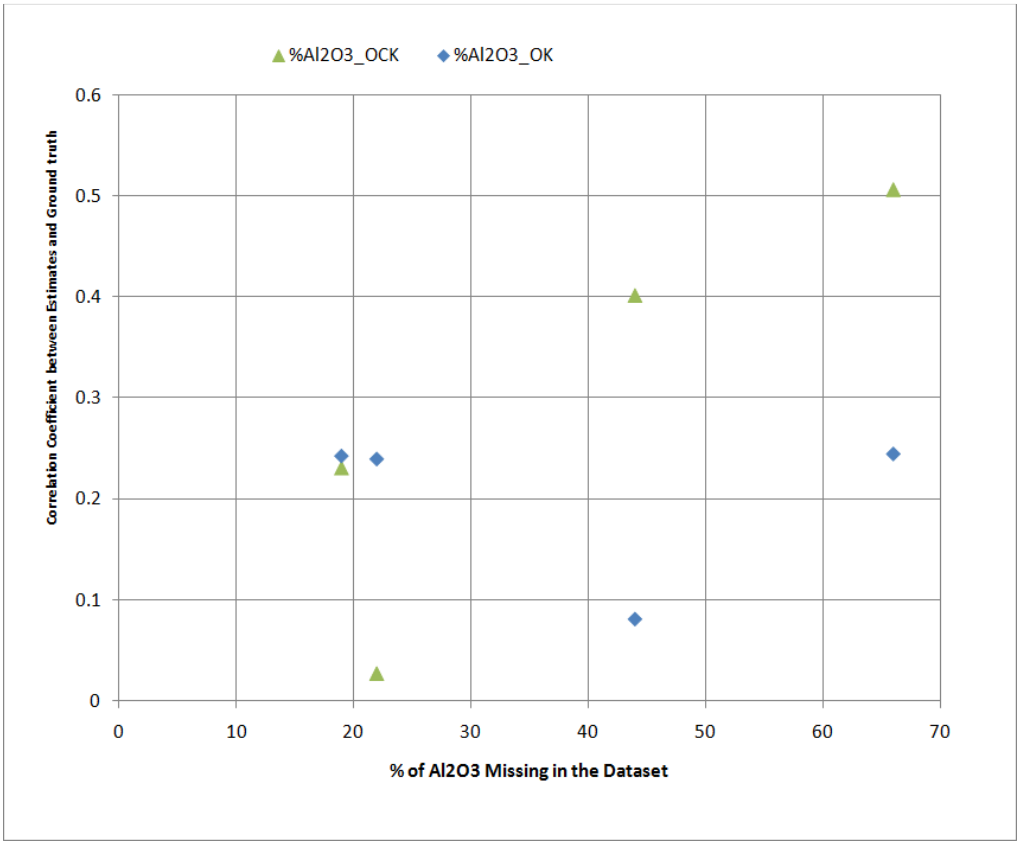


Figure 56: Correlation coefficient for %Al_2O_3 at different percentage of samples missing against ground truth.

It is a well-known phenomenon within literature that cokriging is beneficial when some of the variables are under-sampled; more so if the primary variable is under-sampled and the secondary variable is highly sampled. A potential drawback with this approach is that if the secondary variable is intensively sampled, a significant screening effect may exist (depending upon variogram model and search parameters), potentially resulting in large negative weightings (and possibly negative estimates as a consequences). A test was carried out on Al_2O_3 as a primary variable with different threshold of data missing, to see at what percentage threshold is using OCK of benefit to OK.

Figure 56 shows that as percentage of Al_2O_3 missing in the dataset above 44% percentage threshold tested; OCK is a preferred estimator of Al_2O_3 to that of OK.

8 CONCLUSION

The conclusion drawn from the study is that OK and OCK performs equally when the primary and secondary variables are sampled at the same locations; as observed in **Figure 55** in that estimating Fe as a primary variable using OK and OCK displays similar correlation coefficient tested against the five simulations ran. The study has confirmed as with most literatures that cokriging is not worthwhile if primary and secondary variables are sampled at the same locations (isotopic situation). However the study has also demonstrated a motivating factor for performing OCK, in that it enforces the relationship between variables as shown in **Table 9**.

The study has also shown the advantage of OCK when there is under-sampling, thus the heterotopic situation as shown in **Figure 56** using Al_2O_3 as a primary variable as an example. In this case OCK displays higher correlation between kriged estimates and ground truth to that of OK, given a test of heterotopic situation at 44% and 66% of Al_2O_3 missing in the dataset.

Table 10: Summary of the results of the two estimation methods

	Summary of Results	
Estimation Method	**OK**	**OCK**
Description	OK unbiased linear estimator that constrains the sum of weights to be 1, therefore the mean does not need to be known.	OCK unbiased linear estimator that allows secondary variable to be integrated into the kriging matrix, forcing the primary data weights to sum to one whereas the weights of each secondary variables are constrained to sum to zero
Time Required for Execution	Medium	High
Reduce Kriging Variance	No	Yes
Increase Regression Slope	Yes	Yes
Correlation with Ground Truth	Higher	High
Order of Preference(Isotopic Data)	1	2
Order of Preference(Heterotopic Data, Data Correlated)	2	1

Ultimately the choice of estimation method may depend on a number of factors:

- The type of dataset whether heterotopic or isotopic
- The geometry of the dataset whether is closely spaced or sparse
- The quality of the variogram /cross variogram – it is not easy to derive variograms from a sparse dataset thus alternative method such as normalising of the dataset.

9 REFERENCES

1. Armstrong, M. (1998) Basic Linear Geostatistics. Springer-Verlag Berlin Capability, Perth, Australia, p 231.

2. Bohling, G. (2005) Kriging. Kansas Geological Survey.

3. Cairncross, B. and Dixon, R. (1995) Minerals of South Africa. Geol. Soc. S.Africa, Johannesburg, p 290.

4. Coombes, J. (2008) The Art and Science of Resource Estimation.

5. Deutsch, C.V. and Journal, A.G. (1998) GSLIB – Geostatistical Software Library and User's guide. Oxford University Press, p 363.

6. De-Vitry, C., Vann, J., and Arvidson, H. (2007) Multivariate Iron Ore Deposit Resource Estimation – A Practitioner's Guide to Selecting Methods. *Applied Earth Science (Trans. Inst.Min. Metall. B),* Vol. 119 No. 3: p 154-165.

7. Glacken, I. M. and Snowden, D .V. (2001) Mineral Resource Estimation, in *Mineral Resource and OreReserve Estimation – The AusIMM Guide to Good Practice* (Ed: A CEdwards), (The Australasian Institute of Mining and Metallurgy: Melbourne), p 189-198.

8. Goovaerts, P., (1998) Ordinary Cokriging Revisited. Mathematical Geology, vol.30, No.1.

9. *http://www.biddle.com/documents/bcg_comp_chapter2.pdf (*Accessed on the 25 September 2012).

10. Isaaks, E and Srivastava, R.M. (1989) An Introduction to Applied Geostatistics, Oxford University Press, p 56.

11. Journel, A.G. and Huijbregts, CH.J (1978) Mining Geostatistics. Academic Press Inc, London, p303.

12. Moore, J.M., Tsikos, H. and Polteau, S. (2001). Deconstructing the Transvaal Supergroup, South Africa: Implications for Palaeoproterozoic Palaeoclimate Models. *Journal of African Earth Sciences.* Vol. 33: p 437-444.

13. Morris, R.C., Thornber M.R. and Ewers, W.E.(1980). Deep Seated Iron Ores from Banded Iron Formation. Nature 288, p 250 -252.

14. Meyers, D.E. (1992) Cokriging, Radial Basis Functions and the role of Positive Definiteness. Computers Math. Applications 24, p 139-148.

15. Myers, D.E. (1994) Statistical Methods for Interpolation of Spatial Data. J. Applied Science and Computations 1, p 283- 318.

16. Nel, D., *Personal Communication*, 17th October 2013.

17. Netshiozwi, S.T. (2002), Origin of High Grade Hematite Ores at Thabazimbi Mine, Limpopo Province, South Africa. Dissertation, Rand Afrikaans University.

18. Snowden, D.V. (1996), *Practical Interpretation of Mineral Resource and Ore Reserve Classification Guidelinesftp://www.ige.unicamp.br/pub/ge_902/.../reservas_snowden.pdf (Accessed on the 18th October 2011).*

19. Vann, J., Jackson, S. and Bertoli, O. (2003). Quantitative Kriging Neighbourhood Analysis for the Mining Geologist – A Description of the Method with Worked Case Examples. In: Proceedings Fifth International Mining Geology Conference, (The Australasian Institute of Mining and Metallurgy: Melbourne), p 215-223.

20. Vann, J., Jackson, S. and Bertoli, O. (2002). An Overview of Geostatistical Simulation for Quantifying Risk. In: Proceedings to Geostatistical Association of Australian symposium "Quantifying Risk and Error".

21. Van Schalkwyk,J.F., and Beukes, N.J. (1986). The Sishen iron ore deposit, Griqualand West, 931 – 956. In: Anhaeusser, C.R. and Maske, S., Eds., Mineral Deposits of Southern Africa, I: Geol. Soc. S. Afr., Johannesburg. 1020 pp.

22. Welmer, F.W., 1998. Statistical Evaluations in Exploration for Mineral Deposits Springer - Verlag, Berlin.

APPENDIX: 1 STATISTICS

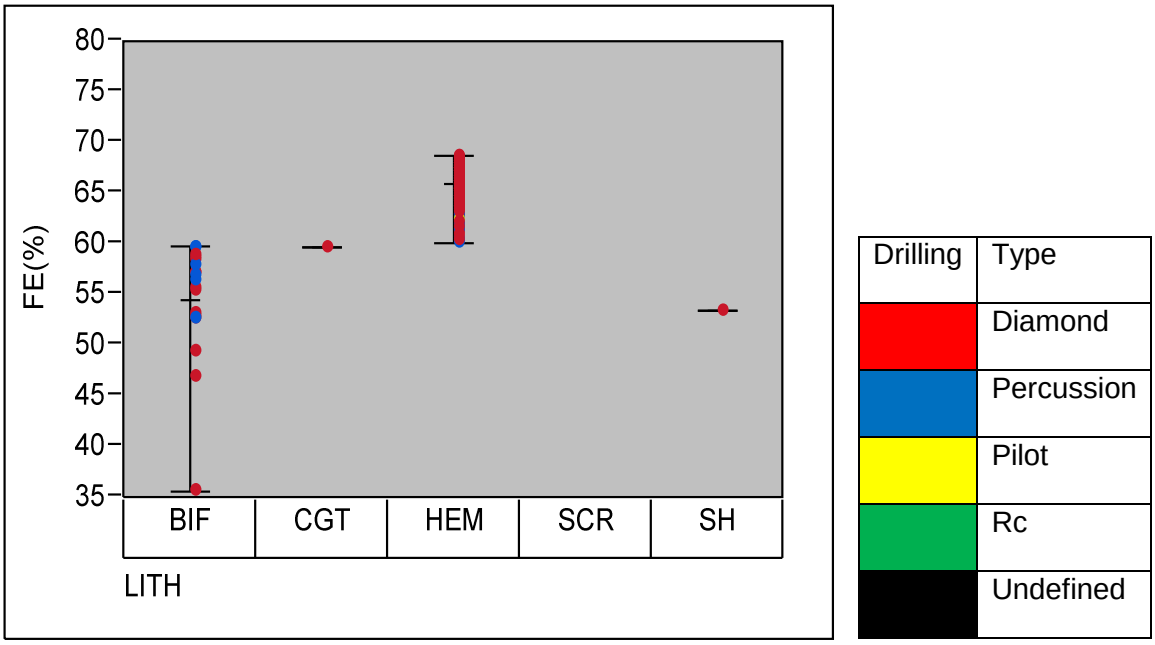


Figure 57: %Fe grade Variation in different rock types

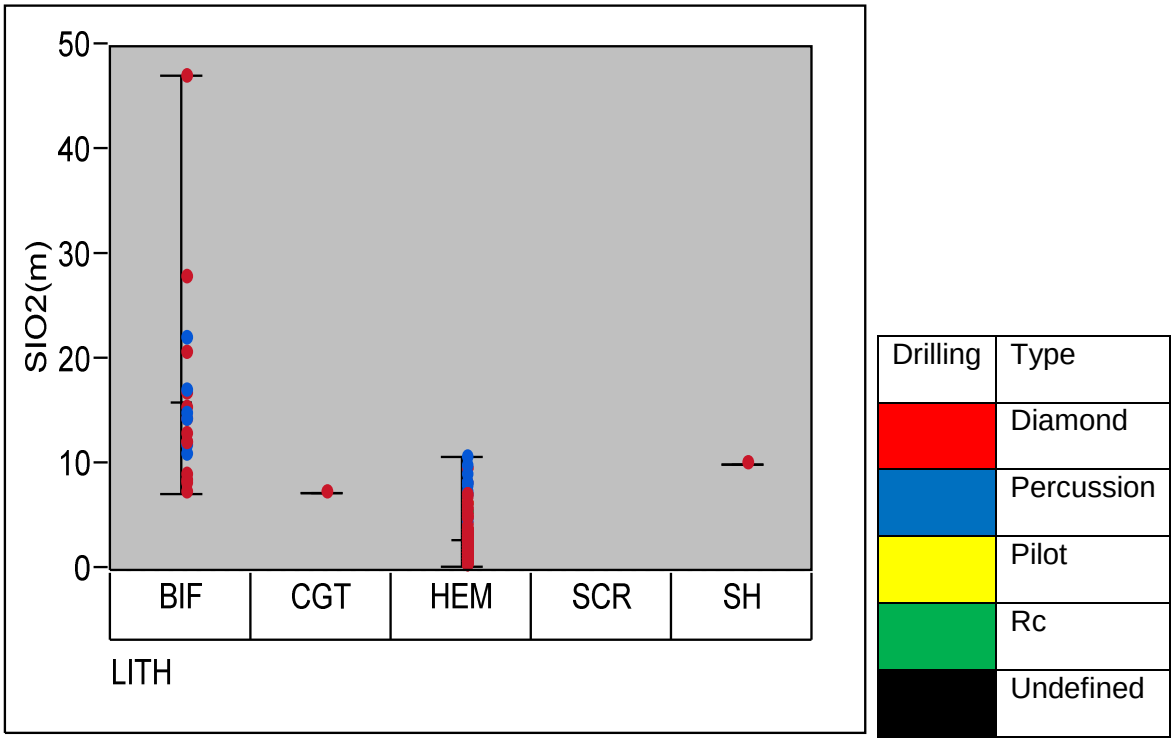


Figure 58: %SiO_2 Variation in different rock types

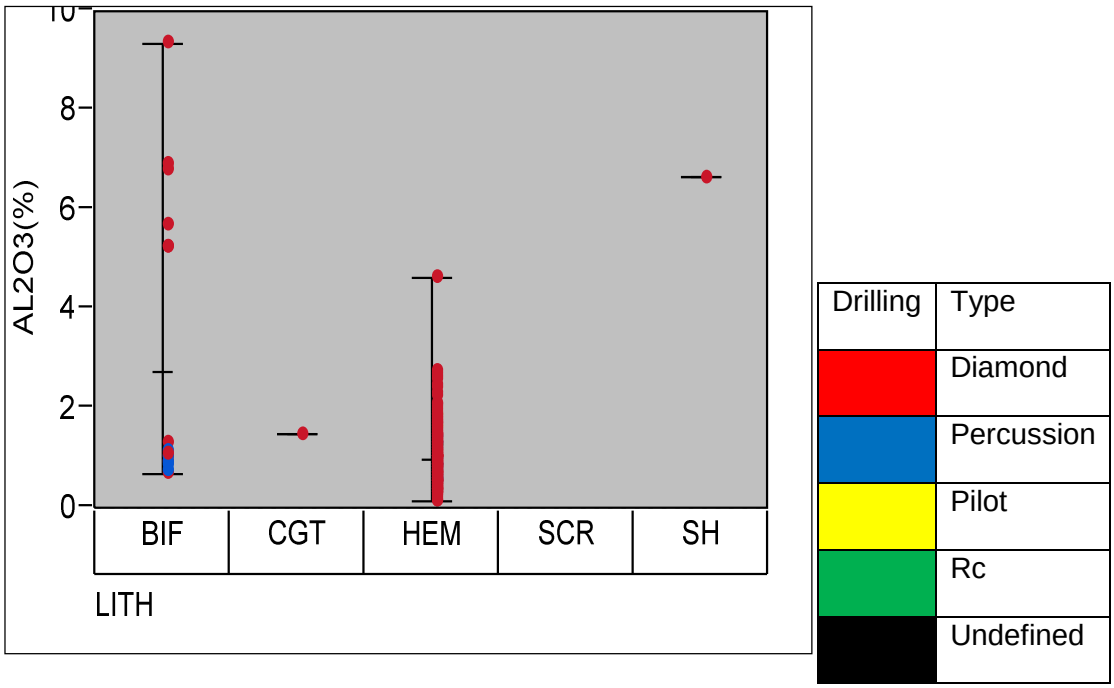


Figure 59: %Al_2O_3 Variability in different rock types

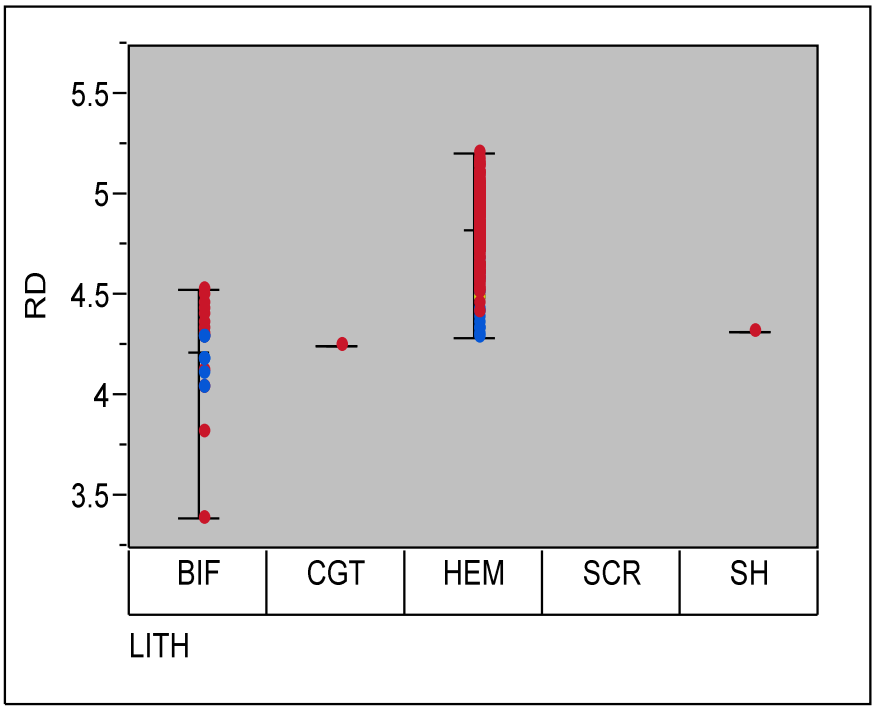


Figure 60: RD Variation in different rock types

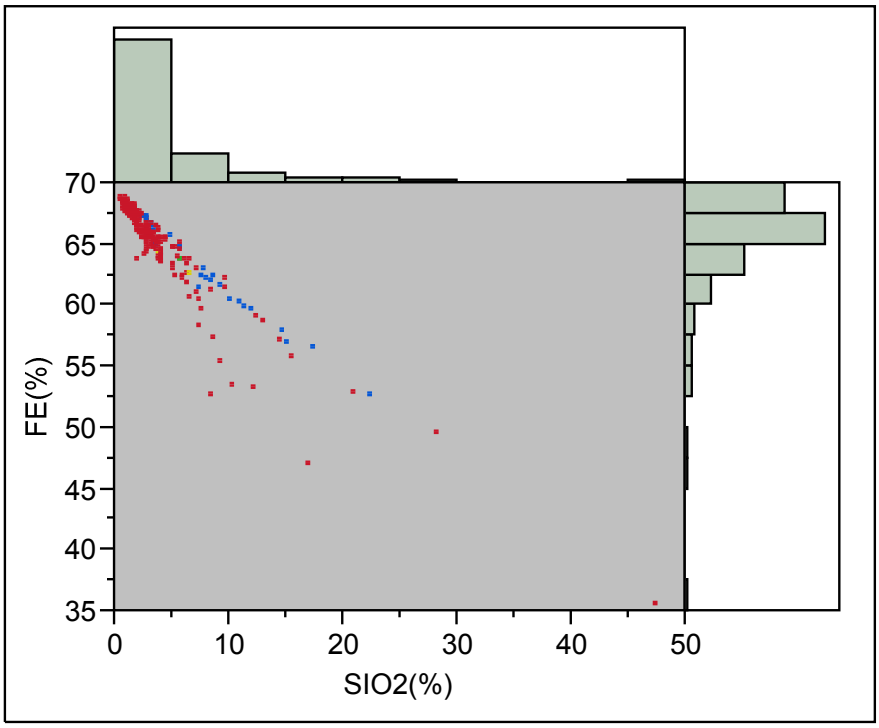


Figure 61: Scatterplot of %Fe vs %SiO_2

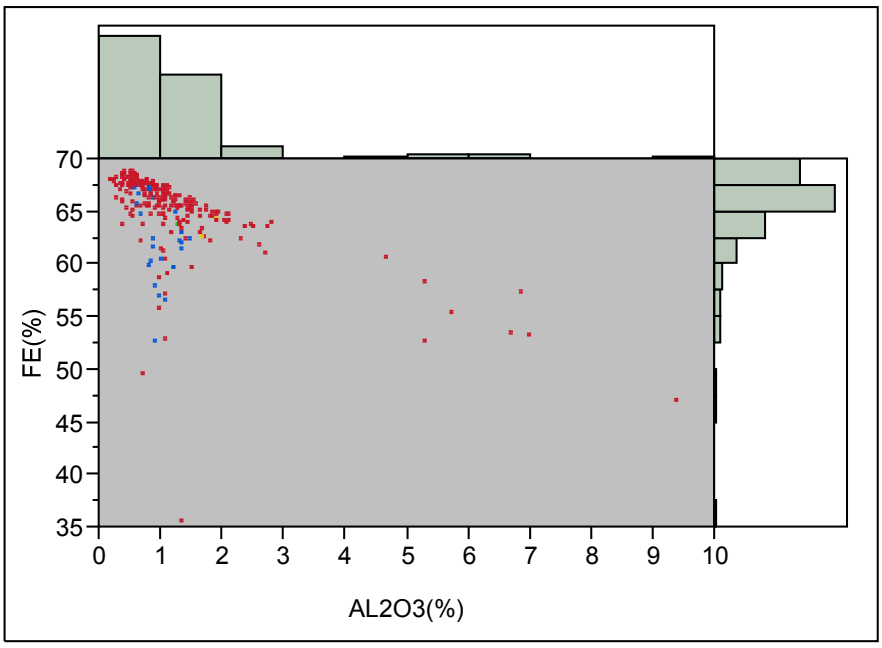


Figure 62: Scatterplot %Fe vs %Al_2O_3

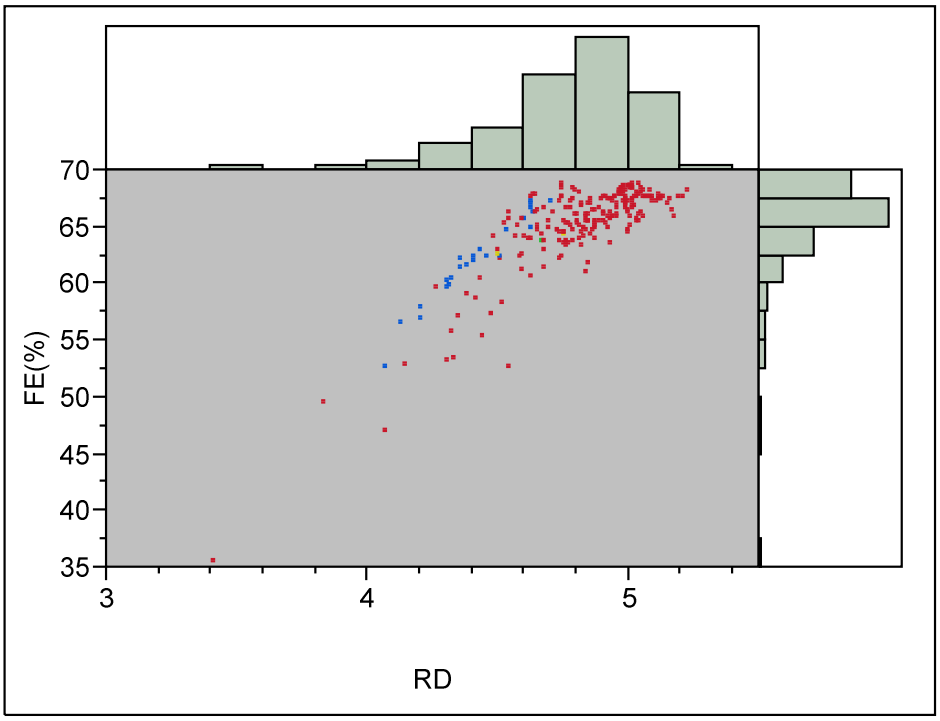


Figure 63: Scatterplot %Fe vs RD

APPENDIX: 2 VARIOGRAM BOREHOLE DATA WITH BOTH DIAMOND DRILLED AND PERCUSSION SAMPLES

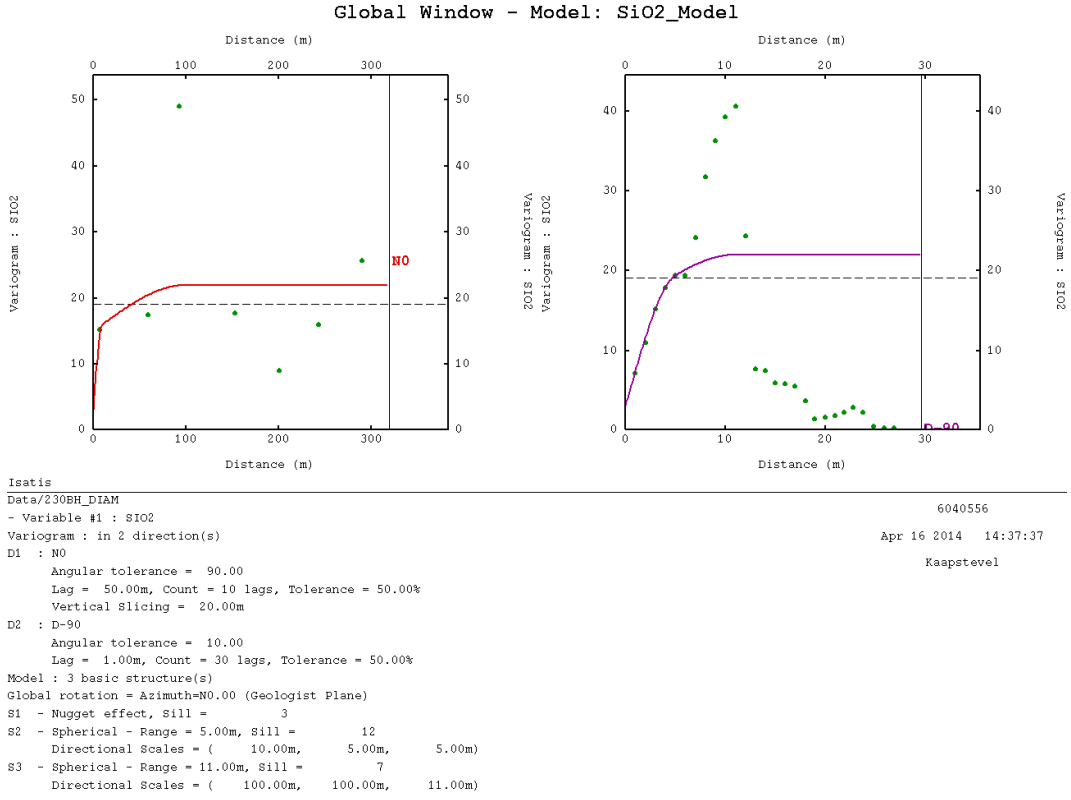


Figure 64: Experimental Variogram %SiO_2Variogram

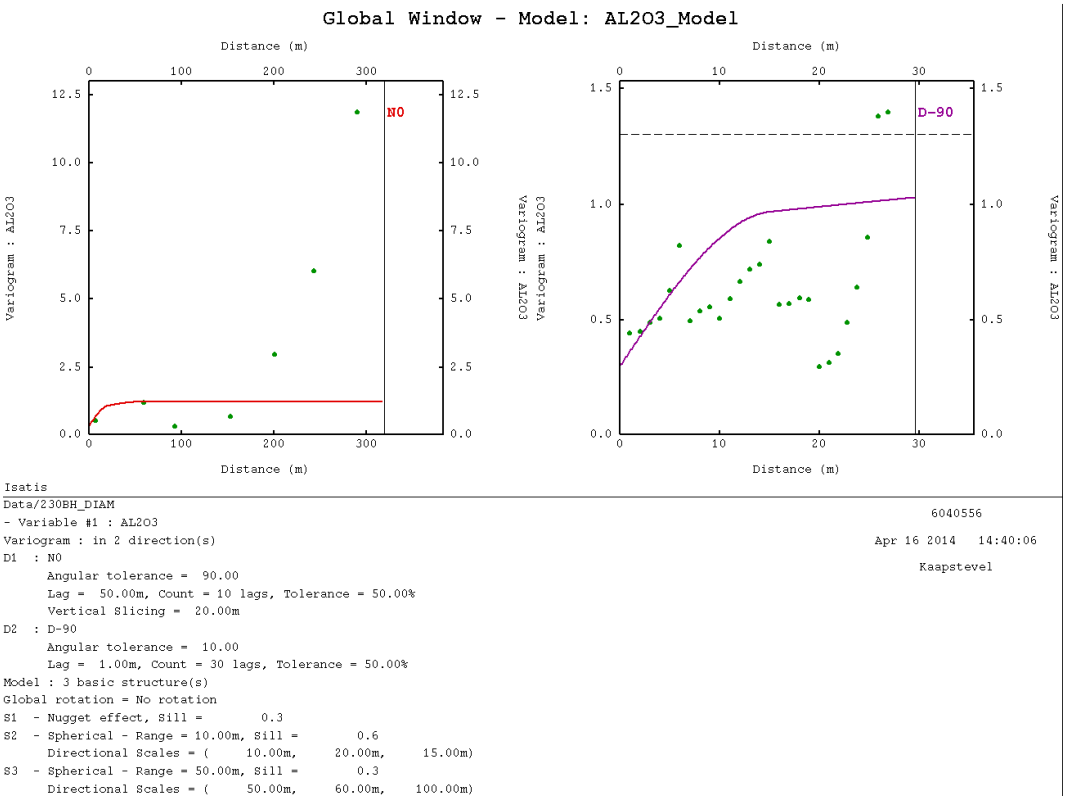


Figure 65: Experimental Variogram %Al_2O_3 Variogram

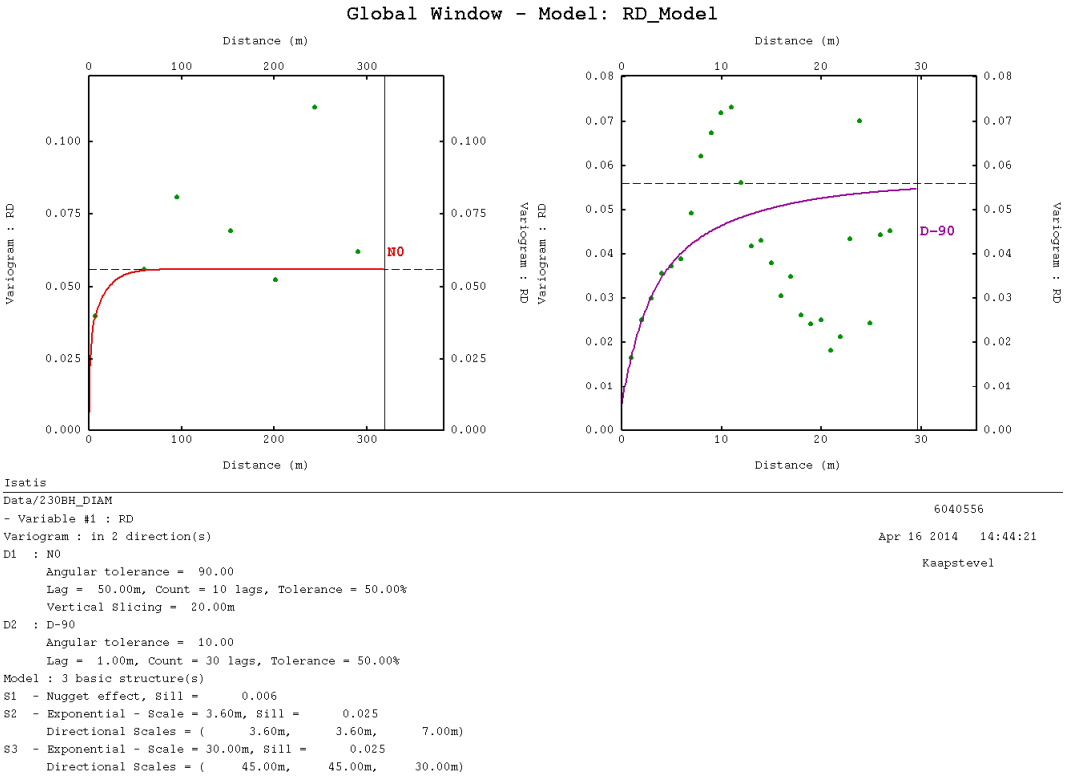


Figure 66: Experimental Variogram RD Variogram

APPENDIX: 3 GAUSSIAN ANARMORPHOSIS TRANSFORMATION

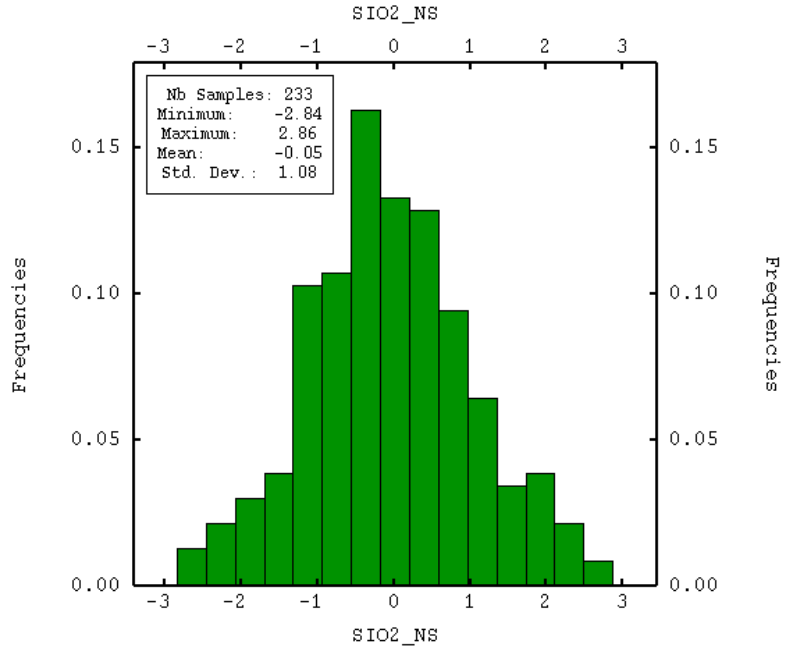


Figure 67: %SiO_2 GAUSSIAN Anamorphosis Transformation

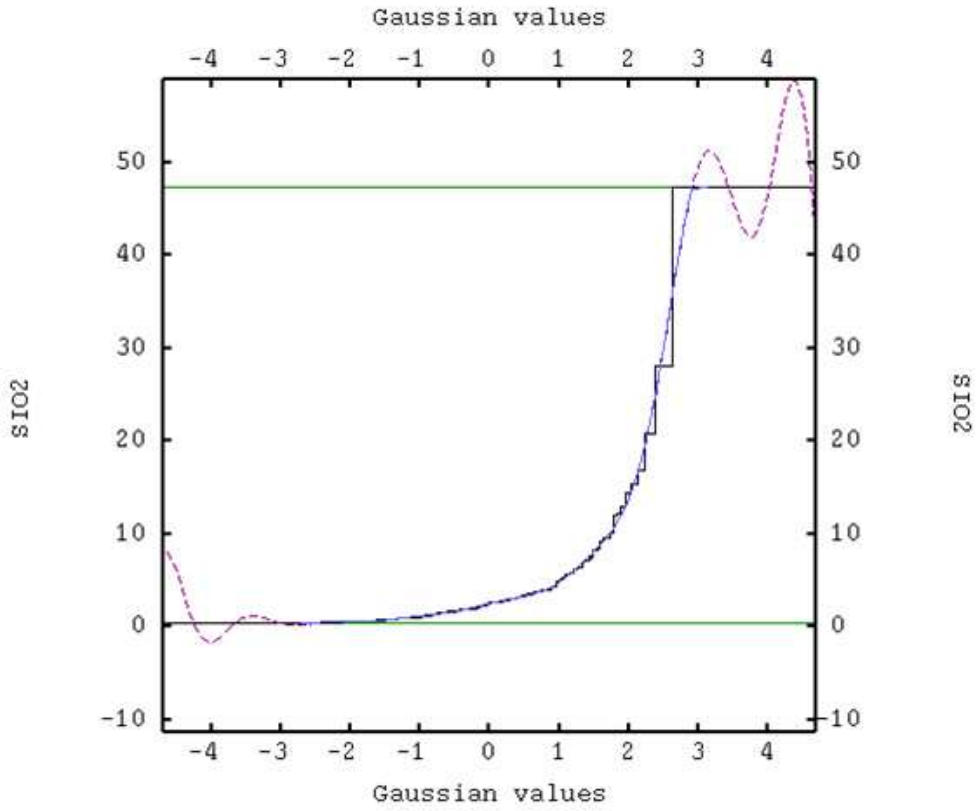


Figure 68: %SIO_2 GAUSSIAN Anamorphosis Transformation Model

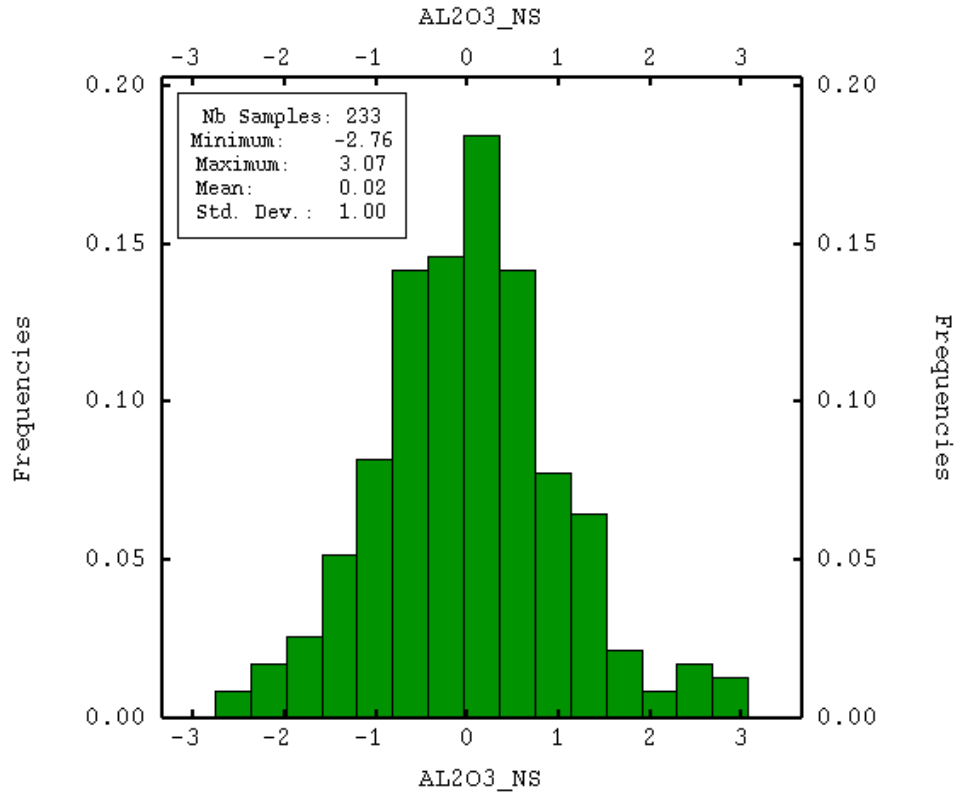


Figure 69: %Al_2O_3 GAUSSIAN Anamorphosis Transformation

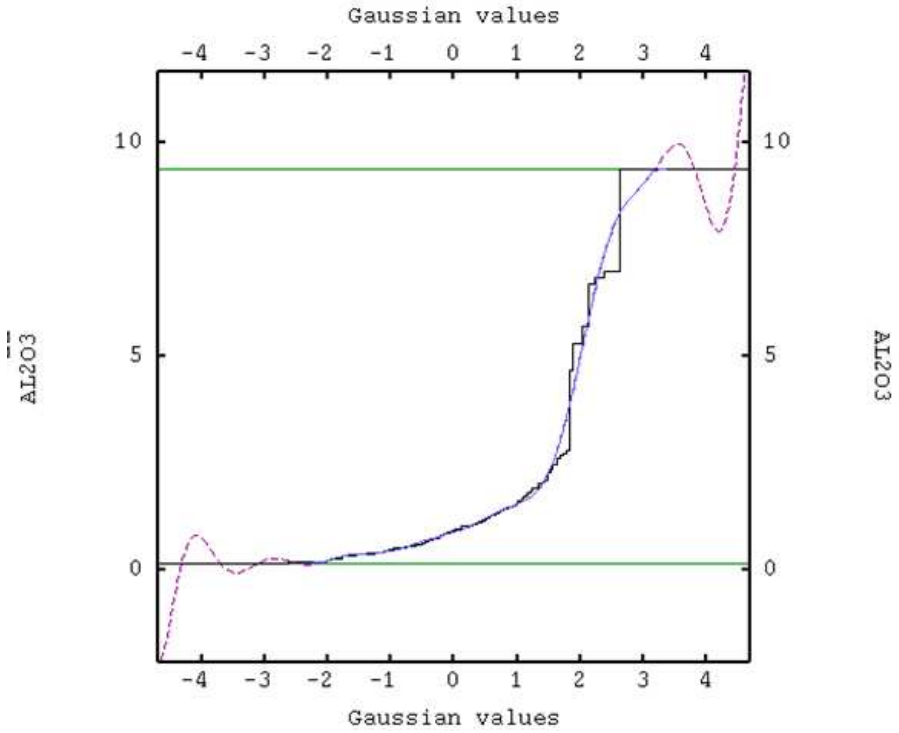


Figure 70: %Al_2O_3 GAUSSIAN Anamorphosis Transformation Model

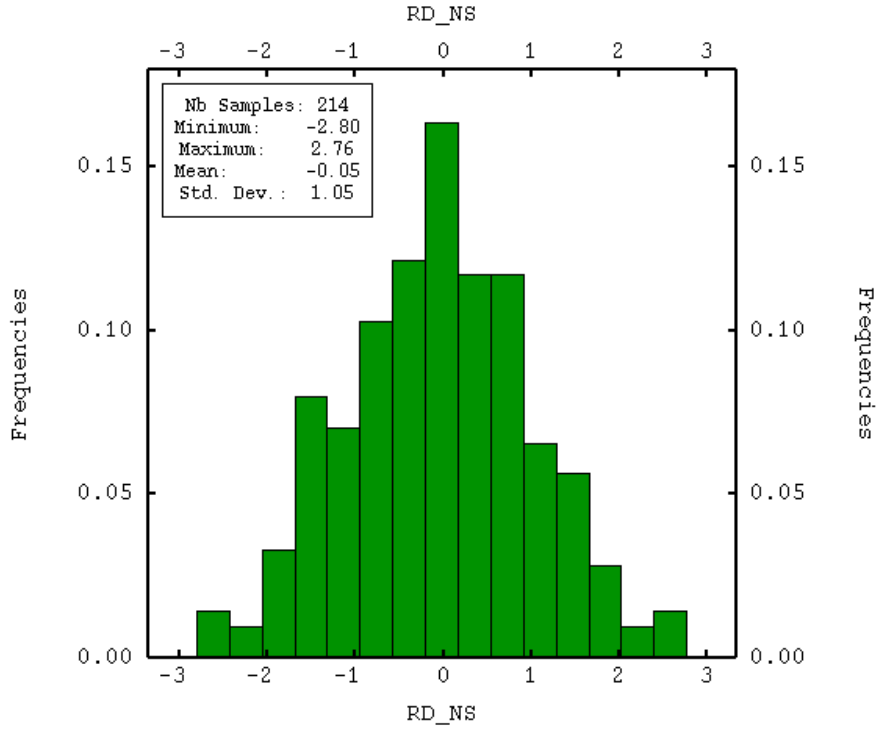


Figure 71: RD GAUSSIAN Anamorphosis Transformation

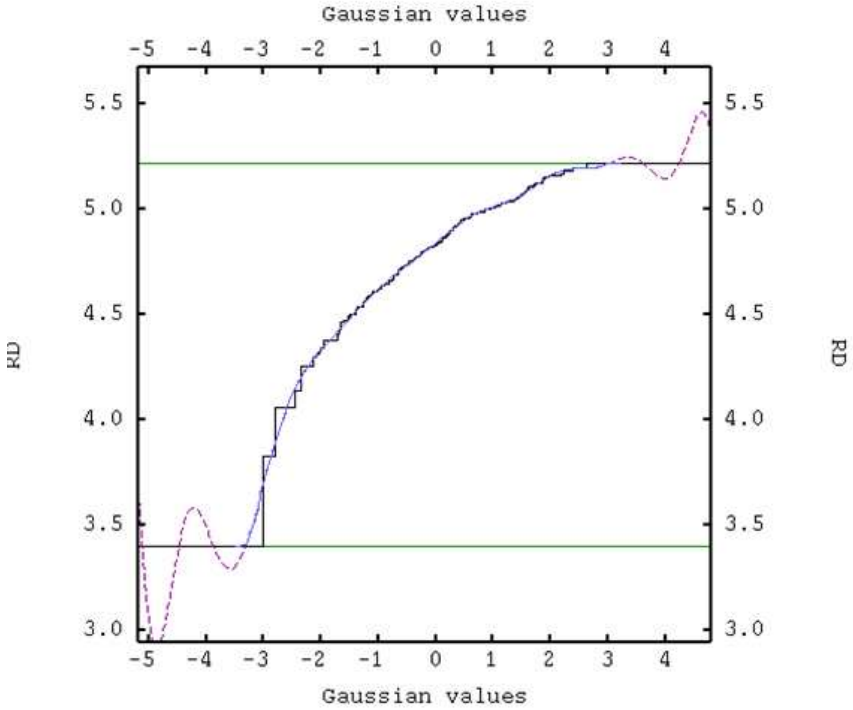
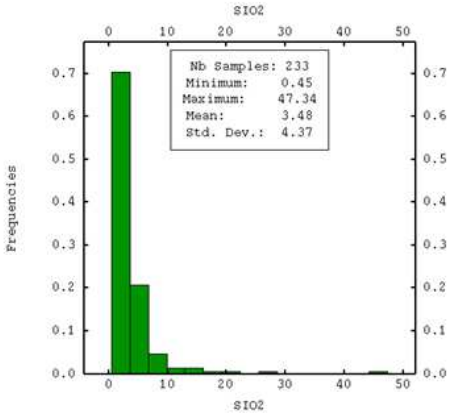
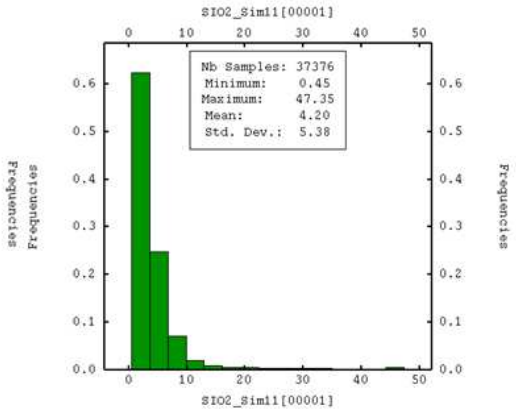
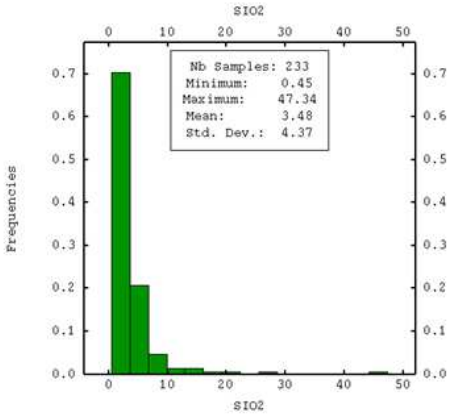


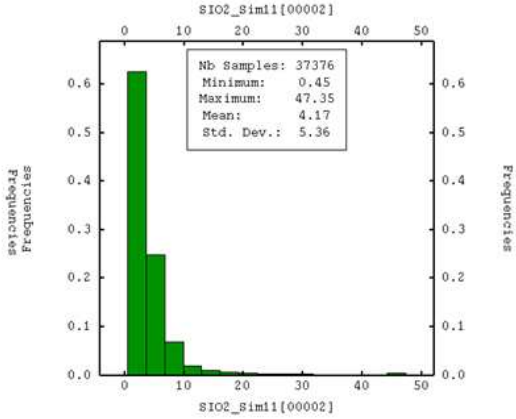
Figure 72: RD GAUSSIAN Anamorphosis Transformation Model

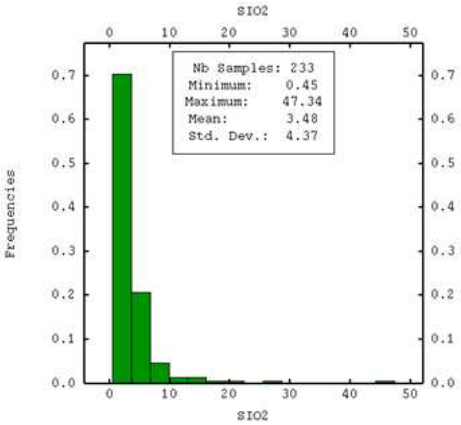
APPENDIX: 4 CONDITIONAL SIMULATION PROPERTIES

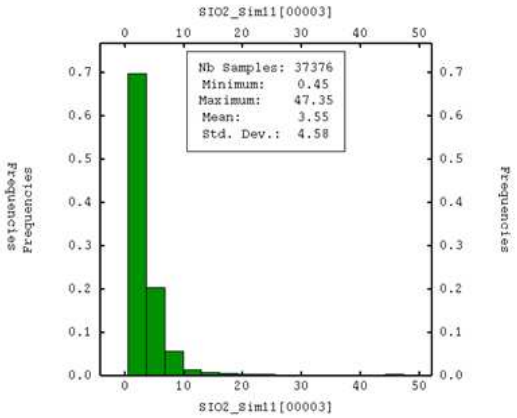


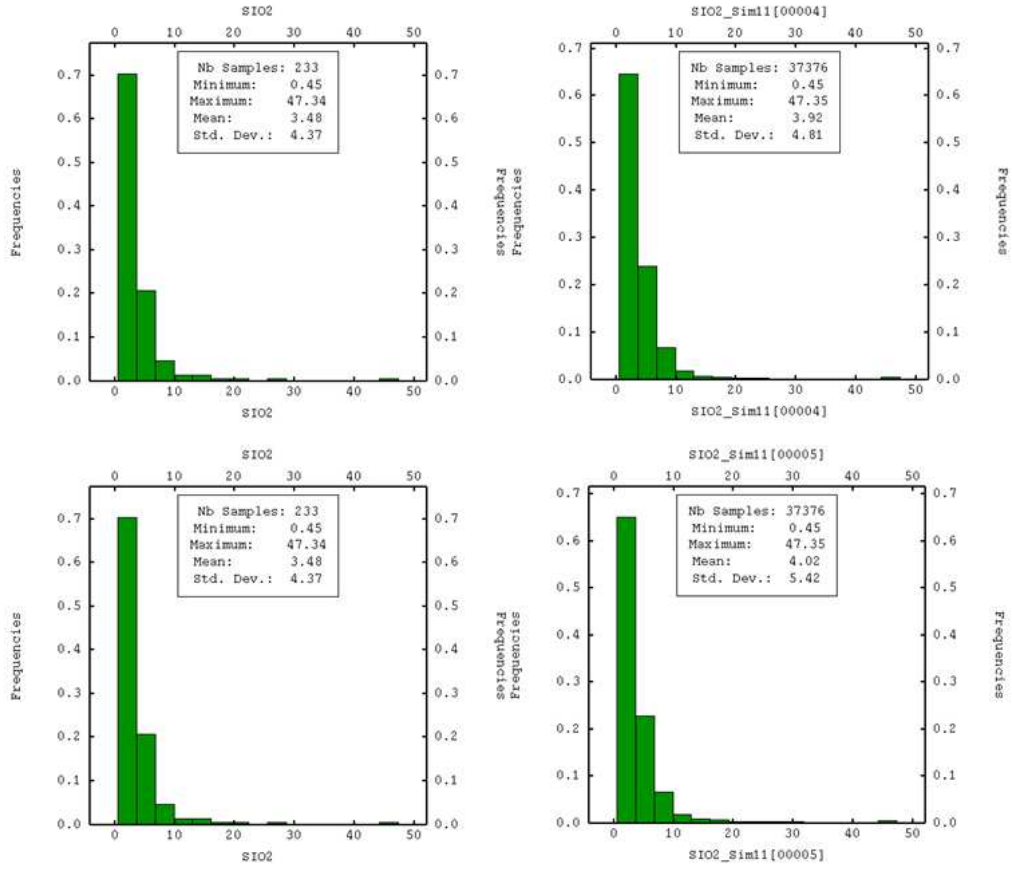


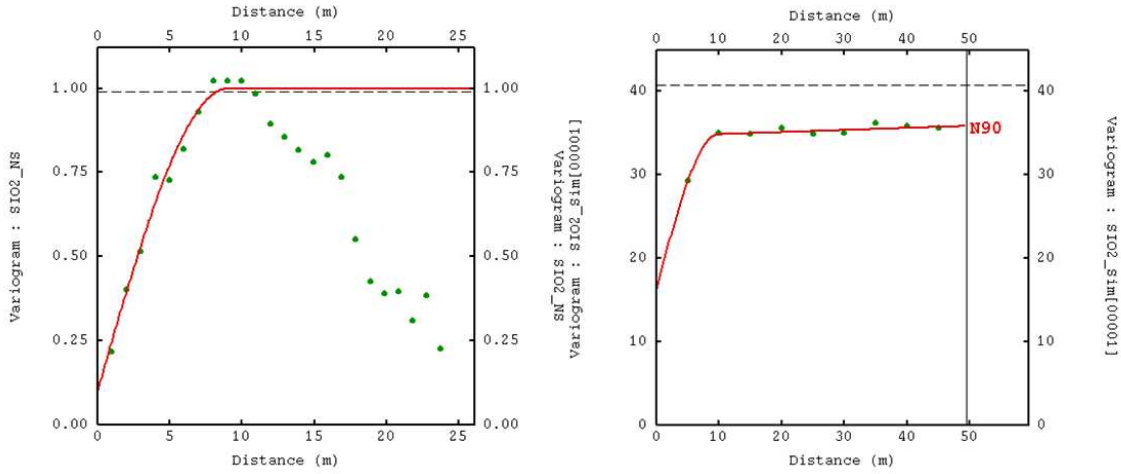


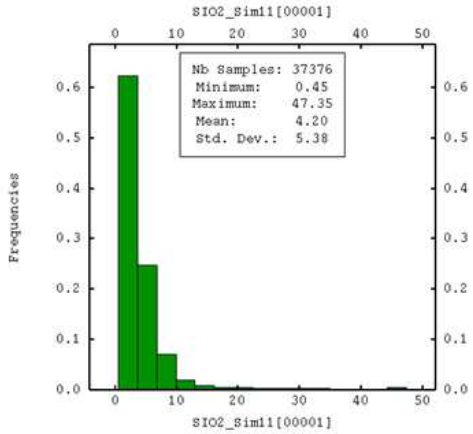


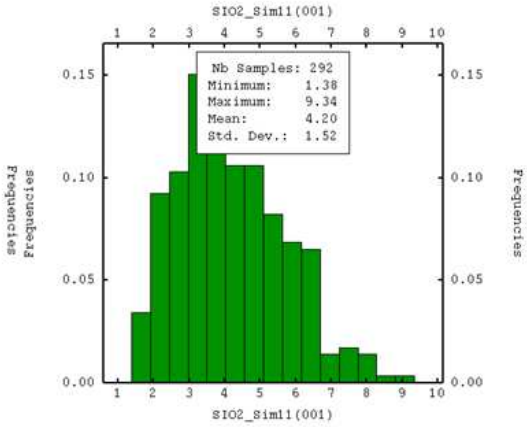


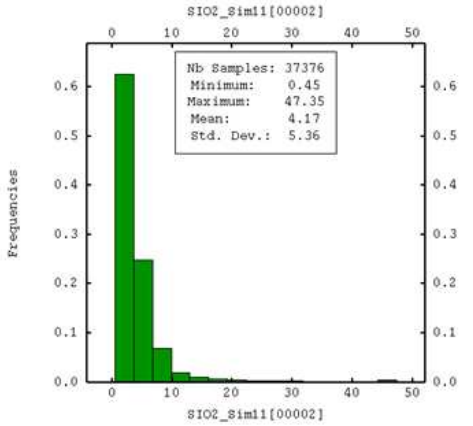


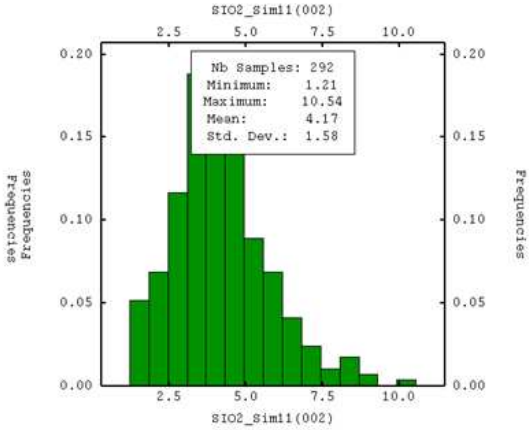

SIO2
Nb Samples: 233
Minimum: 0.45
Maximum: 47.34
Mean: 3.48
Std. Dev.: 4.37
Frequencies
SIO2_Sim11[00004]
Nb Samples: 37376
Minimum: 0.45
Maximum: 47.35
Mean: 3.92
Std. Dev.: 4.81
SIO2_Sim11[00005]
Nb Samples: 37376
Minimum: 0.45
Maximum: 47.35
Mean: 4.02
Std. Dev.: 5.42

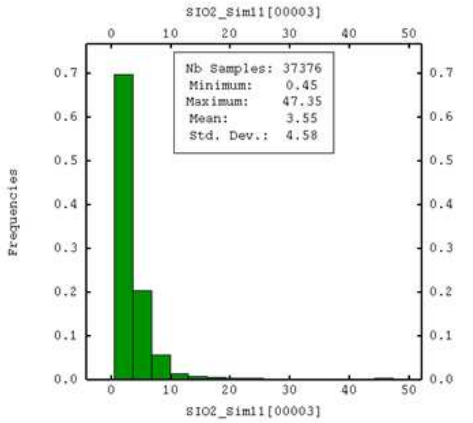

Distance (m)
Variogram : SIO2_NS
Variogram : SIO2_Sim[00001]
N90

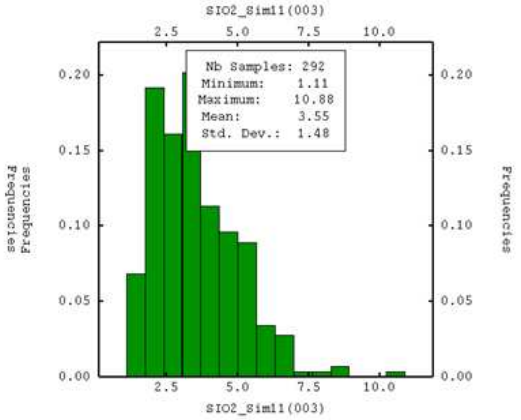

SIO2_Sim11[00001]
Nb Samples: 37376
Minimum: 0.45
Maximum: 47.35
Mean: 4.20
Std. Dev.: 5.38
Frequencies
SIO2_Sim11[00001]


SIO2_Sim11(001)
Nb Samples: 292
Minimum: 1.38
Maximum: 9.34
Mean: 4.20
Std. Dev.: 1.52
Frequencies
SIO2_Sim11(001)


SIO2_Sim11[00002]
Nb Samples: 37376
Minimum: 0.45
Maximum: 47.35
Mean: 4.17
Std. Dev.: 5.36
Frequencies
SIO2_Sim11[00002]


SIO2_Sim11(002)
Nb Samples: 292
Minimum: 1.21
Maximum: 10.54
Mean: 4.17
Std. Dev.: 1.58
Frequencies
SIO2_Sim11(002)


SIO2_Sim11[00003]
Nb Samples: 37376
Minimum: 0.45
Maximum: 47.35
Mean: 3.55
Std. Dev.: 4.58
Frequencies
SIO2_Sim11[00003]


SIO2_Sim11(003)
Nb Samples: 292
Minimum: 1.11
Maximum: 10.88
Mean: 3.55
Std. Dev.: 1.48
Frequencies
SIO2_Sim11(003)

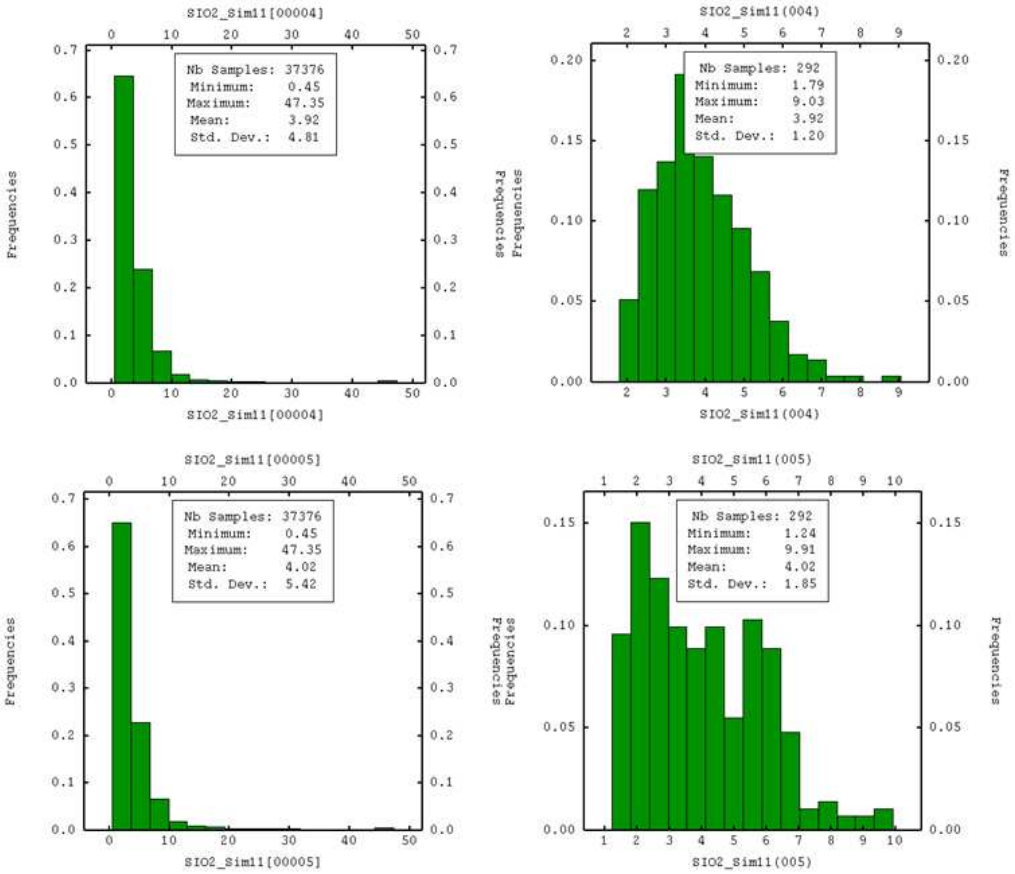
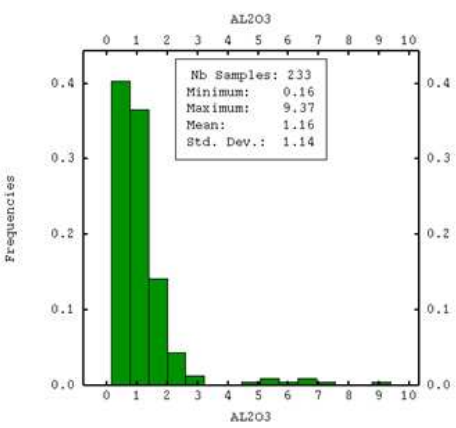
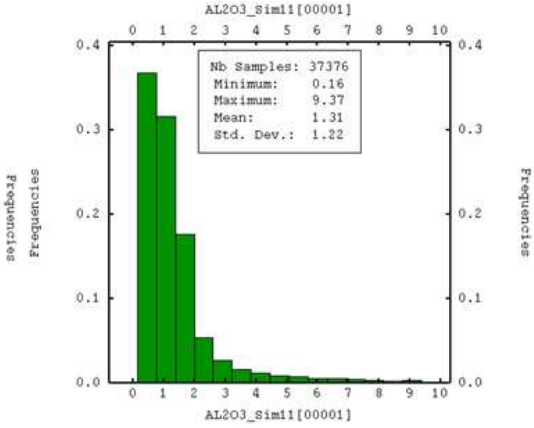
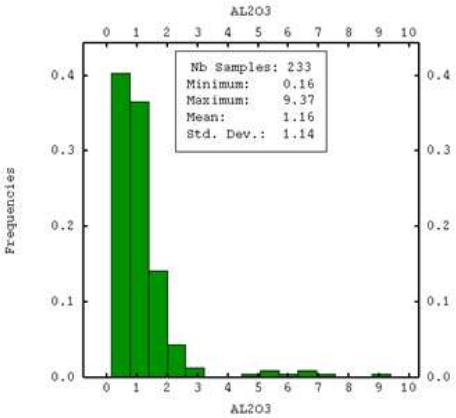
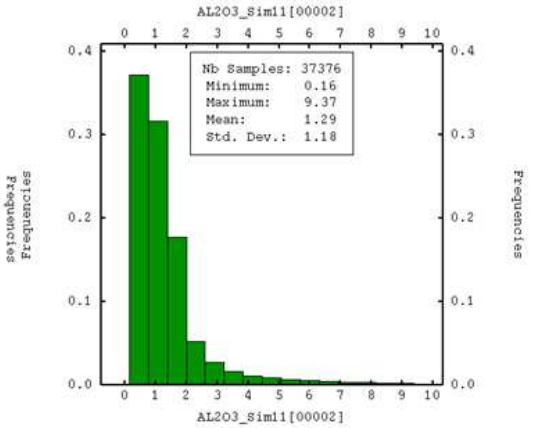


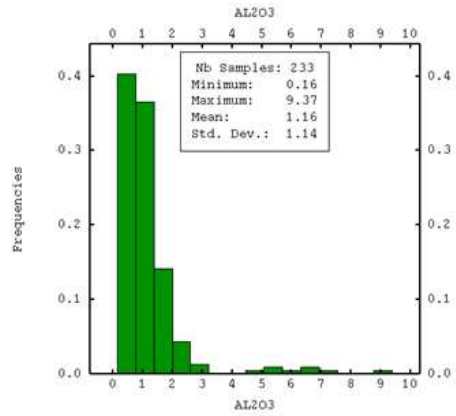
Figure 73: %SiO_2 Conditional Properties

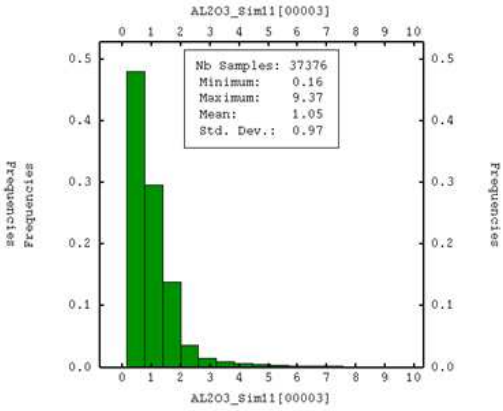

AL2O3
Nb Samples: 233
Minimum: 0.16
Maximum: 9.37
Mean: 1.16
Std. Dev.: 1.14
Frequencies
AL2O3

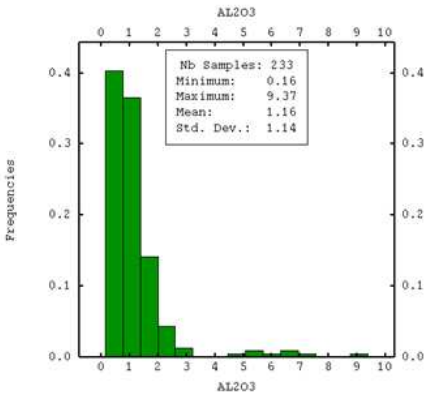

AL2O3_Sim11[00001]
Nb Samples: 37376
Minimum: 0.16
Maximum: 9.37
Mean: 1.31
Std. Dev.: 1.22
Frequencies
AL2O3_Sim11[00001]

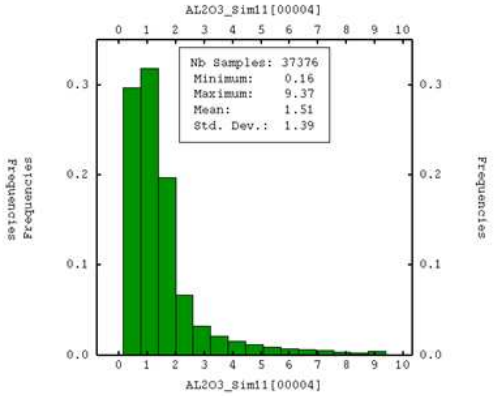

AL2O3
Nb Samples: 233
Minimum: 0.16
Maximum: 9.37
Mean: 1.16
Std. Dev.: 1.14
Frequencies
AL2O3

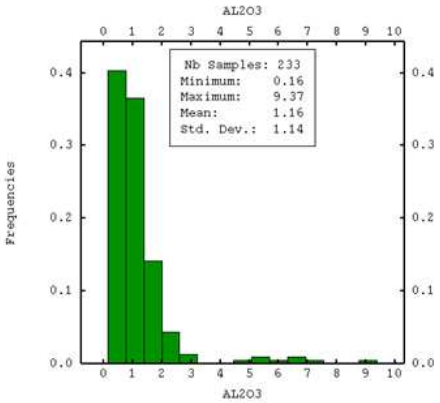

AL2O3_Sim11[00002]
Nb Samples: 37376
Minimum: 0.16
Maximum: 9.37
Mean: 1.29
Std. Dev.: 1.18
Frequencies
AL2O3_Sim11[00002]

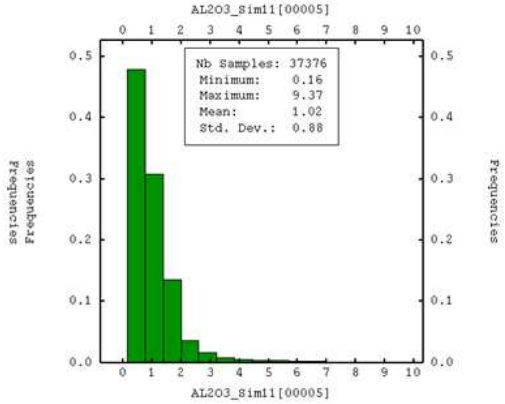

AL2O3
Nb Samples: 233
Minimum: 0.16
Maximum: 9.37
Mean: 1.16
Std. Dev.: 1.14
Frequencies
AL2O3

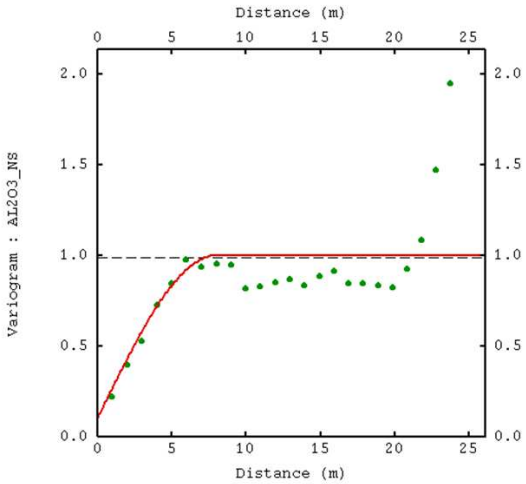

AL2O3_Sim11[00003]
Nb Samples: 37376
Minimum: 0.16
Maximum: 9.37
Mean: 1.05
Std. Dev.: 0.97
Frequencies
AL2O3_Sim11[00003]

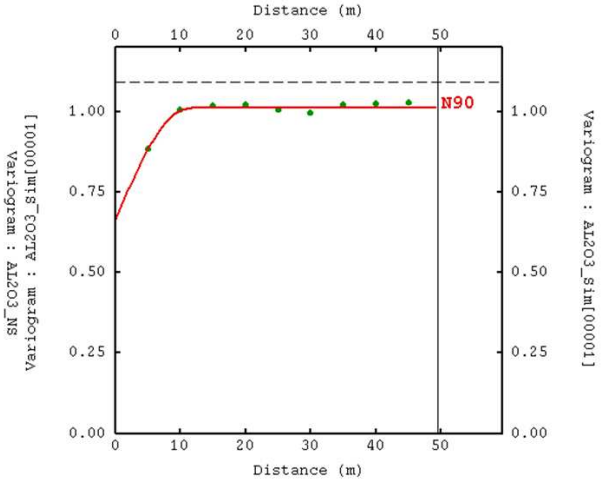

AL2O3
Nb Samples: 233
Minimum: 0.16
Maximum: 9.37
Mean: 1.16
Std. Dev.: 1.14
Frequencies
AL2O3

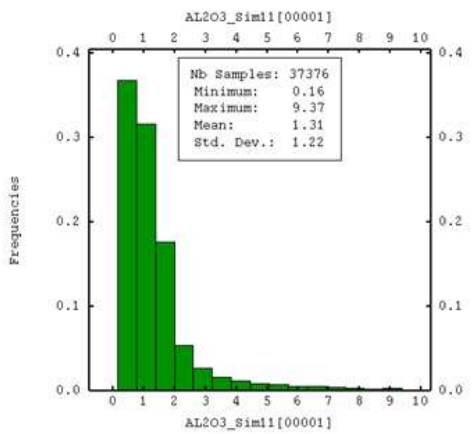

AL2O3_Sim11[00004]
Nb Samples: 37376
Minimum: 0.16
Maximum: 9.37
Mean: 1.51
Std. Dev.: 1.39
Frequencies
AL2O3_Sim11[00004]

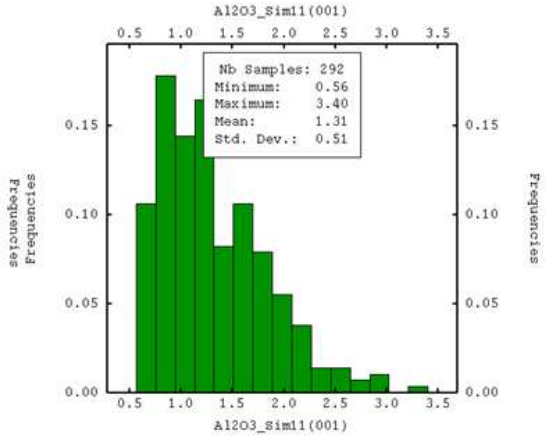

AL2O3
Nb Samples: 233
Minimum: 0.16
Maximum: 9.37
Mean: 1.16
Std. Dev.: 1.14
Frequencies
AL2O3

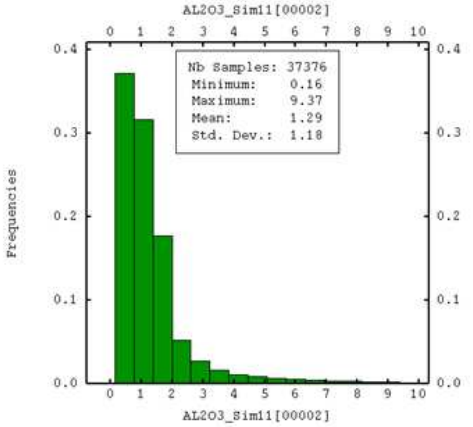

AL2O3_Sim11[00005]
Nb Samples: 37376
Minimum: 0.16
Maximum: 9.37
Mean: 1.02
Std. Dev.: 0.88
Frequencies
AL2O3_Sim11[00005]

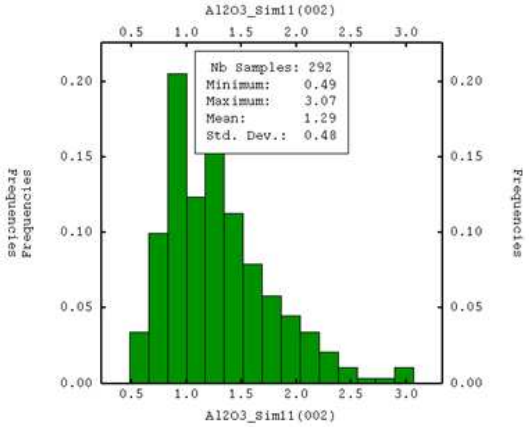

Distance (m)
Variogram : AL2O3_NS
Distance (m)

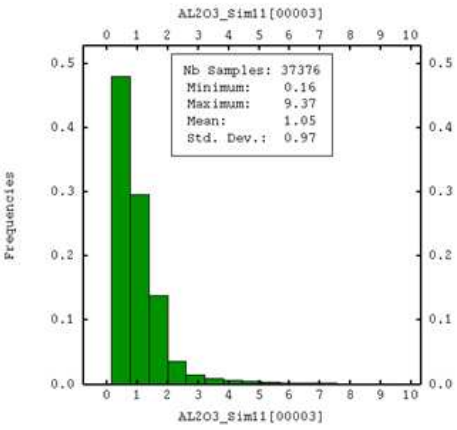

Distance (m)
N90
Variogram : AL2O3_NS
Variogram : AL2O3_Sim[00001]
Distance (m)

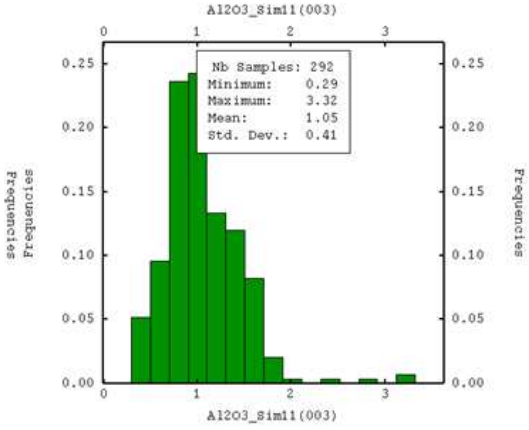

AL2O3_Sim11[00001]
Nb Samples: 37376
Minimum: 0.16
Maximum: 9.37
Mean: 1.31
Std. Dev.: 1.22
Frequencies
AL2O3_Sim11[00001]


Al2O3_Sim11(001)
Nb Samples: 292
Minimum: 0.56
Maximum: 3.40
Mean: 1.31
Std. Dev.: 0.51
Frequencies
Al2O3_Sim11(001)


AL2O3_Sim11[00002]
Nb Samples: 37376
Minimum: 0.16
Maximum: 9.37
Mean: 1.29
Std. Dev.: 1.18
Frequencies
AL2O3_Sim11[00002]


Al2O3_Sim11(002)
Nb Samples: 292
Minimum: 0.49
Maximum: 3.07
Mean: 1.29
Std. Dev.: 0.48
Frequencies
Al2O3_Sim11(002)


AL2O3_Sim11[00003]
Nb Samples: 37376
Minimum: 0.16
Maximum: 9.37
Mean: 1.05
Std. Dev.: 0.97
Frequencies
AL2O3_Sim11[00003]


Al2O3_Sim11(003)
Nb Samples: 292
Minimum: 0.29
Maximum: 3.32
Mean: 1.05
Std. Dev.: 0.41
Frequencies
Al2O3_Sim11(003)

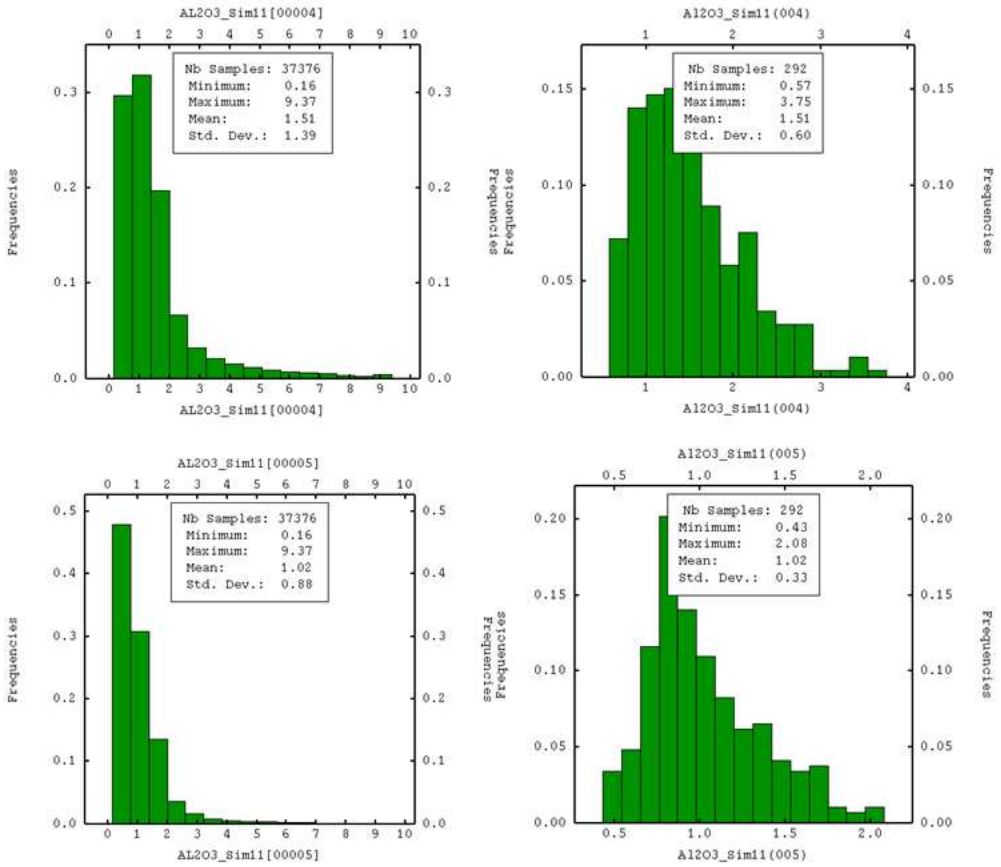
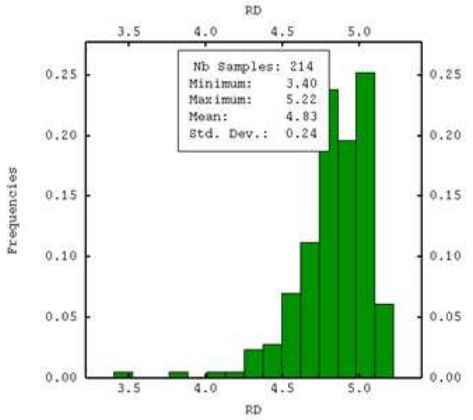
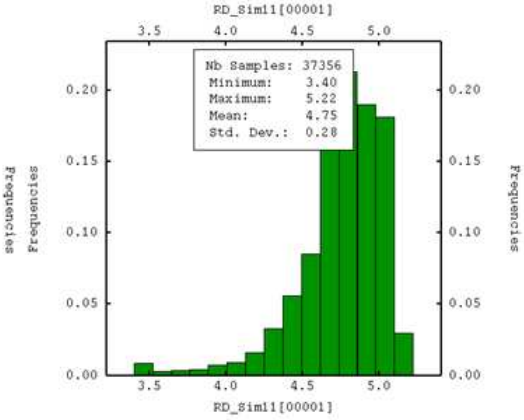
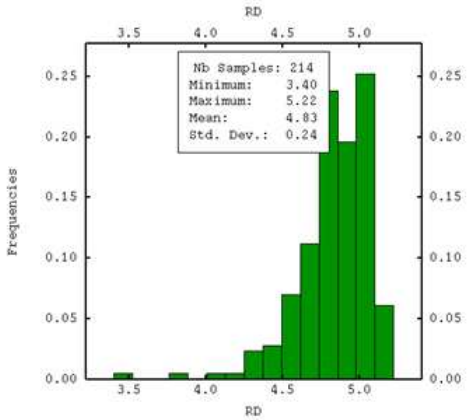
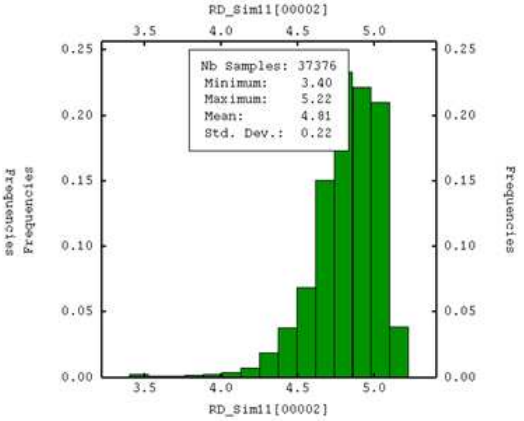


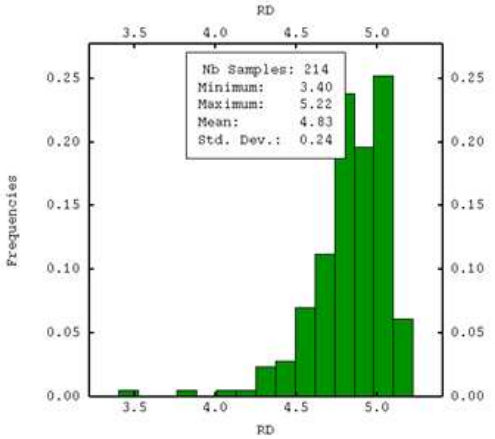
Figure 74: $\%Al_2O_3$ Conditional Properties

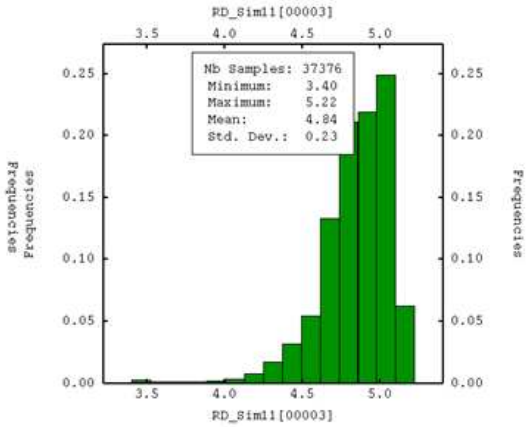

RD
Nb Samples: 214
Minimum: 3.40
Maximum: 5.22
Mean: 4.83
Std. Dev.: 0.24
Frequencies
RD

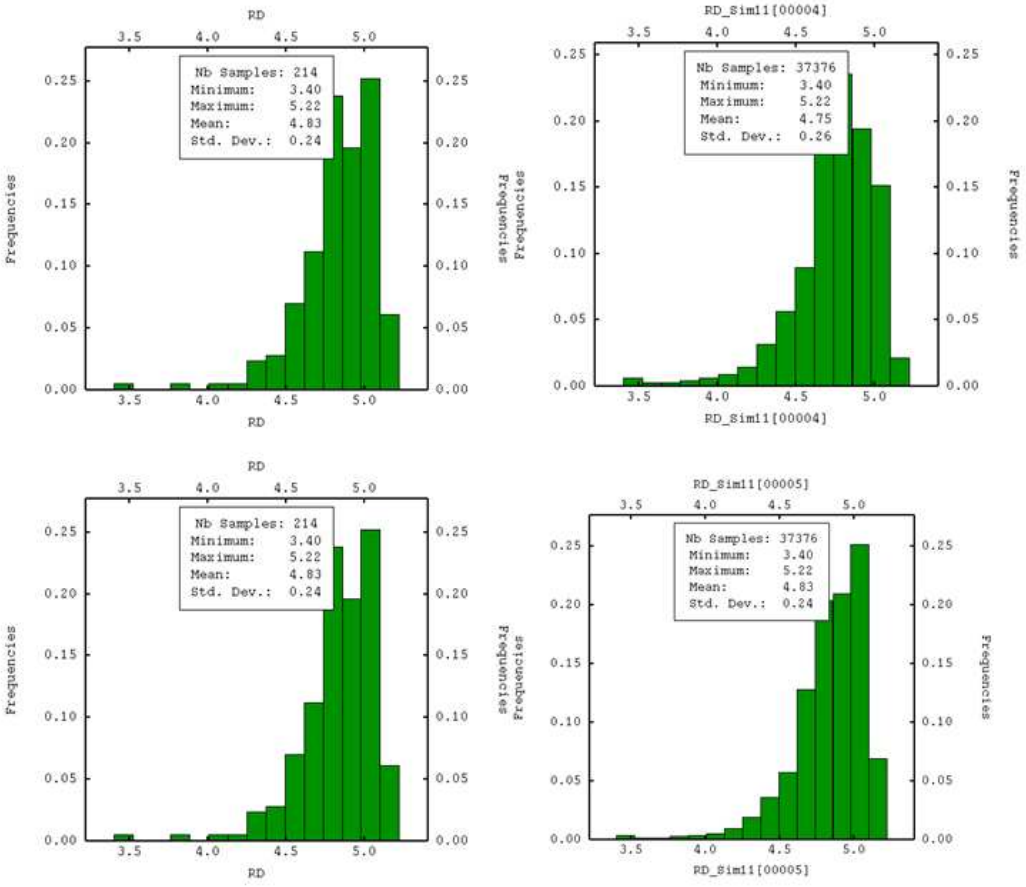

RD_Sim11[00001]
Nb Samples: 37356
Minimum: 3.40
Maximum: 5.22
Mean: 4.75
Std. Dev.: 0.28
Frequencies
RD_Sim11[00001]

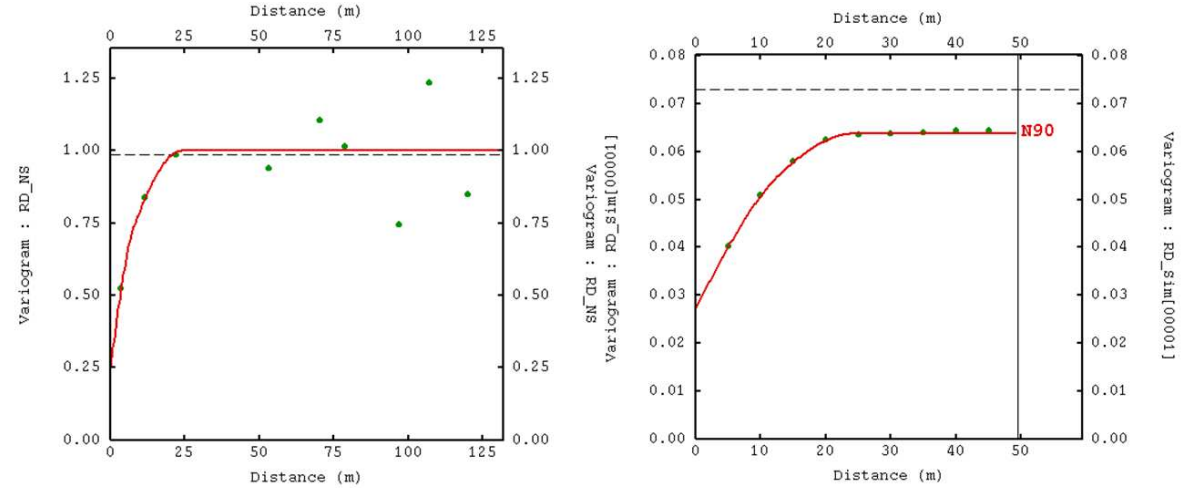

RD
Nb Samples: 214
Minimum: 3.40
Maximum: 5.22
Mean: 4.83
Std. Dev.: 0.24
Frequencies
RD

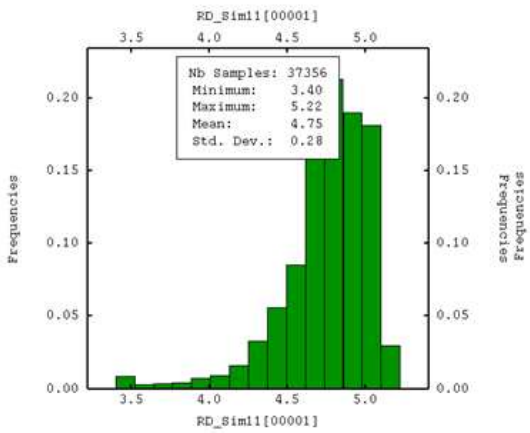

RD_Sim11[00002]
Nb Samples: 37376
Minimum: 3.40
Maximum: 5.22
Mean: 4.81
Std. Dev.: 0.22
Frequencies
RD_Sim11[00002]

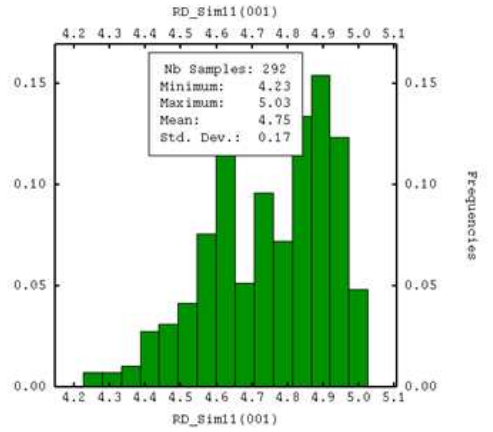

RD
Nb Samples: 214
Minimum: 3.40
Maximum: 5.22
Mean: 4.83
Std. Dev.: 0.24
Frequencies
RD

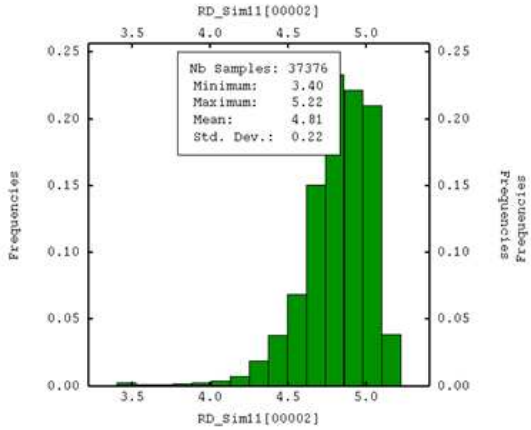

RD_Sim11[00003]
Nb Samples: 37376
Minimum: 3.40
Maximum: 5.22
Mean: 4.84
Std. Dev.: 0.23
Frequencies
RD_Sim11[00003]

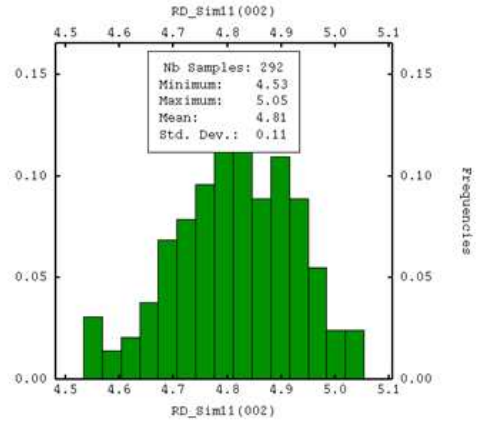

RD
Nb Samples: 214
Minimum: 3.40
Maximum: 5.22
Mean: 4.83
Std. Dev.: 0.24
RD_Sim11[00004]
Nb Samples: 37376
Minimum: 3.40
Maximum: 5.22
Mean: 4.75
Std. Dev.: 0.26
RD_Sim11[00005]
Nb Samples: 37376
Minimum: 3.40
Maximum: 5.22
Mean: 4.83
Std. Dev.: 0.24
Frequencies

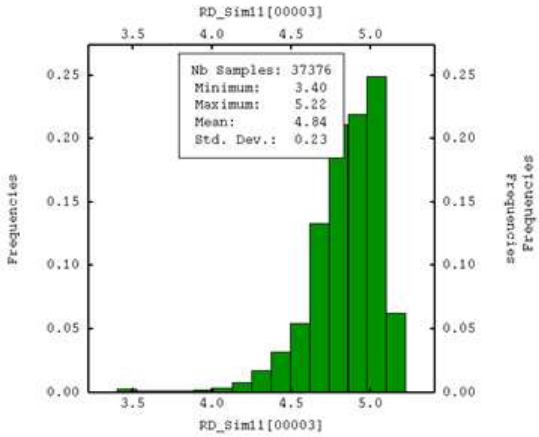

Distance (m)
Variogram : RD_NS
Variogram : RD_Sim[00001]
N90

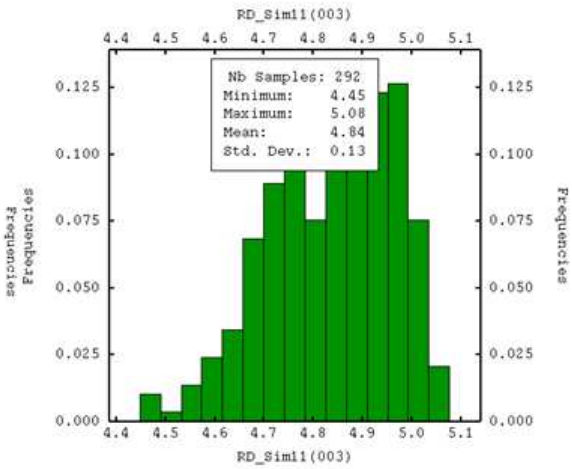

RD_Sim11[00001]
Nb Samples: 37356
Minimum: 3.40
Maximum: 5.22
Mean: 4.75
Std. Dev.: 0.28
Frequencies
RD_Sim11[00001]


RD_Sim11(001)
Nb Samples: 292
Minimum: 4.23
Maximum: 5.03
Mean: 4.75
Std. Dev.: 0.17
Frequencies
RD_Sim11(001)


RD_Sim11[00002]
Nb Samples: 37376
Minimum: 3.40
Maximum: 5.22
Mean: 4.81
Std. Dev.: 0.22
Frequencies
RD_Sim11[00002]


RD_Sim11(002)
Nb Samples: 292
Minimum: 4.53
Maximum: 5.05
Mean: 4.81
Std. Dev.: 0.11
Frequencies
RD_Sim11(002)


RD_Sim11[00003]
Nb Samples: 37376
Minimum: 3.40
Maximum: 5.22
Mean: 4.84
Std. Dev.: 0.23
Frequencies
RD_Sim11[00003]


RD_Sim11(003)
Nb Samples: 292
Minimum: 4.45
Maximum: 5.08
Mean: 4.84
Std. Dev.: 0.13
Frequencies
RD_Sim11(003)

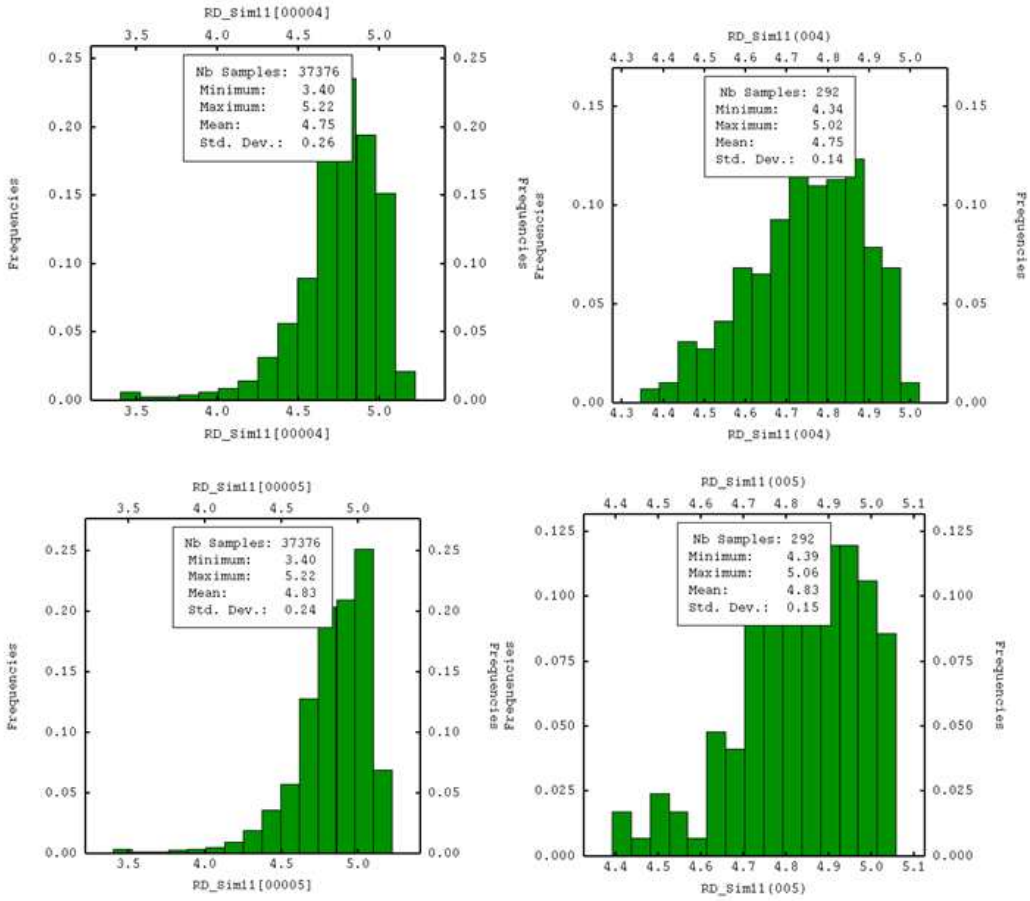
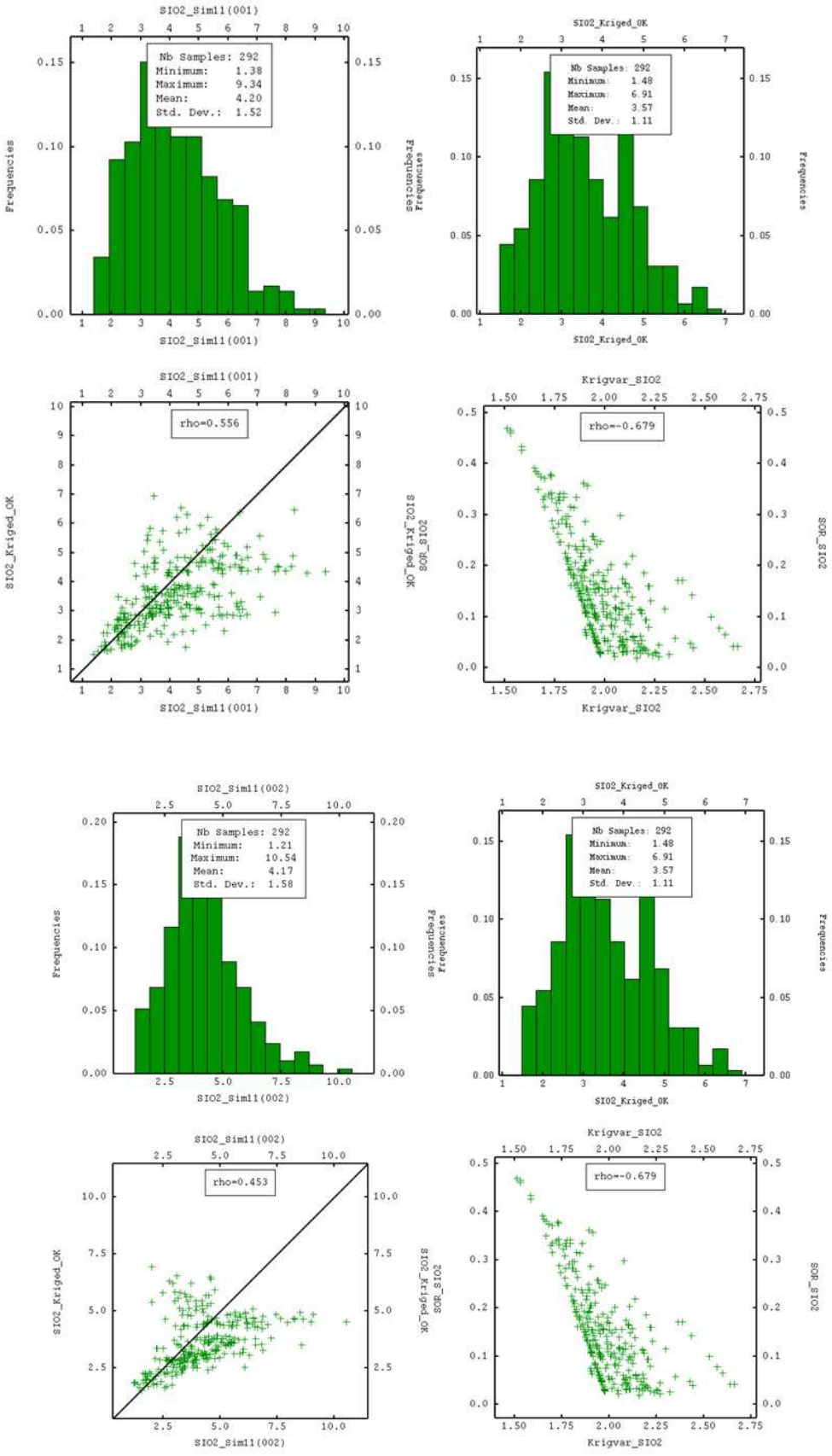
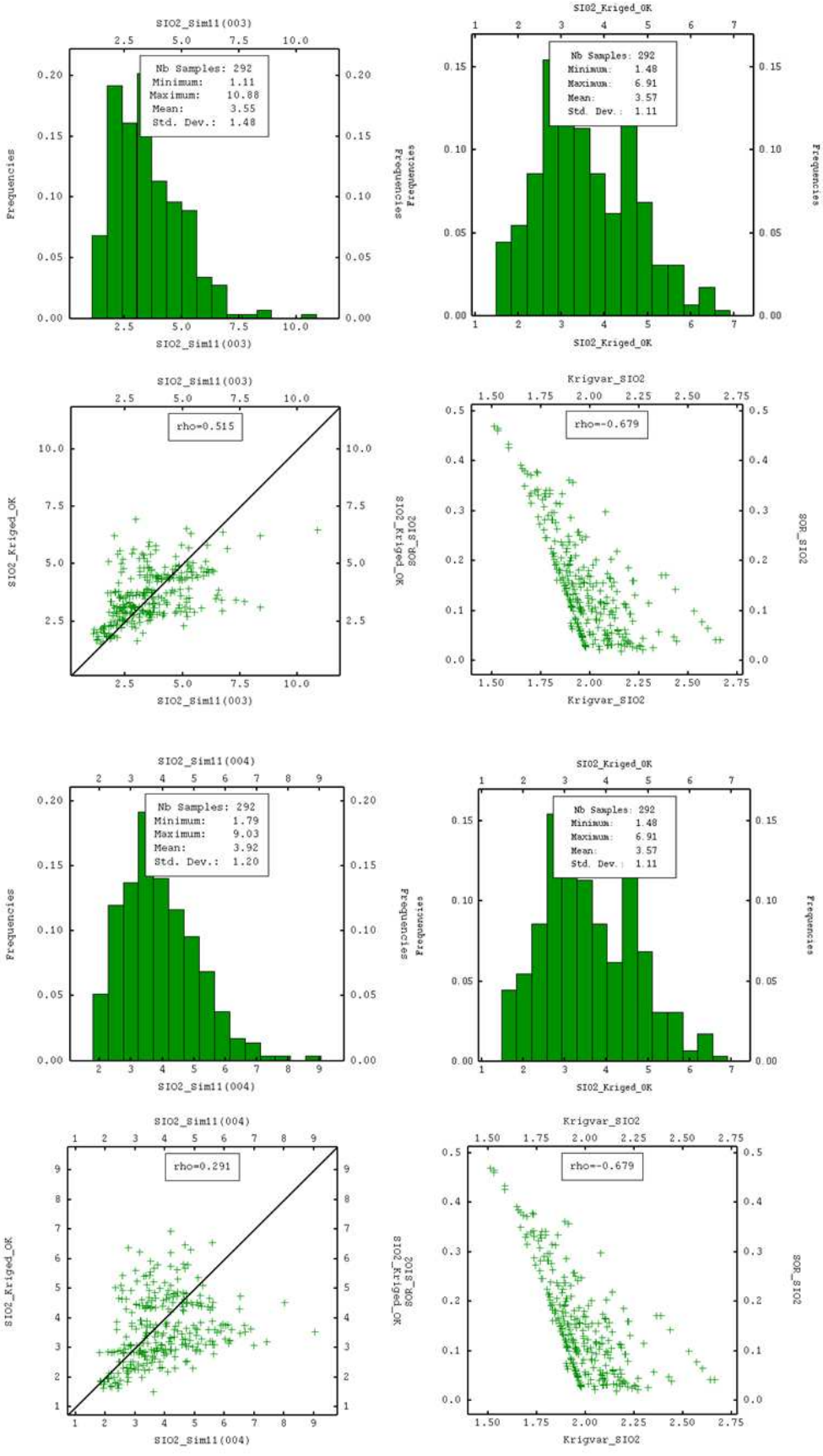


Figure 75: RD Conditional Properties

APPENDIX: 5 ORDINARY KRIGING




SIO2_Sim11(003)
Nb Samples: 292
Minimum: 1.11
Maximum: 10.88
Mean: 3.55
Std. Dev.: 1.48
Frequencies
SIO2_Kriged_OK
Nb Samples: 292
Minimum: 1.48
Maximum: 6.91
Mean: 3.57
Std. Dev.: 1.11
rho=0.515
rho=-0.679
Krigvar_SIO2
SOR_SIO2
SIO2_Sim11(004)
Nb Samples: 292
Minimum: 1.79
Maximum: 9.03
Mean: 3.92
Std. Dev.: 1.20
rho=0.291
rho=-0.679

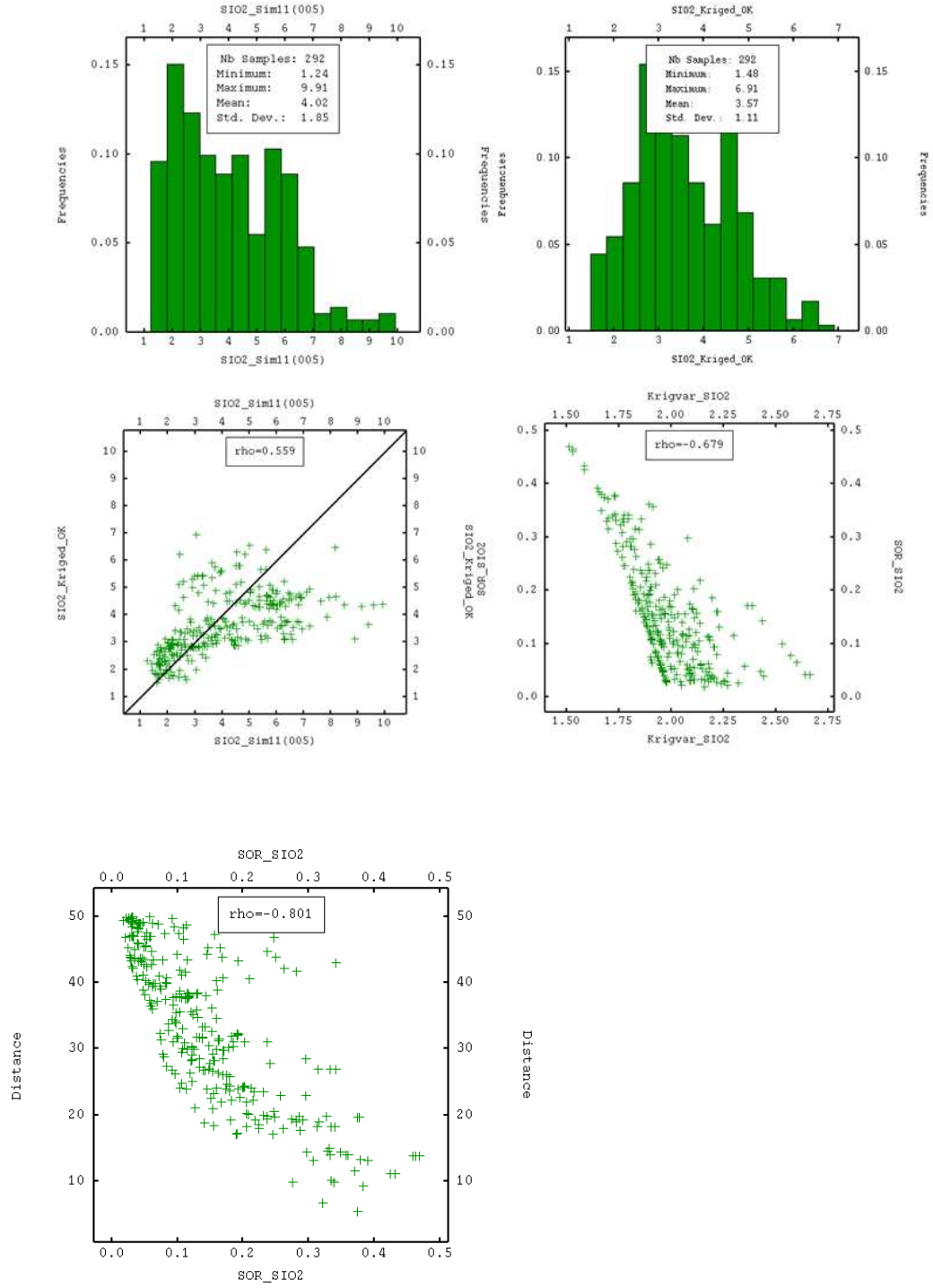
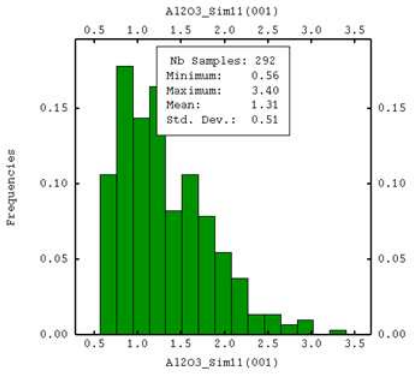
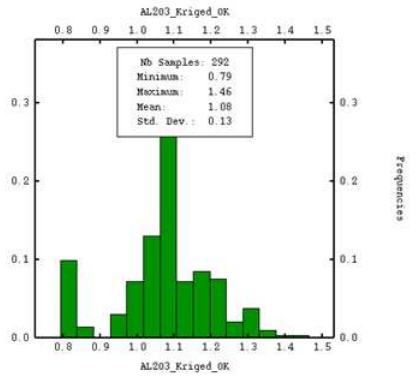
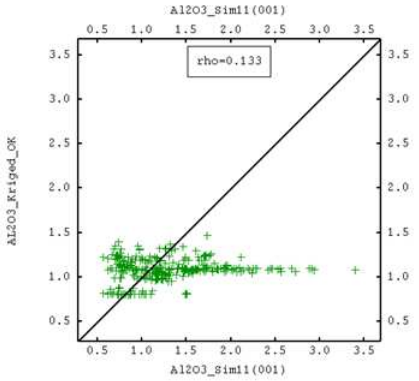
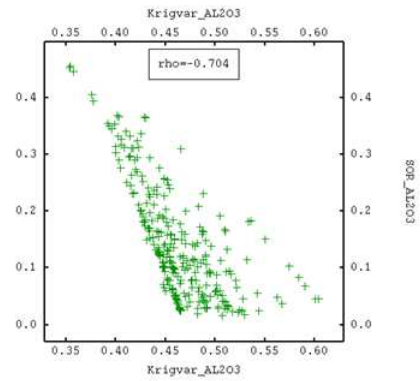


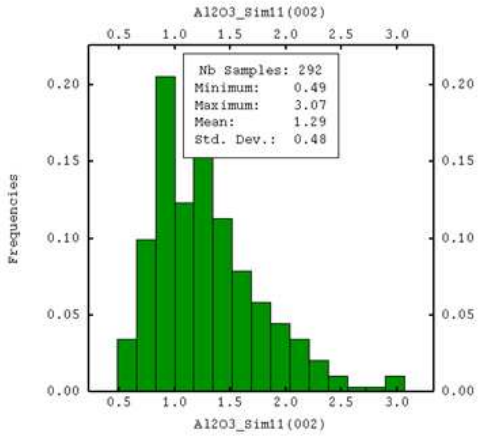
Figure 76: SIO_2 Results

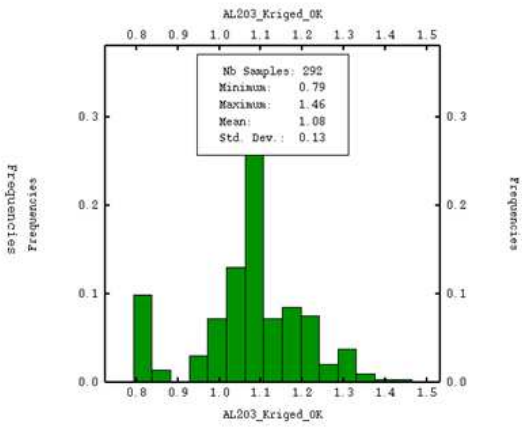

Al2O3_Sim11(001)
Nb Samples: 292
Minimum: 0.56
Maximum: 3.40
Mean: 1.31
Std. Dev.: 0.51
Frequencies
Al2O3_Sim11(001)

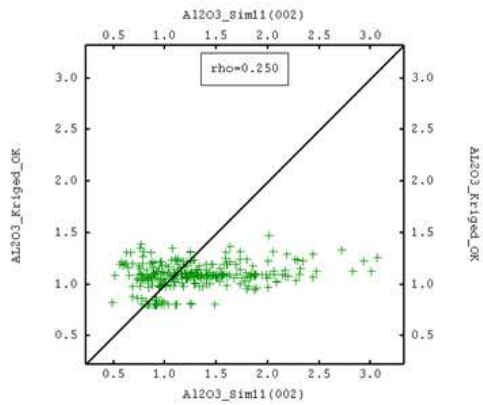

AL203_Kriged_OK
Nb Samples: 292
Minimum: 0.79
Maximum: 1.46
Mean: 1.08
Std. Dev.: 0.13
Frequencies
AL203_Kriged_OK

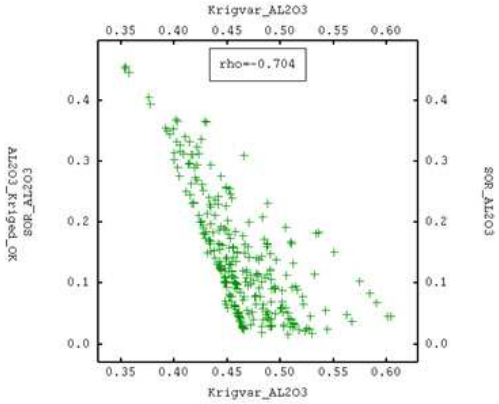

Al2O3_Sim11(001)
rho=0.133
AL203_Kriged_OK
Al2O3_Sim11(001)

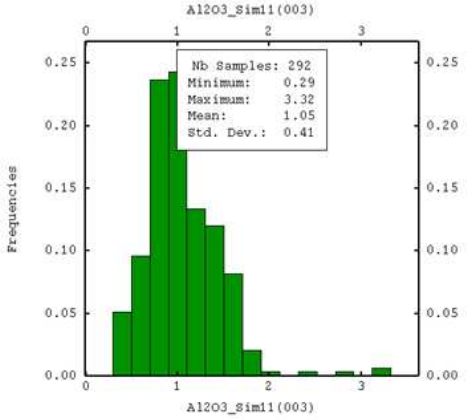

Krigvar_AL2O3
rho=-0.704
SOR_AL2O3
Krigvar_AL2O3

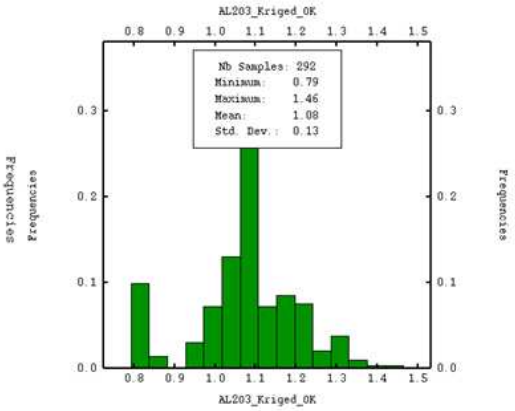

Al2O3_Sim11(002)
Nb Samples: 292
Minimum: 0.49
Maximum: 3.07
Mean: 1.29
Std. Dev.: 0.48
Frequencies
Al2O3_Sim11(002)

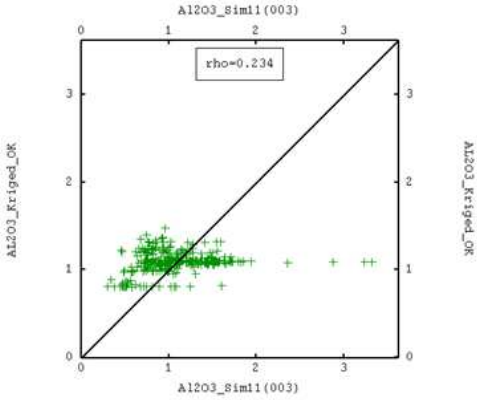

AL203_Kriged_OK
Nb Samples: 292
Minimum: 0.79
Maximum: 1.46
Mean: 1.08
Std. Dev.: 0.13
Frequencies
AL203_Kriged_OK

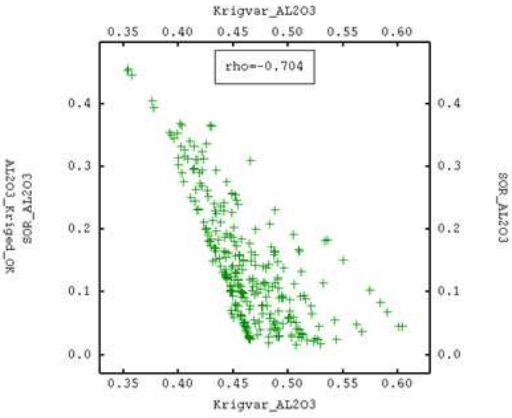

Al2O3_Sim11(002)
rho=0.250
AL203_Kriged_OK
Al2O3_Sim11(002)

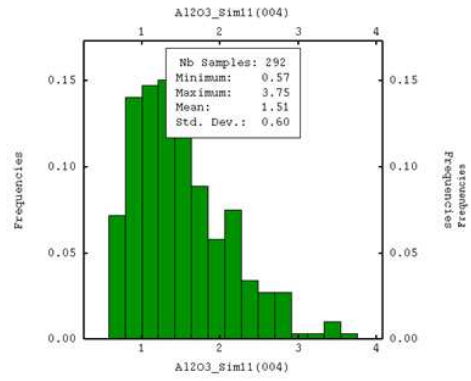

Krigvar_AL2O3
rho=-0.704
SOR_AL2O3
Krigvar_AL2O3

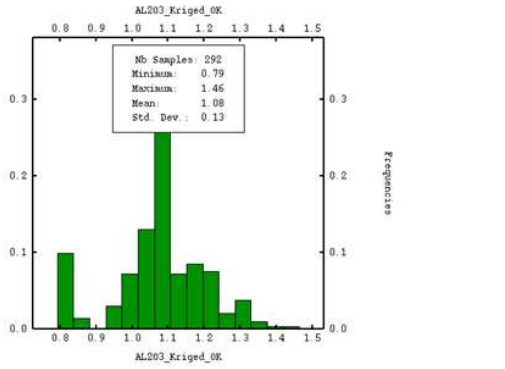

Al2O3_Sim11(003)
Nb Samples: 292
Minimum: 0.29
Maximum: 3.32
Mean: 1.05
Std. Dev.: 0.41
Frequencies
Al2O3_Sim11(003)

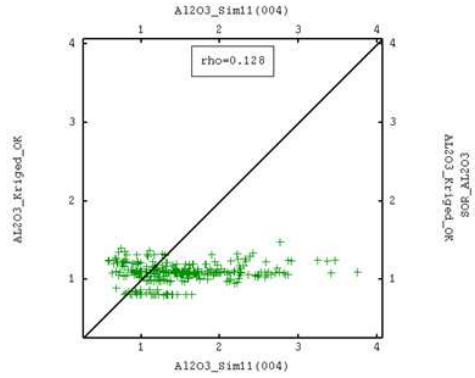

AL2O3_Kriged_OK
Nb Samples: 292
Minimum: 0.79
Maximum: 1.46
Mean: 1.08
Std. Dev.: 0.13
Frequencies
AL2O3_Kriged_OK

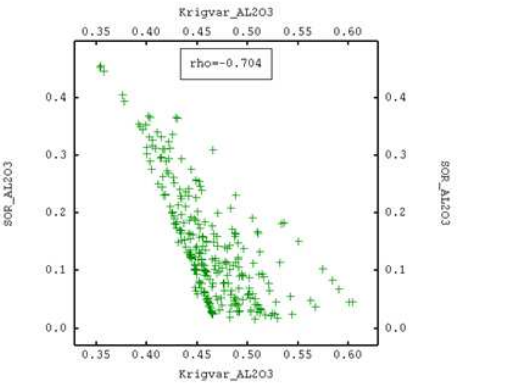

Al2O3_Sim11(003)
rho=0.234
Al2O3_Kriged_OK
Al2O3_Sim11(003)


Krigvar_AL2O3
rho=-0.704
AL2O3_Kriged_OK SOR_AL2O3
SOR_AL2O3
Krigvar_AL2O3


Al2O3_Sim11(004)
Nb Samples: 292
Minimum: 0.57
Maximum: 3.75
Mean: 1.51
Std. Dev.: 0.60
Frequencies
Al2O3_Sim11(004)


AL2O3_Kriged_OK
Nb Samples: 292
Minimum: 0.79
Maximum: 1.46
Mean: 1.08
Std. Dev.: 0.13
Frequencies
AL2O3_Kriged_OK


Al2O3_Sim11(004)
rho=0.128
Al2O3_Kriged_OK
Al2O3_Sim11(004)


Krigvar_AL2O3
rho=-0.704
AL2O3_Kriged_OK SOR_AL2O3
SOR_AL2O3
Krigvar_AL2O3

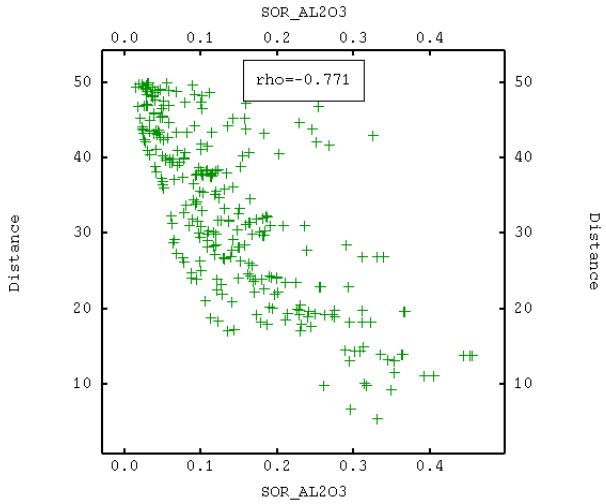
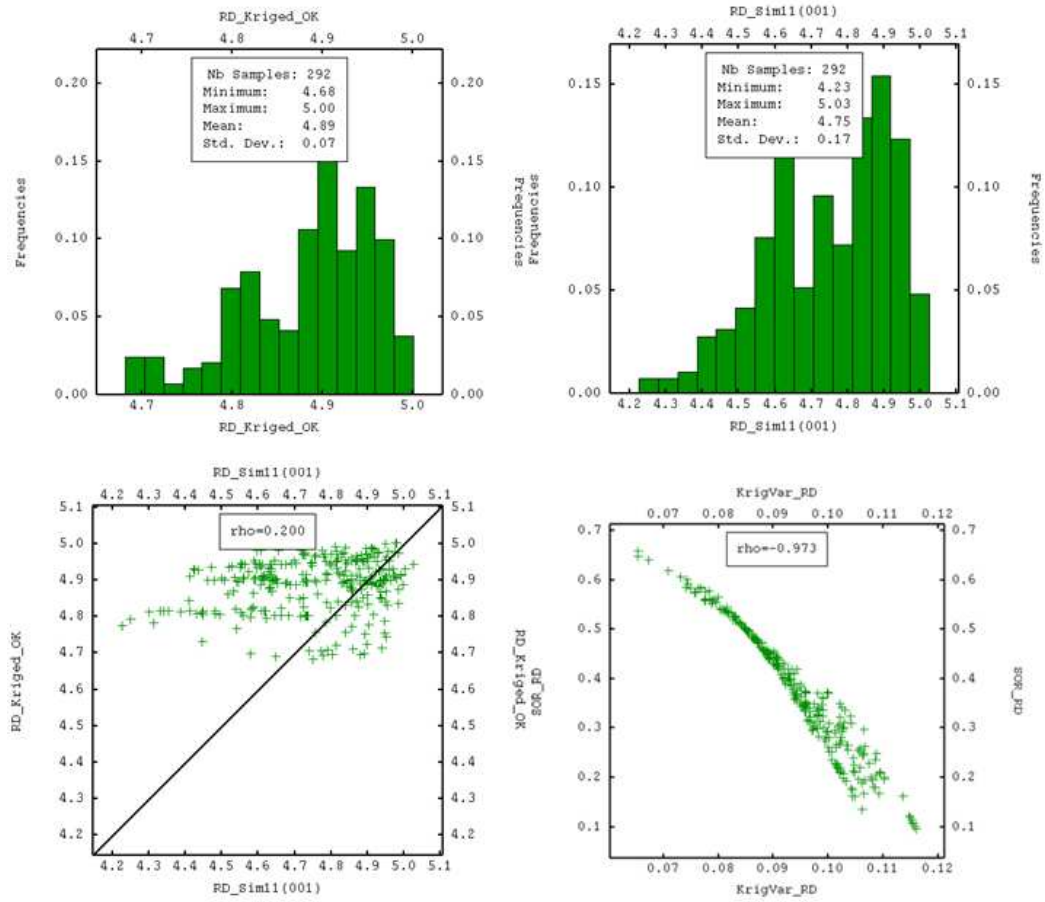
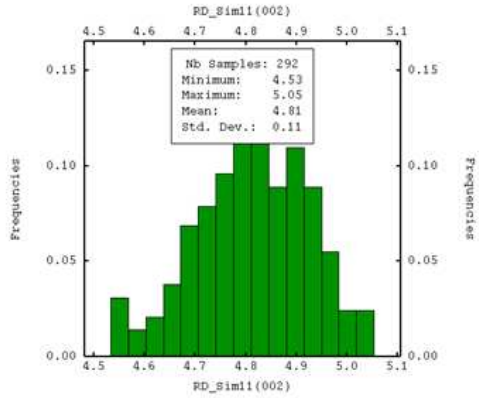
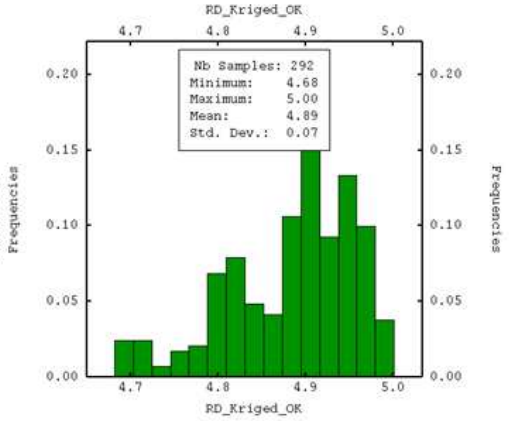
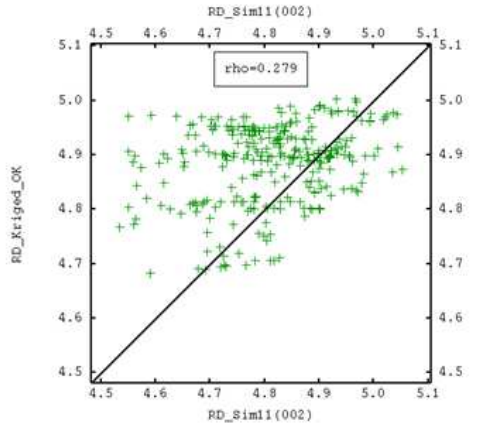


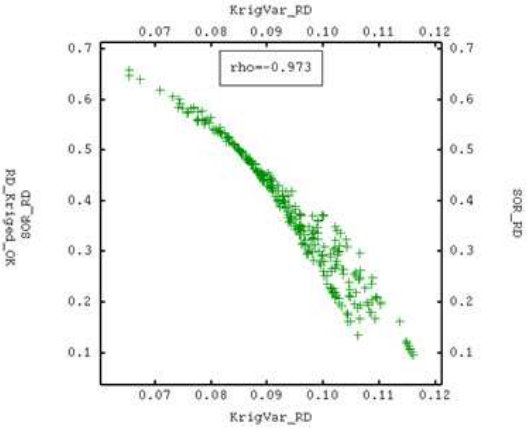
Figure 77: Al_2O_3 Results

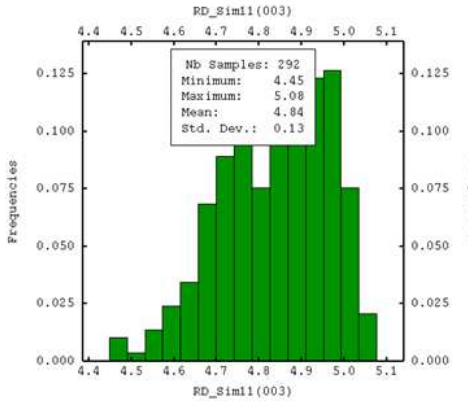


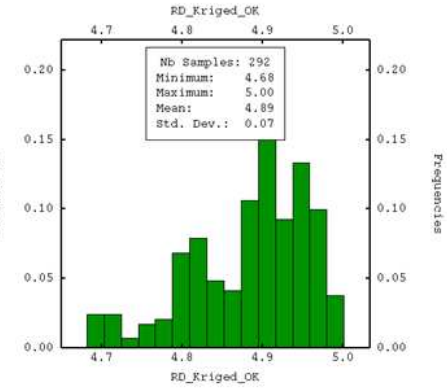

RD_Sim11(002)
Nb Samples: 292
Minimum: 4.53
Maximum: 5.05
Mean: 4.81
Std. Dev.: 0.11
Frequencies
RD_Sim11(002)

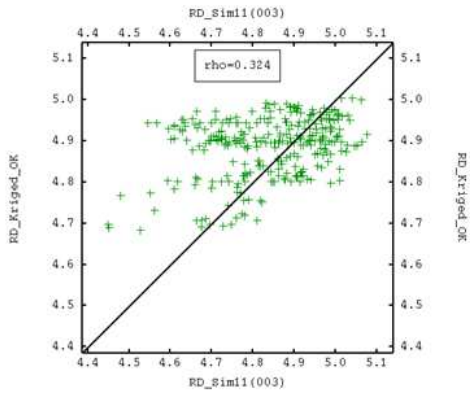

RD_Kriged_OK
Nb Samples: 292
Minimum: 4.68
Maximum: 5.00
Mean: 4.89
Std. Dev.: 0.07
Frequencies
RD_Kriged_OK

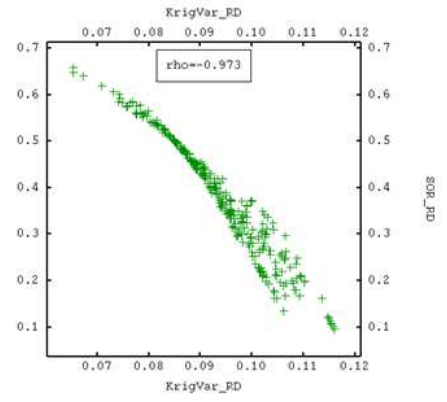

RD_Sim11(002)
rho=0.279
RD_Kriged_OK
RD_Sim11(002)

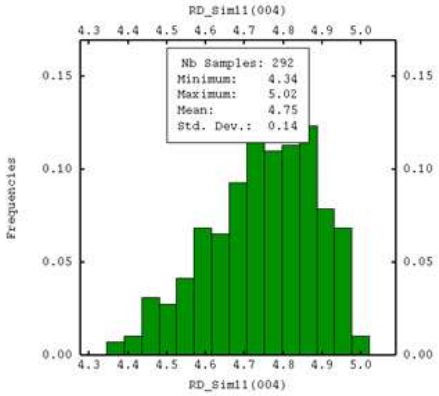

KrigVar_RD
rho=-0.973
RD_Kriged_OK
SOR_RD
KrigVar_RD

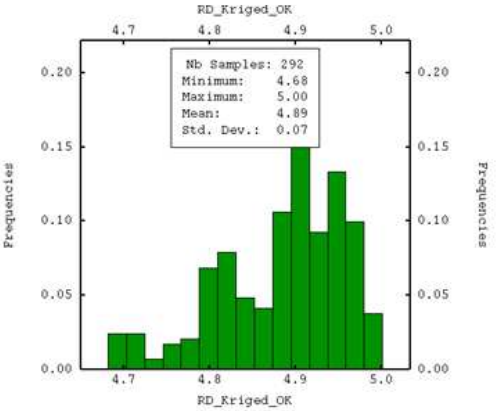

RD_Sim11(003)
Nb Samples: 292
Minimum: 4.45
Maximum: 5.08
Mean: 4.84
Std. Dev.: 0.13
Frequencies
RD_Sim11(003)

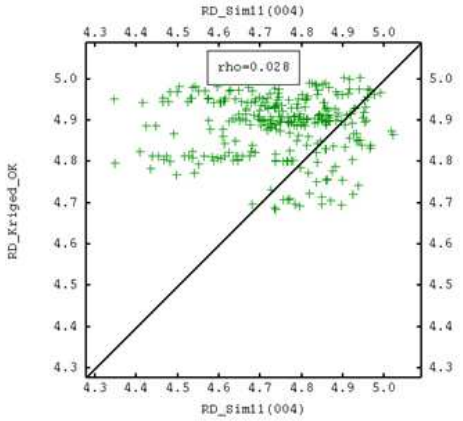

RD_Kriged_OK
Nb Samples: 292
Minimum: 4.68
Maximum: 5.00
Mean: 4.89
Std. Dev.: 0.07
Frequencies
RD_Kriged_OK

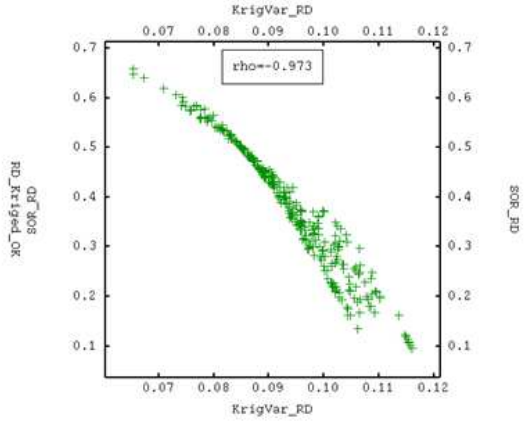

RD_Sim11(003)
rho=0.324
RD_Kriged_OK
RD_Sim11(003)


KrigVar_RD
rho=-0.973
RD_Kriged_OK
SOR_RD
KrigVar_RD


RD_Sim11(004)
Nb Samples: 292
Minimum: 4.34
Maximum: 5.02
Mean: 4.75
Std. Dev.: 0.14
Frequencies
RD_Sim11(004)


RD_Kriged_OK
Nb Samples: 292
Minimum: 4.68
Maximum: 5.00
Mean: 4.89
Std. Dev.: 0.07
Frequencies
RD_Kriged_OK


RD_Sim11(004)
rho=0.028
RD_Kriged_OK
RD_Sim11(004)


KrigVar_RD
rho=-0.973
SOR_RD
KrigVar_RD

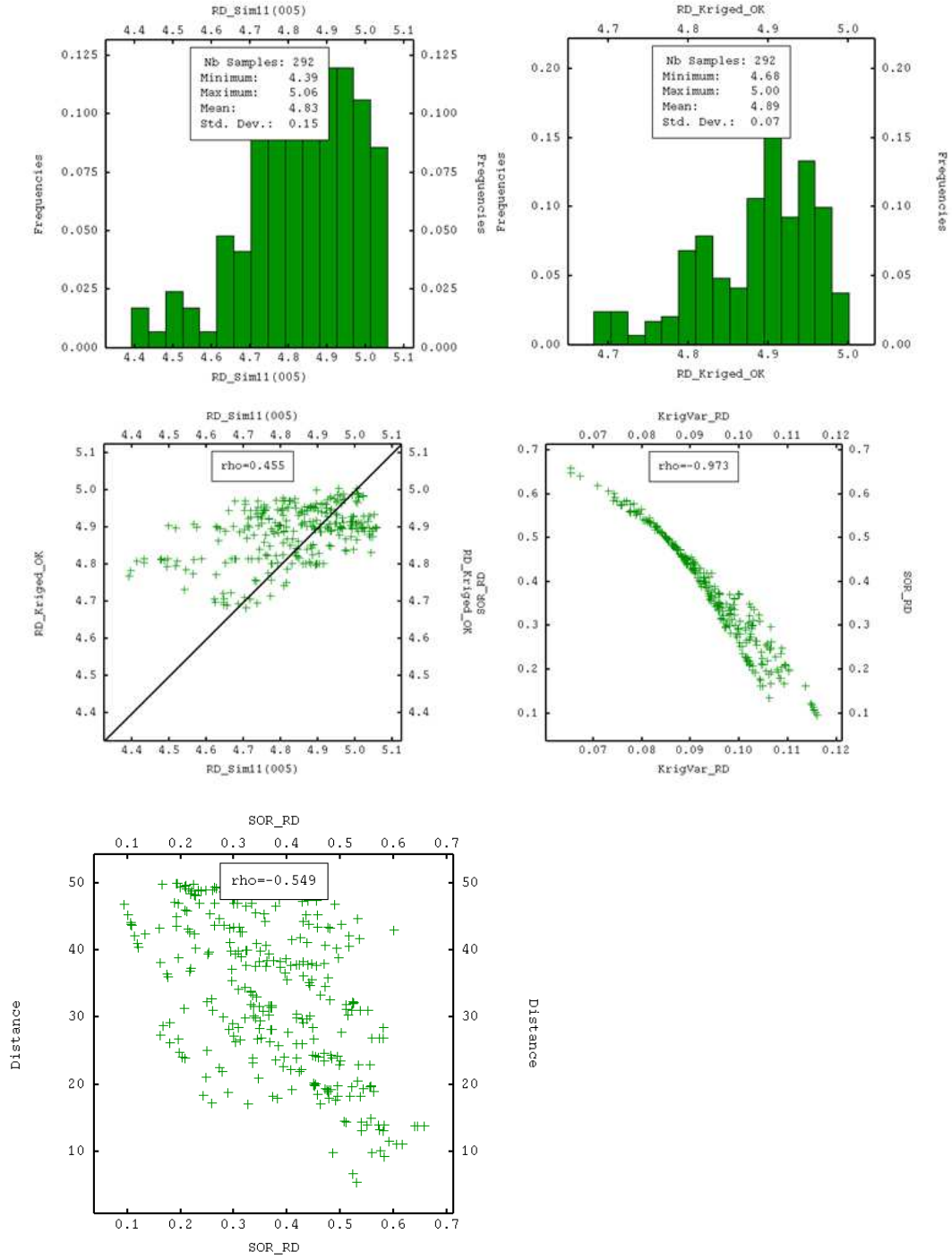
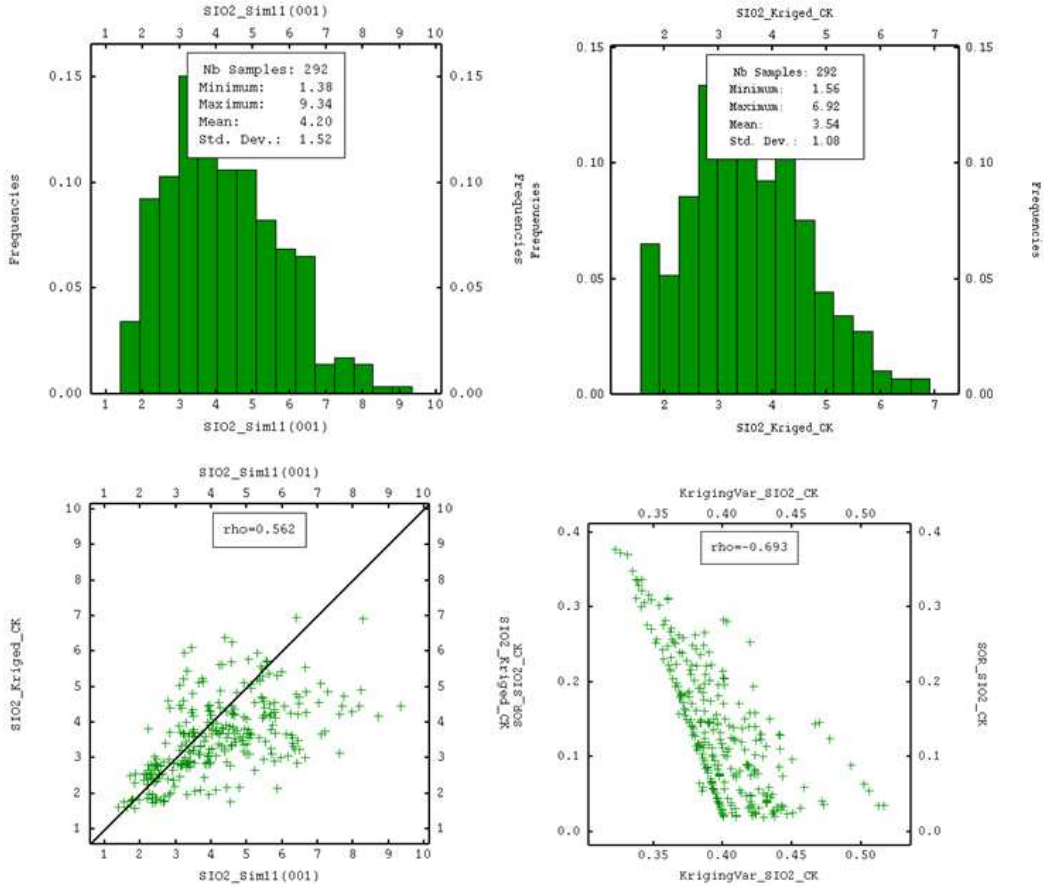
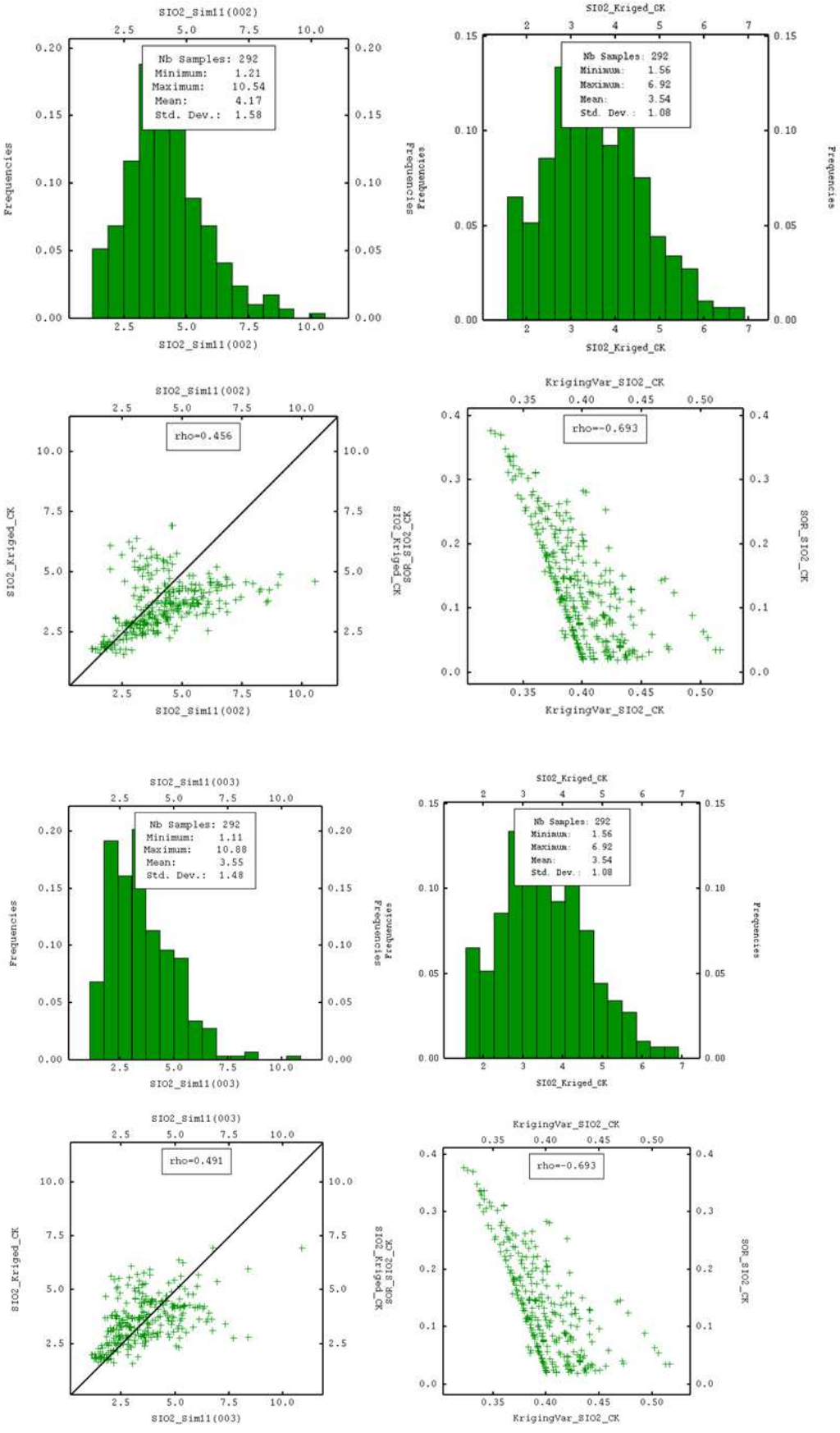
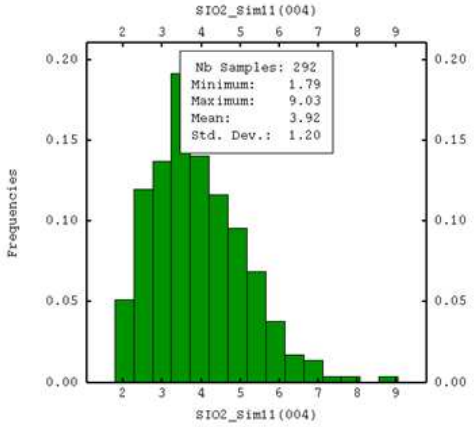


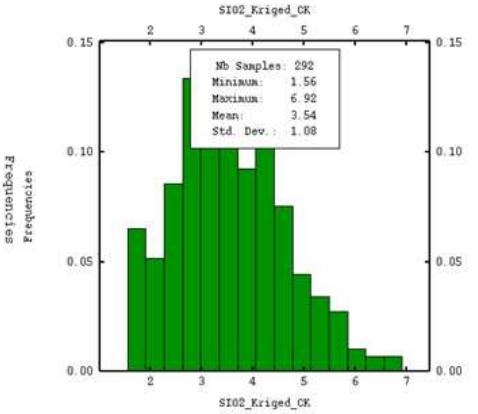
Figure 78: RD Results

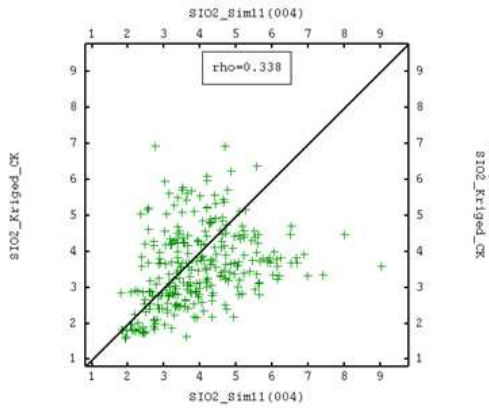
APPENDIX: 6 ORDINARY COKRIGING

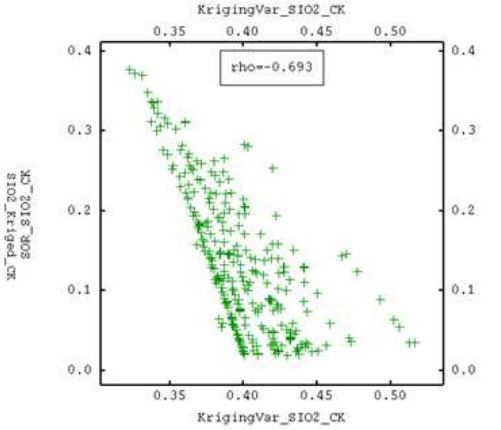



SIO2_Sim11(002)
Nb Samples: 292
Minimum: 1.21
Maximum: 10.54
Mean: 4.17
Std. Dev.: 1.58
Frequencies
SIO2_Kriged_CK
Nb Samples: 292
Minimum: 1.56
Maximum: 6.92
Mean: 3.54
Std. Dev.: 1.08
rho=0.456
rho=-0.693
KrigingVar_SIO2_CK
SOR_SIO2_CK
SIO2_Sim11(003)
Nb Samples: 292
Minimum: 1.11
Maximum: 10.88
Mean: 3.55
Std. Dev.: 1.48
rho=0.491
rho=-0.693


SIO2_Sim11(004)
Nb Samples: 292
Minimum: 1.79
Maximum: 9.03
Mean: 3.92
Std. Dev.: 1.20
Frequencies
SIO2_Sim11(004)


SIO2_Kriged_CK
Nb Samples: 292
Minimum: 1.56
Maximum: 6.92
Mean: 3.54
Std. Dev.: 1.08
Frequencies
SIO2_Kriged_CK


SIO2_Sim11(004)
rho=0.338
SIO2_Kriged_CK
SIO2_Sim11(004)


KrigingVar_SIO2_CK
rho=-0.693
SIO2_Kriged_CK
SOR_SIO2_CK
KrigingVar_SIO2_CK

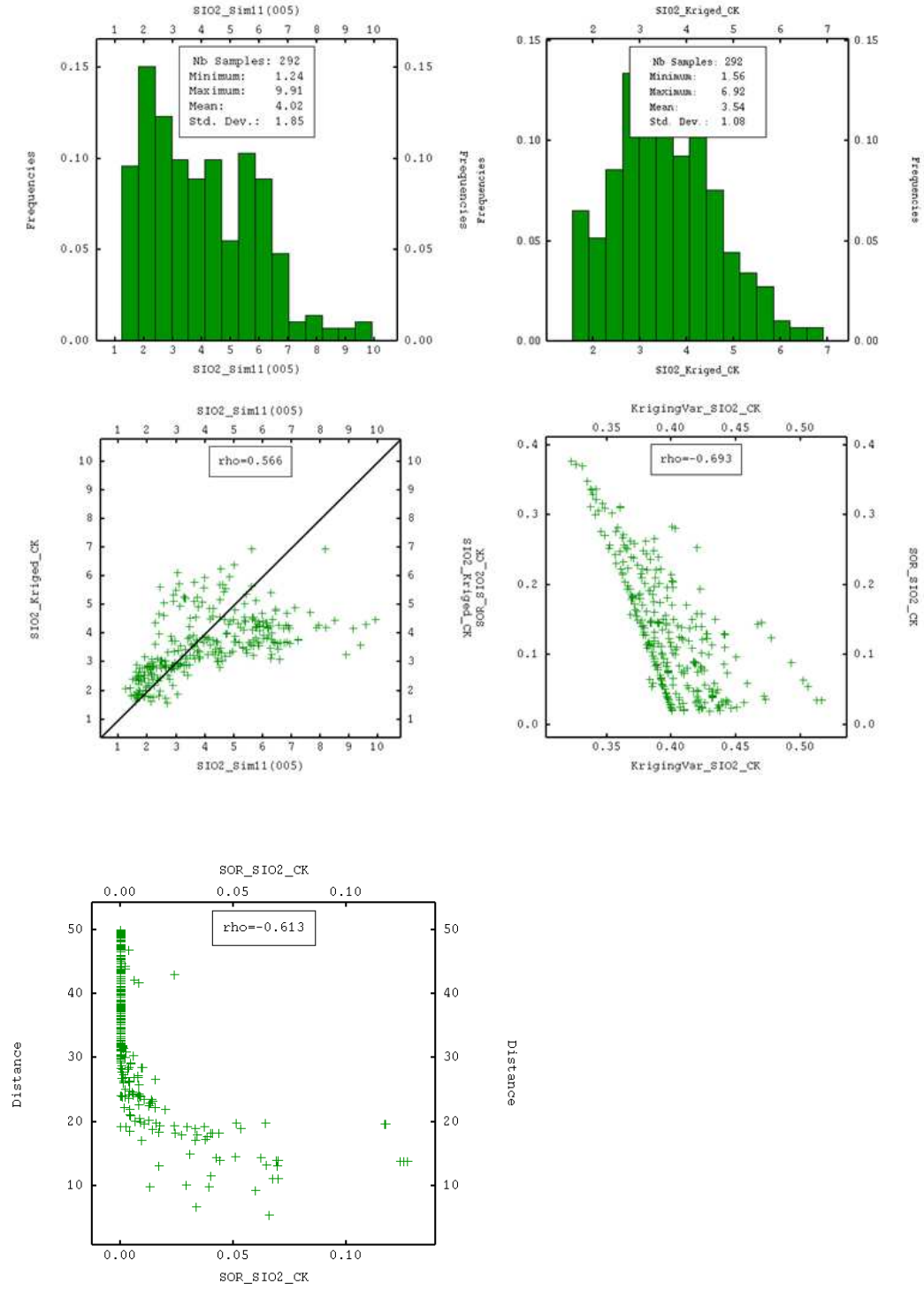
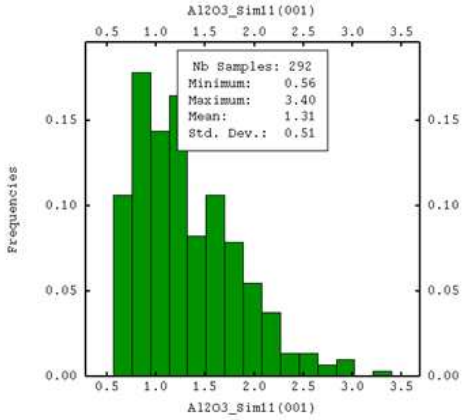
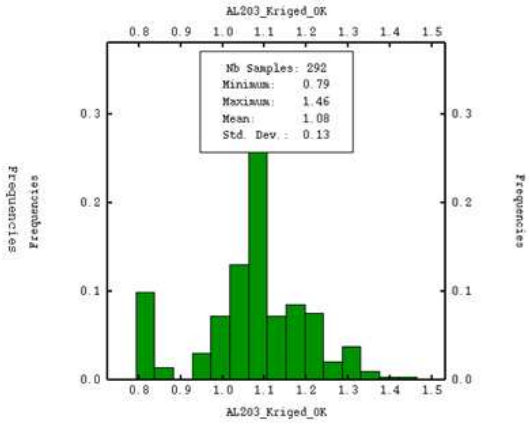
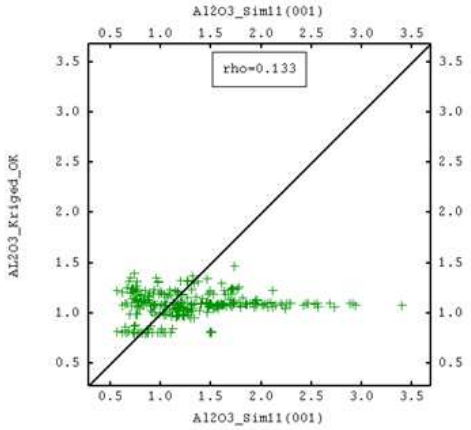
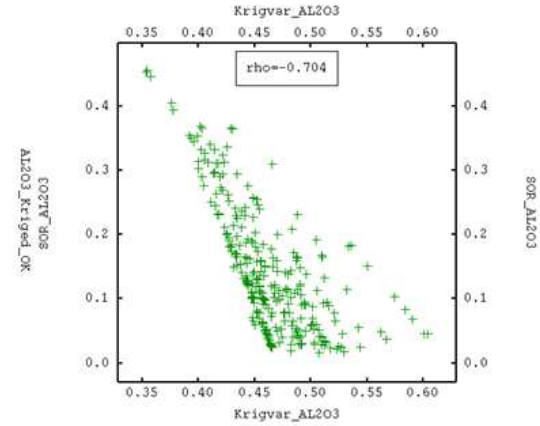


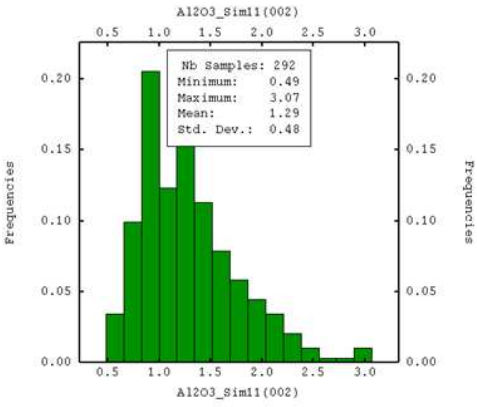
Figure 79: SIO_2 Results

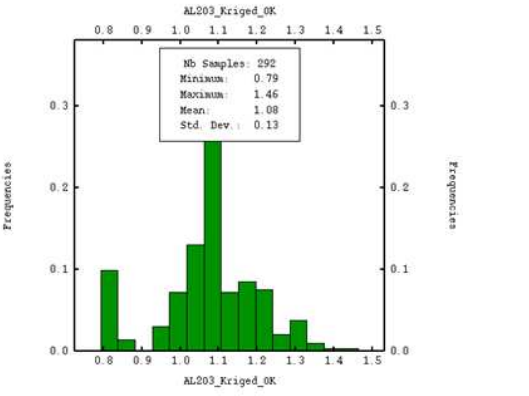

Al2O3_Sim11(001)
Nb Samples: 292
Minimum: 0.56
Maximum: 3.40
Mean: 1.31
Std. Dev.: 0.51
Frequencies
Al2O3_Sim11(001)

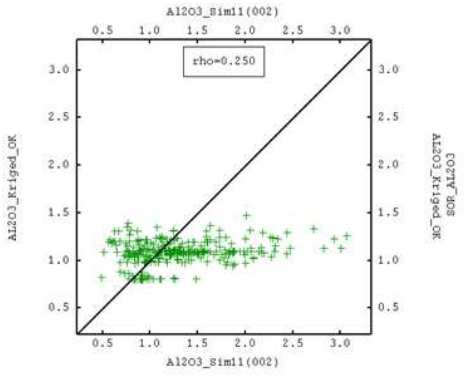

AL203_Kriged_OK
Nb Samples: 292
Minimum: 0.79
Maximum: 1.46
Mean: 1.08
Std. Dev.: 0.13
Frequencies
AL203_Kriged_OK

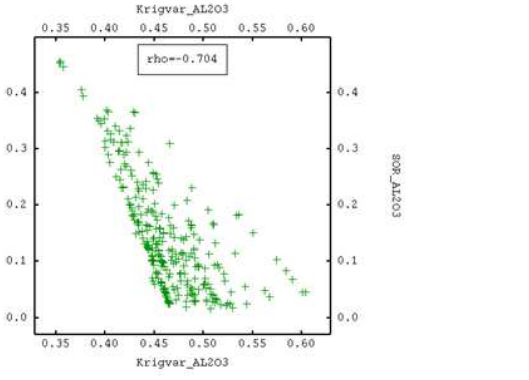

Al2O3_Sim11(001)
rho=0.133
Al2O3_Kriged_OK
Al2O3_Sim11(001)

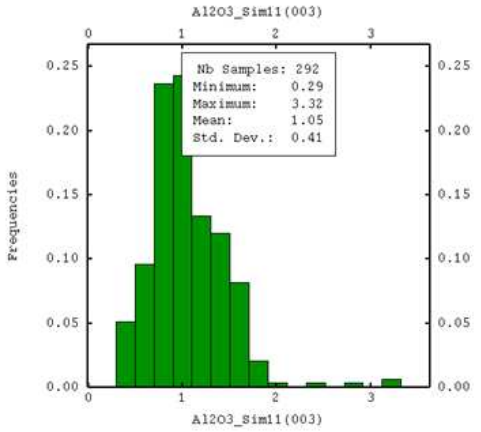

Krigvar_AL2O3
rho=-0.704
SOR_AL2O3
Krigvar_AL2O3

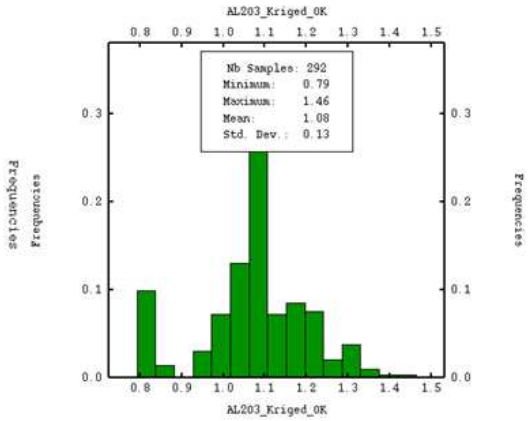

Al2O3_Sim11(002)
Nb Samples: 292
Minimum: 0.49
Maximum: 3.07
Mean: 1.29
Std. Dev.: 0.48
Frequencies
Al2O3_Sim11(002)

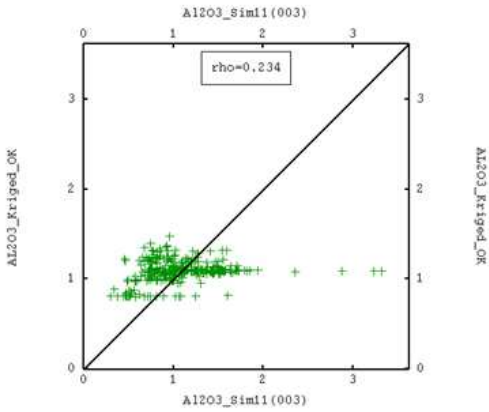

AL203_Kriged_OK
Nb Samples: 292
Minimum: 0.79
Maximum: 1.46
Mean: 1.08
Std. Dev.: 0.13
Frequencies
AL203_Kriged_OK

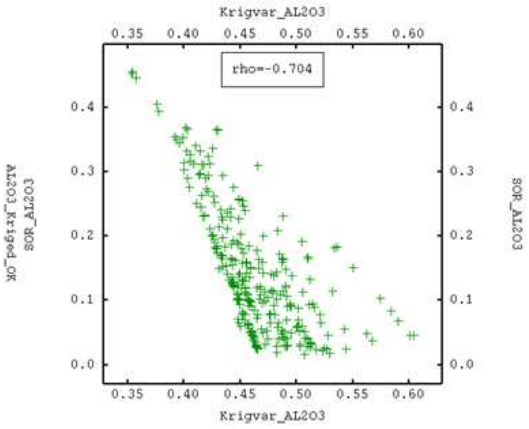

Al2O3_Sim11(002)
rho=0.250
Al2O3_Kriged_OK
Al2O3_Sim11(002)

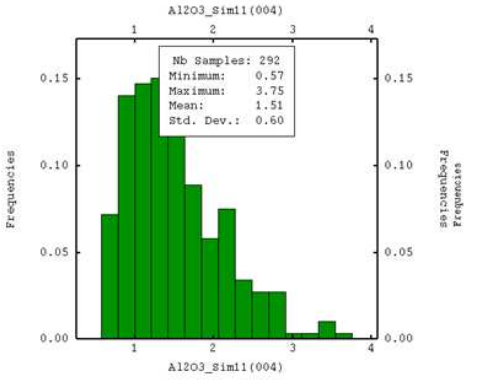

Krigvar_AL2O3
rho=-0.704
SOR_AL2O3
Krigvar_AL2O3

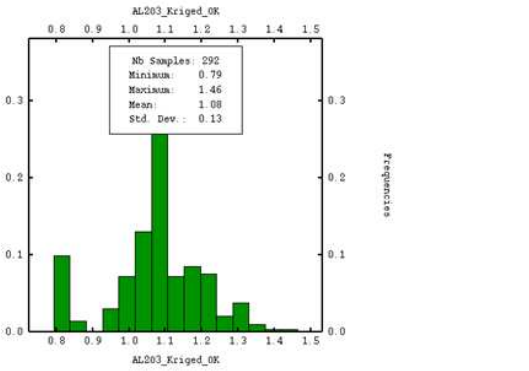

Al2O3_Sim11(003)
Nb Samples: 292
Minimum: 0.29
Maximum: 3.32
Mean: 1.05
Std. Dev.: 0.41
Frequencies
Al2O3_Sim11(003)

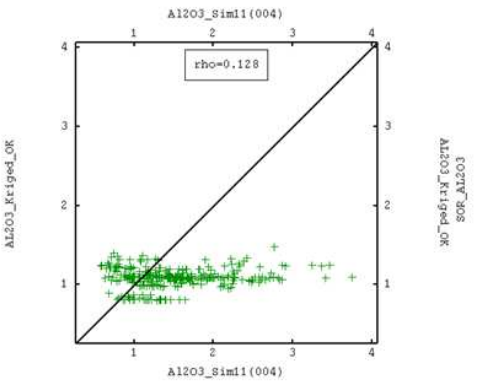

AL2O3_Kriged_OK
Nb Samples: 292
Minimum: 0.79
Maximum: 1.46
Mean: 1.08
Std. Dev.: 0.13
Frequencies
AL2O3_Kriged_OK

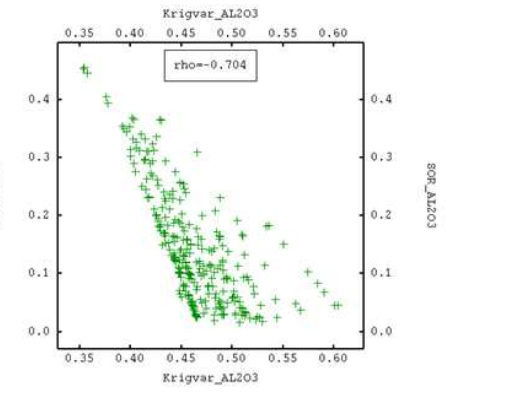

Al2O3_Sim11(003)
rho=0.234
AL2O3_Kriged_OK
Al2O3_Sim11(003)


Krigvar_AL2O3
rho=-0.704
AL2O3_Kriged_OK
SOR_AL2O3
Krigvar_AL2O3


Al2O3_Sim11(004)
Nb Samples: 292
Minimum: 0.57
Maximum: 3.75
Mean: 1.51
Std. Dev.: 0.60
Frequencies
Al2O3_Sim11(004)


AL2O3_Kriged_OK
Nb Samples: 292
Minimum: 0.79
Maximum: 1.46
Mean: 1.08
Std. Dev.: 0.13
Frequencies
AL2O3_Kriged_OK


Al2O3_Sim11(004)
rho=0.128
AL2O3_Kriged_OK
Al2O3_Sim11(004)


Krigvar_AL2O3
rho=-0.704
AL2O3_Kriged_OK
SOR_AL2O3
Krigvar_AL2O3

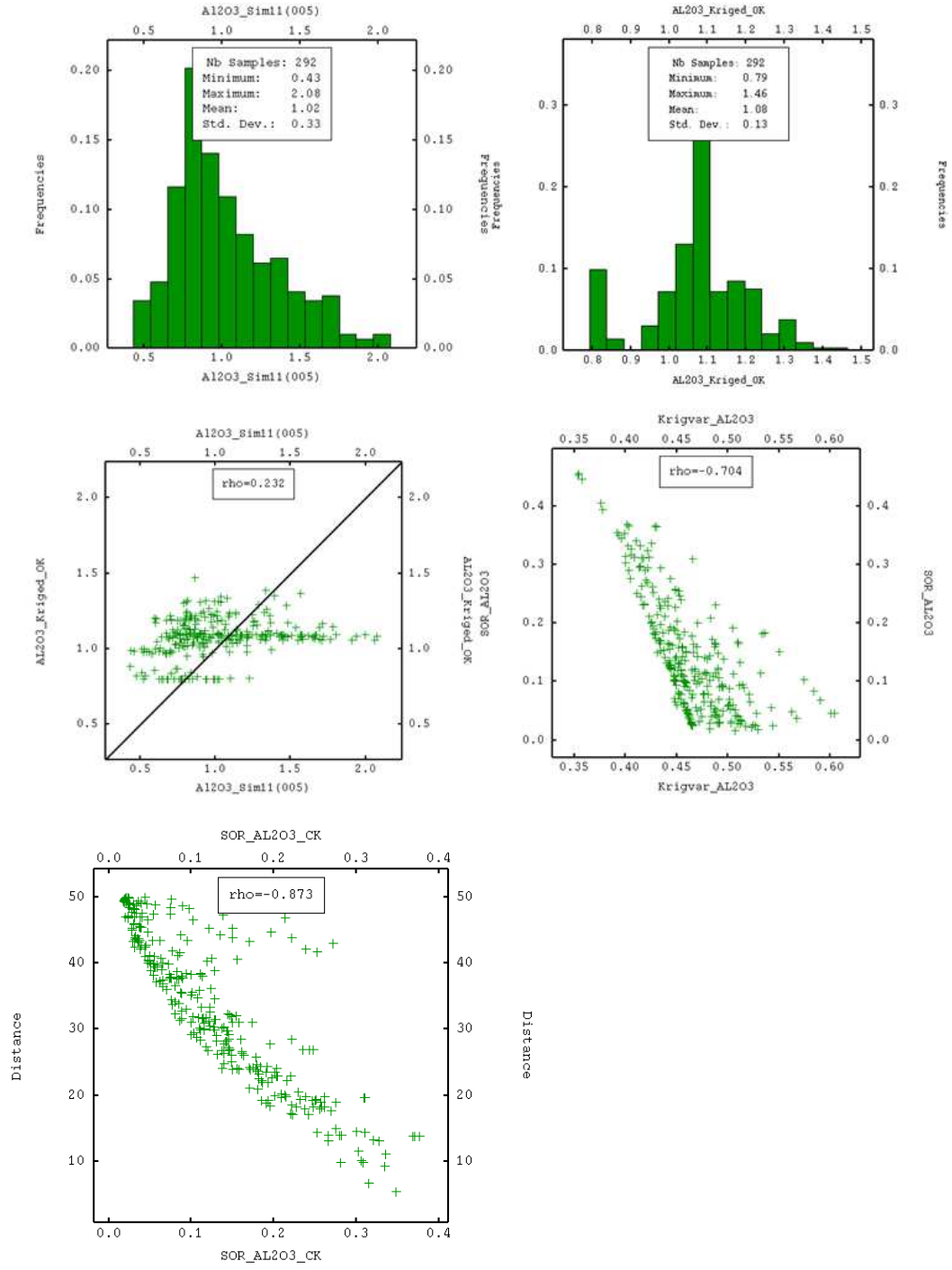
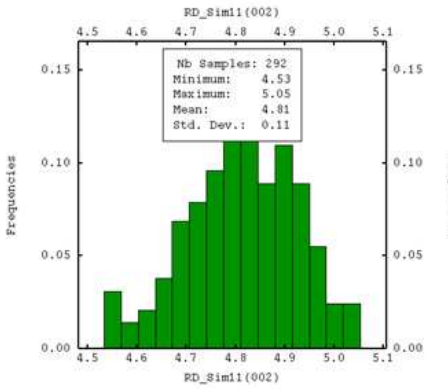
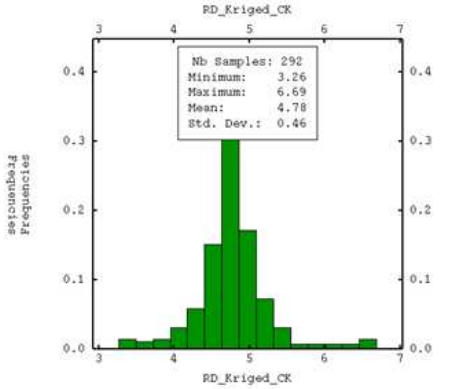
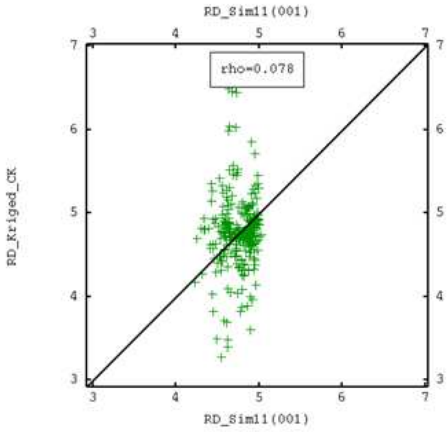
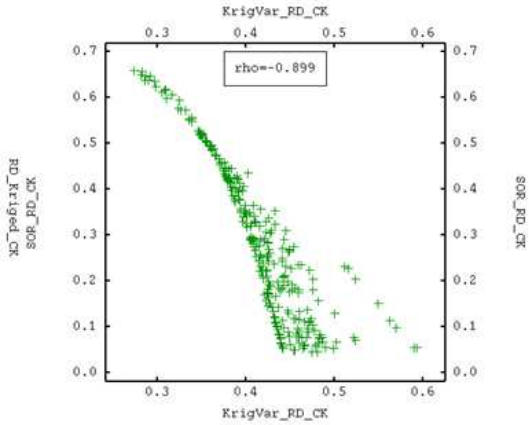


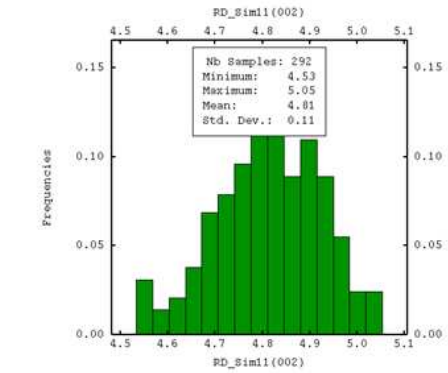
Figure 80: Al_2O_3 Results

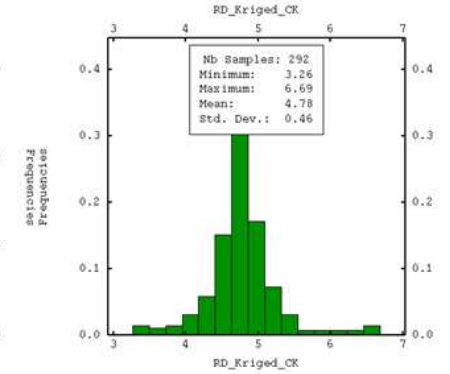

RD_Sim11(002)
Nb Samples: 292
Minimum: 4.53
Maximum: 5.05
Mean: 4.81
Std. Dev.: 0.11
Frequencies
RD_Sim11(002)

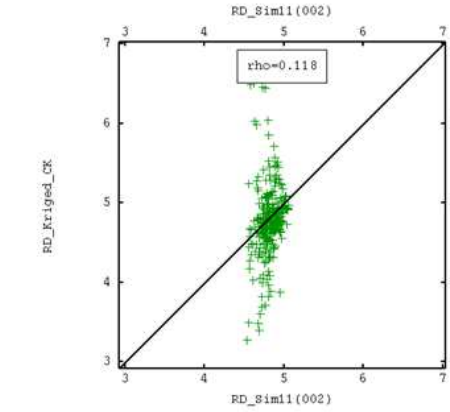

RD_Kriged_CK
Nb Samples: 292
Minimum: 3.26
Maximum: 6.69
Mean: 4.78
Std. Dev.: 0.46
Frequencies
RD_Kriged_CK

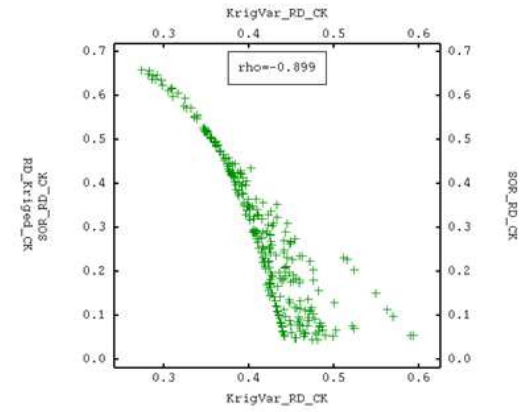

RD_Sim11(001)
rho=0.078
RD_Kriged_CK
RD_Sim11(001)

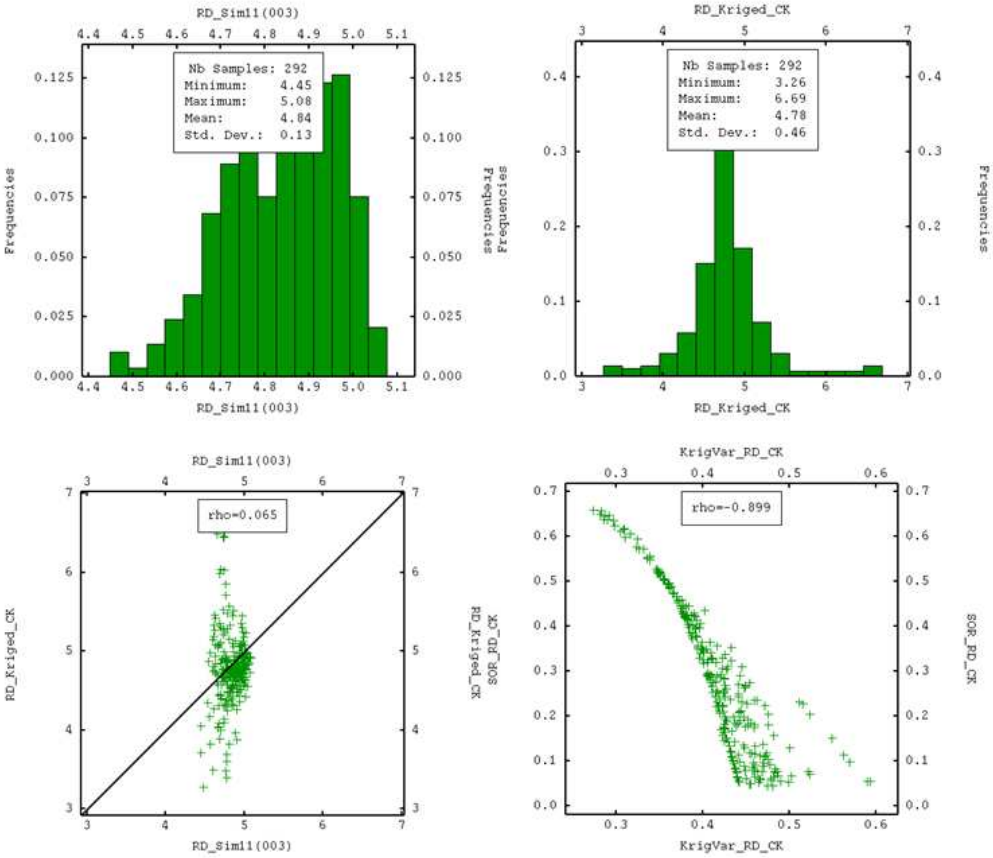

KrigVar_RD_CK
rho=-0.899
RD_Kriged_CK
SOR_RD_CK
KrigVar_RD_CK

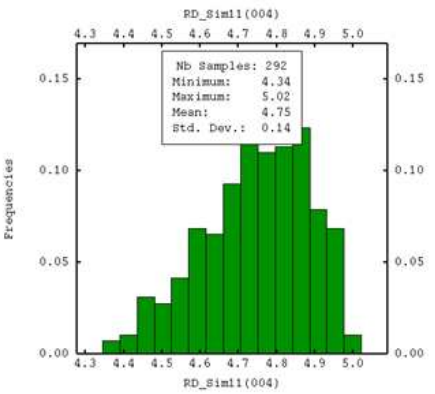

RD_Sim11(002)
Nb Samples: 292
Minimum: 4.53
Maximum: 5.05
Mean: 4.81
Std. Dev.: 0.11
Frequencies
RD_Sim11(002)

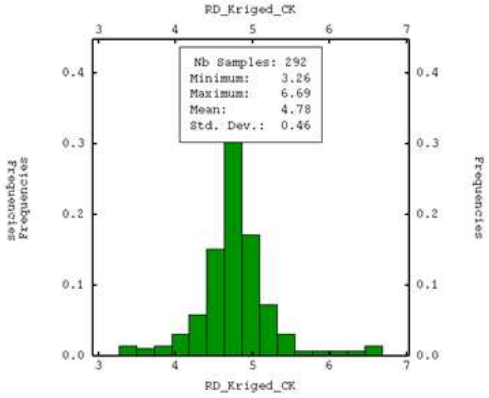

RD_Kriged_CK
Nb Samples: 292
Minimum: 3.26
Maximum: 6.69
Mean: 4.78
Std. Dev.: 0.46
Frequencies
RD_Kriged_CK

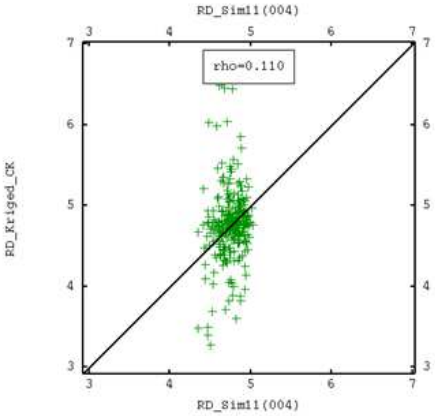

RD_Sim11(002)
rho=0.118
RD_Kriged_CK
RD_Sim11(002)

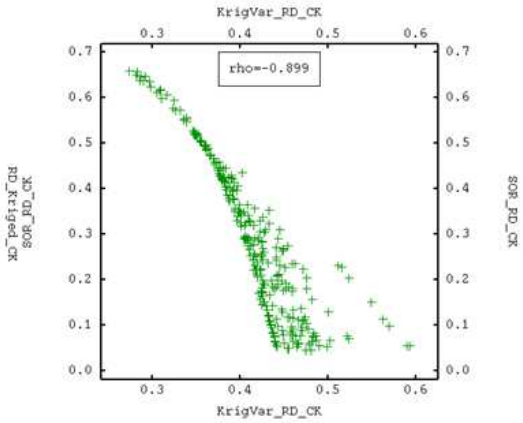

KrigVar_RD_CK
rho=-0.899
RD_Kriged_CK
SOR_RD_CK
KrigVar_RD_CK


RD_Sim11(003)
Nb Samples: 292
Minimum: 4.45
Maximum: 5.08
Mean: 4.84
Std. Dev.: 0.13
Frequencies
RD_Kriged_CK
Nb Samples: 292
Minimum: 3.26
Maximum: 6.69
Mean: 4.78
Std. Dev.: 0.46
rho=0.065
rho=-0.899
KrigVar_RD_CK
SOR_RD_CK


RD_Sim11(004)
Nb Samples: 292
Minimum: 4.34
Maximum: 5.02
Mean: 4.75
Std. Dev.: 0.14
Frequencies
RD_Sim11(004)


RD_Kriged_CK
Nb Samples: 292
Minimum: 3.26
Maximum: 6.69
Mean: 4.78
Std. Dev.: 0.46
Frequencies
RD_Kriged_CK


RD_Sim11(004)
rho=0.110
RD_Kriged_CK
RD_Sim11(004)


KrigVar_RD_CK
rho=-0.899
RD_Kriged_CK
SOR_RD_CK
KrigVar_RD_CK

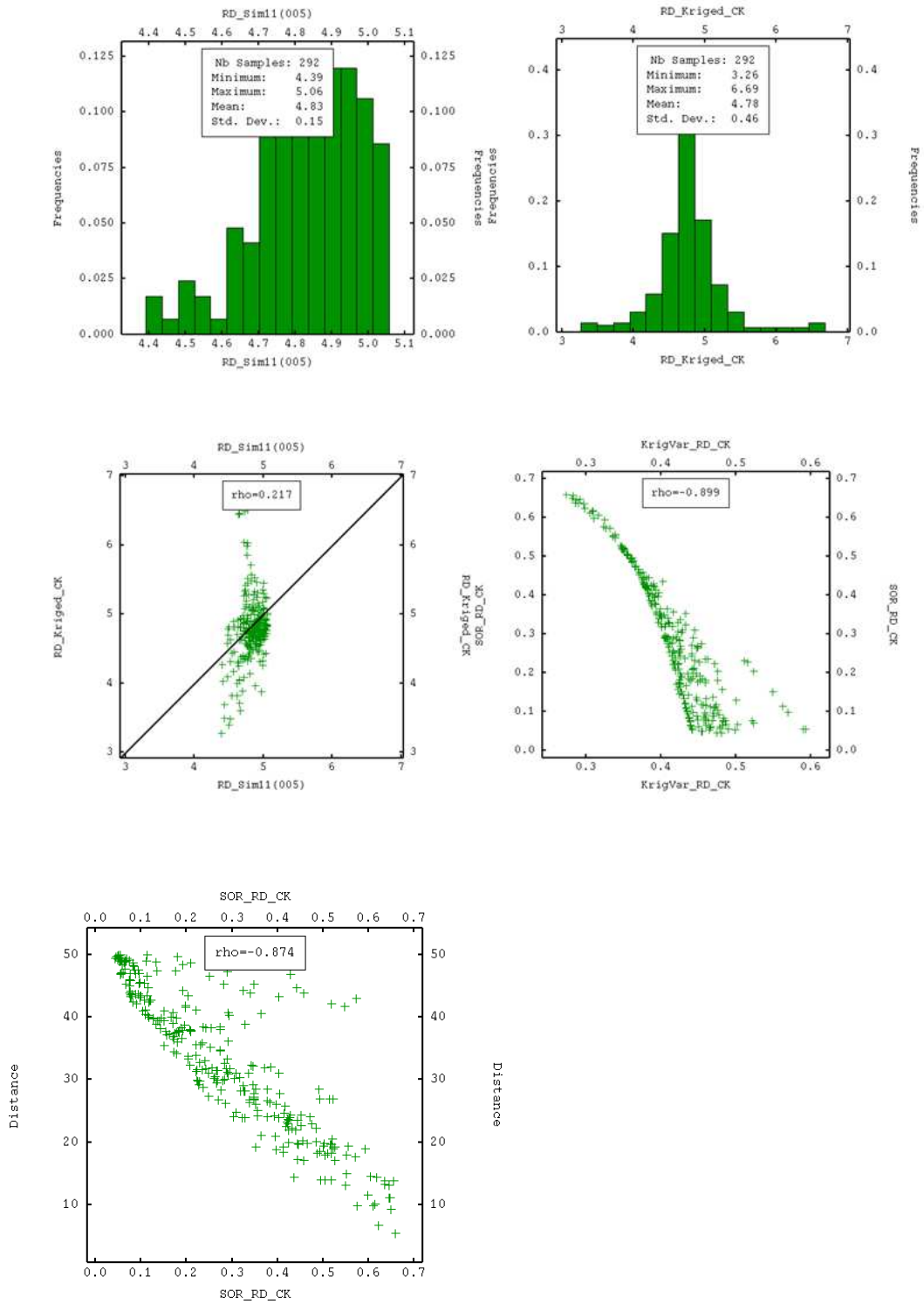
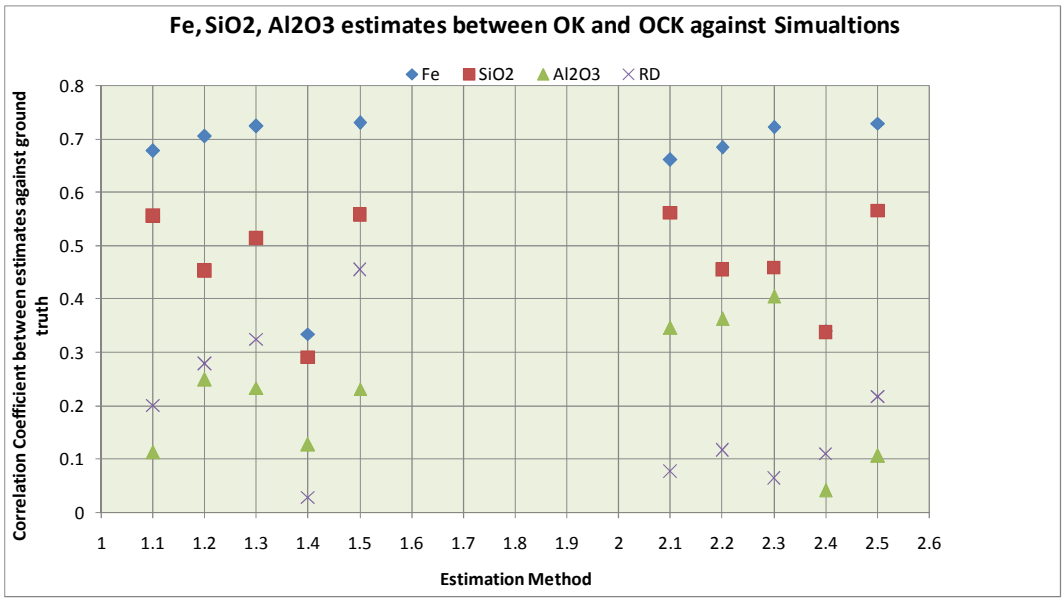


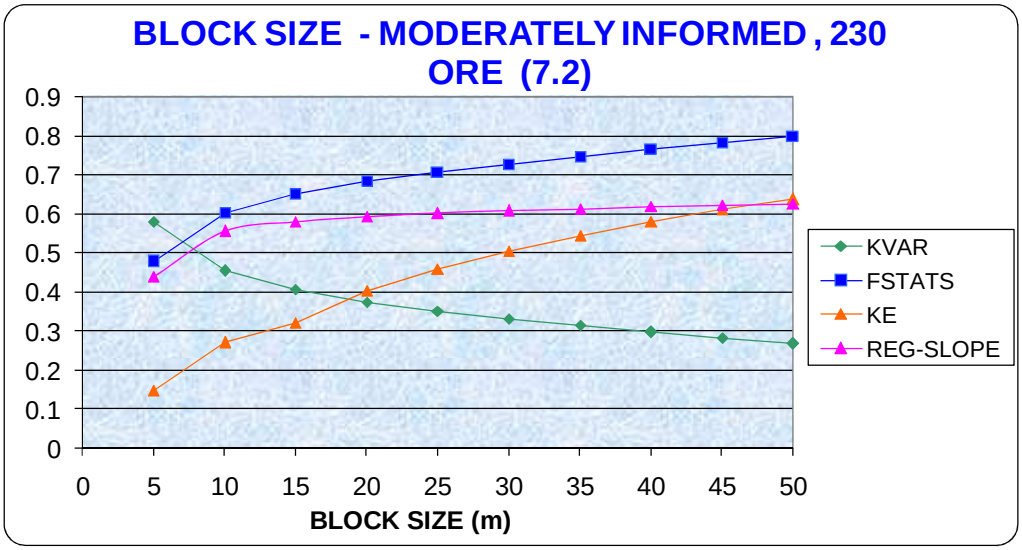
Figure 81: RD Results

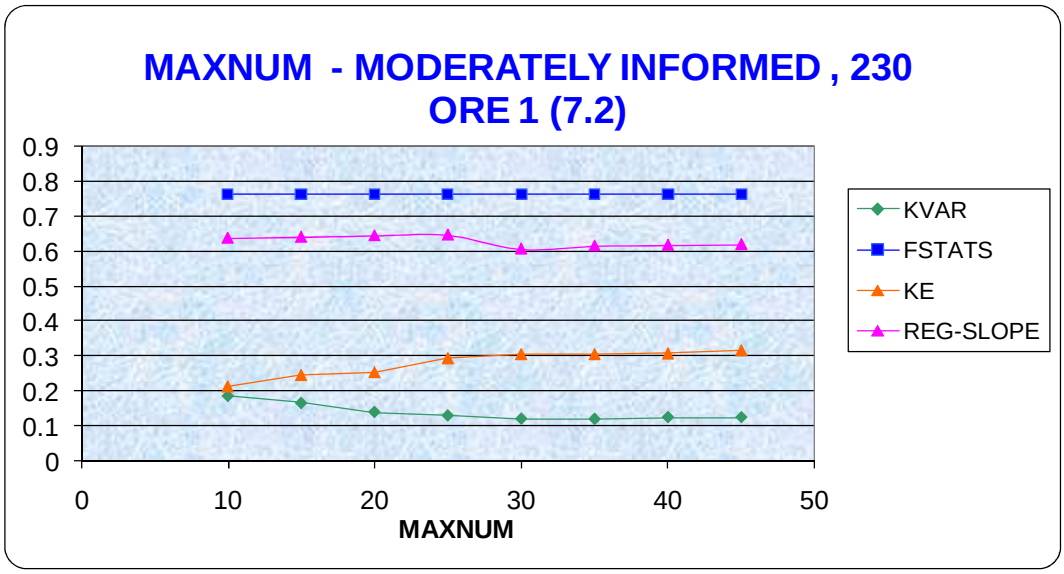
APPENDIX: 7 CORRELATION COEFFICIENT FOR % SiO_2, Al_2O_3 and RD AGAINST GROUND TRUTH

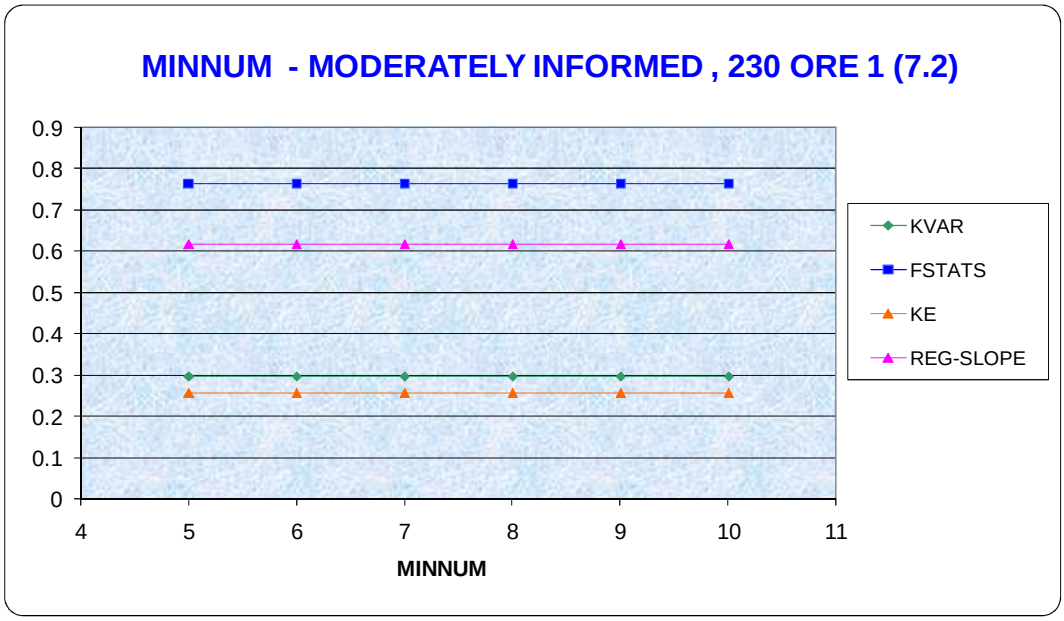


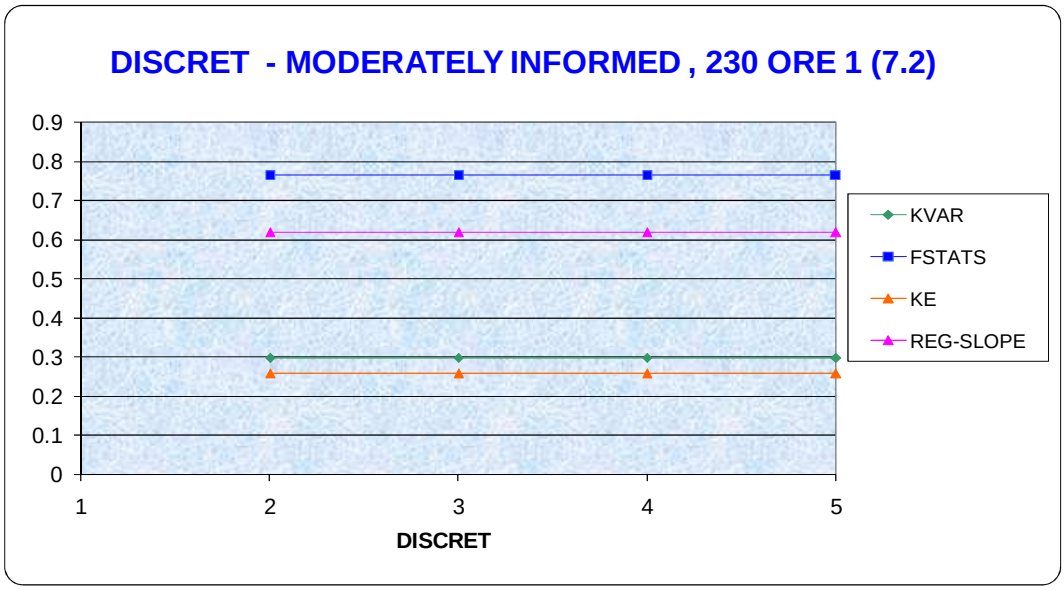
APPENDIX: 8 QUANTITATIVE NEIGHBOURHOOD ANALYSIS

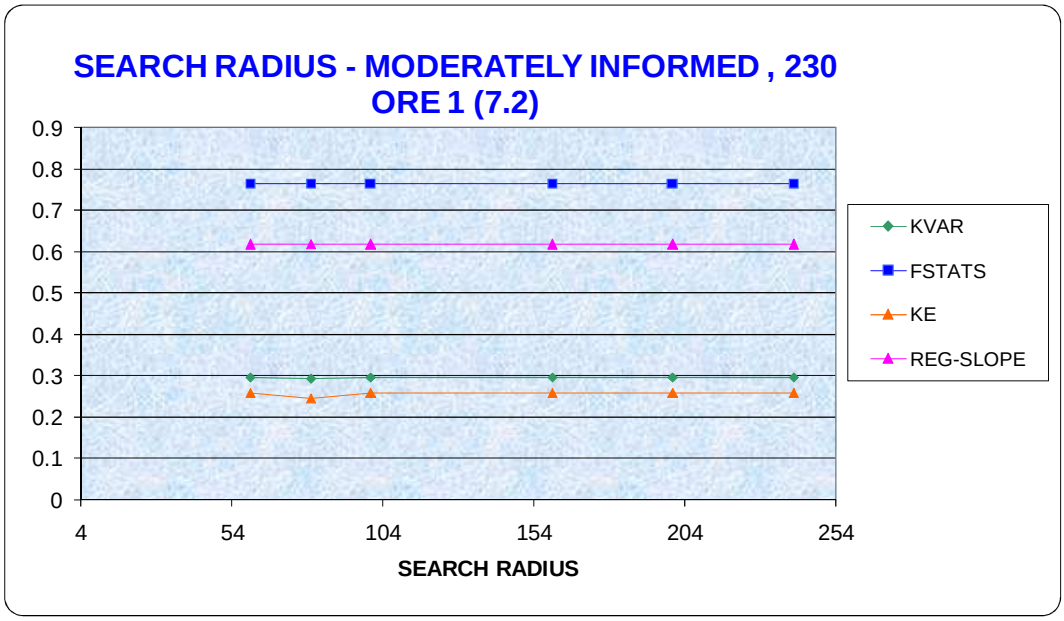
BLOCK 7.2 QKNA STUDY ANALYSIS



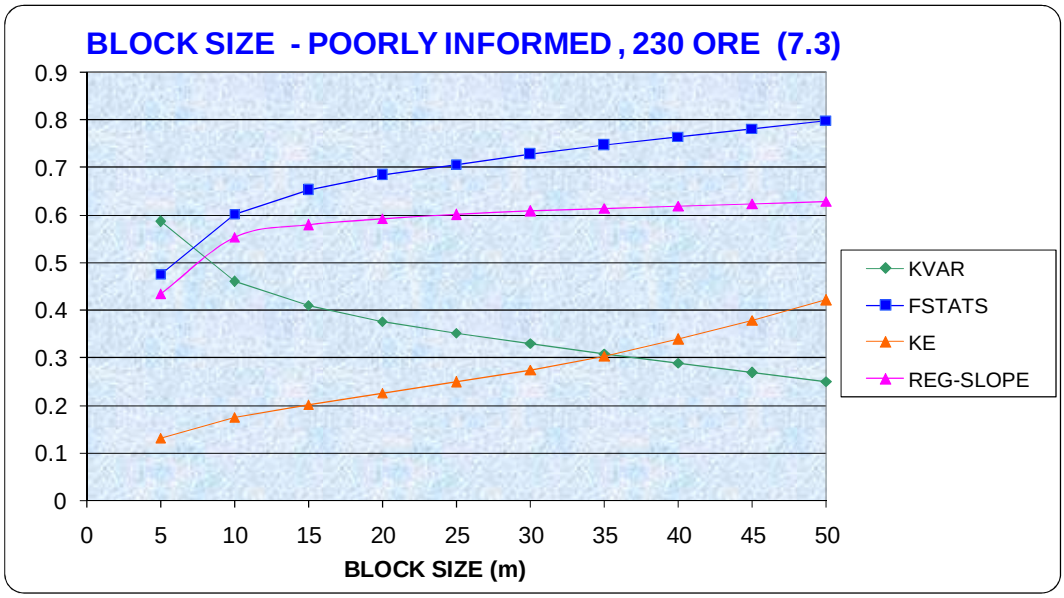


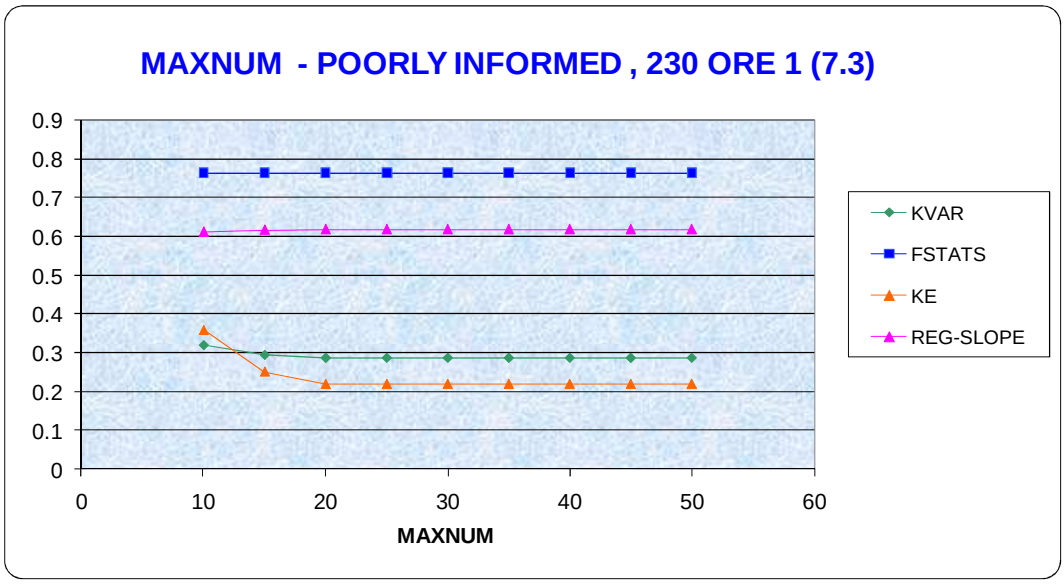

MINNUM - MODERATELY INFORMED , 230 ORE 1 (7.2)
0.9
0.8
0.7
0.6
0.5
0.4
0.3
0.2
0.1
0
4
5
6
7
8
9
10
11
MINNUM
KVAR
FSTATS
KE
REG-SLOPE

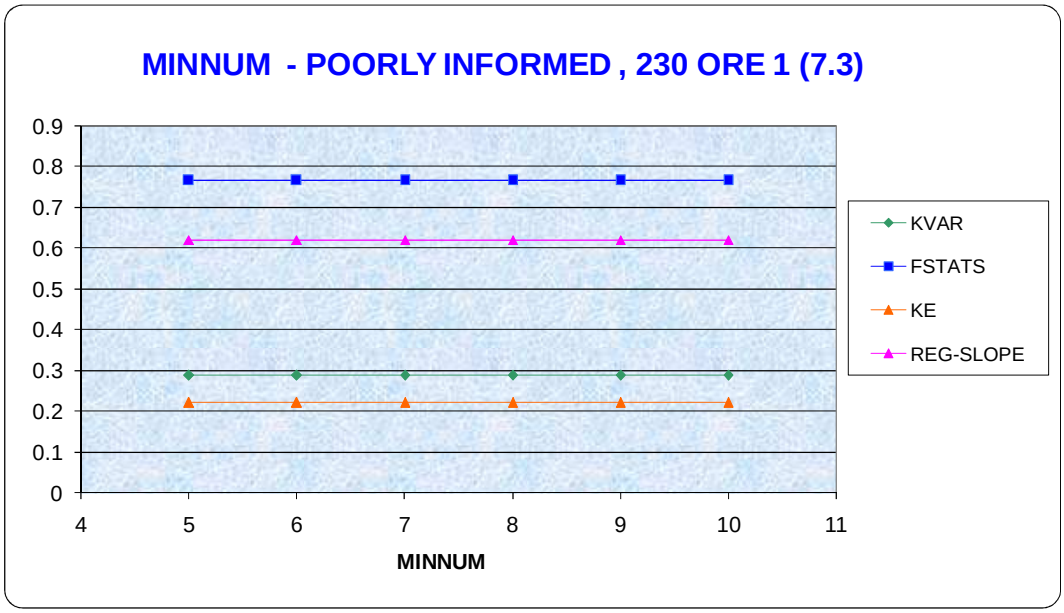

DISCRET - MODERATELY INFORMED , 230 ORE 1 (7.2)
0.9
0.8
0.7
0.6
0.5
0.4
0.3
0.2
0.1
0
1
2
3
4
5
DISCRET
KVAR
FSTATS
KE
REG-SLOPE

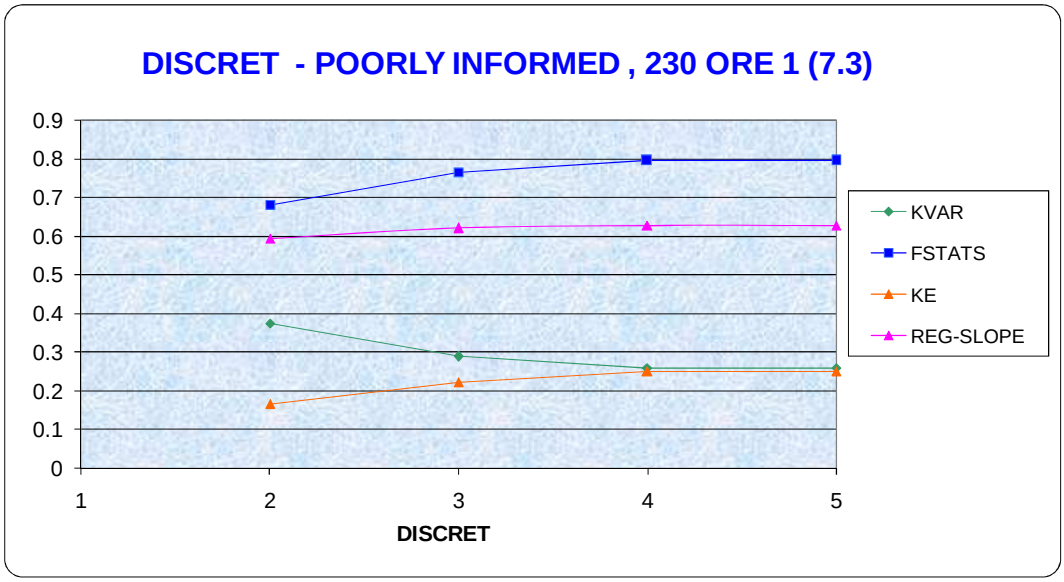

SEARCH RADIUS - MODERATELY INFORMED , 230 ORE 1 (7.2)
0.9
0.8
0.7
0.6
0.5
0.4
0.3
0.2
0.1
0
4
54
104
154
204
254
SEARCH RADIUS
KVAR
FSTATS
KE
REG-SLOPE

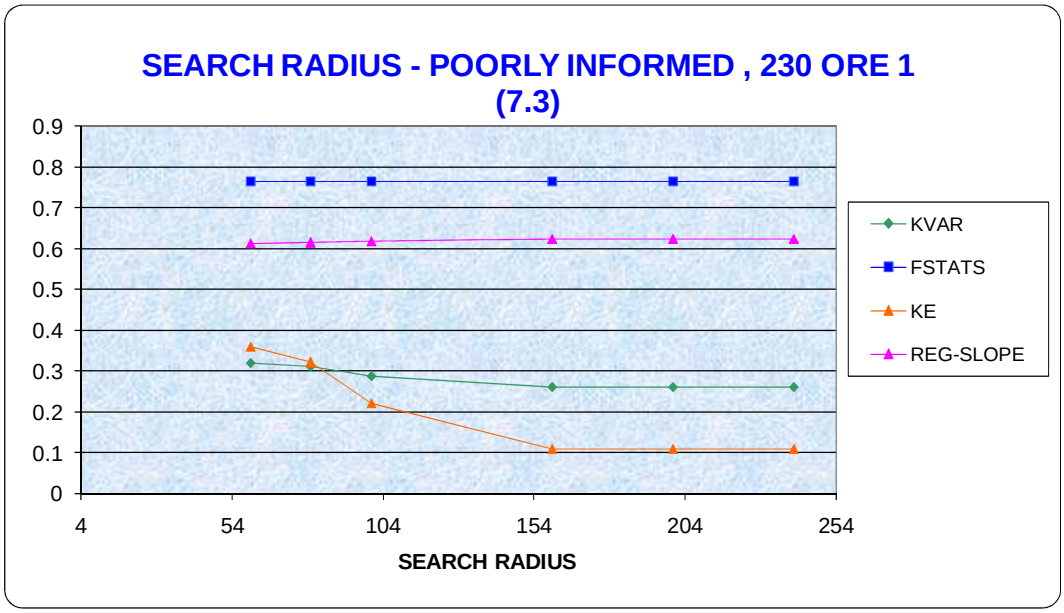
BLOCK 7.3 QKNA STUDY ANALYSIS






MINNUM - POORLY INFORMED , 230 ORE 1 (7.3)
0.9
0.8
0.7
0.6
0.5
0.4
0.3
0.2
0.1
0
4
5
6
7
8
9
10
11
MINNUM
KVAR
FSTATS
KE
REG-SLOPE


DISCRET - POORLY INFORMED , 230 ORE 1 (7.3)
0.9
0.8
0.7
0.6
0.5
0.4
0.3
0.2
0.1
0
1
2
3
4
5
DISCRET
KVAR
FSTATS
KE
REG-SLOPE


SEARCH RADIUS - POORLY INFORMED , 230 ORE 1 (7.3)
0.9
0.8
0.7
0.6
0.5
0.4
0.3
0.2
0.1
0
4
54
104
154
204
254
SEARCH RADIUS
KVAR
FSTATS
KE
REG-SLOPE